CALCIUM SILICATE-BASED BIOCERAMICS DERIVED FROM NATURAL RESOURCES FOR BONE TISSUE ENGINEERING

THESIS

SUBMITTED IN PARTIAL FULFILMENT OF THE REQUIREMENTS FOR THE AWARD OF THE DEGREE OF

Doctor of Philosophy

IN
PHYSICS
BY

PALAKURTHY SRINATH
(Roll No. 716188)

Dr. P. ABDUL AZEEM

Prof. K. VENUGOPAL REDDY

RESEARCH SUPERVISORS

DEPARTMENT OF PHYSICS
NATIONAL INSTITUTE OF TECHNOLOGY
WARANGAL-506004, (T. S.), INDIA

JULY – 2021

DECLARATION

I hereby declare that the matter embodied in this thesis entitled "**Calcium silicate-based bioceramics derived from natural resources for bone tissue engineering**" is based entirely on the results of the investigations and research work carried out by me under the supervision of **Dr. P. Abdul Azeem** and **Prof. K. Venugopal Reddy**, Department of Physics, National Institute of Technology, Warangal. I declare that this work is original and has not been submitted elsewhere in part or full for the award of any degree.

Place: Warangal

Date:.....

(PALAKURTHY SRINATH)

Roll No. 716188

NATIONAL INSTITUTE OF TECHNOLOGY
WARANGAL – 506004
PHYSICS DEPARTMENT

CERTIFICATE

This is to certify that the work presented in the thesis entitled **"Calcium silicate-based bioceramics derived from natural resources for bone tissue engineering"** is a bonafide work done by **Mr. Palakurthy Srinath** under our guidance and was not submitted elsewhere for the award of any degree.

(Dr. P. Abdul Azeem) **(Prof. K. Venugopal Reddy)**

ACKNOWLEDGEMENTS

I would like to express my sincere gratitude to Prof. K. Venugopal Reddy for his constant support, relentless encouragement and mentoring me with this research study and for all his knowledge and constructive criticism. His guidance and mentoring was not limited to this research study, it helped me personally as well.

My deepest gratitude to Dr. Abdul Azeem for his continued support, fruitful guidance and persistent encouragement every step of the way through this research study. His expertise in the area, passion for research, patience and motivation not only helped me in this research and writing of the thesis but also inspired me to work in cutting edge areas. This research work would not have been possible without him.

I extend my heartfelt thanks to the Director, National Institute of Technology, Warangal for giving me the opportunity to conduct research work and for allowing me to submit the thesis.

I would like to express my sincere thanks to Prof. D. Dinakar, Head Department of Physics, NIT Warangal for his valuable suggestions and support.

I would like to express my sincere thanks to Former Heads, Department of Physics, NIT Warangal for their valuable suggestions and support.

I greatly acknowledge the financial assistance, in the form of fellowship from the Ministry of Human Resource and Development (MHRD), New Delhi.

I sincerely thank the members of the Doctorial scrutiny committee Prof. D. Dinakar, Prof. D. M. Vinod Kumar and Dr. T. Venkatappa Rao for their valuable suggestions at every step of research work.

I am very much thankful to Prof. Bramanandam Manavathi and group, School of Life Science, University of Hyderabad for permitting me to perform cell culture studies in their laboratory.

I take this opportunity to express my sincere gratitude to Prof. L.R.G Reddy, Prof. R.L.N Sai Prasad, Dr. P. Syam Prasad, Dr. B. Sobha, Dr. Sourabh Roy, Dr. K. Thangaraju, Dr. D. Haranath, Dr. Kusum Kumari, Dr. D. Paul Joseph, Dr. V Jayalakshmi. Dr. Rakesh Kumar, Dr. Vijay Kumar, Dr. Udaykumar, Dr. Surya K. Ghosh, Dr. Hitesh Borkar, Dr. Aalu Boda, faculty, Department of Physics, NIT Warangal for their valuable suggestions and encouragement.

I am very thankful to Dr. M Raja Vishwanathan, Department of Humanities & Social Science, NIT Warangal for his assistance in correcting the papers.

I gladly acknowledge the help given by my seniors, Dr. S. Rajkumar, Dr. B. Evangeline, Dr. V. Himamaheswara Rao, Dr. P.V.N Kishore Dr. Harikrishna, Dr. Ashish Kumar, Dr. Mohanbabu, Dr. Rama Rajan, Gnaneswar, Lalsingh and Sravanthi. I would like to acknowledge the pleasant company of my co-scholars, Nagaraju, Manjula, VDR Pavan, Buchaiah, Purushotham reddy, Ramesh, Akshay kranth, Koustav Dey, Krishnam Raju, Sathaiah, Vishnu vikesh jaiswal, Prasad, Sushil patel, Jayaram babu and other research scholars .I will relish your memories for years to come. I convey my thanks to all non-teaching and supporting staff, Department of Physics for their help during my research work.

Last but not least; my deep debt of gratitude goes to my beloved family members who with all their patience, prayers, and faith in the almighty, awaited all these years to see me reach this stage. Their blessings and care always gave me new fervour and gusto to do something more. I will always remember and cherish the encouragement provided by my mother and sister. Special thanks to all the people behind the curtain and well-wishers who helped me during the course of my research work.

(Palakurthy Srinath)

Dedicated to…..

My Parents

&

My Gurus

A PERSON WHO

NEVER MADE A MISTAKE

NEVER TRIED ANYTHING NEW

- Albert Einstein

Abstract

Bioactive ceramics are defined as synthesized inorganic materials with a crystalline structure, used for the repair and regeneration of damaged or diseased parts of the human tissue. Bioactive ceramics are highly promising in terms of their capability (i) to bond to hard tissue (and soft tissues) through the development of hydroxyapatite without any inflammatory effects when interacting with physiological fluid (ii) to release biologically active ions which stimulate osteogenesis, (iii) to promote vascular ingrowth during new tissue growth. Several bioceramics have been explored as potential candidates for tissue engineering applications beginning with alumina (Al_2O_3) and zirconia (ZrO_2) to calcium phosphate, borate and calcium silicate-based ceramics owing to their excellent biocompatibility and osteoconductivity. Calcium silicate-based bioactive materials including $CaSiO_3$ and Ca – Si – x (x = Zr, Ti, Zn, Mg, Sr) ceramics, are an emerging subject of research for bone tissue engineering. The release of Ca and Si ions at specific concentrations induces osteoblast cells proliferation and differentiation being a significant feature of calcium silicate-based materials. In the present study, β-wollastonite (β-$CaSiO_3$) incorporated with trace metal oxides (Ag, Zr and Mg) were prepared using bio-waste such as rice husk ash (RHA) as a source of silica and eggshells as a source of calcium oxide through sol-gel method. A detailed study of *in vitro* bioactivity, degradation rate, cytocompatibility and mechanical properties of prepared bioceramics was made for bone tissue engineering. X-ray powder diffraction (XRD), Thermogravimetric-differential thermal analysis (TG-DTA), Scanning electron microscopy (SEM), Fourier transforms infrared (FTIR) and Energy-dispersive spectrometry (EDS) were used to assess the crystalline phase, thermal behavior, microstructure, functional groups and composition, respectively. The bioactivity of the prepared samples was tested by means of ability as well as the rate of apatite mineralization on the surface in simulated body fluid (SBF). Degradation rate was studied by testing the weight loss in Tris-HCl buffer

solution according to ISO 10993-14 standard. Cytocompatibility by human osteoblast-like cells and their proliferation were studied using MTT assay. Mechanical properties such as microhardness, fracture toughness and compressive strength were obtained on cylindrical type of ceramic samples, and bending strength and elasticity modulus were obtained using ceramics bars. *In vitro* bioactivity results clearly showed that apatite crystals were close-packed and fine, and the growth rate was faster on β-$CaSiO_3$ ceramics synthesized by sol-gel method using bio-waste resources than on β-$CaSiO_3$ prepared using tetraethylorthosilicate (TEOS) and calcium nitrate tetra hydrate ($Ca(NO_3)_2.4H_2O$). The addition of Ag results in the improvement of apatite layer formation rate. The antimicrobial activity test demonstrated that Ag doped wollastonite exhibits excellent inhibition zone of pathogens such as E. coli and S. aureus than pure form of wollastonite. In case of ZrO_2 substituted β-$CaSO_3$ ceramics, it was observed that the microhardness and compressive strength increased from 19.3 ± 1.3 to 45.1 ± 2.8 HV and 40 ± 2.4 to 86 ± 2.1 MPa, respectively, with an increase in zirconia content from 0 to 5 mol%. The bending strength and elasticity modulus increased from 10.2 ± 0.7 to 23.6 ± 1.2 MPa and 1.44 ± 0.1 to 5.8 ± 0.2 GPa, respectively. Zr-W ceramics show good bioactivity with the formation of hydroxyapatite, while the apatite formation rate slightly reduced with increasing zirconia content. Degradation tests demonstrated that the addition of zirconia decreased the rate of degradation of wollastonite. Cytocompatibility tests demonstrated Zr-W ceramics have no toxic effect on MG-63 cells. Pure phase of diopside ($CaMgSi_2O_6$) was successfully attained at significantly low temperature (800 °C) with good mechanical properties especially compressive strength (210 ± 12.5 MPa), fracture toughness (2.8 ± 0.3 MPa $m^{1/2}$), bending strength (86.7 ± 7.3 MPa) and elasticity modulus (17.5 ± 2.3 GPa), which were comparable to that of human cortical bone, and which came with enhanced mechanical stability. Diopside ceramics possessed apatite growth on the surface in SBF and exhibited excellent cytocompatibility with MG-63 cells. Therefore, all the prepared

bioceramics from bio-waste such as RHA and eggshells showed good bioactivity, cytocompability, degradation rate and mechanical properties. Therefore, these materials might be potential low cost candidates for bone tissue engineering.

Keywords: Bioceramics, bone tissue engineering, *in vitro* bioactivity, hydroxyapatite, cytocompatibility, mechanical properties, degradation

CONTENTS

LIST OF FIGURES

LIST OF TABLES

ABBREVATIONS

BTE	Bone Tissue Engineering
CSD	Critical Size Defect
HAP	Hydroxyapatite
HCA	Hydroxyl Carbonate Apatite
TCP	Tricalcium phosphate
ECM	Extracellular matrix
ALP	Alkaline Phosphatase Activity
HOB	Human Osteoblast like cells
HBDC	Human Bone Derived Cells
SBF	Simulated Body Fluid
PBS	Phosphate Buffer Saline
DMEM	Dulbecco Modified Eagle's Medium
FBS	Fetal Bovine Serum
TEOS	Tetraethylorthosilicate
TMOS	Tetramethyl orthosilicate
RHA	Rice Husk Ash
ES	Eggshells
PVA	Polyvinyl alcohol
XRF	X-ray Fluorescent
TG-DTA	Thermo Gravimetric-Differential Thermal Analysis
XRD	X-ray diffraction
SEM	Scanning Electron Microscopy
EDS	Energy Dispersive Spectroscopy
FTIR	Fourier Transform Infrared

Chapter 1

Introduction

In this chapter, bone, bone healing processes and the development of bone tissue engineering using a variety of biomaterials have been discussed. In particular, a comprehensive overview of the features of calcium silicate-based ceramics in terms of their preparation techniques, mechanism of bioactivity, biocompatibility, ion releasing capacity, mechanical strength and stability have been described, with the possibility of multiple potential applications in biomedical field. A detailed literature review on calcium silicate-based bioceramics has been presented which informed the rational for the research while the primary objectives of the research embodied in the thesis present at the end of the chapter.

1.1 Bone

Bone is a complex tissue that provides the foundation for physical movement in humans, load-bearing capacity to the skeleton, biological elements necessary for hematopoiesis and protection from injuries to internal organs. It stores about 85% of the body's phosphorus and 99% of calcium and plays a vital role in maintaining homeostasis in the circulating body fluids [1]. Bone is divided into two types at the macro level: cortical and cancellous bones, which are characterized by different micro-level entities, and consequently have different functions and mechanical properties (Table 1.1). All the bones inside the body contain both cortical and cancellous bone types, but the distribution ratio varies based on the anatomical site [2]. Cortical bone is dense and solid with average density of 1.8 g/cm^3 and possesses low porosity of around 2-13%, and is located in the very outer part of the tissue. The structural unit of the cortical bone is designated the osteon or haversian system in which the lamellae are organized into concentric circles of about 3 μm thickness, surrounding a vertical haversian canal containing blood vessels and nerves (Fig.1.1 (a)). On the other hand, cancellous bone contains a sponge-like structure with interconnecting porosity of 50-90% and low density of around 0.2 g/cm^3, and is located at the internal section of the bone. The cancellous bone is composed of honeycomb-like network of trabecular plates with large spaces, and the spaces between trabeculae are filled with bone marrow because of which there is light and porous bone that is strong against multidirectional forces and is crucial for initiating body movement [3, 4].

Table 1.1 Mechanical properties of cancellous and cortical bones

Property	**Cortical bone**	**Cancellous bone**
Compressive strength	100-230 MPa	2-12MPa
Tensile strength	50-100 MPa	10-20 MPa
Fracture toughness	2-12 MPa $m^{1/2}$	-
Bending strength	50-150 MPa	-
Young's modulus	7-30 GPa	0.5-0.05 GPa

In a material science perspective, bone is a heterogeneous composite material consisting of 20% of water and 80% of solid matrix that is made up of organic phase and inorganic phases:

- Organic phase is about 30-35% (weight) in which the major component is type I collagen of ~ 90%, ~ 5% non-collagenous proteins (NCPs) and ~ 2% lipids. Type I collagen is a structural protein very well organized in fibers (Fig. 1.1(b)) that gives viscoelasticity to the bone, stabilizes the extracellular matrix and supports the mineral deposition. Non-collagenous proteins such as albumin, fibronectin, decorin, osteonectin are important for matrix organization, cell signalling, metabolism and mineralization.
- Inorganic phase of hydroxyapatite (C_{10} $(PO_4)_6$ $(OH)_2$) is about 65-70% (weight). These crystals gradually grow on collagen fibers that provide structural reinforcement; In fact, they are responsible for bone hardness and stiffness [5].

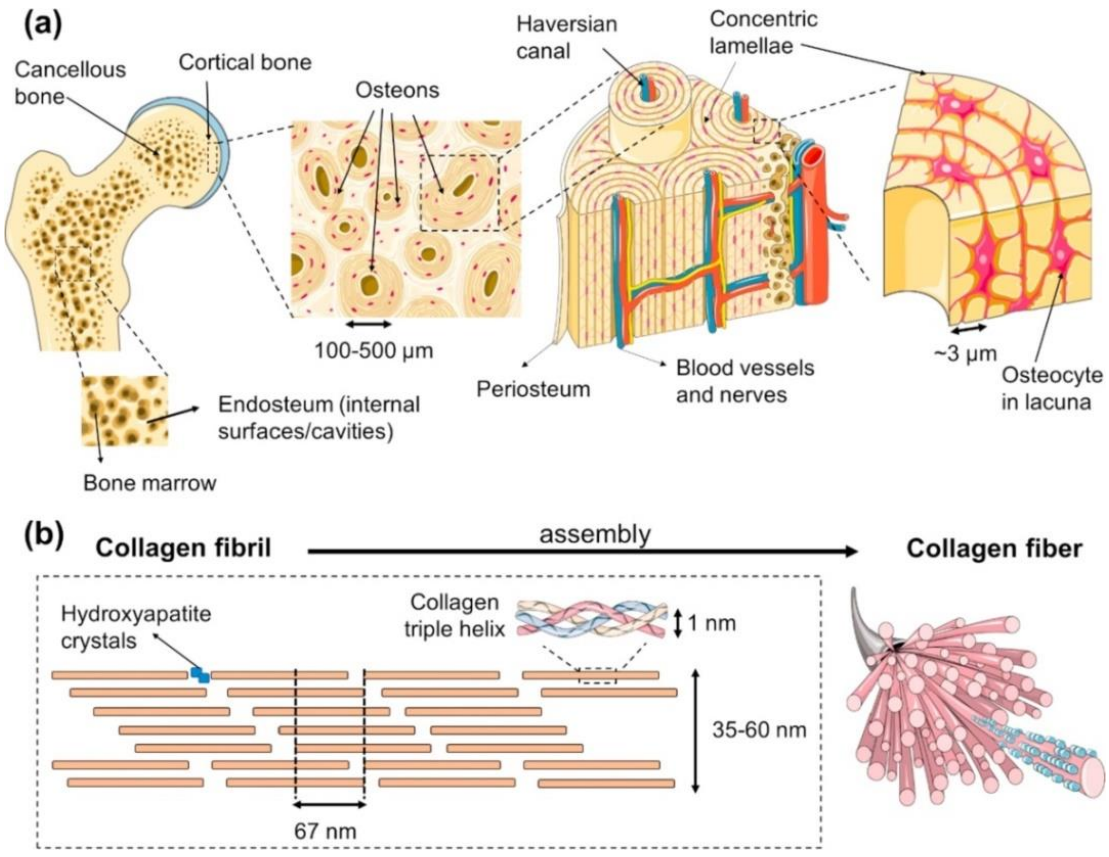

Fig. 1.1 Inter scale representation of bone: a) a macroscopic-to-microscopic view of cancellous and cortical bone and b) bone tissue is constituted at the nanometric scale by collagen fibers that contain the mineral phase [2].

Bone is engaged in a constant cycle of resorption and regeneration that is subject to continuous chemical exchange and structural reconstruction due to internal mediators and external mechanical demands. Bone tissue exhibits a high capacity for remodelling and self-regeneration [1]. Upon fracture, bone healing is a complex process that requires many events of intramembraneous and endochondral bone formation [6]. During the initial healing process, there is an inflammatory response to the formation of hematoma. Necrotic cells release danger signals, which activate the inflammatory response and replace the clotting cascade with a temporary fibrin network that replaces the hematoma. In the meantime, macrophages remove bone fragments and induce the recruitment of mesenchymal and osteogenic cells. Due to the lack of vascularization, the fracture site is hypoxic. Hence, mesenchymal cells become chondrocytes and they produce cartilage that forms a bridge to the fracture site to capture bone fragments. Soft callus provides a template for mechanical stability and vascularization and subsequent mineralization. Through a process called endochondral ossification, bone cells replace soft tissue with woven (or immature hollow) bone. Woven bone and the cartilage matrix are removed by osteoclasts and the bone begins to remodel [7].

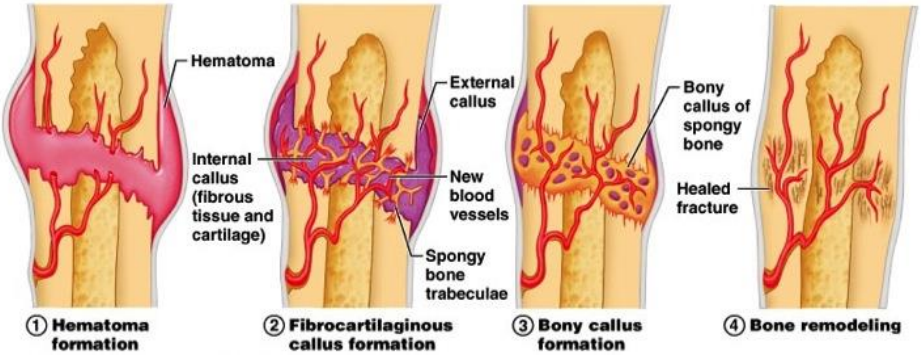

Fig.1.2 Schematic representation of bone healing process

1.2 Bone Tissue Engineering (BTE)

As discussed previously, bone has high regeneration potential, and can repair itself when the wound is smaller than the "critical size defect" while the newly formed bone is indistinguishable from healthy ones. The non-regenerative threshold of bone fracture is called critical sized defect (CSD) [8, 9]. In such cases, extensive studies have been reported for bone repair, including autografts and allografts using autologous and allogeneic transplantations. Autografts are the gold standard for bone repair in which cancellous iliac bone is taken from the same patient and used as a graft. Autografts have indispensable components needed to achieve osteoconduction, osteogenesis and osteoinduction without the risk of an immunogenic response because they are perfectly histocompatible [10]. However, autograft transplants are very expensive techniques, and they are associated with substantial donor site injury, illness, disability, scarring, and the risks of surgery, bleeding, inflammation, infection, and chronic pain. Autologous transplantations may be a null treatment option in cases where the defect site needs larger bones than is possible or obtainable [11]. Allogeneic transplantation is the process of bone-grafting in which bone is taken from a living human donor or from a cadaver (freeze-dried bone), or from xenografts (animal origin). Allografts are associated with low revascularization and integration compared to autografts. Moreover, they demonstrate different kinetics of remodelling, risks of immunogenic response and the transmission of viral pathologies [4].

The field of bone tissue engineering (BTE) came into existence almost three decades ago. Interest and progress in the BTE field has grown tremendously over the years with increasing number of studies. BTE focuses on alternate treatment strategies that will ideally eliminate the previously described shortcomings of current clinically used treatments (i.e., infection, vascular injuries, immune rejection, chronic donor-site pain, and morbidity) by using a combination of materials science, engineering principles, and cell biology. BTE seeks

to develop strategies for the regeneration of diseased or damaged bone through: (i) a biocompatible scaffold that closely mimics the extracellular matrix of natural bone, (ii) osteogenic cells to form the bone tissue matrix, (iii) morphogenic signals that help to direct the cells to the phenotypically desirable type and (iv) adequate vascularization to meet the growing tissue nutrient supply and clearance requirements [12].

1.3 Biomaterials in Bone Tissue Engineering

Biomaterial has been described in many ways in the literature. The American National Institute of Health defined the term "biomaterial" as “unlike drugs, a substance or combination of substances, to be used to replace parts of a living system or to function in intimate contact with living tissue [13]. A significant amount of attention has been paid to this field in the last few decades since biomaterial alignment warranted availability, reproduction, international standard and reliability [14]. The success of biomaterials in health care applications depends entirely on biocompatibility, host response, immunological reactions and cell-biomaterial interaction [15]. In Bone Tissue Engineering, biomaterials can be divided into three categories: i) first generation biomaterials ii) second generation biomaterials and iii) third generation biomaterials (Fig.1.3).

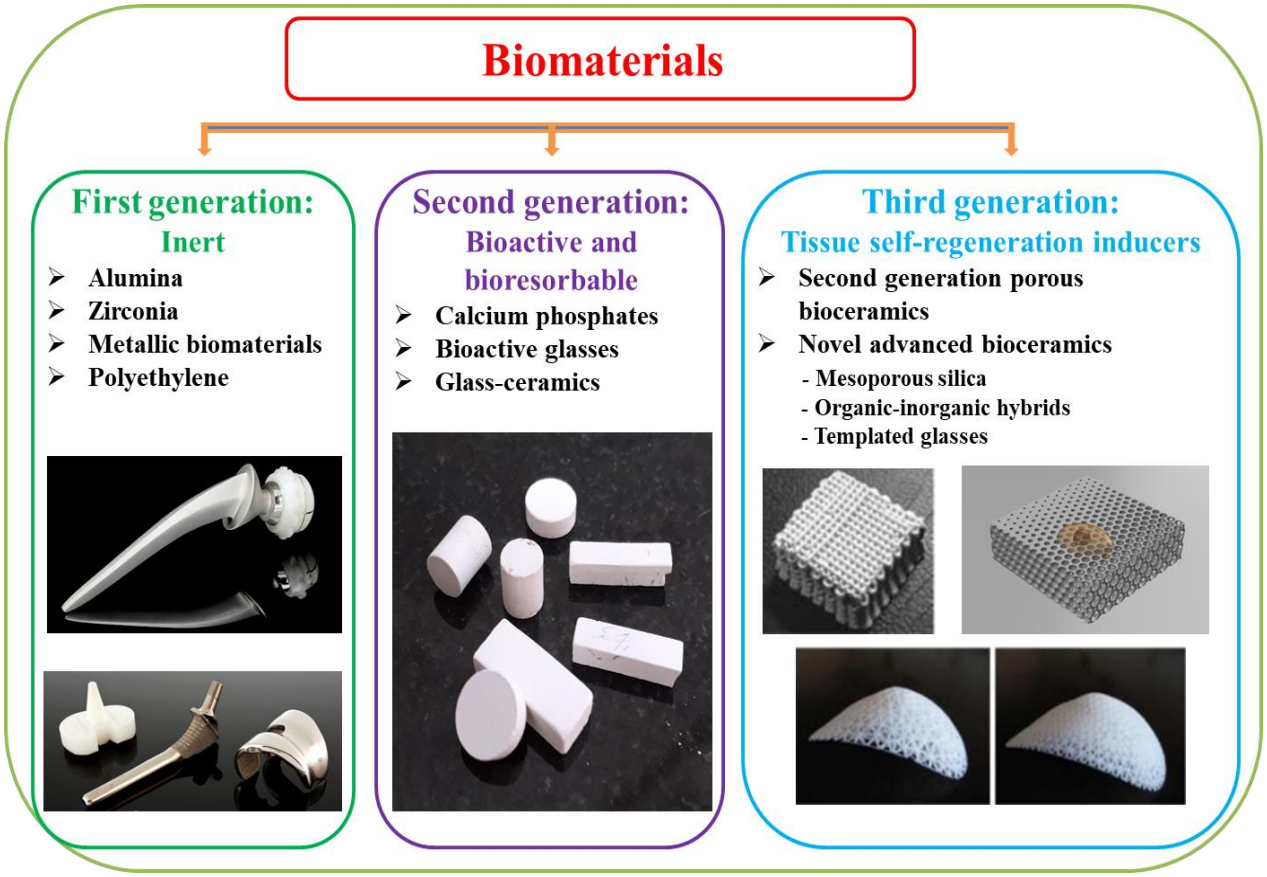

Fig. 1.3 Schematic representation of three generations of biomaterials

1.3.1 First generation: Inert

First generation biomaterials were developed during the 1960s and 1970s. At the time, synthetic substances were used for the first time in biomedical field, to achieve the optimal combination of physical and mechanical properties to match the substituted tissue with least toxic reaction in the host. Therefore, biologically inert or nearly inert biomaterials were designed to match the mechanical properties of the host tissue in order to avoid the phenomenon of stress shielding and consequently bone resorption. Most of these materials are commercially available materials with a high level of purity. For example, titanium, zirconia, alumina and poly-ethylene are bio-inert materials, which compensate for the deficiency without triggering foreign body response in the host's immune system. The implantation of such materials in the body promotes pro inflammatory process that elicits a

foreign fibrous capsule around the material, which isolates it from the surrounding tissue. The thickness of the fibrous layer between the tissue and the material is related to the condition of the material, the tissue and the mechanical load [16].

1.3.2 Second generation: Bioactive and bioresorbable

The field of biomaterials began to receive prominence beginning by 1984 from exclusively achieving bioinert tissue response. The focus of second generation biomaterials is to produce a stable interface with the host tissue due to controlled action and reaction in the physiological conditions that determines the progress of the tissue regeneration process without any inflammatory effects. Therefore, second-generation biomaterials have been developed as bioactive, which "permit the formation of direct bond between the tissue and the material through a specific biological response at the interface of the material, resulting in the nucleation and crystallization of a biologically active hydroxyl-carbonate apatite (HCA) layer, equivalent to the chemical and crystallographic structure to the inorganic bone mineral phase, which exhibits osteoconductive property for bone growth" [17]. Many new bioactive materials such as bioactive glasses (45S5 Bioglass®), glass-ceramics, A-W glass ceramics, dense calcium phosphate ceramics (synthetic hydroxyapatite), calcium silicates ceramics, bioactive composites and bioactive coatings have been discovered in the field of bioactive materials and have reached clinical use in a wide variety of orthopedic and dental applications (Table 1.2).

Table 1.2 Clinical usages of bioactive materials

Bioactive material	**Clinical use**	**Ref.**
Hydroxyapatite (HAP)	Bone defect repair	[18]
45S5 Bioglass and glass-ceramics	Endoscopic ridge maintenance implants to restore the ossicular chain and treat carrier hearing loss, middle ear prostheses, and protect the alveolar ridge from bone resorption	[19]
A-W glass ceramics	Vertebrae replacement in patients with spinal tumours	[20]
Tricalcium phosphate (TCP)	Orthopedic joint replacements	[18, 21]
HAP/TCP	Bone replacement materials (synthetic bone grafts)	
Metal/polymer containing bioactive molecules	Dental applications	[22]
Collagen	Augmentation as cosmetic surgery	[23]
Chitosan	Wound tissue repair	
Gelatin	Implants for urinary incontinence	
HAP/collagen	Vascular grafts	
HAP + polyethylene matrix bioactive composites	Repair and replacement of bones in the middle ear	[22, 24]
Biodegradable polymer + HAP + cells	Skin substitutes	

Bioresorbable biomaterials are also included under the category of second generation biomaterials, which degrade and resorb upon implantation, allowing the proliferation and seeding of osteogenic cells. The cells secrete their own extracellular matrix and eventually the material is completely replaced with new bone. As the products of degradation are absorbed into the body, they must be biologically accepted. Furthermore, the rate of degeneration of the resorbable implant must match the rate of regeneration of the bone to ensure proper support. Nowadays, it is common to use resorbable polymers as clinical sutures. Resorbable fracture fixation plates and screws in orthopaedics and controlled-release drug delivery systems have been introduced [25].

1.3.3 Third generation: Tissue self-regeneration inducers

In the first decade of the twenty-first century, the concepts of bioactive and resorbable materials come together; bioactive materials are made into resorbable. Therefore, third generation biomaterials are designed to induce specific reactions directly in the cells that stimulate regeneration of living tissues through molecular modifications of polymers, bioactive glasses, glass-ceramics and composites hierarchical porous foams [24]. There are two alternate methods of repair that use new molecularly designed third generation biomaterials. The first approach involves the use of materials in the form of solutions, powders or doped nano or micro particles to stimulate local tissue repair. The materials release macromolecular growth factors or ionic soluble products, at controlled rates that activate the cells in contact with the stimuli. Cells produce additional growth factors that stimulate multiple generations of growing cells to self-assemble in the tissues necessary for the site. In the next method, the pores of the molecularly modified resorbable scaffolding are filled with progenitor cells outside the body, where the cells grow and differentiate and mimic naturally occurring tissues. The tissue-engineered structures are then implanted into

the diseased or damaged parts of the body in patients. The scaffolds are resorbed and replaced over time by the host tissues, which have a viable blood supply and nerves [24, 26].

1.4 Introduction to calcium silicate-based bioceramics

Calcium and silica are mainly two significant ions in calcium silicate-based bioceramics. Human body contains about 2% of Ca in which 98% exists in bones. The body fluid and cells contain 10 to 15 mg per 100 mg. Ca is present in the active region of the natural bone and plays an essential role in blood vessels and bone growth [27]. Extracellular calcium plays a biological role in regulating bone restoration independent of hormones by stimulation of cation-sensing receptors [28]. For instance, extracellular Ca can enhance the usefulness of insulin-like growth factor (IGF) II, which explicitly regulates proliferation of osteoblasts. Extracellular Ca concentrations can also enhance the release of osteoblast glutamate [29]. Several studies have been conducted over the past few decades to investigate the potential role of silica in bone growth. Si is generally absorbed in the form of metasilicate, which is extensively disseminated in connective tissue. Si is essential for the metabolic process associated with bone calcification and is favourable for enhancing bone density and inhibiting osteoporosis [30]. Specifically, in the initial period of bone matrix calcification, Si contents in new bone can develop a certain degree of osteogenesis [31]. Aqueous Si was able to induce precipitation of inorganic phase of bone i.e. hydroxyapatite [32]. Some reports have revealed that Si can also stimulate proliferation and differentiation of osteoblast and regulate the activation of bone-related gene expression [33]. Along with Ca and Si other important ions in calcium silicate-based bioceramics such as Mg, Zn, Zr and Sr are also plays significant role in bone metabolism. A detained biological response to ionic dissolution products of calcium silicate-based ceramics is presented in table 1.3.

Table 1.3 Biological responses to ionic dissolution products of calcium silicate-based ceramics

Ion	Biological response	Ref.
Ca	❖ favours osteoblast proliferation, differentiation and extracellular matrix (ECM) mineralization ❖ activates Ca-sensing receptors in osteoblast cells, increases expression of growth factors, e.g. IGF-I or IGF-II	[28, 34]
Si	❖ essential for metabolic process and calcification of bone tissue ❖ favourable for enhancing bone density and inhibiting osteoporosis ❖ aqueous Si was able to induce precipitation of hydroxyapatite ❖ $Si(OH)_4$ stimulates collagen I formation and osteoblastic differentiation	[31, 35]
Mg	❖ stimulates new bone formation ❖ increase adhesion and growth of osteoblast cells	[36, 37]
Zr	❖ shows superior biocompatibility and favours osseointegration ❖ enhance mechanical strength and stability	[38]
Zn	❖ exhibits antimicrobial activity, anti-fungal activity and virus inactivation properties ❖ favours osteoblast proliferation, enhances alkaline phosphatase (ALP) activity in bone tissue and inhibits osteoclastic bone resorption	[39]
Sr	❖ enhances osteoprogenitor cell replication and collagen synthesis ❖ promising agent for treating osteoporosis	[40]

Calcium silicate ceramics have the ability to induce hydroxyapatite in simulated body fluid (SBF) in the form of ceramics, powders and ceramic coatings. The mechanism of

hydroxyapatite formation on the surface of calcium silicate bioceramics is shown in Fig. 1.4. When calcium silicate ceramic is soaked in SBF, Ca^{2+} ions from the surface are first exchanged with H^{+} ions in the solution, and they subsequently increase pH level of body fluid. The ion exchange leads to the development of leached layer rich in silanols (Si-OH) on the surface of ceramics. In the next step, Ca^{2+} ions in the SBF are electrostatically attracted to the newly developed negatively charged silica-rich layer; the Ca^{2+} ions are initially attached to negatively charged silica-rich surface and then there is adsorption of PO_4^{3-}/HPO_4^{2-} on Ca^{2+} ions followed by the growth of bone-like apatite layer onto the surface [41].

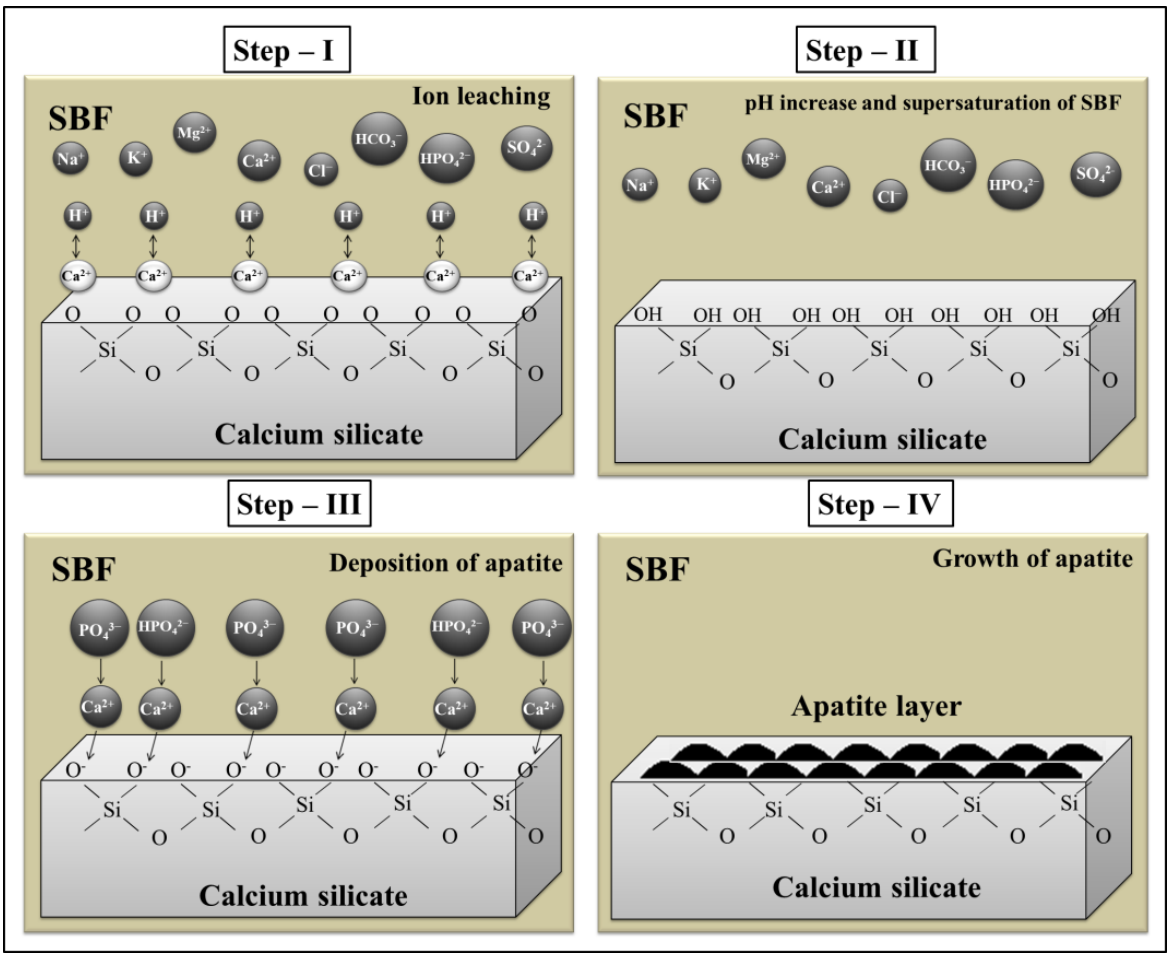

Fig. 1.4 Schematic illustration of the mechanism of apatite formation on calcium silicate ceramics in SBF

Three important Ca-Si compounds have been observed with variation in Ca/Si ratio, such as tricalcium silicate (Ca_3SiO_5), dicalcium silicate (Ca_2SiO_4) and monocalcium silicate

($CaSiO_3$). Dicalcium silicate and tricalcium silicate are the main constituents of Portland cement, hydrated and hardened when combined with liquid phase. Dicalcium silicate has five different polymorphs denoted by α, α′H, α′L, β and γ symbols. The α, α′H, α′L phases are stable at high temperature, γ phase is stable at ambient temperature and β phase is not thermodynamically stable but is hydration active at ambient temperature. Tricalcium silicate phase is stable between 1200 – 1900 °C and beyond 1900 °C the phase disassociates into CaO and Ca_2SiO_4. Tricalcium silicate hydrates quietly and greatly influence the setting and improvement of early strength while dicalcium silicate hydrates much more slowly than tricalcium silicate and are accountable for the latter's strength [42]. Monocalcium silicate is a most extensively studied ceramics for bone repair and regeneration applications for its progressive bio-functionalities compared to dicalcium silicate and tricalcium silicate ceramics. It exists in two forms: low temperature form β – wollastonite (β – $CaSiO_3$) and high temperature form α – wollastonite (α – $CaSiO_3$). Another important aspect that the substitution of trace elements (Mg, Zn and Zr) into Ca-Si system leads to the formation of calcium silicate-based minerals such as akermanite ($Ca_2MgSi_2O_7$), Diopside ($CaMgSi_2O_6$), bredigite ($Ca_7MgSi_4O_{16}$), merwinite ($Ca_3MgSi_2O_8$), monticellite ($CaMgSiO_4$), hardystonite ($Ca_2ZnSi_2O_7$) and baghdadite ($Ca_3ZrSi_2O_9$). Each of these calcium silicate-based ceramics has their own significance and surviving as bone implant materials. Along with wollastonite bredigite ceramics exhibit superior apatite formation ability with rapid dissolution rate. Diopside, monticellite and baghdadite demonstrate moderate apatite formation ability with slow dissolution rate. No noticeable apatite formation could be observed for hardystonite ceramics and their dissolution rate is also quite low. Whereas, Akermanite and merwinite display good apatite formation with reasonable dissolution rate and promote enhanced osteoblasts adhesion, proliferation and osteogenic differentiation, including osteopontin, alkaline phosphatase, bone sialoprotein and osteocalcin compared with β-TCP.

1.5 Motivation and scope of the present work

Interest in research on bioactive materials is growing day by day as they are very promising in terms of their capability (i) to initiate complex chemical and biological processes due to interaction with living cells that determines the progress of the tissue regeneration process without any inflammatory effects, (ii) to release biologically active ions which stimulate osteogenesis, (iii) to promote vascular ingrowth during new tissue formation. The revolution in the field of bone tissue engineering was took place in 1969 with the development of calcium silicate bio-glass (45S5Bioglass) by Hench. In fact, such bio-glass plays their role as synthetic bone with host tissues after few days [43]. Over the past few decades, a wide variety of bioactive materials have been developed, which can show high performance and improved biological response. In addition, loading of bioactive materials with drugs has also been explored for therapeutic functions such as anti-tumor and antibacterial effects [13]. Among various bioactive materials that have been developed, widespread ceramic products are based on calcium phosphates including hydroxyapatite [$Ca_{10}(PO_4)6(OH)_2$] and tricalcium phosphate [$Ca_3(PO_4)_2$], which have molecular composition equivalent to that of human bone. These are potentially used in orthopaedic applications for bone tissue repair and extensively studied to induce bone regeneration because of its exceptional adaptation under human body environment [44]. Although the calcium phosphate-based ceramics applications have made great advances, it should be indicated that the primary premise of ideal bone substitutes is that the mechanical properties must be consistent with human bone and that the body's own biological tissues can regenerate over time through resorption. The resorption procedure is initiated by both dissolution of the material as well as by osteoclastic cells. However, sintered calcium phosphates usually have low fracture toughness and compressive strength. Moreover, low dissolution rate of calcium phosphate ceramics normally marks low kinetics of resorption [45].

Calcium silicate-based ceramics are being presently explored as an alternative to calcium phosphate ceramics. Literature reviews have shown that important features of calcium silicate-based ceramics are excellent bioactivity, biodegradability and tendency to release ions at a concentration that promotes osteoblast proliferation and differentiation [46]. The rate of apatite mineralization on the surface of the calcium silicate-based ceramics is found to be faster than calcium phosphates and any other glass ceramics due to the presence of silicon ion which efficiently takes part in the metabolism during bone growth and cell proliferation. Moreover, the relatively wide range of calcium silicate-based materials in chemical compositions have great influence on regulating mechanical strength, making them capable of stress and load-bearing applications [47]. These materials are also widely used in various medical applications such as biocompatible polymer-ceramic composites, bioactive coating of metallic implants and drug delivery.

In spite of various methods that have been reported for preparation of calcium silicate ceramics, sol-gel synthesized calcium silicates have proven to be potential candidates for its biomedical application due to their enhanced chemical homogeneity and higher bioactivity. The traditional powder manufacture technology using melt-quenching method or solid-state sintering for the fabrication of calcium silicate ceramics requires more than 1200 °C temperature; in contrast, the sol-gel technique requires reasonably low temperature of 800 °C [48]. A typical sol-gel method for synthesis of calcium silicates require high purity calcium nitrate tetra hydrate ($Ca(NO_3)_2 \cdot 4H_2O$) as calcium oxide source and tetraethylorthosilicate (TEOS) as silica source which are expensive. In addition, the method requires gelation of TEOS and ($Ca(NO_3)_2 \cdot 4H_2O$) via acid or base hydrolysis of TEOS. TEOS hydrolysis is extremely slow in neutral medium and this method requires the addition of acid or base catalyst during gelation. Without any catalyst, the presence of water alone leads to elastic homogeneous gel formation, which requires long drying time [49].

Accelerating utilisation and recycling of waste volumes to produce valuable biomaterials is a significant increasing research interest worldwide [50]. Managing waste to recapture resources and turning them back into virgin raw materials is always an impetus for promoting sustainable living in the future. In the field of agriculture, rice husk is highest waste production across the world. Researchers have reported that rice husk has rich amount of silica in the form of rice husk ash (RHA) which could be easily extracted from the rice husk after calcination at high temperatures [51]. It has also been reported that these biogenic forms of silica produced in rice husk ash shows good biocompatibility over synthetic forms of silica [52]. Also, since 11% of the total mass of egg represents eggshell, millions of tons of eggshells are generated as bio waste. It has been reported that eggshells has ample amount of calcium carbonate as ~94%, and remaining constituents are ~1% of calcium phosphate, ~1% of magnesium carbonate and ~4% of other organic matters. High temperature treatment of crushed eggshells produce ~99% of calcium oxide along with traces of biologically beneficial ions such as Mg^{2+}, Sr^{2+} and F^{-} [53]. Moreover, the calcium oxide produced in eggshell can impart antimicrobial activity to the composition [54]. Therefore, the use of these biogenic forms of silica and calcium oxides as alternatives to synthetic forms to produce biomaterials for biomedical applications not only reduces the total production cost, but also shows myriad biological beneficial effects.

Furthermore, the degradation rate of calcium silicate ceramics is relatively high when used in the form of 3D scaffold because porous scaffolds have significantly higher specific surface area than ceramic discs, leading to abrupt change in pH value of local environment by dissolution ions, which may negatively affect surrounding cells [55]. Additionally, the high solubility rate, which indicates their chemical instability, is likely reason for failure of scaffold construction before the creation of appropriate extracellular matrix (ECM) and new bone. Literature studies have shown that the dissolution rate of calcium silicate ceramics can

be control by substitution of ions (Ag, Mg, Zn, Zr and Sr) that leads to formation of new materials with modified crystal structure. Such complicated crystal structures with various bond strengths between ions and with improved density decreases dissolution rate of Ca and Si ions concentration which in turn create a suitable pH value that promotes osteoblast proliferation, differentiation and gene expression

Therefore, in the current study, as a part of dissertation, natural resources such as rice husk and eggshells have been chosen as source materials for silica and calcium oxide, respective to produce calcium silicate ($CaSiO_3$) bioceramics by sol-gel technique for bone tissue engineering. Different trace metals like Ag, Zr and Mg were incorporated in produced calcium silicate phase to regulate the properties for bone tissue engineering. Different techniques like XRF, TG-DTA, XRD, FTIR, SEM-EDS and Particle analyzer were used to characterize the prepared samples. Bioactivity was studied based on the rate of hydroxyapatite formation using *in vitro* experiments in simulated body fluid (SBF). Weight loss studies were performed in SBF and also in Tris-HCl buffer solutions to know the degradation behaviour of the synthesized ceramics. Biocompatibility was estimated by osteoblastic cells (MG – 63) using MTT assay. Mechanical properties such as microhardness, compressive strength, fracture toughness and elasticity modules were tested to know the nature of the prepared ceramics whether they are mechanically compatible with the bone tissue or not.

1.6 Brief review of the work done on calcium silicate-based bioceramics

The traditional method of preparing bioactive material is through melt quenching; only a limited composition range of Ca-Si binary system can be melted. The Ca–Si system phase diagram shows the liquid – liquid miscibility gap is asymmetric at 1871 °C upper critical solution temperature and at 1705 ± 10 °C solvus temperature [56, 57], while

quenching glasses from above 1700 °C have a white opaque Ca-rich phase and clear siliceous phase, which makes it impossible to synthesize glasses with composition in this area by conventional melt quenching method [56]. This could be the reason for the development of research on Ca-Si binary system is less mature for biomedical field. However, Hayashi T and Saito H [58] who first reported in 1980 an incapability to produce Ca-Si binary system by sol-gel procedure used high purity Ca metal reacting with ethanol. They struggled with alkoxides hydrolysis, resulting in precipitation of hydrolysed product. Hayashi T and Saito H [58] also reported that when they used calcium nitrate as calcium source, a translucent or opaque gel was obtained which gave rise to crystalline $Ca(NO_3)_2$. nH_2O containing fully white powders at higher temperatures. Bansal NP [57] in 1992 was able to successfully obtain a transparent gel by using calcium nitrate tetra hydrate as precursor of calcium where alcoholic solution of calcium nitrate tetra hydrate was mixed with tetraethyl orthosilicate (TEOS). Catauro M et al. [59] in 1997 produced similar results with tetramethyl orthosilicate (TMOS) and $Ca(NO_3)_2.4H_2O$ as precursors for glass composition of $2CaO.3SiO_2$. Later Vallet-Regi and co-workers [60, 61] reported a succession of publications on the biological properties of $CaO\text{-}SiO_2$ binary system.

Several *in vitro* and *in vivo* studies have been carried out to examine the bioactivity and biocompatibility of dicalcium silicate and tricalcium silicates. For example, Liu X et al. [62] investigated the formation and evolution of hydroxyapatite on dicalcium silicate coatings and found excellent bioactivity of dicalcium silicate when used as coatings for titanium alloy substrates. Sun J et al. [63, 64] demonstrated that plasma-sprayed coatings of dicalcium silicate are favourable for the proliferation and differentiation of osteoblast-like MG63 cells and regulation of osteoclastogenic gene expression. Jiang Chang and co-workers examined *in vitro* bioactivity and self-setting property of dicalcium silicate [65, 66] and tricalcium silicate [67, 68], demonstrating that these cement pastes are bioactive self-setting materials which can

be used as injectable implants for bone repair applications. Sun M et al. [69] described the systematic *in vitro* and *in vivo* investigation on β-Ca_2SiO_4 cements in comparison with calcium phosphate cement, suggesting that β-Ca_2SiO_4 biocement is a promising candidate for bone tissue engineering.

Monocalcium silicate ($CaSiO_3$) is a most extensively studied ceramics for bone repair and regeneration applications for its progressive bio-functionalities compared to dicalcium silicate and tricalcium silicate ceramics. Siriphannon P et al. [70] showed that carbonated hydroxyapatite (CHA) growth rate on wollastonite was faster than on other bioactive glass ceramics and A-W glass ceramics. *In vitro* cell culture assessments demonstrated that wollastonite ceramics can support the attachment of osteoblast-like cells and bone marrow mesenchymal stem cell, as well as their proliferation and differentiation [71–73]. Wollastonite shows improved performance in terms of mechanical properties such as higher fracture toughness and bending strength when compared with calcium phosphate ceramics [74, 75]. Furthermore, some of the *in vivo* functions of wollastonite have also been reported. De Aza PN et al. [76] examined the morphology and chemistry of the reconstructed interface between wollastonite implant and the surrounding bone in the femoral condyle of rats, showing that wollastonite implant seemed to serve as a physical support where cells with osteoblastic capability were found to migrate and develop. Xue W et al. [77] investigated the bioactivity behaviour of wollastonite coatings by implanting them in dog's muscle and in cortical bone marrow, and found that the bone like apatite layer was grown on the surface of wollastonite coating when it was implanted in the muscle, while the bone tissue could extend and grow along the surface of wollastonite coating when implanted in cortical bone. Xu S et al. [78] evaluated the resorption and bone regenerative ability of β – $CaSiO_3$ porous scaffolds in a rabbit calvarial defect model, and the results revealed that β – $CaSiO_3$ has better bone

regenerative capability and much more resorption rate compared with porous β – tricalcium phosphate.

Several studies have also been reported on substitution of trace metal ions such as magnesium (Mg), zinc (Zn) and zirconium (Zr) into calcium silicates to overcome the drawbacks such as weak mechanical strength and high degradation rate. Jiang Chang's group [79, 80] investigated *in vitro* and *in vivo* assessment, and mechanical properties of calcium magnesium silicate bioceramics. The results show that the mechanical properties were increased and promote greater osteogenesis and biodegradation with Mg doping. The rate of bone formation is faster in calcium magnesium silicates than in β-tricalcium phosphate at late-stage implantations [81, 82]. Comparative studies on *in vitro* degradation, apatite forming-ability and cytocompatibility of magnesium containing calcium silicate bioceramics have shown that their mechanical properties are improved, activation energy of Si ions release increased and degradation rate decreased with increase of Mg contents in ceramics, whereas apatite formation rate in SBF solution decreased [83–85]. Li HC et al. [86] showed that the incorporation of ZrO_2 or ZnO decreases the total pore volume, indicating ZrO_2 or ZnO increase the density of wollastonite. ZrO_2 or ZnO enhances the bending strength and elastic moduli of wollastonite ceramics that matches the human body bone. The addition of ZrO_2 or ZnO decreases the degradation rate of wollastonite. Hala Zreiqat's group [87–89] extensively studied the potential biomedical applications of calcium zinc silicates. Their studies revealed that compared to wollastonite, zinc incorporated wollastonite have shown considerably improved attachment of osteoblast-like cells (HOBs), cellular proliferation and differentiation. In addition, addition of zinc promoted the development of mature and efficient osteoclasts and formed resorption imprints. Ramaswamy Y et al. [90] examined the effect of calcium zirconium silicate on proliferation and differentiation of osteoclasts (OC), human osteoblast like cells (HOB) and endothelial cells to determine the potential use of

ceramics for bone tissue engineering. The results of these studies revealed that zirconium containing calcium silicate ceramics support the attachment of human osteoblast-like cells with systematized cytoskeleton structure, promoted enhanced cell proliferation and differentiation compared to wollastonite. Osteoclast activity is enhanced when osteoclasts are cultured, demonstrating that zirconium containing calcium silicates can stimulate bone restoration procedures while accelerating the formation of new bone. In addition, zirconium containing calcium silicate supports endothelial cells attachment, which indicates endothelial cell markers; ZO-1 and VE-Cadherin.

1.7 The objectives of the present study

1. To obtain low temperature calcium silicate-based bioceramics from natural resources which will function as a bone implant material.
2. To study the *in vitro* bioactivity of prepared bioceramics in simulated body fluid.
3. To ensure the mechanical properties of prepared materials match the mechanical properties of human bone.
4. To obtain a controlled degradation rate i.e. the degradation rate of prepared bioceramic and its kinetics of conversion to hydroxyapatite must match.
5. To assess the cytocompatibility and the ability to promote cell proliferation of prepared bioceramics by MTT assay.
6. To assess the antimicrobial activity of prepared bioceramics

1.8 References

1. Walsh JS. Normal bone physiology, remodelling and its hormonal regulation. Surgery (Oxford). 2018;36(1):1-6.

2. Lopes D, Martins-Cruz C, Oliveira MB, Mano JF. Bone physiology as inspiration for tissue regenerative therapies. Biomaterials. 2018;185:240-275.

3. Tzelepi V, Tsamandas AC, Zolota V, Scopa CD. Bone Anatomy, Physiology and Function. Bone Metastases. Cancer Metastasis – Biology and Treatment. 2009;12:3-30.

4. Henkel J, Woodruff MA, Epari DR, Steck R, Glatt V, DIckinson IC, et al. Bone Regeneration Based on Tissue Engineering Conceptions-A 21st Century Perspective. Bone Research. 2013;1(3):216-48.

5. Boskey AL. Bone composition: relationship to bone fragility and anti-osteoporotic drug effects. Bonekey Rep. 2015; 4:710.

6. Fazzalari NL. Bone Fracture and bone fracture repair. In: Osteoporosis International. 2011;22(6):2003-6.

7. Loi F, Córdova LA, Pajarinen J, Lin T hua, Yao Z, Goodman SB. Inflammation, fracture and bone repair. Bone. 2016;86:119-30.

8. Cacchioli A, Spaggiari B, Ravanetti F, Martini FM, Borghetti P, Gabbi C. the Critical Sized Bone Defect: Morphological Study of Bone Healing. Ann Fac Med Vet di Parma. 2006; 26:97-110.

9. Schemitsch EH. Size Matters: Defining Critical in Bone Defect Size! J Orthop Trauma. 2017; 5:S20-S22.

10. Hsiong SX, Mooney DJ. Regeneration of vascularized bone. Periodontology 2000. 2006;41(1):109-122.

11. Salgado AJ, Coutinho OP, Reis RL. Bone tissue engineering: State of the art and future trends. Macromolecular Bioscience. 2004;4(8):743-65.

12. O'Keefe RJ, Mao J. Bone tissue engineering and regeneration: From discovery to the clinic-an overview. Tissue Engineering - Part B: Reviews. 2011;17(6):389-392.

13. Vallet-Regí M, Ruiz-Hernández E. Bioceramics: From bone regeneration to cancer nanomedicine. Advanced Materials. 2011;23(44):5177-218.

14. Hench LL. Biomaterials: A forecast for the future. In: Biomaterials. 1998;19(16):1419-1423.

15. Basu B, Katti DS, Kumar A. Advanced Biomaterials: Fundamentals, Processing, and Applications. Fundamentals of Biomaterials and Biocompatibility. The American

Ceramic Society. 2010;1-18.

16. Hench LL. Biomaterials. Science (80-). 1980;1(1):1-64.

17. Hench LL, Splinter RJ, Allen WC, Greenlee TK. Bonding mechanisms at the interface of ceramic prosthetic materials. J Biomed Mater Res. 1971;5(6):117-141.

18. Hench LL. Bioactive Ceramics: Theory and Clinical Applications. In: Bioceramics. 1994;3-14.

19. Larry L. HenchJune Wilson. Clinical Perfomance of Skeletal Prostheses. 1995.

20. Hench LL, Wilson J, Yamamuro T. A/W GLASS-CERAMIC: CLINICAL APPLICATIONS. In: An Introduction to Bioceramics. 1993;89-103.

21. de Groot K. Clinical applications of calcium phosphate biomaterials: A review. Ceramics International. 1993;19(5):363-366.

22. Zhao X, Courtney J, Qian H. Bioactive materials in medicine design and application. 2011.

23. Puppi D, Chiellini F, Piras AM, Chiellini E. Polymeric materials for bone and cartilage repair. Progress in Polymer Science (Oxford). 2010;35(4):403-440.

24. Hench LL, Thompson I. Twenty-first century challenges for biomaterials. Journal of the Royal Society Interface. 2010; 7(4):S379-S391.

25. Cao W, Hench LL. Bioactive materials. Ceram Int. 1996; 22(6):493-507.

26. Place ES, Evans ND, Stevens MM. Complexity in biomaterials for tissue engineering. Nat Mater. 2009; 8:457-470.

27. Pravina P, Sayaji D, Avinash M. Calcium and its role in human body. Int J Res Pharm Biomed Sci. 2013;4(2):659-668.

28. Marie PJ. The calcium-sensing receptor in bone cells: A potential therapeutic target in osteoporosis. Bone. 2010;46(3):571-6.

29. Midha S, van den Bergh W, Kim TB, Lee PD, Jones JR, Mitchell CA. Bioactive Glass Foam Scaffolds are Remodelled by Osteoclasts and Support the Formation of Mineralized Matrix and Vascular Networks In Vitro. Adv Healthc Mater. 2013; 2(3):490-9.

30. Zhou X, Zhang N, Mankoci S, Sahai N. Silicates in orthopedics and bone tissue engineering materials. Journal of Biomedical Materials Research - Part A. 2017;105(7):2090-2102.

31. Carlisle EM. Silicon: A possible factor in bone calcification. Science. 1970; 167(3916):279–80.

32. Damen JJM, Ten Cate JM. Silica-induced Precipitation of Calcium Phosphate in the Presence of Inhibitors of Hydroxyapatite Formation. J Dent Res. 1992; 71(3):453–7

33. Bose S, Tarafder S, Banerjee SS, Davies NM, Bandyopadhyay A. Understanding in vivo response and mechanical property variation in MgO, SrO and SiO2 doped β-TCP. Bone. 2011; 48(6):1282–90.

34. Valerio P, Pereira MM, Goes AM, Leite MF. Effects of extracellular calcium concentration on the glutamate release by bioactive glass (BG60S) preincubated osteoblasts. Biomed Mater. 2009; 4(4):045011.

35. Carlisle EM. Silicon: A requirement in bone formation independent of vitamin D1. Calcif Tissue Int. 1981; 33(1):27–34.

36. Zreiqat H, Howlett CR, Zannettino A, Evans P, Schulze-Tanzil G, Knabe C, et al. Mechanisms of magnesium-stimulated adhesion of osteoblastic cells to commonly used orthopaedic implants. J Biomed Mater Res. 2002;62(2):175-84.

37. Yamasaki Y, Yoshida Y, Okazaki M, Shimazu A, Uchida T, Kubo T, et al. Synthesis of functionally graded $MgCO_3$ apatite accelerating osteoblast adhesion. J Biomed Mater Res. 2002;62(1):99-105.

38. Ramaswamy Y, Wu C, Van Hummel A, Combes V, Grau G, Zreiqat H. The responses of osteoblasts, osteoclasts and endothelial cells to zirconium modified calcium-silicate-based ceramic. Biomaterials. 2008;29(33):4392–402.

39. Yamaguchi M. Role of zinc in bone formation and bone resorption. J Trace Elem Exp Med. 1998; 11(2–3):119–35.

40. Marie PJ, Ammann P, Boivin G, Rey C. Mechanisms of action and therapeutic potential of strontium in bone. Calcified Tissue International. 2001;69(3):121-9.

41. Liu X, Ding C, Chu PK. Mechanism of apatite formation on wollastonite coatings in simulated body fluids. Biomaterials. 2004;25(10):1755–61.

42. Saghiri MA, Orangi J, Asatourian A, Gutmann JL, Garcia-Godoy F, Lotfi M, et al. Calcium silicate-based cements and functional impacts of various constituents. Dental Materials Journal. 2017;36(1):8–18.

43. Hench LL. The story of Bioglass®. In: Journal of Materials Science: Materials in Medicine. 2006;17(11):967-78.

44. Xin R, Leng Y, Chen J, Zhang Q. A comparative study of calcium phosphate formation on bioceramics in vitro and in vivo. Biomaterials. 2005; 26(33):6477–86.

45. Bouler JM, Pilet P, Gauthier O, Verron E. Biphasic calcium phosphate ceramics for bone reconstruction: A review of biological response. Acta Biomaterialia. 2017.

46. Valerio P, Pereira MM, Goes AM, Leite MF. The effect of ionic products from

bioactive glass dissolution on osteoblast proliferation and collagen production. Biomaterials. 2004;53:1-12.

47. Wu C, Chang J. A review of bioactive silicate ceramics. Biomedical Materials (Bristol). 2013;8(3):032001.

48. Hench LL, West JK. The Sol-Gel Process. Chem Rev. 1990;90(1):33–72.

49. Meiszterics A, Sinkó K. Sol-gel derived calcium silicate ceramics. Colloids Surfaces A Physicochem Eng Asp. 2008;319(1–3):143–8.

50. Xu C, Nasrollahzadeh M, Selva M, Issaabadi Z, Luque R. Waste-to-wealth: biowaste valorization into valuable bio(nano)materials. Chem Soc Rev. 2019;48:4791-4822.

51. Abu R, Yahya R, Neon S. Production of High Purity Amorphous Silica from Rice Husk. Procedia Chem. 2016;19:189–95.

52. Alshatwi AA, Athinarayanan J, Periasamy VS. Biocompatibility assessment of rice husk-derived biogenic silica nanoparticles for biomedical applications. Mater Sci Eng C. 2015;47:816.

53. Jayasree R, Velkumar J, Sampath Kumar TS. Egg shell derived apatite cement for the treatment of angular periodontal defects: A preliminary clinical and radiographic assessment. Dent Oral Craniofacial Res. 2017;4(2):1-4.

54. Ohshima Y, Takada D, Namai S, Sawai J, Kikuchi M, Hotta M. Antimicrobial Characteristics of Heated Eggshell Powder. Biocontrol Sci. 2015;20(4):239-46.

55. Kohn DH, Sarmadi M, Helman JI, Krebsbach PH. Effects of pH on human bone marrow stromal cells in vitro: Implications for tissue engineering of bone. J Biomed Mater Res. 2002; 60(2):292–9.

56. Johnson JR. Phase Diagrams for Ceramists. Nucl Sci Eng. 1965; 22(2):275–6.

57. Bansal NP. Influence of Several Metal lons on the Gelation Activation Energy of Silicon Tetraethoxide. J Am Ceram Soc. 1990; 73(9):2647–52.

58. Hayashi T, Saito H. Preparation of CaO-SiO_2 glasses by the gel method. J Mater Sci.1980; 15:1971–7.

59. Catauro M, Laudisio G, Costantini A, Fresa R, Branda F. Low Temperature Synthesis, Structure and Bioactivity of $2CaO{\cdot}3SiO_2$ Glass. J Sol-Gel Sci Technol.1997; 10:231–7.

60. Martinez A, Izquierdo-Barba I, Vallet-Regi M. Bioactivity of a CaO - SiO_2 binary glasses system. Chem Mater. 2000; 12(10):3080–8.

61. Salinas AJ, Vallet-Regi M, Izquierdo-Barba I. Biomimetic apatite deposition on calcium silicate gel glasses. J Sol-Gel Sci Technol.2001; 21:13–25.

62. Liu X, Tao S, Ding C. Bioactivity of plasma sprayed dicalcium silicate coatings. Biomaterials. 2002; 23(3):963–8.

63. Sun J, Wei L, Liu X, Li J, Li B, Wang G, et al. Influences of ionic dissolution products of dicalcium silicate coating on osteoblastic proliferation, differentiation and gene expression. Acta Biomater. 2009; 5(4):1284–93.

64. Sun J, Li J, Liu X, Wei L, Wang G, Meng F. Proliferation and gene expression of osteoblasts cultured in DMEM containing the ionic products of dicalcium silicate coating. Biomed Pharmacother. 2009; 63(9):650–7.

65. Gou Z, Chang J. Synthesis and in vitro bioactivity of dicalcium silicate powders. J Eur Ceram Soc. 2004; 24(1):93–9.

66. Gou Z, Chang J, Zhai W, Wang J. Study on the self-setting property and the in vitro bioactivity of β-Ca_2SiO_4. J Biomed Mater Res - Part B Appl Biomater. 2005; 73(2):244–51.

67. Zhao W, Chang J. Sol-gel synthesis and in vitro bioactivity of tricalcium silicate powders. Mater Lett. 2004; 58(19):2350–3.

68. Zhao W, Wang J, Zhai W, Wang Z, Chang J. The self-setting properties and in vitro bioactivity of tricalcium silicate. Biomaterials. 2005; 26(31):6113–21.

69. Sun M, Liu A, Ma C, Shao H, Yu M, Liu Y, et al. Systematic investigation of β-dicalcium silicate-based bone cements in vitro and in vivo in comparison with clinically applied calcium phosphate cement and Bio-Oss®. RSC Adv. 2015; 6(1):586–96.

70. Siriphannon P, Kameshima Y, Yasumori A, Okada K, Hayashi S. Influence of preparation conditions on the microstructure and bioactivity of α-$CaSiO_3$ ceramics: Formation of hydroxyapatite in simulated body fluid. J Biomed Mater Res. 2000; 52(1):30–9.

71. Ni S, Chang J, Chou L. A novel bioactive porous $CaSiO_3$ scaffold for bone tissue engineering. J Biomed Mater Res - Part A. 2006; 76A(1):196–205.

72. Ni S, Chang J, Chou L, Zhai W. Comparison of osteoblast-like cell responses to calcium silicate and tricalcium phosphate creamics in vitro. J Biomed Mater Res - Part B Appl Biomater. 2007; 80(1):174–83.

73. Wang C, Lin K, Chang J, Sun J. Osteogenesis and angiogenesis induced by porous β-$CaSiO_3$/PDLGA composite scaffold via activation of AMPK/ERK1/2 and PI3K/Akt pathways. Biomaterials. 2013; 34(1):64–77.

74. Gao C, Peng S, Feng P, Shuai C. Bone biomaterials and interactions with stem cells. Bone Research. 2017; 5:17059.

75. Lin K, Zhai W, Ni S, Chang J, Zeng Y, Qian W. Study of the mechanical property and in vitro biocompatibility of $CaSiO_3$ ceramics. Ceram Int. 2005; 31(2):323–6.

76. De Aza PN, Luklinska ZB, Martinez A, Anseau MR, Guitian F, De Aza S, et al. Morphological and structural study of pseudowollastonite implants in bone. J Microsc. 2000; 197(1):60–7.

77. Xue W, Liu X, Zheng X Bin, Ding C. In vivo evaluation of plasma-sprayed wollastonite coating. Biomaterials. 2005; 26(17):3455–60.

78. Xu S, Lin K, Wang Z, Chang J, Wang L, Lu J, et al. Reconstruction of calvarial defect of rabbits using porous calcium silicate bioactive ceramics. Biomaterials. 2008;29(17):2588–96.

79. Wu C, Chang J. A novel akermanite bioceramic: Preparation and characteristics. J Biomater Appl. 2006; 21(2):119–29.

80. Huang Y, Jin X, Zhang X, Sun H, Tu J, Tang T, et al. In vitro and in vivo evaluation of akermanite bioceramics for bone regeneration. Biomaterials. 2009; 30(28):5041–8.

81. Xia L, Yin Z, Mao L, Wang X, Liu J, Jiang X, et al. Akermanite bioceramics promote osteogenesis, angiogenesis and suppress osteoclastogenesis for osteoporotic bone regeneration. Sci Rep. 2016; 6(1):22005.

82. Wu C, Chang J, Wang J, Ni S, Zhai W. Preparation and characteristics of a calcium magnesium silicate (bredigite) bioactive ceramic. Biomaterials. 2005; 26(16):2925–31.

83. Chen X, Ou J, Wei Y, Huang Z, Kang Y, Yin G. Effect of MgO contents on the mechanical properties and biological performances of bioceramics in the MgO-CaO-SiO2 system. J Mater Sci Mater Med. 2010; 21:1463-1471.

84. Wu C, Chang J. Degradation, bioactivity, and cytocompatibility of diopside, akermanite, and bredigite ceramics. J Biomed Mater Res - Part B Appl Biomater. 2007; 88(1):153–60.

85. Xie J, Yang X, Shao H, Ye J, He Y, Fu J, et al. Simultaneous mechanical property and biodegradation improvement of wollastonite bioceramic through magnesium dilute doping. J Mech Behav Biomed Mater. 2016; 54:60–71.

86. Li HC, Wang DG, Chen CZ. Effect of zinc oxide and zirconia on structure, degradability and in vitro bioactivity of wollastonite. Ceram Int. 2015;41(8):10160–9.

87. Ramaswamy Y, Wu C, Zhou H, Zreiqat H. Biological response of human bone cells to zinc-modified Ca-Si-based ceramics. Acta Biomater. 2008; 4(5):1487–97.

88. Wu C, Ramaswamy Y, Chang J, Woods J, Chen Y, Zreiqat H. The effect of Zn contents on phase composition, chemical stability and cellular bioactivity in Zn-Ca-Si system ceramics. J Biomed Mater Res - Part B Appl Biomater. 2008; 87B(2):346-353.

89. Wu C. Methods of improving mechanical and biomedical properties of Ca-Si-based ceramics and scaffolds. Expert Rev Med Devices. 2009; 6(3):237-41.

90. Ramaswamy Y, Wu C, Van Hummel A, Combes V, Grau G, Zreiqat H. The responses of osteoblasts, osteoclasts and endothelial cells to zirconium modified calcium-silicate-based ceramic. Biomaterials. 2008; 29(33):4392–402.

Chapter 2

Experimental methods and Characterization

In this chapter, the purification steps of raw materials used are described in detail. The comprehensive description of the conventional sol-gel method and the proposed sol-gel method in the present study are presented. The methodologies of different biological studies such as in vitro bioactivity, cytocompatibility, degradation studies and antimicrobial activity, which will evaluate the performance of prepared material for bone tissue engineering, are described. The detailed explanation of working principle and methodology of apparatus used (XRF, TG-DTA, XRD, SEM-EDS, FTIR, UTM, Microhardness testing and Particle analyzer) are presented.

2.1 Materials

The conventional sol-gel preparation of calcium silicate-based bioceramics requires calcium nitrate tetrahydrate ($Ca(NO_3)_2.\ 4H_2O$) and tetraethyl orthosilicate (TEOS; $Si(OC_2H_5)_4$) as precursor materials for calcium oxide and silica, respectively. They were procured from Sigma Aldrich, India. In the proposed sol-gel method for the present study, rice husk was used as silica source and eggshells were used as calcium oxide source. Rice husk was obtained from a rice mill in Warangal, Telangana, India and the eggshells were collected from NIT Warangal mess. Other precursor materials for dopants such as silver nitrate ($AgNO_3$), zirconium (IV) oxynitrate hydrate ($Zr\ (NO_3)_2.\ x\ H_2O$) and magnesium nitrate hexahydrate ($Mg\ (NO_3)_2.\ 6H_2O$) were also purchased from Sigma Aldrich, India.

Sodium chloride (NaCl), potassium chloride (KCl), sodium bicarbonate ($NaHCO_3$), potassium hydrogen phosphate trihydrate ($K_2HPO_4.3H_2O$), magnesium chloride hexahydrate ($MgCl_2.\ 6H_2O$), calcium chloride ($CaCl_2$), sodium sulphate (Na_2SO_4), Hydrochloric acid (HCl) were procured from Sisco Research Laboratories Pvt. Ltd. (SRL), India.

Dulbecco Modified Eagle's Medium (DMEM; Gibco, 11965092), 3-(4,5-dimethylthiazol-2-yl)-2,5-diphenyltetrazolium bromide (MTT; Himedia, TC191), Nonidet P-40 (NP-40; Sigma, I8896), Fetal bovine serum (FBS; Gibco, 10270106), Phosphate buffered saline (PBS; Gibco, 10010023), Antibiotic-Antimycotic (Gibco, 15240062), Trypsin-EDTA (Gibco, 25200056), Sodium pyruvate (Gibco, 11360070) and Isopropyl alcohol were purchased from Invitrogen, India.

The human osteoblast-like MG-63 cells were procured from National Centre for Cell Science, Pune, India. The expression of different symptoms by these cells facilitates in investigating the osteoblast response on different biomaterials as they originate from osteosarcoma cells.

2.1.1 Rice husk ash (RHA)

Rice husk was first washed with running tap water to remove dirt and water soluble impurities. Then the washed rice husk was treated with 0.5 M concentration of hot hydrochloric acid at ~ 60 °C for half an hour under constant stirring. After removing the acid solution, the rice husk was rinsed with distilled water until it was free from acids. It was first air-dried and later dried in a hot air-oven at 110 °C for 24 h. Consequently, the dried rice husk was placed in muffle furnace and heated at 600 °C for 4 h [1, 2]. Brown residues turned to white in colour, indicating the formation of silica. The rice husk ash obtained was characterized by XRD and XRF and after characterization it was directly used without any further purification.

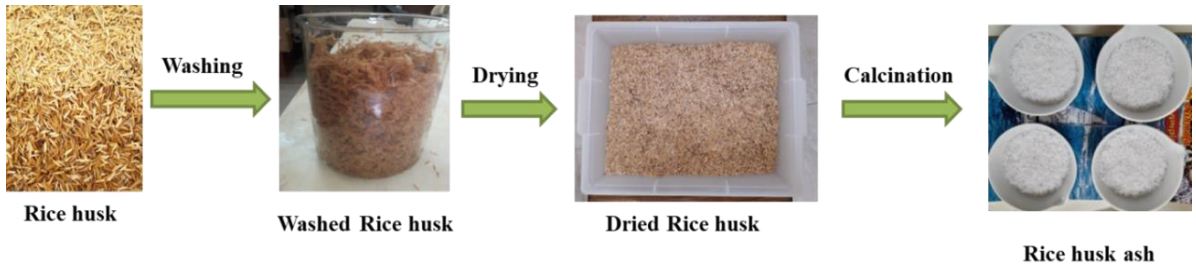

Fig. 2.1 Schematic representation of process used to convert rice husk into silica

2.1.2 Eggshells (ES)

Boiled hen eggshells were collected and the unwanted protein coatings were detached from the shells, rinsed thoroughly using distilled water, and then dried at 120 °C for 2 h. The dried eggshells were ground using mortar and pestle to get fine powder. Subsequently, the ground eggshell powder was placed in a muffle furnace for two step thermal treatment. The first step involved heating it at 450 °C for 2 h at a heating rate of 5 °C / min; at this stage, any organic residue is destroyed and the second step involved heating the mixture at 900 °C for 2 h, but at a heating rate of 0.5 °C / min; at this stage, the eggshell powder is converted into

calcium oxide with the release of carbon dioxide [3]. The calcinated eggshell powder was characterized by XRD and XRF and after characterization it was directly used without any further purification.

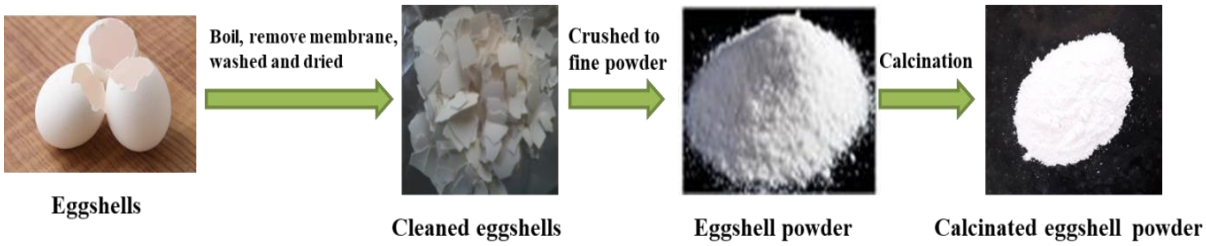

Fig. 2.2 Schematic representation of process used to convert eggshells into calcium oxide

2.2 Preparation techniques

SiO_2 and CaO at a molar ratio 1:1 were synthesized by sol-gel technique using rice husk ash (RHA) as the source of silica and eggshell powder as the source of calcium oxide. Calcium oxide thus obtained from eggshells was dissolved in 2M hydrochloric acid to obtain a clear calcium chloride solution ($CaCl_2$). Sodium silicate solution (Na_2SiO_3) was prepared by boiling the rice husk ash (RHA) at 60 °C for 30 min in 2M sodium hydroxide solution. Sodium silicate solution was then added to calcium chloride solution under constant stirring. A thick white colour solution was obtained which was allowed to age for 3 days at room temperature, followed by washing four to five times with deionised water to eliminate NaCl by-product. The residual liquid was separated by filtration and the filtered sample was then dried at 70 °C for 24 h and at 120 °C for another 6 h. The resultant dried sample was crushed and ground into fine powder. The powder was calcinated at 600 °C for 2 h. The ceramic specimens were prepared to get different dimensions for different characterizations using stainless steel dyes and 5 wt% polyvinyl alcohol (PVA) water solution binders. An appropriate amount of PVA water solution binders was added to the calcinated powder and then the mixture was uniaxially pressed at 200 MPa with manual hydraulic press and compact

blocks were sintered at the desired temperature according to crystallization temperature obtained from TG-DTA analysis.

Later series of ceramic batches were synthesized using trace metal ions such as Ag, Zr and Mg as the dopends at the expense Ca in the above prepared calcium silicate ceramic. The schematic demonstration of the synthesis procedure is shown in fig. 2.3.

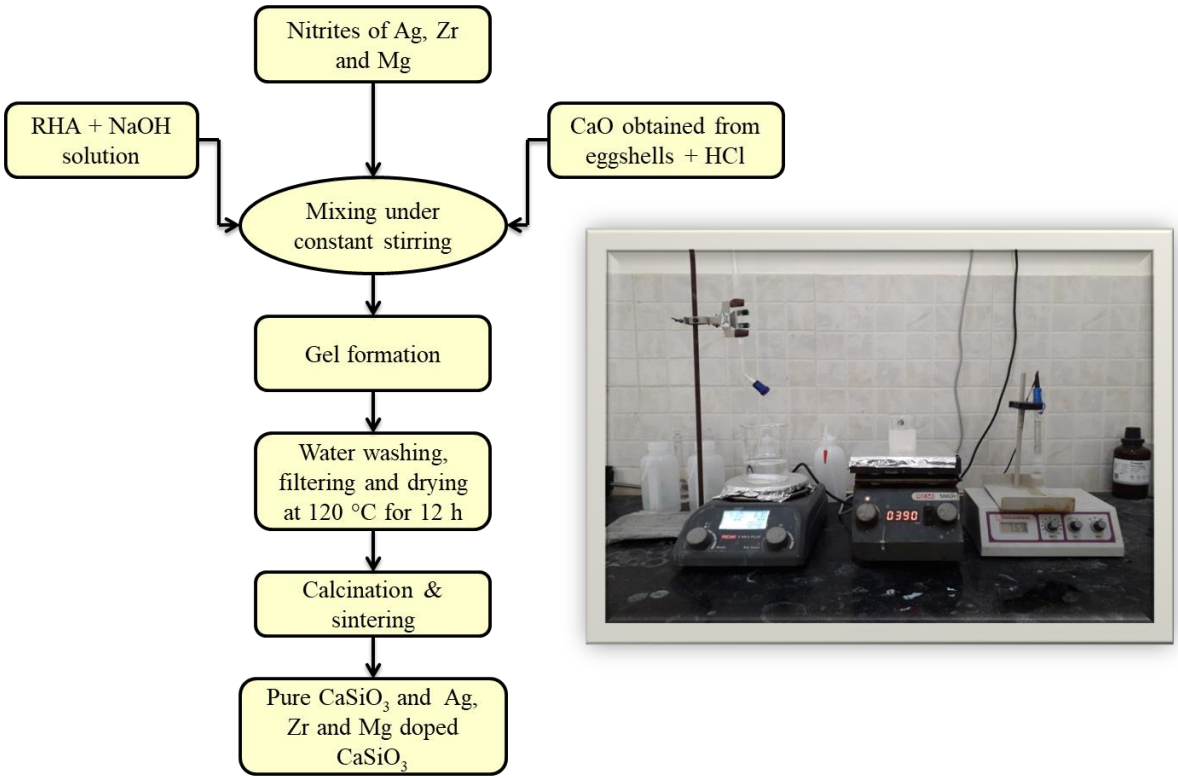

Fig. 2.3 Flow chart and photograph of sol-gel procedure using RHA and eggshells are the source material

SiO_2 and CaO at a molar ratio of 1:1 were also synthesized by conventional sol-gel technique using calcium nitrate tetrahydrate ($Ca(NO_3)_2.\ 4H_2O$) and tetraethyl orthosilicate (TEOS; $Si(OC_2H_5)_4$) as source materials for calcium oxide and silica, respectively for the purpose of comparison. The general process for sol-gel method including hydrolysis and aging was obtained from Ref. [4]. TEOS was mixed with 2 mol/L HNO_3 and absolute ethanol (molar ratio of (HNO_3 + H_2O): TEOS: ethanol = 10:1:10), after 1 hour of stirring, the

necessary quantity of Ca $(NO_3)_2 \cdot 4H_2O$ was added to the resulting mixture and stirring was continued for 1 hour. After that, the sol solution was kept at 60 °C for 1 day in a sealed container for aging followed by drying at 120 °C for 24 h. Calcium silicates were obtained by sintering at the desired temperature according to crystallization temperature obtained from TG-DTA analysis.

2.3 Material characterization techniques

2.3.1 X-Ray fluorescence spectroscopy (XRF)

Energy Dispersive X-ray Fluorescence spectroscopy (XRF) is a non-destructive method for determining the elemental composition of sample materials, both quantitatively and qualitatively. The schematic diagram of XRF is shown in Fig. 2.4. When matter is excited by primary X-radiation, the inner shell electrons are knocked out and the outer shell electrons fill the resulting voids by releasing fluorescent radiation which is characteristic of the energy distribution in a particular material. The detector detects the energy distribution of fluorescent radiation and then produces characteristic measurement signals for chemical elements in the sample.

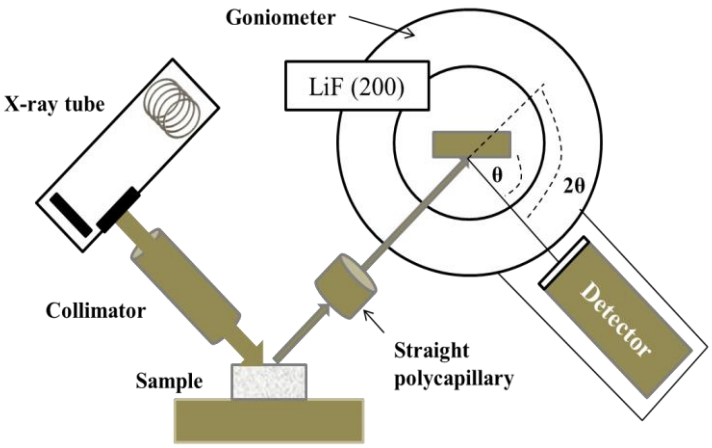

Fig. 2.4 Schematic diagram of X-ray fluorescence (XRF) spectroscopy

The purity of silica produced in rice husk and the purity of CaO produced in eggshells were estimated by wavelength dispersive X-ray fluorescence (XRF) spectrometer (Rigaku ZSX primus) (Fig. 2.5). The analysis was performed at ambient condition along with P-10 gas (Ar 90%, CH_4 10 %) for the flow proportional counter (F-PC).

Fig. 2.5 X-ray fluorescence spectrometer (Rigaku ZSX primus)

2.3.2 Thermo gravimetric and differential thermal analysis (TG-DTA)

Thermal property analysis of all the prepared bioceramics were studied using TG-DTA instrument. Fig. 2.6 shows the schematic representation of TG-DTA experimental setup. It is a simultaneous thermal analyzer that can characterize multiple thermal properties of a specimen in a single experiment. The TG measures the mass changes and the corresponding temperatures associated with dehydration, decomposition, oxidation and desorption that occurs in the sample. The DTA measures the temperature difference between an inert reference and a sample material during a

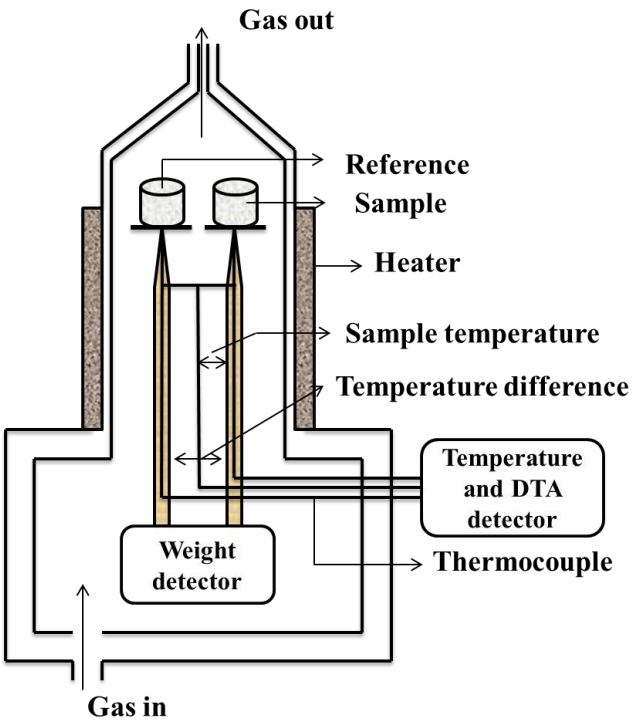

Fig. 2.6 Black diagram of thermo gravimetric and differential thermal analysis (TG-DTA)

programmed change of temperature. If the temperature of the sample lags behind that of the reference material, endothermic curve is observed and if the temperature of the sample exceeds that of the reference material, exothermic curve is observed. The glass transition temperature (T_g), onset crystallization temperature (T_x), peak crystallization temperature (T_c) and melting temperature (T_m) can be found using the outline of exothermic and endothermic peaks in DTA curve. The temperature difference should be zero until a thermal event such as decomposition, melting, crystallization or glass transition occurs.

STA 2500 Regulus (Model: NETZSCH, Germany) simultaneous Thermogravimetric Analysis (TGA) and Differential Thermal Analysis (DTA) (Fig. 2.7) were used to study the thermal behavior of dried gels under argon atmosphere from room temperature to 1200 °C at a heating rate of 10 °C/min.

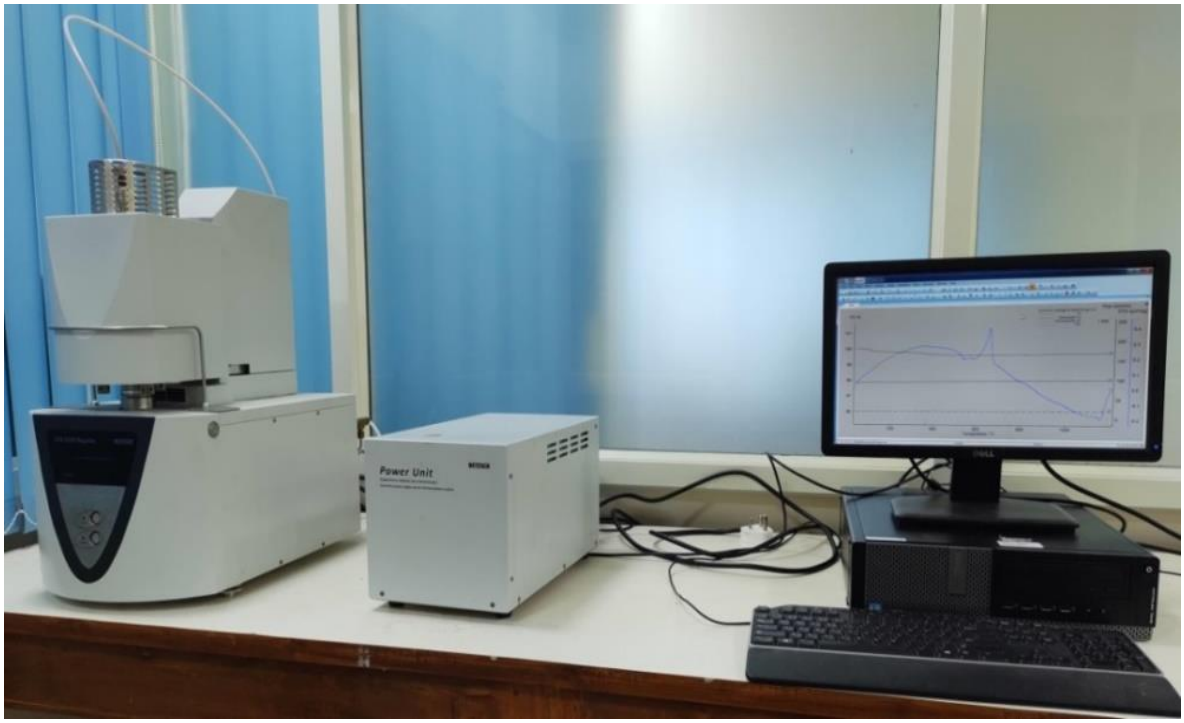

Fig. 2.7 Thermogravimetric and differential thermal analyzer (NETZSCH)

2.3.3 X-ray diffraction (XRD)

X-ray diffraction (XRD) is a rapid non-destructive technique that detects the phase of a material and also provides information about crystalline sizes based on Bragg's law ($n\lambda = 2d \sin\theta$). Fig. 2.8 shows the schematic representation of XRD experimental setup. A monochromatic beam of X-rays is made incident on the sample surface, and the reflected X-rays are detected by a detector. The XRD peak spectrum is generated by the constructive interference of a monochromatic beam of X-rays scattered at specific angles from each lattice plane in a sample. The atomic position in the lattice planes determines the intensities of the peaks. Therefore, the XRD peak pattern is a characteristic of periodic atomic arrangements in the sample material. Standard database for X-ray powder diffraction patterns provides quick identification of a large variety of crystalline materials.

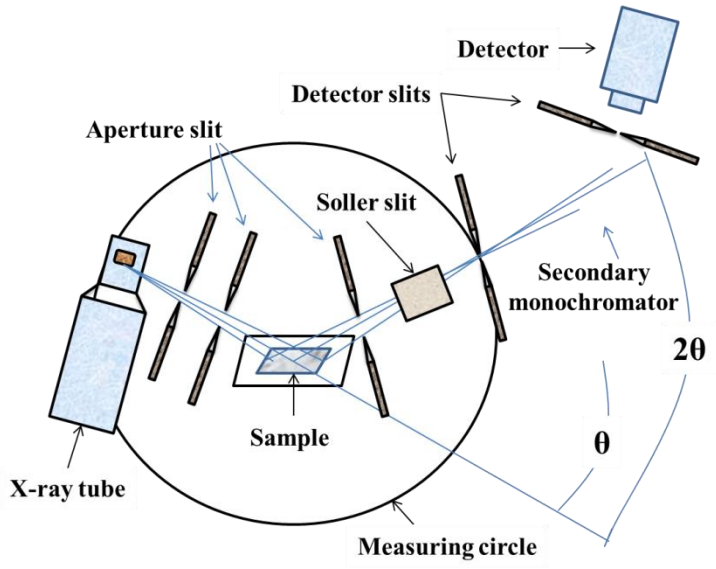

Fig. 2.8 Schematic representation of X-ray diffraction (XRD) apparatus

The phase identification of all the prepared samples was assessed using powder X-ray diffractometer (Model: PANALYTICAL XPERT POWDER, UK) (Fig. 2.9) before and after immersion in SBF solution using Cu Kα radiation source in the 2θ scan range between 10 to 80°. During measurement, the step size was 0.02° and the time per step was 50 s.

Fig. 2.9 X-ray diffractometer (PANALYTICAL)

2.3.4 Fourier transforms infrared (FTIR) spectroscopy

Fourier transform infrared (FTIR) spectroscopy is a technique used to obtain transmission or absorption spectrum by translating the raw data (interferogram) using a mathematical process (Fourier transform). The method is based on the fact that the atoms in a molecule vibrate relative to each other with frequencies that correspond to infrared-wavelength light, and hence can be easily excited with such a radiation. When the molecule is irradiated by infrared light of various wavelengths, if the photon energy matches with the energy quantum needed to increase a molecular vibration one level up, it will be absorbed by

the molecule, and photons of other energies will pass through molecule. By measuring the transmitted light intensity for a broad range of wavelengths, it is possible to obtain a spectrum.

The schematic diagram of FTIR spectrometer is shown in Fig. 2.10. A beam of infrared light of different wavelengths is sent through a beam splitter, half of which is made incident on a fixed mirror and another half on a mirror moving at a constant velocity. The two split beams are then reflected back and incident on the beam splitter but with a path difference between them. Depending on the path difference between the reflected beams, an interference pattern is generated. The interference pattern (or interferogram) is sent to the sample, and the transmitted portion of the interferogram is sent to a detector. After comparison with a reference sample beam spectrum in the detector, a Fourier transform is performed to obtain the full spectrum as a function of wavenumber.

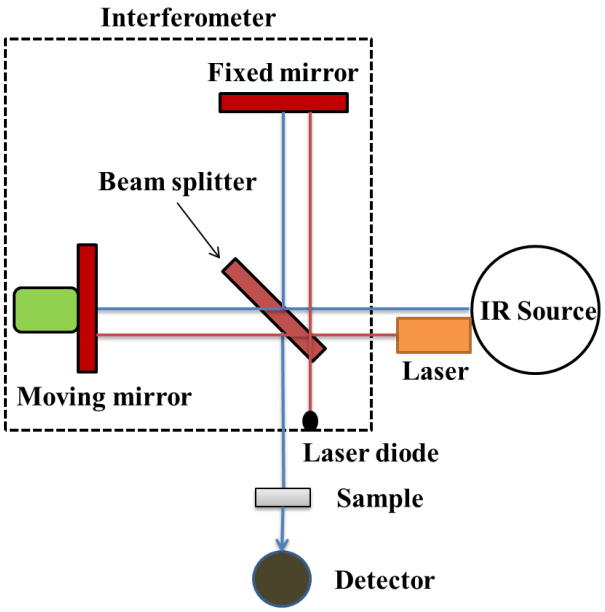

Fig. 2.10 Schematic diagram of Fourier transform infrared (FTIR) spectroscopy

The infrared spectra of all the samples before and after *in vitro* test were obtained by KBr pelleted samples using Fourier transform infrared (FTIR) spectrometer (model: ALPHA II; Bruker, Germany) (Fig. 2.11) in the range of 400–4000 cm^{-1} with a transmission mode and 4 cm^{-1} resolution.

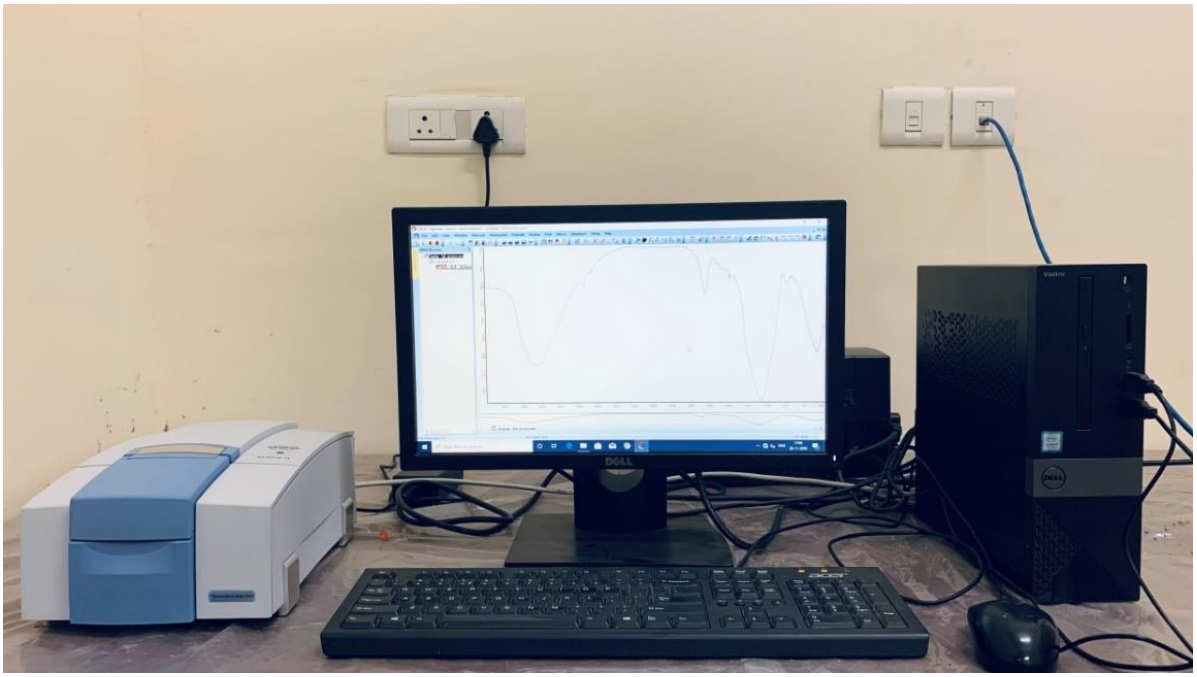

Fig. 2.11 Fourier transforms infrared spectrometer (ALPHA II; Bruker)

2.3.5 Scanning electron microscope-energy dispersive spectroscopy (SEM-EDS)

The scanning electron microscope (SEM) is a type of microscope that can produce high-resolution images of the sample surface. The principle of the electron microscope is similar to that of an optical microscope, but instead of using visible light, it uses high-energy electrons as a light source. The resolution of an optical microscope is limited by its wavelength, whereas the wavelength of electrons in an electron microscope varies with the applied voltage (2.1).

$$\lambda = \frac{1.5}{\sqrt{V}}\, nm \qquad (2.1)$$

The short wavelength electrons produced by the electron gun provide an opportunity to see the atomic structures of the specimens. The schematic diagram of the SEM is shown in Fig. 2.12. Electrons emitted from an electron gun are accelerated with an accelerating voltage of V_0. The electrons in the high vacuum column, called the primary electrons, are focused

through the electronic lens to produce a narrow scan beam that bombards the object, resulting in secondary electrons being emitted from each point on the object. The angle and velocity of the secondary electrons relates to the microstructure of the object. A detector detects the secondary electrons and produces an electronic signal that can be amplified and transformed into a digital image.

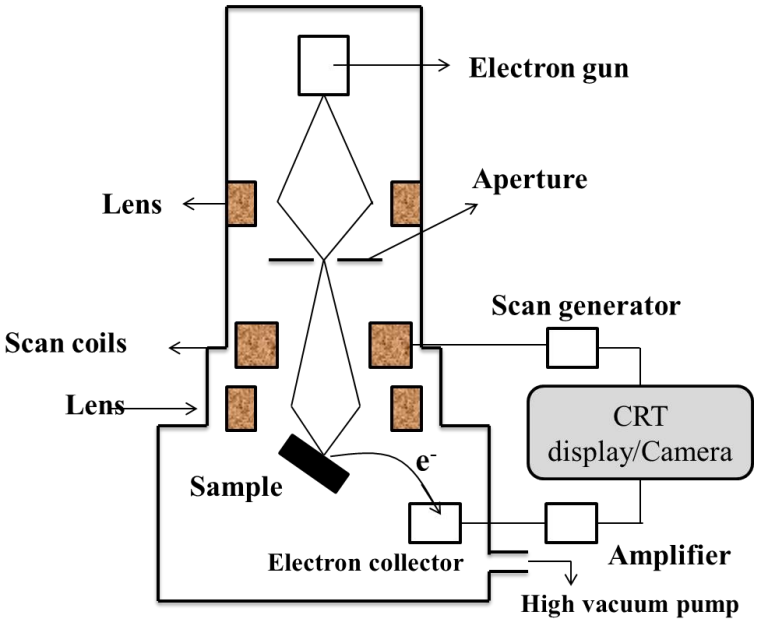

Fig. 2.12 Schematic diagram of SEM

The resolution of any microscope is determined by the spot size on the surface of the sample, quality of lenses and performance of the electron gun. The sharpness and visibility of an image depends on electron probe current (i_p), electron probe size (d_p), electron probe convergence angle (α_p) and electron beam accelerating voltage (V_0). Brightness (β) also depends on the above four parameters and is defined as the beam current area per unit of solid angle. The smaller the spot size, the higher the brightness.

When atoms in the material are ionized by high energy radiation, they emit characteristic X-rays. EDS is an acronym describing a technique of X-ray spectroscopy that is based on the collection and energy dispersion of characteristic X-rays. EDS system consists of a source of high energy radiation, usually electrons; a sample; a solid state detector, usually made from a lithium-drifted silicon, Si (Li); and a signal processing electronics. EDS spectrometers are most frequently attached to the electron column instruments. X-rays that enter Si (Li) detector are converted into an X-ray energy histogram. This X-ray spectrum consists of a series of peaks representing the type and relative amount of each element in the

sample. The number of column in each peak may be further converted into elemental weight concentration either by comparison with standards or using standardless calculations.

The structural morphologies and elemental evaluation of gold sputter-coated bioceramics and the formation of hydroxyapatite crystals after soaking them in SBF solution were analyzed using SEM jointly equipped with EDS. The analysis was performed on 5WEGA 3 LMU; TESCAN, UK model microscope (Fig. 2.13) using a beam energy of 15.0 kV and a working distance of 10 mm.

Fig. 2.13 SEM-EDS (5WEGA 3 LMU; TESCAN)

2.3.6 Microhardness testing

Microhardness testing is a technique for determining the hardness of a specimen by means of a pyramid-shaped diamond indenter. The microhardness test can measure core hardness from the surface on carburized or case-hardened parts as well as surface conditions such as carburization and grinding burns. Vickers hardness test was used to determine the hardness of the sintered samples by Matsuzawa (Via – S) micro hardness tester. A load (P) of

100 g on each sample was applied for a fixed residence time of 15 seconds, leaving a square-shaped indentation on the surface of the tested specimen (Fig. 2.14). The average diagonal length of the indentation (d) was calculated by fixing it optically using a microscope equipped with an instrument. The hardness (Hv) values for sintered samples were calculated using equation 2.2. The indentation fracture toughness (K_{IC}) was estimated using equation 2.3 with an applied load of 4.9 N. The average values were obtained by taking five measurements at different locations on the samples. Matsuzawa (Via – S) micro hardness tester is showed in Fig. 2.15

$$\text{Hv} = \frac{1.854\,P}{d^2}\,(\text{N/m}^2) \tag{2.2}$$

$$K_{IC} = 0.0824 \times \left(\frac{P}{C^{3/2}}\right) \tag{2.3}$$

Where Hv is the microhardness, d the average diagonal length of the indentation, K_{IC} the fracture toughness (MPa $m^{1/2}$), C the radial crack length and P is the applied indenter load.

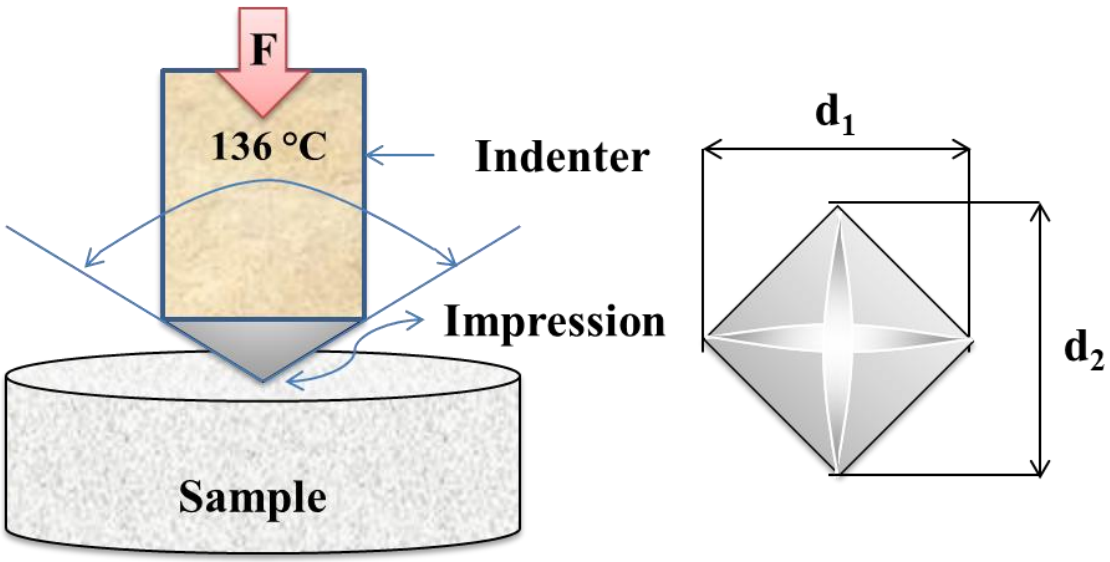

Fig. 2.14 Schematic representation of Vickers hardness test

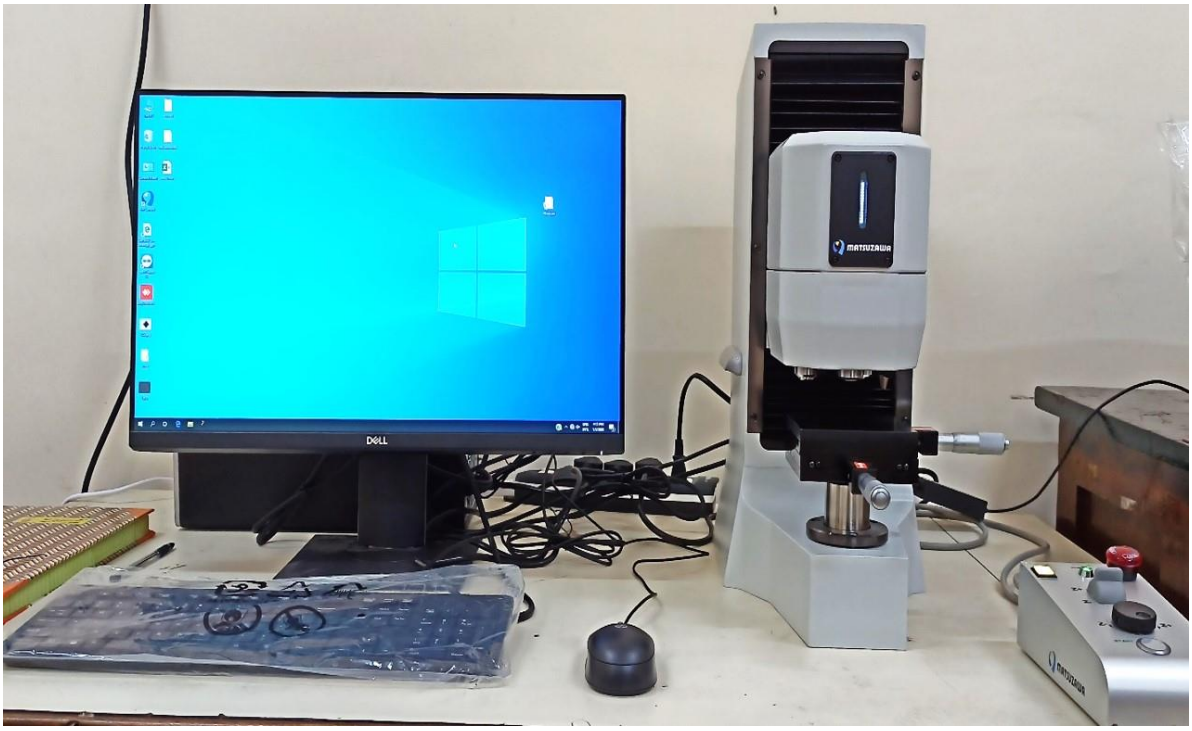

Fig. 2.15 Micro hardness tester (Matsuzawa (Via – S))

2.3.7 Universal testing machine (UTM)

The universal testing machine (UTM) is used to determine the mechanical properties such as compression, tension, flexural, friction, etc. of a given test sample by applying compressive, tensile, or transverse stresses. The machine is so named because it can perform extensive tests on a wide variety of materials. Fig.2.16 shows the schematic diagram of the universal testing machine (a) under compression mode and (b) under three point bending mode. The compressive mechanical analysis of prepared ceramics (n=3; Ø 8 mm × 12 mm) was measured using universal testing machine (Model: WDW-1000S). The compressive strength was obtained by applying a load cell of 5 kN at a crosshead of 0.5 mm min^{-1} until the ceramic structures reported failure. Elasticity modulus and bending strength of ceramic bars (n=3; 38 mm × 3 mm × 4mm) were studied by employing three-point bending technique using universal testing machine with a 0.5 mm min^{-1} crosshead speed and a sample span of

30 mm. The test outcomes were calculated as per equations 2.4 and 2.5. WDW-1000S universal testing machine was showed in Fig. 2.17

$$\sigma_f = \frac{3PL}{2bh^2} \tag{2.4}$$

$$E = \frac{L^3(P_2 - P_1)}{4bh^3(Y_2 - Y_1)} \times 10^{-3} \tag{2.5}$$

Where E is modulus of elasticity (GPa), σ_f bending strength (MPa), P fracture load, b sample width (mm), h sample height (mm) and L length of the support span (mm).

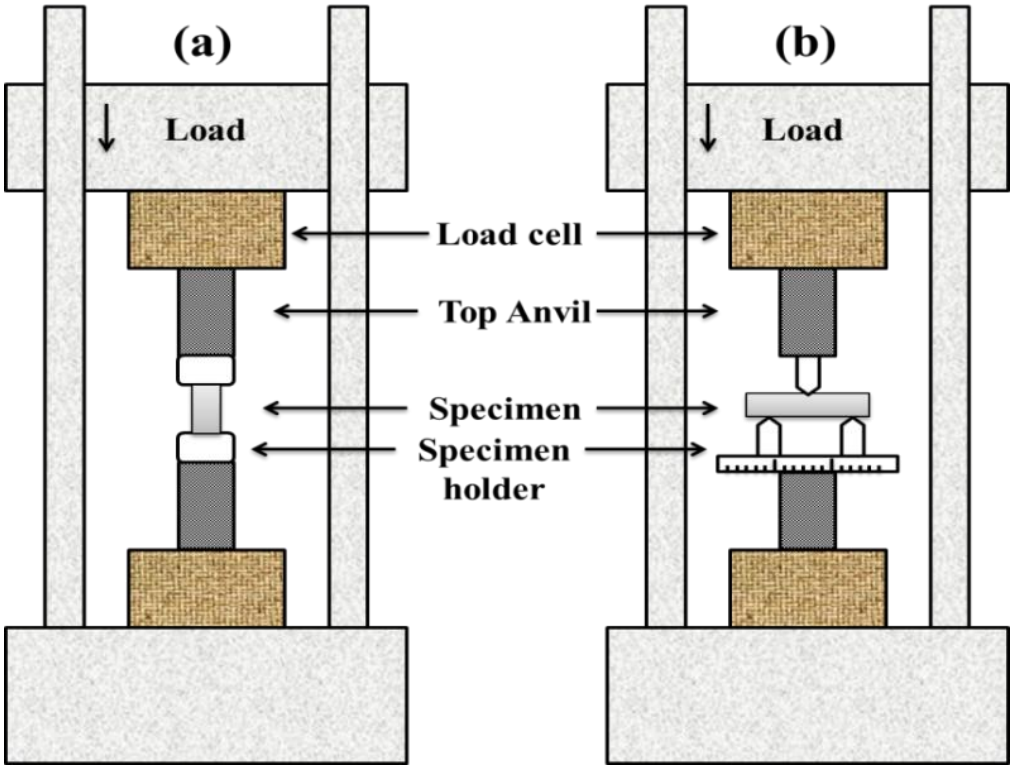

Fig. 2.16 Schematic diagram of universal testing machine compression mode (a) and bending mode (b)

Fig. 2.17 Universal testing machine (WDW-1000S)

2.4 Biological studies

2.4.1 In vitro bioactivity evaluation

The International Organization for Standardization (ISO 10993-14) has approved the use of simulated body fluid (SBF) as a preliminary test to assess the *in vitro* bioactivity of materials. SBF solution mimics human extracellular fluid in terms of ion concentrations and pH. SBF solution was prepared as per a well-established procedure by Kokubo and his colleagues [5, 6]. Fig. 2.18 shows the schematic representation of SBF solution preparation. In brief, all the bottles, beakers etc. were immersed in diluted HCl for several hours and after

that removed from solution and washed with ultra-purified water and the mouths covered with wrapping film. 750 ml of double deionized water was taken into 1000 ml of torsion beaker and covered with aluminium foil. The temperature of the water in the beaker was maintained at 37 °C by placing it in a water bath on a magnetic stirrer. The

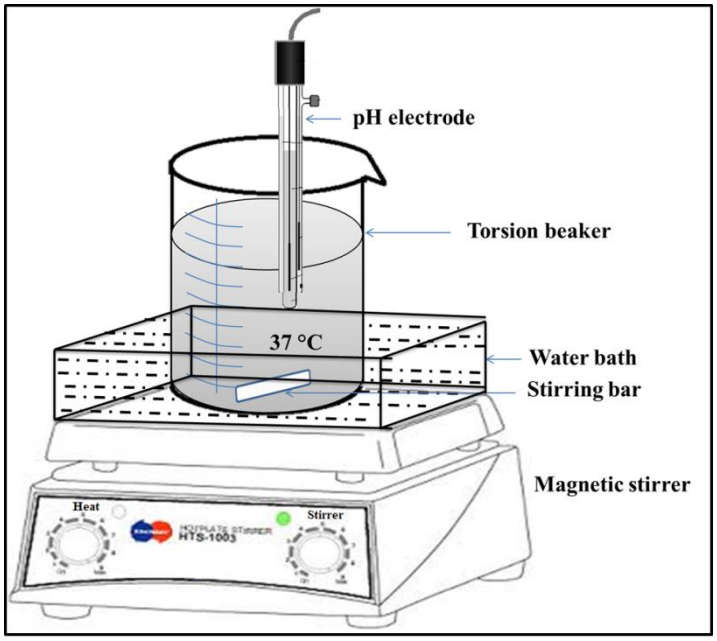

Fig. 2.18 Preparation of SBF solution

first eight reagents given in Table 2.1 were dissolved in the solution one by one in the same order mentioned in the table and after dissolving, the pH electrode was inserted into the solution, with a pH value between 2.0 ± 1.0. Now the 9th reagent i.e. Tris was added into the solution little by little taking careful note of the pH variation. Tris was stopped being added into the solution when the pH of the solution reached 7.5. The remaining Tris and 1M HCl were added alternately into the solution keeping the pH within the range of 7.42 - 7.45. The final pH of the solution was adjusted to 7.4 exactly at 37 °C. Further, deionized water was added to the solution to adjust the total volume of the solution to 1000 ml.

Table 2.1 Order and amounts of reagents for preparation of 1000 ml of SBF solution

Order	**Reagent**	**Amount**
1	NaCl	8.035 g
2	$NaHCO_3$	0.355 g
3	KCl	0.225 g
4	$K_2H\ PO_4.\ 3H_2O$	0.231 g
5	$MgCl_2.\ 6H_2O$	0.311 g
6	1 M HCl	39 ml

7	$CaCl_2$	0.292 g
8	Na_2SO_4	0.072 g
9	Tris	6.118 g
10	1 M HCl	0 – 5 ml

To emphasize the potential of apatite layer formation rate of the prepared bioceramics, the ceramic specimens (Ø 10 mm × 3 mm) were soaked in SBF solution and incubated at 37 °C for various time periods such as 3, 7, 14 and 21 days (Fig. 2.19). The assessment was performed under static condition to monitor pH values over immersion time. The difference in pH level of SBF solution for the period of soaking was recorded every day. After the soaking process in SBF solution, the samples were collected, cleaned with deionised water, and dried. The changes in chemical composition of surface and microstructural properties were examined by XRD, SEM-EDS and FTIR analysis.

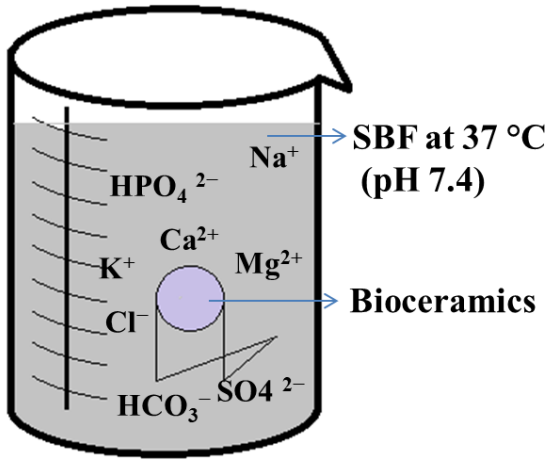

Fig. 2.19 A specimen in the SBF

2.4.2 In vitro degradation evaluation

The degradation behaviour of prepared ceramic specimens was studied using Tris-(hydroxymethyl)-aminomethane and hydrochloric acid (Tris-HCl) solution according to ISO 10993-14 standard. Tris-HCl buffer solution was used to study the degradation behaviour because it does not contain ions, thus confirming maximum solubility and minimum reprecipitation activity of material [7]. 0.05 M concentration of Tris-HCl was prepared by dissolving pure Tris in deionised water under constant stirring while monitoring the pH of the solution. The final pH of the solution was adjusted to 7.4 using 1 M HCl solution. The

sintered ceramic specimens (10 mm diameter × 3 mm thickness) were immersed in Tris-HCl buffer solution by maintaining the surface area of the sample to volume of the solution ratio as 1:10 and incubated at 37 °C for different time periods like 1, 3, 7, 14 and 21 days. Tris-HCl buffer solution was exchanged with fresh solution every 3 days. At the end of each immersion time, the samples were collected from the solution and thoroughly cleaned with deionised water and then dried at 95 °C for 3 h. The change in weight loss was measured based on initial weight. The rate of degradation was calculated using equation 2.6. The test was performed in triplicate and the relative weight loss percentage was determined with respect to soaking time.

$$\text{Weight loss\%} = \frac{W_i - W_f}{W_i} \times 100 \qquad (2.6)$$

Where W_i is the initial weight and W_f is the final weight of the sample

2.4.3 Cytotoxicity and cell proliferation studies

Cytotoxicity was assessed using MTT [3-(4,5-dimethylthiazol-2-yl)-2,5-diphenyltetrazoliumbromide] assay, a standard assay for testing the cytotoxicity of materials and performed according to ISO 10993-5:1999 standard [8]. The MTT colorimetric assay is based on the transformation of a yellow tetrazolium salt to purple formazan crystals with live cells. Viable cells contain NAD (P) H-based oxidoreductase enzymes that transform MTT to formazan. Insoluble formazan crystals are dissolved using a solvent solution and the resulting color solution absorption is calculated using a multi-well spectrophotometer. The darker the purple colored solution, the greater number of viable cells (Fig. 2.20).

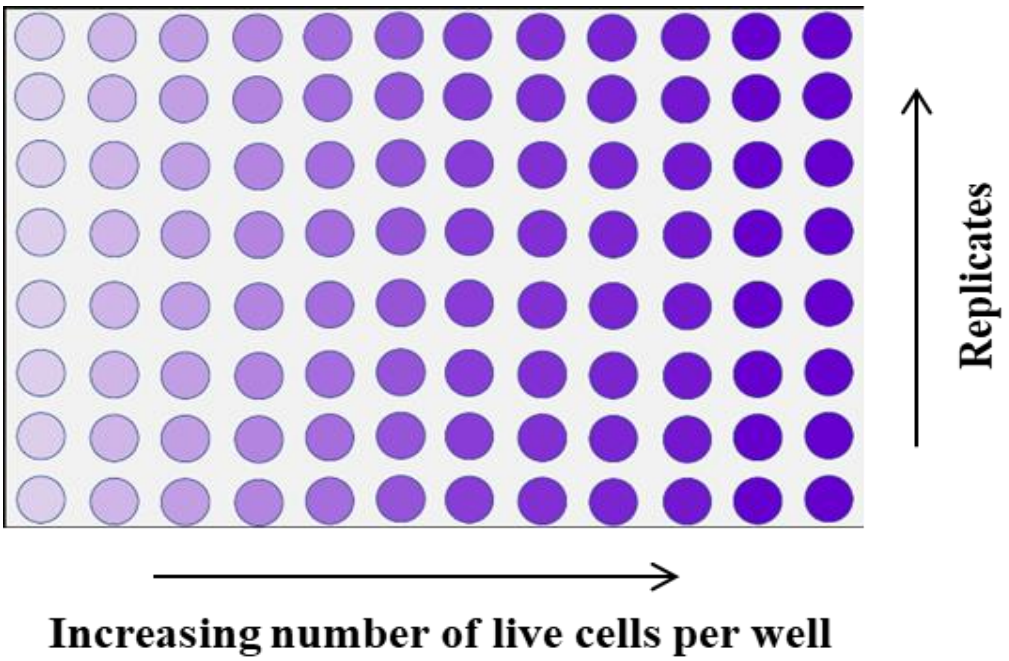

Fig. 2.20 Metabolism of MTT to a formazan salt by viable cells in 96 wells plate

Human osteosarcoma cells (MG-63 cells) were used to examine the cytotoxicity and cell proliferation ability of prepared bioceramics. Dulbecco Modified Eagle's Medium (DMEM) supplemented with 10% fetal bovine serum (FBS) was added to MG-63 cells and stored in humidified air with 5% CO_2 incubator at 37 °C. After that, the cells were detached from the vessel using a proteolytic enzyme known as trypsin. Trypsin cleaves peptide chains mainly at the end of carboxyl group of the amino acids such as Lysine and Arginine, when it is not accompanied by Proline in the cells. Consequently, it dissociates the adherent cells from the vessel in which they are being cultured for further treatment. The density of cell suspension was adjusted to 5×10^4/ml. 100 µL of cell suspension was seeded into each well of culture plate of 96 wells and incubated in humidified atmosphere at 37 °C for 24 hours to allow the cells to attach to the wells. Different concentrations of dilution extracts (50, 100, 200, 500 and 1000 µg/mL) of ceramics were prepared by adding ceramic particles to DMEM with 10% FBS. The 96 wells plate was divided into experimental groups. Sample extracts were added to experimental group to replace the original culture medium, and this was

incubated at 37 °C for 48 hours in humidified atmosphere. After 48 hours, 20µL (5 mg/mL) MTT reagent was added to the culture wells. After 4 hours of incubation, the culture medium with MTT of all wells was removed and then 100 µL of acidified isopropanol was added to each well followed by incubation for half an hour to solubilize the formazan crystals. The optical density (OD) values of each well were measured photometrically at 570 nm using a micro plate reader. Three test results were achieved for each concentration. % of cell viability was calculated using the equation 2.7.

$$\%Cell\ Viability\ = \frac{[OD]test}{[OD]control} \times 100 \qquad (2.7)$$

The effect of ionic dissolution of prepared bioceramics on osteoblast-like MG-63 cell proliferation was studied for a prolonged time period up to 7 days. We monitored similar procedure for proliferation assay. The diluted extracts were added to 96 wells plate containing 5×10^3 cells/well and incubated at 37 °C for 1, 3, 5 and 7 days. The absorbance was measured at the end of each incubation period.

2.4.4 Antimicrobial activity test

The antimicrobial activity of prepared bioceramics was determined by disc diffusion method against bacterial microbes such as *Staphylococcus aureus (S. aureus)* and *Escherichia coli (E. coli)* because *S. aureus* and *E. coli* are two main possible sources of infection in wounds. The growth of pathogens was carried out in nutrient agar medium. The gently warmed molten nutrient agar medium was poured into sterilized petri dishes. Hundred microliters of the bacterial culture were dispersed on the agar plates and after dispersion, the ceramic discs of 10 mm diameter were positioned in the agar plates. The plates were incubated at 37 °C for 24 h. Antibacterial activity was assessed by determining the diameter of the inhibition zone against bacteria after the incubation period.

2.5 Statistical analysis

All the data were expressed as mean ± standard deviation. One-way ANOVA tests were used to compare the data between the samples. All tests were performed using origin 8.5 software and in all cases, the results were considered statistically significant with a p-value of less than 0.05.

2.6 References

1. Abu R, Yahya R, Neon S. Production of High Purity Amorphous Silica from Rice Husk. Procedia Chem. 2016;19:189–95.
2. Nayak JP, Bera J. Preparation of silica aerogel by ambient pressure drying process using rice husk ash as raw material. Trans Indian Ceram Soc. 2009;68(2):91–4.
3. Ho WF, Hsu HC, Hsu SK, Hung CW, Wu SC. Calcium phosphate bioceramics synthesized from eggshell powders through a solid state reaction. Ceram Int. 2013;39(6):6467–73.
4. Ding S-J, Shie M-Y, Wang C-Y. Novel fast-setting calcium silicate bone cements with high bioactivity and enhanced osteogenesis in vitro. J Mater Chem. 2009;19(8):1183.
5. Kokubo T, Takadama H. How useful is SBF in predicting in vivo bone bioactivity? Biomaterials. 2006;27: 2907–15.
6. Kokubo T, Kushitani H, Sakka S, Kitsugi T, Yamamuro T. Solutions able to reproduce in vivo surface-structure changes in bioactive glass-ceramic A-W3. J Biomed Mater Res. 1990; 24(6):721-34.
7. EN-ISO-10993-14. Biological evaluation of medical devices - Part 14: Identification and quantification of degradation products from ceramics. ISO 10993-142001. 2001.
8. International Organization for Standardization. Biological evaluation of medical devices - Part 5: Tests for in vitro cytotoxicity. Iso 10993–5. 2009.

Chapter 3

In vitro biological and degradation behaviour of wollastonite derived from bio-waste

In this chapter, initially, the preparation of β-wollastonite using bio-waste such as rice husk ash (RHA) and eggshells as sources of silica and calcium oxide through sol-gel method has been discussed. The required optimum calcination and sintering temperatures to achieve pure phase of β-wollastonite have been described using thermal analysis. In vitro apatite forming ability, degradation behaviour, cytocompatibility and mechanical properties of synthesized wollastonite have been discussed.

3.1 Introduction

Wollastonite is the most extensively studied calcium silicate ceramic. It has a wide combination of properties such as thermal stability, low thermal conductivity, corrosion resistance, chemical inertness and low dielectric constant [1, 2]. Wollastonite is used in ceramics to reduce the baking temperature and duration, as filling agent in rubber, paper and plastic, as milking agent in paint, bonding agents for abrasives, and metallurgical applications [3, 4]. Wollastonite is a polymeric substance existing in two mineral forms: low temperature form; where β-wollastonite crystallizes in a chain silicate and high temperature form; where α-wollastonite crystallizes in a triclinic lattice [5].

Wollastonite has been studied for being a promising bone implantable material because of its advanced bio-functionalities, excellent bioactivity and biocompatibility [6-10] The presence of Ca and Si ions in wollastonite shows its important role in the formation of hydroxyapatite layer, affects mineralization process and plays a role in bone bonding mechanism [11, 12]. The ionic products released from calcium silicate ceramics could promote gene expression and improve the efficiency of insulin-like growth factor (IGF), which is especially related to cell proliferation. Wollastonite ceramic shows better performance in terms of mechanical properties such as higher bending strength and fracture toughness when compared with calcium phosphate and Hydroxyapatite (HA) [13, 14]. However, the relatively high dissolution rate of wollastonite, which accounts for higher pH level in the surrounding environment, has a limit on its clinical applications. The problem can be solved by emerging multiphase materials comprising highly dissolvable phases [15].

Different methods went into the preparation of wollastonite: solid phase reaction [16, 17], co-precipitation [18], sol-gel method [19], hydrothermal method [20], microwave synthesis [21] and solution combusting method [22]. Synthesis technique plays an important

role in biomedical application of wollastonite. Sol-gel derived wollastonite exhibit unique surface chemistry and higher bioactivity [23–26]. In sol-gel process, metal alkoxides like tetraethylorthosilicate (TEOS) and tetramethylorthosilicate (TMOS) were used as silica precursor and calcium nitrate tetra hydrate ($Ca(NO_3)_2.4H_2O$) was used as calcium oxide precursor. However, these precursors are expensive. The present work provides an environmentally beneficial and cost-free production of wollastonite by using rice husk ash (RHA) and eggshells which form source materials for silica and calcium oxide respectively.

The aim of the present work is to synthesize wollastonite ceramic using RHA and eggshells by sol-gel method. *In vitro* bioactivity, degradation and cytocompatibility were investigated to analyse its potential application as a bone implant material.

3.2 Results and discussion

3.2.1 Raw materials characterization

XRD patterns of raw eggshell powder, extracted CaO and SiO_2 are showed in Fig. 3.1 (a & b). Raw eggshells powder primarily composed of calcite ($CaCO_3$) whereas the eggshells powder calcined at 900 °C for 2 hours showed the formation of cubic phase in accordance with JCPDS No. 82-1690 in terms of CaO. Rice husk ash calcinated at 600 °C for 4 hours showed the broad diffused peak with maximum intensity at $2\theta = 22°$, indicating amorphous nature of silica [27]. XRF was used to determine the chemical composition and purity of raw materials. The weight percentages of the oxides are presented in detail in Tables 3.1 for RHA and calcinated eggshell powder. The high purity of about 99.17% for SiO_2 was observed in RHA using XRF analysis. The excess purity of the extracted silica is likely due to the hydrochloric acid leaching and determination of optimum temperature as suggested by Rohani Abu Bakara et al. [27]. Moreover, very low amounts of other metallic impurities were

measured. The obvious 98.47% purity was obtained for CaO produced in calcinated eggshell powder using XRF analysis.

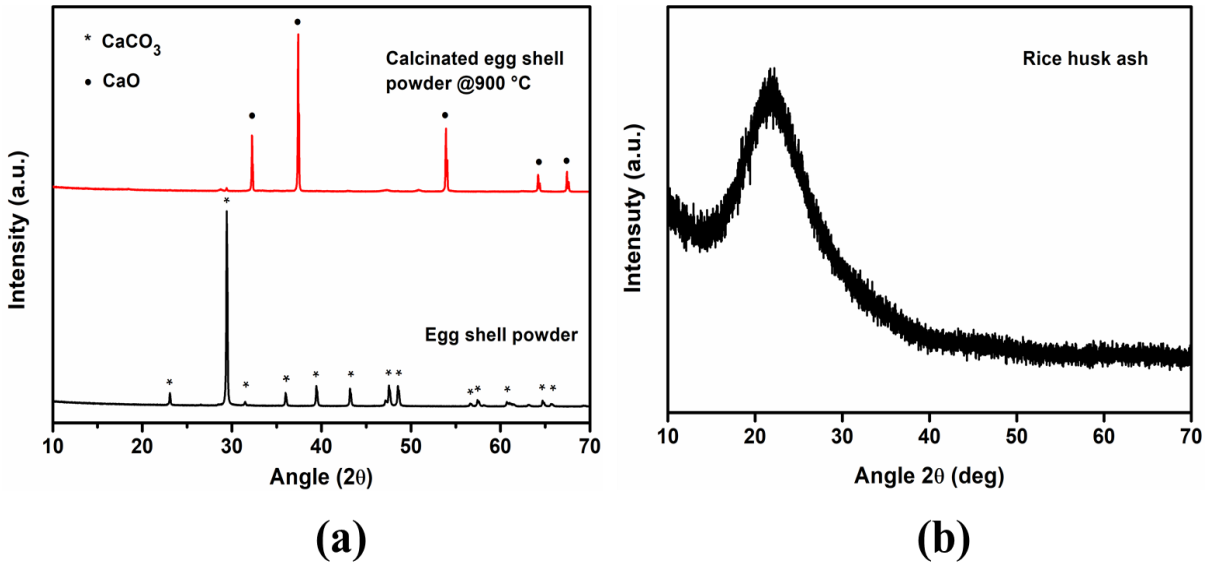

Fig. 3.1 XRD patterns of (a) raw eggshells powder, calcinated eggshells powder at 900 °C and (b) calcinated rice hush at 600 °C

Table 3.1 Rice husk ash and calcinated eggshells oxidic composition measured by XRF

Rice husk ash (RHA)	
Oxide	Weight %
SiO_2	99.172
MgO	0.087
Al_2O_3	0.175
P_2O_5	0.106
SO_3	0.052
K_2O	0.043
CaO	0.172
Fe_2O_3	0.072
ZnO	0.011
Cl	0.057

Calcinated eggshell powder	
Oxide	Weight %
CaO	98.473
MgO	0.821
Al_2O_3	0.132
CuO	0.024
SrO	0.081
P_2O_5	0.214
SO_3	0.117
K_2O	0.091
Fe_2O_3	0.012

3.2.2 Thermal analysis

Fig. 3.2 illustrates the TG-DTA curves of prepared sample after being dried at 120 °C. In the DTA curve, the exothermic peak at 778 °C indicates the starting temperature for crystallisation of β-wollastonite. This crystallization temperature revealed that the wollastonite prepared from RHA and eggshells crystallized at lower temperature when compared to previous reports by other researchers [28, 29]. From TGA curve, it is observed that the thermal decomposition takes place in different steps. The occurrence of 8.4% weight loss was associated with the removal of residual water from room temperature to 220 °C, while the next step which involved from 220 to 600 °C corresponded to a weight loss of 5.18%, while between 600 to 750 °C, it shows a small weight loss of 2.5%. The second and third steps of weight loss might be caused by low temperature and high temperature decarbonation respectively [30]. It was observed that after the temperature reached 800 °C, the weight loss remained constant.

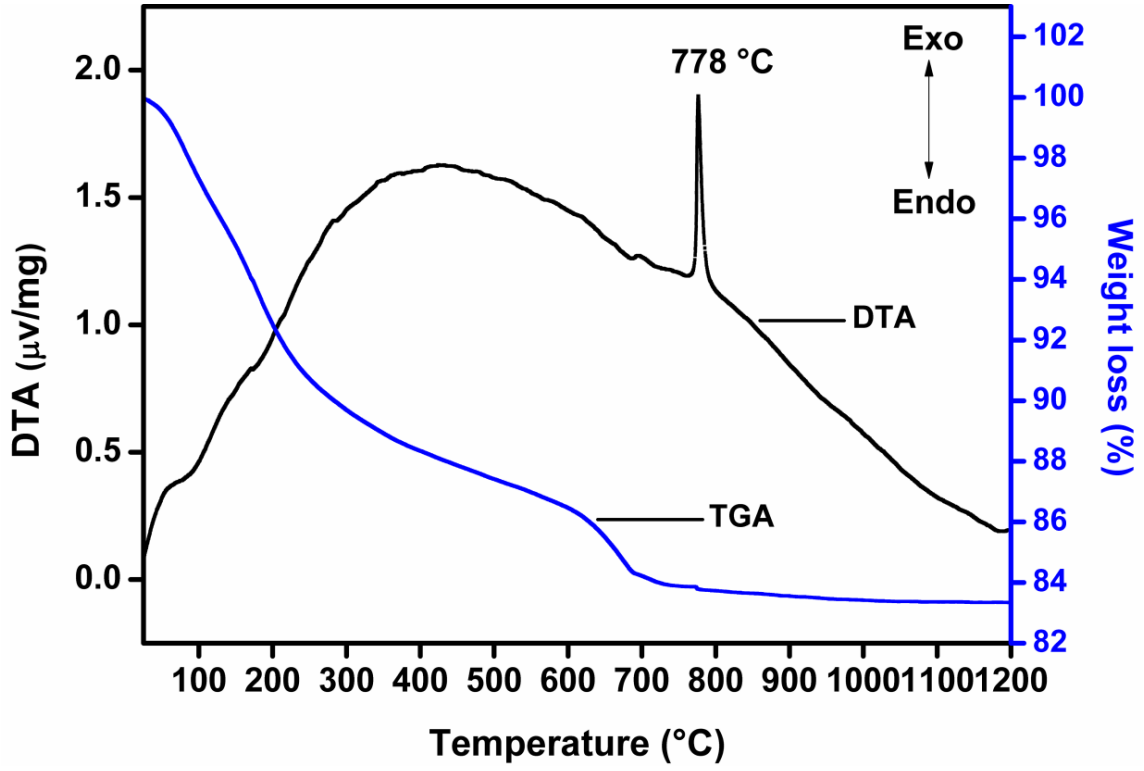

Fig. 3.2 TG-DTA curve of wollastonite sample after dried at 120° C

3.2.3 Structural characterization

The XRD pattern of the prepared sample sintered at 850 °C is shown in fig. 3.3. All the diffraction peaks were indexed to β-wollastonite (JCPDS file no: 42-0547) and no other peaks were observed. The particle size was estimated by Scherrer's formula using full width half maxima (FWHM) of all the diffraction peaks in XRD pattern. The calculated average particle size was in the range of ~ 48 nm.

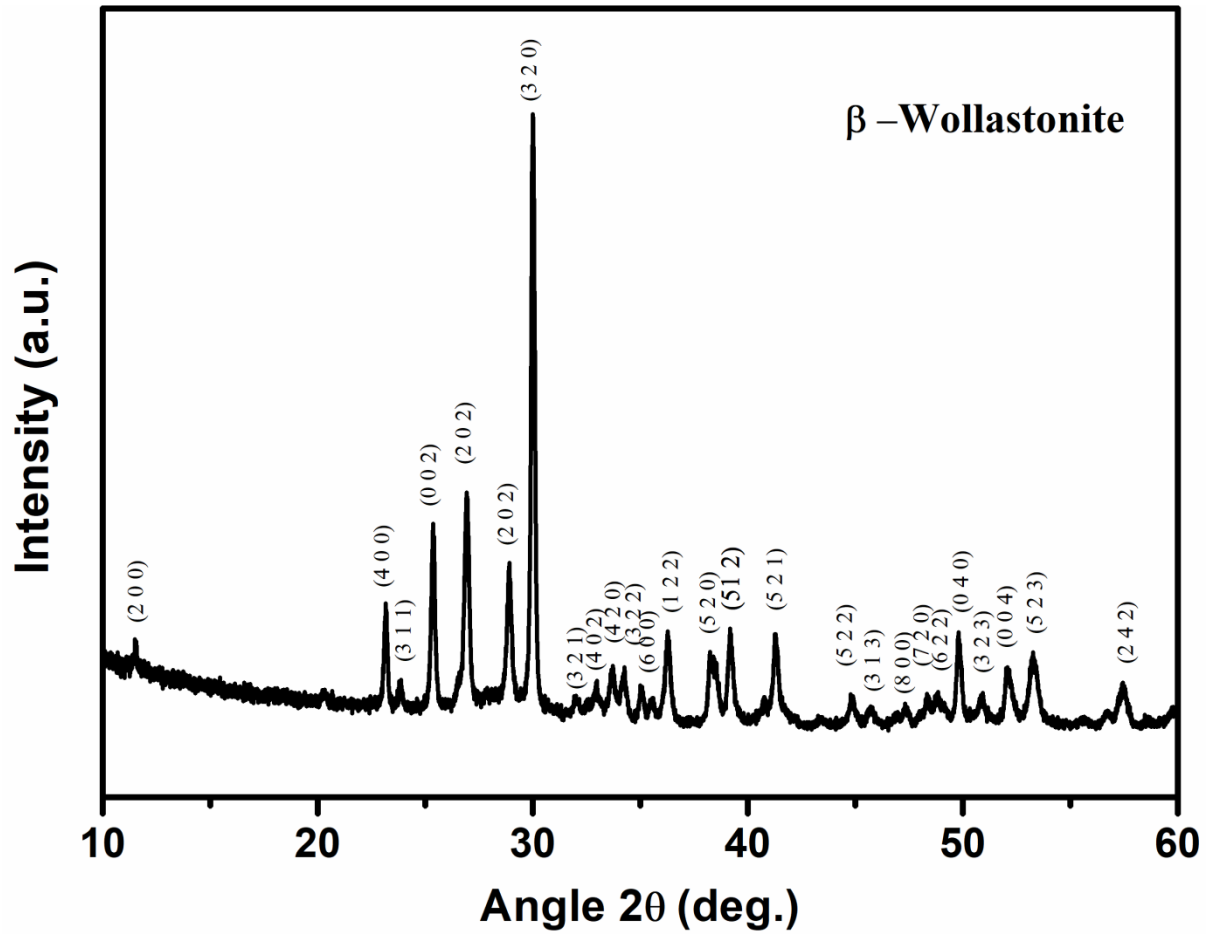

Fig. 3.3 XRD pattern of the prepared wollastonite sample sintered at 850° C

The morphological parameters of synthesized wollastonite ceramics were analyzed by SEM-EDS. Fig. 3.4 shows the surface micrographs and relative elemental spectra of wollastonite ceramics sintered at 850 °C. SEM image of surface of wollastonite pellet showed pores with irregular surface morphology. The appearance of pores on the surface of

wollastonite pellets might be owing to the release of volatile materials through calcination and sintering procedure. The EDS spectra show the presence of all indispensable elements like Ca, Si and O, which further supports the XRD data that pure wollastonite phase was achieved from eggshell and RHA at 850 °C.

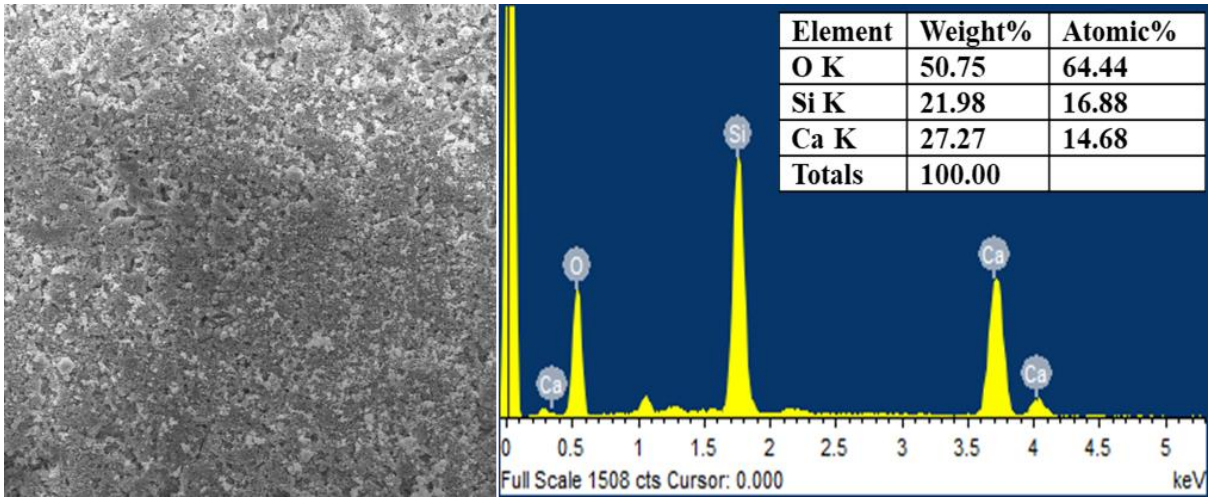

Fig. 3.4 Surface morphology of the prepared wollastonite sample

Fig. 3.5 depicts the FTIR spectra of prepared wollastonite sample. The IR absorption peaks were observed at 1022 and 1075 cm^{-1} corresponding to the asymmetric stretching mode of Si-O-Si and the IR absorption bands at 684 and 641 cm^{-1} were assigned to the symmetric stretching vibration of Si-O-Si. The vibrational bands observed at 902 and 943 cm^{-1} can be associated with the non-bridging silicon-oxygen bond of Si-O-NBO whereas the absorption bands located at 462 and 563 cm^{-1} corresponded to the bending vibrational mode of Si-O-S [31–33].

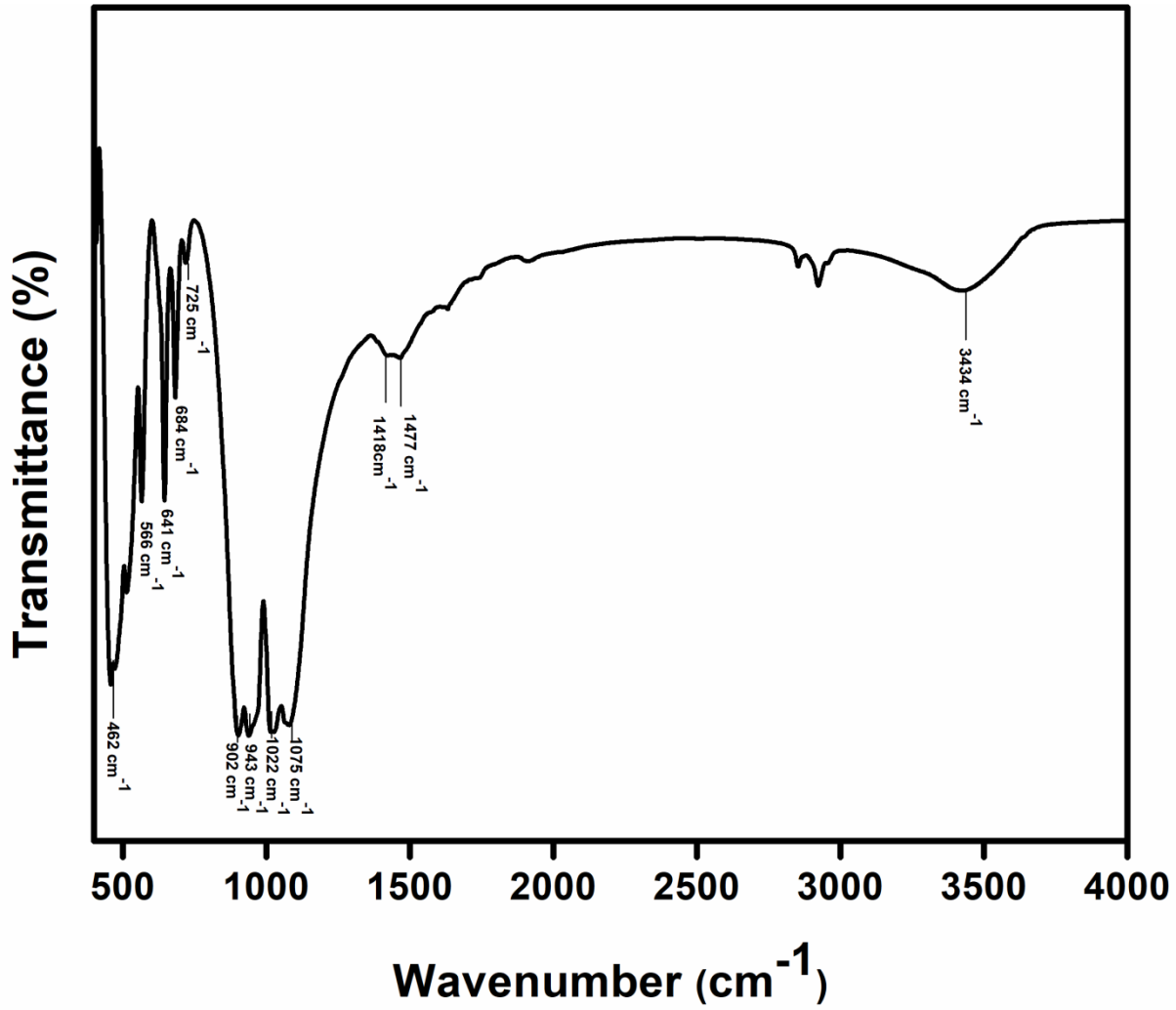

Fig. 3.5 FTIR spectra of wollastonite ceramics

3.2.4 In vitro bioactivity

The growth of hydroxyapatite layer on the surface of wollastonite samples after immersion in SBF solution was assessed by investigating the change of crystallinity, functional groups and surface morphology. Fig. 3.6 shows the XRD pattern of the wollastonite ceramic pellets after soaking in SBF solution. The characteristic peaks of hydroxyapatite ($Ca_{10}(PO_4)_6(OH)_2$) at 2θ = 25.87 (0 0 2), 2θ = 31.78 (2 1 1), 2θ = 46.71 (2 2 2), 2θ = 49.46 (2 1 3), 2θ = 53.14 (0 0 4), 2θ = 57.12 (3 1 3) were found in agreement with JCPDS no: 09-0432, indicating that the hydroxyapatite layer growth started immediately on the sample surface after immersing it in SBF solution. The diffraction intensity of original

wollastonite phase reduced significantly as soaking time increased and was replaced by hydroxyapatite phase. The wollastonite phase was still detected after 21 days of soaking because of non-homogeneous distribution of hydroxyapatite on the surface of the sample.

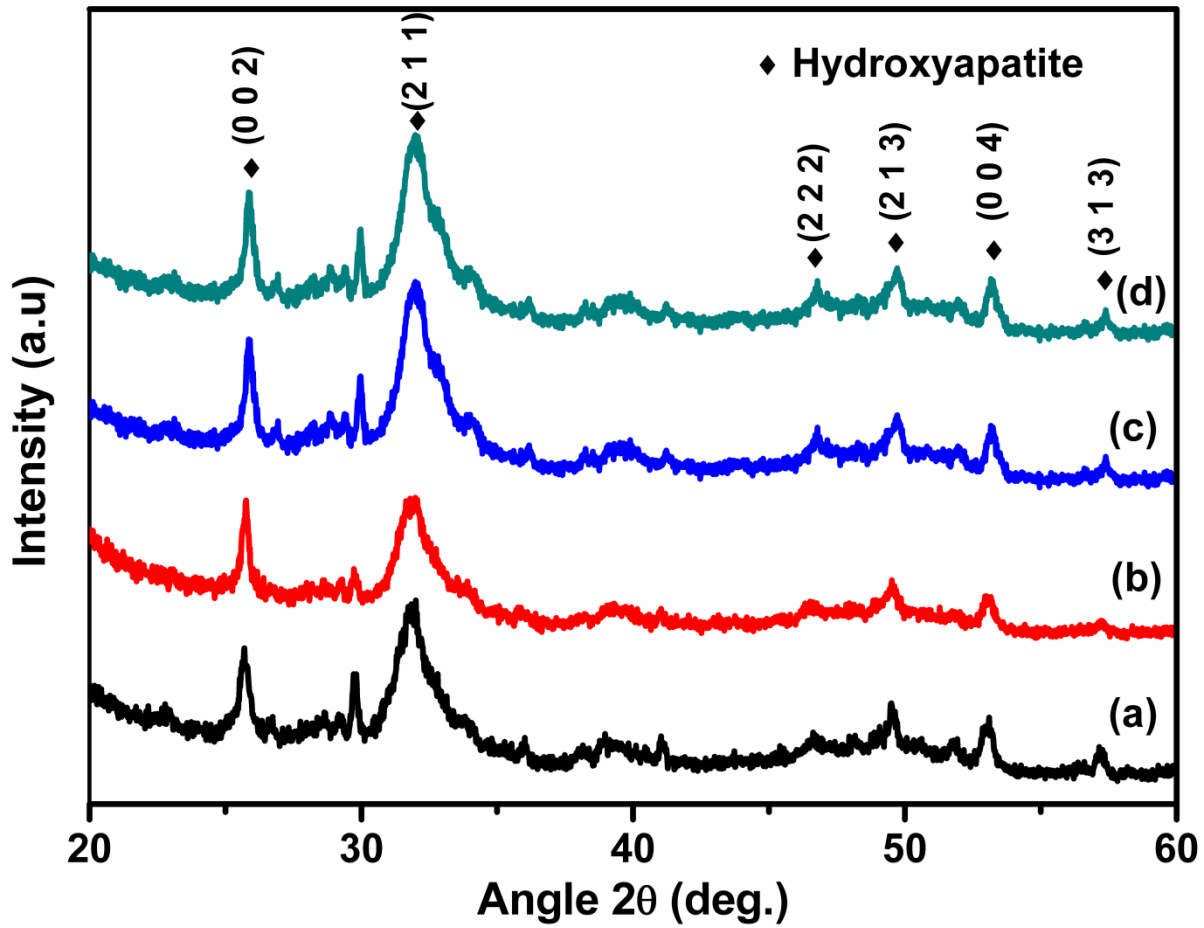

Fig. 3.6 XRD pattern of wollastonite ceramic pellets after soaking in SBF solution

SEM micrographs and elemental analysis of wollastonite samples surfaces after soaking in SBF solution are shown in Fig. 3.7. The growth of spherical shaped white colour agglomerates indicates the setting of hydroxyapatite over the surface of the sample after immersion in SBF solution and this was confirmed with the surface chemical composition obtained from EDS spectra. It is apparent from EDS spectra that there is a strong increase in calcium and phosphorus contents and the atomic ratio of Ca/P increased from 1.24 after 3 days of soaking to 2.1 after 21 days of soaking. The calculated Ca/P ratio after 21 days of

immersion indicated that carbonated hydroxyapatite (CHA) layer formed on the surface of the sample [34, 35].

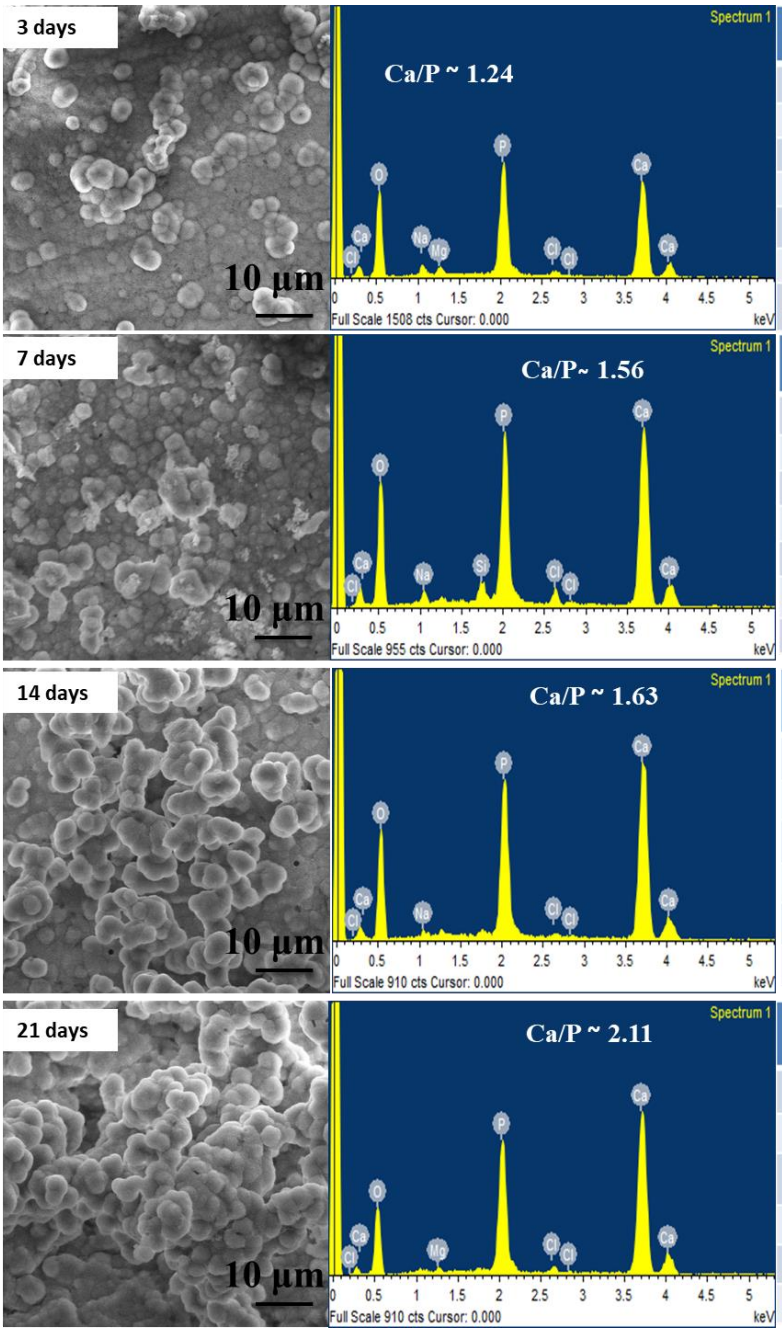

Element	Weight%	Atomic%
O K	51.92±0.68	70.45±0.82
Na K	0.78±1.10	0.73±1.13
Si K	0.94±0.02	0.95±0.13
P K	17.38±0.10	12.19±0.05
Cl K	0.95±0.00	0.58±0.00
Ca K	27.95±0.24	15.14±0.11
Total	100	

Element	Weight%	Atomic%
O K	49.46±0.55	68.72±0.68
Na K	0.61±0.86	0.59±0.84
Si K	1.43±0.00	1.14±0.00
P K	15.41±0.07	11.07±0.04
Cl K	1.82±0.01	1.15±0.00
Ca K	31.24±0.21	17.33±0.09
Total	100	

Element	Weight%	Atomic%
O K	45.98±3.76	65.88±3.30
Na K	0.61±0.07	0.59±0.07
P K	16.85±0.41	12.49±0.70
Cl K	0.87±0.50	0.57±0.33
Ca K	35.67±2.93	20.46±2.33
Total	100	

Element	Weight%	Atomic%
O K	30.19±0.19	50.03±0.30
Mg K	0.3±0.42	0.32±0.45
P K	18.15±0.03	15.53±0.03
Cl K	1.58±0.00	1.18±0.00
Ca K	49.76±0.19	32.91±0.12
Total	100	

Fig. 3.7 SEM micrographs and elemental analysis of wollastonite after *in-vitro* studies

The growth of apatite layer thickness was evaluated separately; SEM images and elemental analysis of cross section for the sample after being soaked for 3 and 7 days in SBF solution are shown in Fig. 3.8. After being soaked for 3 days, a layer thickness of about 48.91

± 0.24 µm was observed. After 7 days of immersion the layer thickness increased to about 112 ± 3.4 µm with increasing amount of phosphate [36].

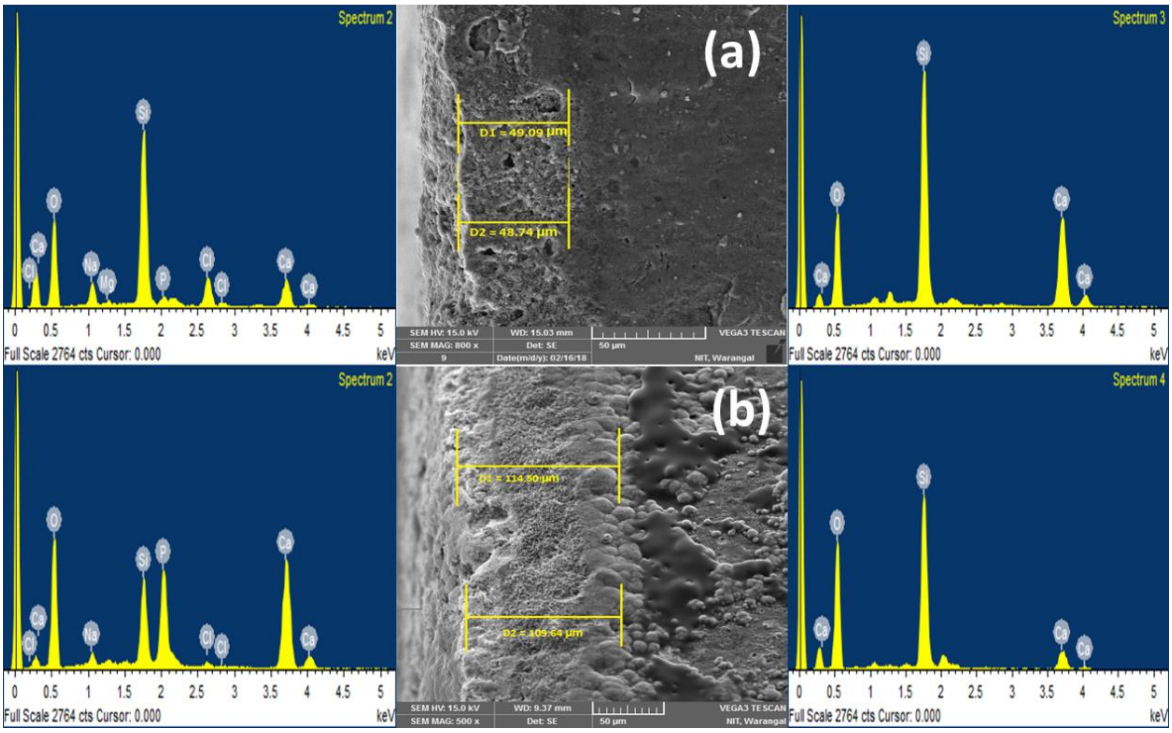

Fig. 3.8 SEM micrographs and EDS analysis of cross-section of wollastonite after soaking in SBF for (a) 3 days and (b) 7days

After soaking in SBF solution, the intensity of the silicate absorption bands decreased and the FTIR spectra (Fig.3.9) of the sample exhibited several new infrared bands at 563, 603, 800, 875, 960, 1033, 1093, 1418, 1487, 1642 and 3434 cm^{-1}. The peaks were observed at 1418, 1487 cm^{-1} and a small shoulder at 875 cm^{-1} was assigned to the C-O stretching of the carbonate group (CO_3^{2-}) [37, 38]; the bands at 1093, 1033, 603 and 563 cm^{-1} could be assigned to the phosphate group (PO_4^{3-}) in which double peaks at 603 and 563 cm^{-1} are representative features of the crystalline phase of phosphate in hydroxyapatite. The bands at 1642 and 3434 cm^{-1} corresponded to the O-H stretching vibrations [39, 40]. In addition to this, Si-O-Si symmetric stretching vibration band was observed at 800 cm^{-1} and a very small peak at 960 cm^{-1}, which was associated with Si-OH symmetric stretching corresponding to

silanol bonds [41, 42]. In accordance with SEM-EDS analysis, the presence of carbonate absorption bands in FTIR spectra after immersion in SBF solution further confirmed that CHA layer formed on the surface of the sample. The bone-like CHA layer, which developed on the surface of sample in SBF solution, suggested that the fabricated wollastonite exhibited excellent bioactivity.

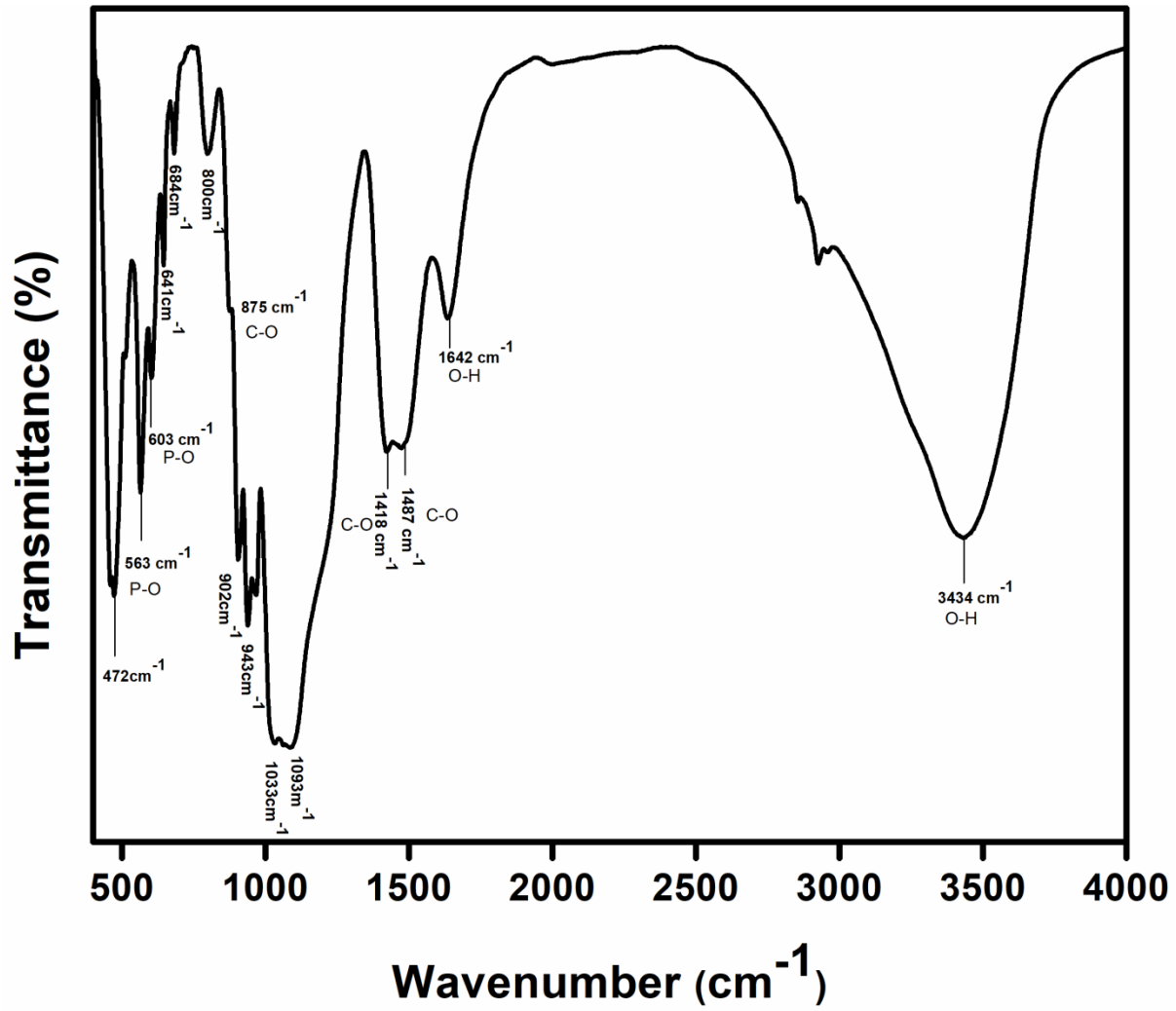

Fig. 3.9 FTIR spectra of wollastonite after immersion in SBF solution

3.2.5 Change in pH of SBF solution

Fig. 3.10 shows the change in pH value of SBF solution during bioactivity test. The obtained pH values increased rapidly for up to 5 days of immersion after the increment in pH

value slowed down. The pH value attained a maximum of ~7.7 on day 11, after which no change was observed for entire recorded time (up to 14 days). The variation in pH value of SBF solution is associated with the mechanism of nucleation and the development of hydroxyapatite layer on the surface of bioactive specimens [43]. When the wollastonite ceramic was immersed in SBF solution the Ca^{2+} ions from its surface exchanged with H^{+} or H_3O^{+} in SBF solution, resulting in rapid increase of pH value of surrounding fluid for initial soaking period. This ion exchange leads to the silica-rich layer formation on the surface of the sample. Once the negatively charged silica-rich layer formed, the Ca ions in SBF solution are first attached to the silica-rich layer and then the ionic activity products of apatite migrate to the surface followed by growth of apatite layer onto the surface [44].

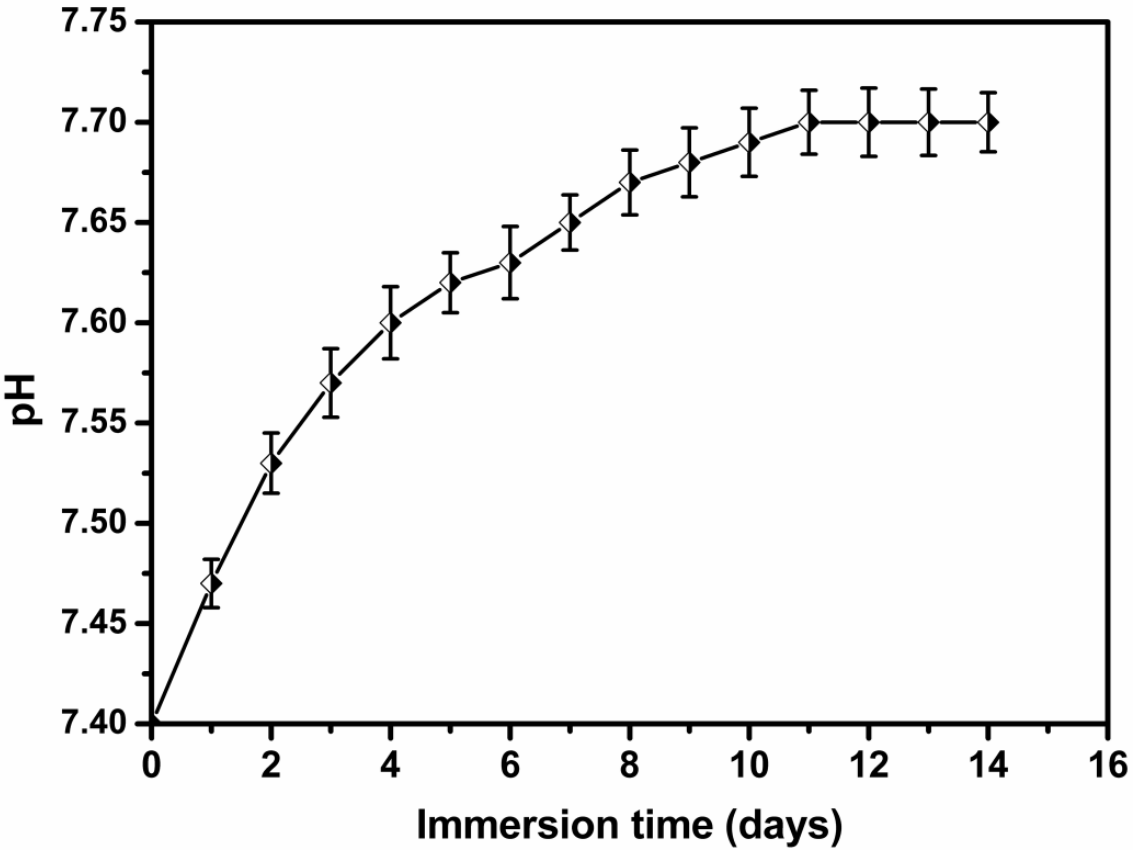

Fig. 3.10 Change in pH value of SBF solution during immersion time for wollastonite

3.2.6 Degradation

Fig. 3.11 illustrates the degradation rate of the immersed ceramic pellets in SBF and Tris buffer solutions for different time durations. During the soaking period, the particles on surface were attacked by the surrounding solution and the ions were leached from the surface, as a result of which gradual weight loss occurred. The degradation of the samples was determined by calculating the weight loss percentage as a function of soaking time. For initial soaking period, weight loss percentage was faster than that of latter and the degradation rate in SBF solution was lower than that of Tris buffer solution because the hydroxyapatite precipitated on the surface in SBF solution whereas no reprecipitation of ions in Tris buffer solution. On day 21, the degradation of wollastonite reached 5.6 % in SBF solution and 16.8 % in Tris buffer solution. The results showed that prepared wollastonite exhibits considerably lower degradation rate followed by slow dissolution, compared to the previous reports by other researchers [45, 46].

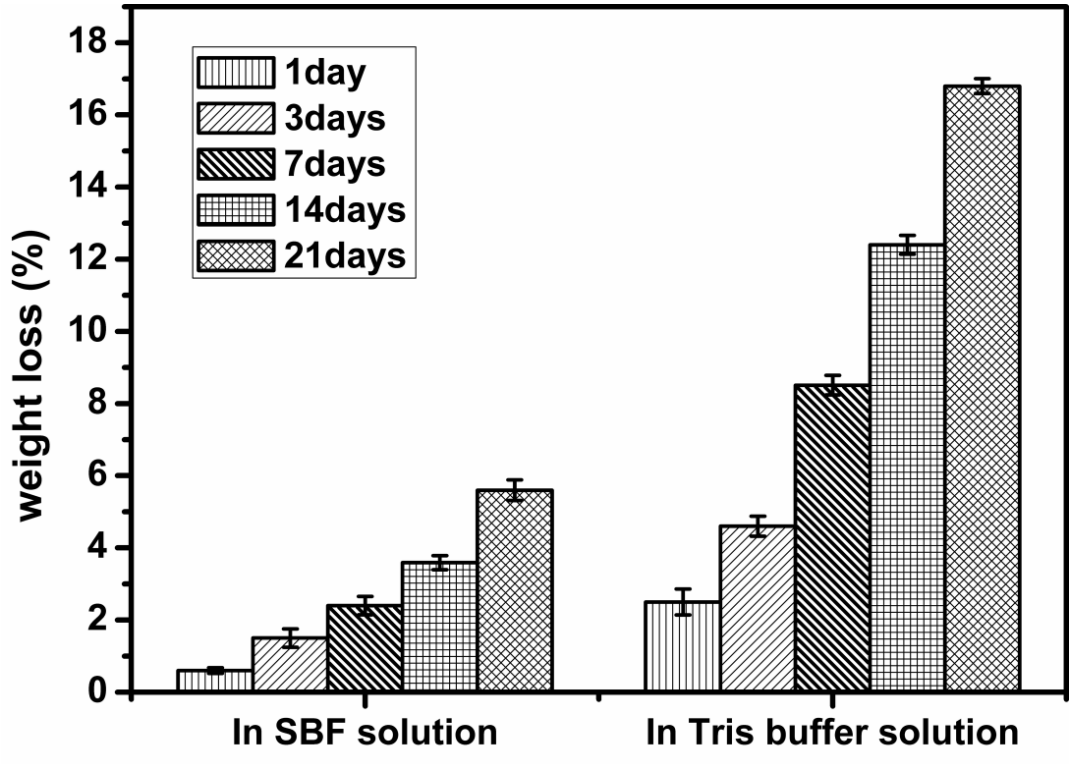

Fig. 3.11 Weight loss of wollastonite as a function of immersion time

The morphology after degradation in SBF and Tris buffer solution were also studied, as shown in the Fig. 3.12. Obviously a lot of spherical shaped hydroxyapatite particles were compactly distributed on the surface in SBF solution and on increasing immersion time period, more precipitation of apatite was observed. On the other hand, in Tris buffer solution, obvious evidence existed for a homogeneous degradation of the wollastonite ceramic. The surface of the ceramic appeared to have a number of cavities and the cavities were deepened into the ceramic on prolonged time period [47]. These results were in agreement with the degradation profile (Fig. 3.11).

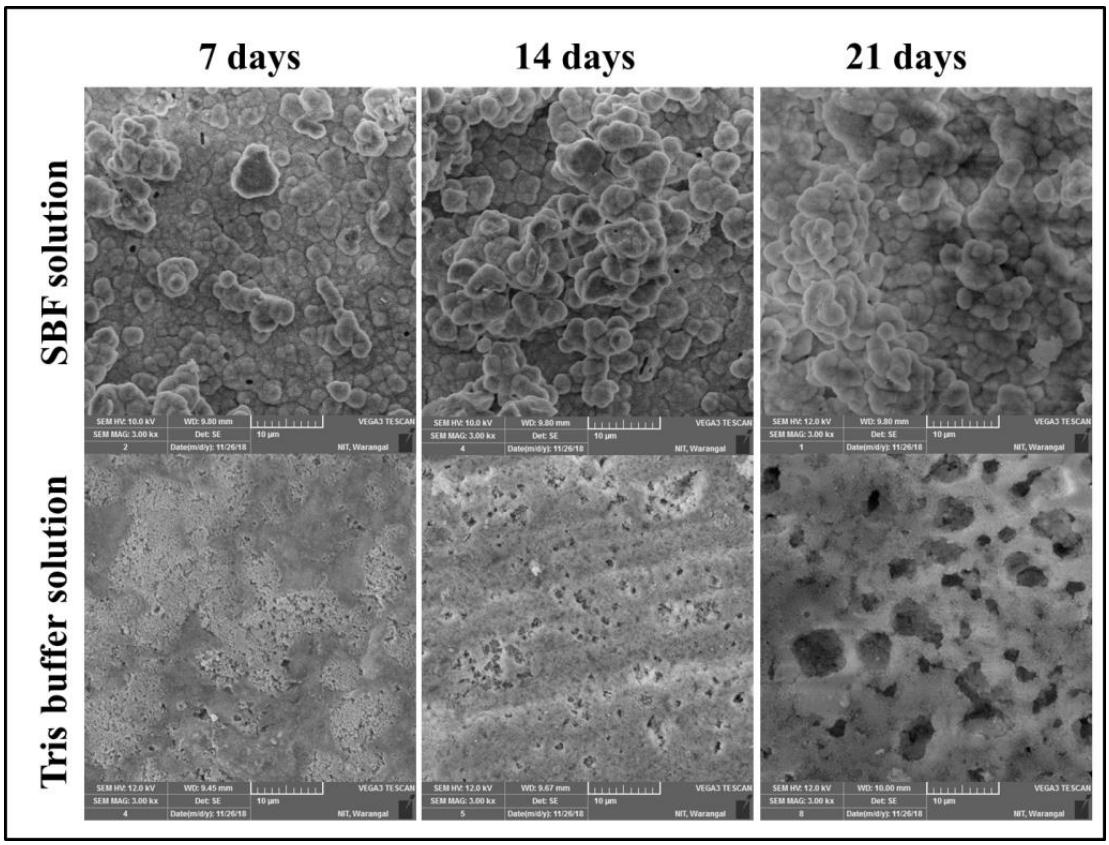

Fig. 3.12 SEM images of wollastonite after degradation studies in SBF and Tris buffer

3.2.7 Cytocompatibility

Cytocompatibility study has been successfully done based on the rate of viability of cells. Fig. 3.13 represents the concentrations vs. cell viability (in %). As can be seen from the

image of cytocompatibility result, there is no significant change in MG-63 cell viability at different dosages (1000µg/mL to 50µg/mL) in osteosarcoma cell line. Moreover, within the experimental settings, the cell viability is unaffected at different doses. According to biological evaluation of medical devices – Part 5: tests for *in vitro* cytocompatibility (ISO 10993 - 5: 2009), if the cell viability of the material is less than 70%, it has cytotoxic potential. On the other hand, in present work, it is observed that cell viability is greater than 70% for wollastonite samples at all different dosages which showed great cytocompatibility result even at higher (1000 µg/mL) concentrations. Hence, Cytocompatibility test indicates that the synthesized wollastonite ceramic has no biological cell toxicity; consequently it has a significantly active role to play in biological applications.

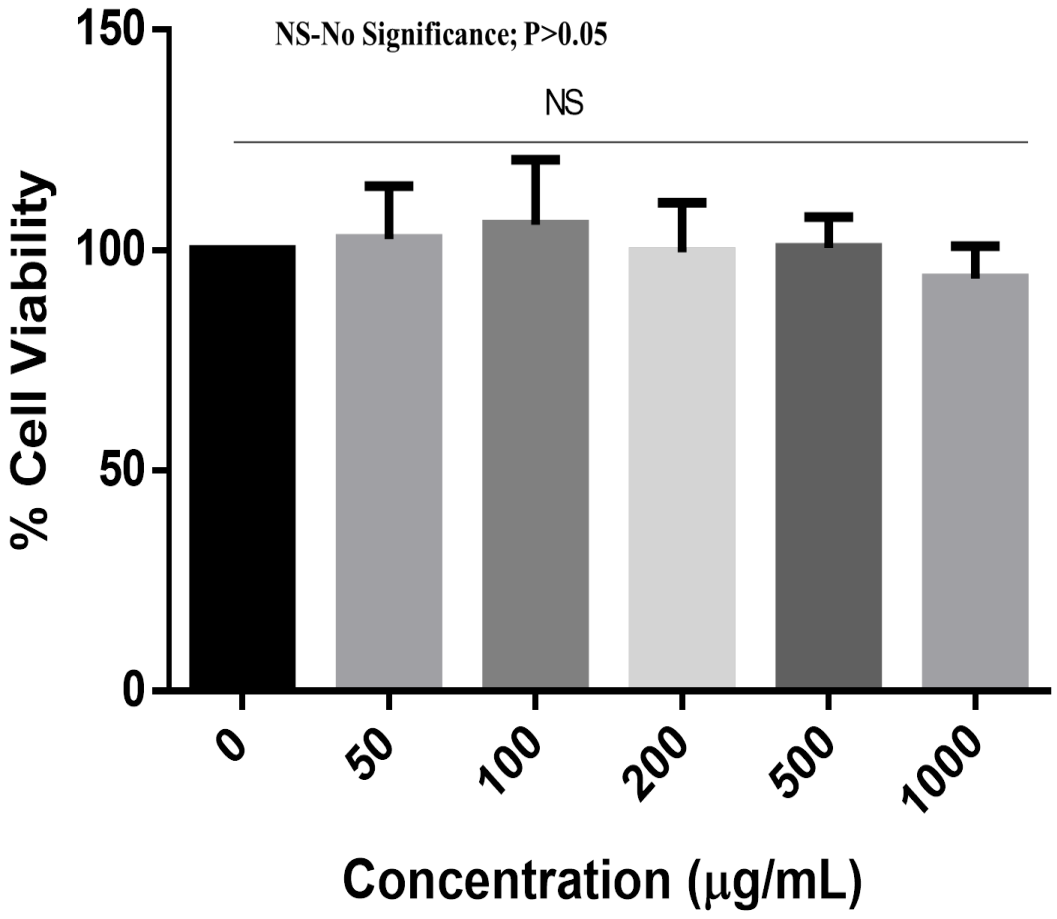

Fig. 3.13 Cell viability of wollastonite with MG-63 cells using MTT assay

3.2.8 Mechanical properties

Micro-hardness and compressive strength values are shown in Table 3.2. These Micro-hardness values are measured at five different locations on the sample given an average value of 20.14 ± 1.85 HV. The detailed view of polished surface of sintered wollastonite sample after Vickers indentation measurement can be seen in Fig. 3.14(a). The measured Micro-hardness value is similar and slightly higher compared to those of other sol-gel produced bioceramics reported in the literature [48–50]. The compressive strength was estimated from stress-strain curve by applying load until the specimen was crushed. Fig. 3.14(b) shows a typical stress-strain curve of wollastonite specimen during the compressive strength test. The stress increased abruptly as a function of strain at the early stage and decreased after the maximum compressive stress was reached. It is evident that the specimen started to be crushed at maximum compressive stress. At the compressive strain of 0.9 % the stress was increased because the crushed fragments were compressed once again. This is a typical characteristic of brittle fracture of bioceramics. The test was performed using at least five samples and given an average value of compressive strength 40.77 ± 2.46 MPa [51–53].

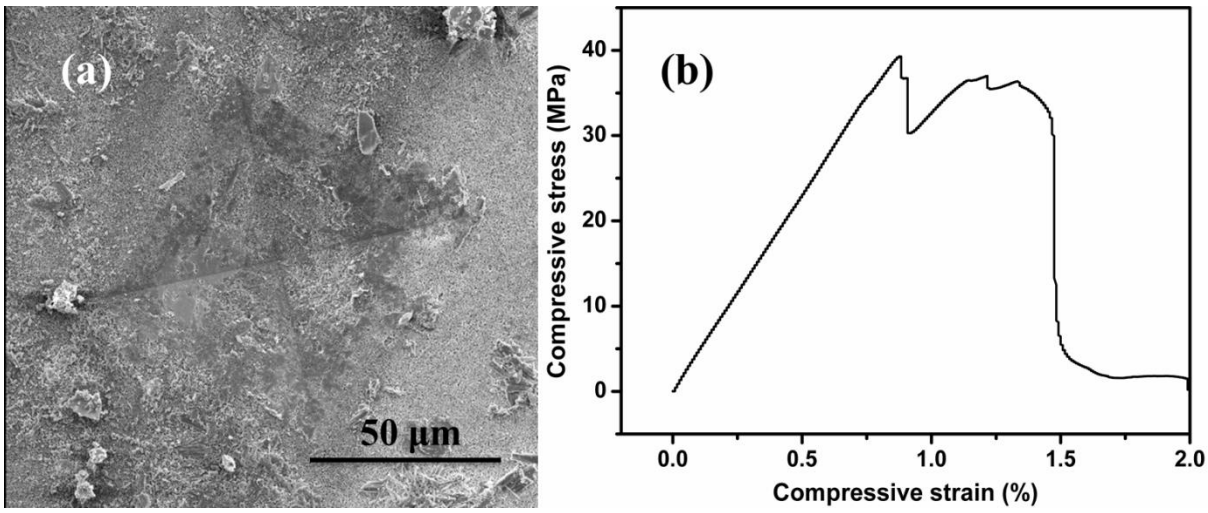

Fig. 3.14 Vickers indentation at 100 g load (a) and a typical stress-strain curve (b) of wollastonite

Table 3.2 The Micro-hardness and compressive strength values of wollastonite

Load (g)	**Dwell Time (s)**	**Hardness (HV)**	**Mean Hardness (HV)**
100	15	18.74	20.14 ± 1.85
		19.07	
		23.24	
		19.17	
		20.52	
Load (kN)	**Crosshead speed (mm/min)**	**Compressive strength (MPa)**	**Mean Compressive strength (MPa)**
5	0.5	39.29	40.77 ± 2.46
		41.11	
		38.26	
		40.49	
		44.72	

3.3 Conclusion

Wollastonite was successfully fabricated from Rice husk ash (RHA) and eggshell powder by sol-gel method. The crystallization of β-wollastonite was obtained by suitable heat treatment according to thermogravimetric and differential thermal analysis (TG/DTA) results. The pure phase β-wollastonite was achieved at a relatively low temperature. *In vitro* studies result revealed that the prepared wollastonite exhibited good bioactivity and cytocompability with higher growth rate of CHA and slow degradation rate. The mechanical properties revealed excellent compressive strength (40.77 ± 2.46 MPa) and Micro-hardness (20.14 ± 1.85 HV) values of wollastonite. Therefore, wollastonite prepared from RHA and eggshells might have potential for use as bioactive implant. The study also provides evidence that the method is effective in recycling natural waste into valuable bioceramics.

3.4 References

1. Azarov GM, Maiorova E V., Oborina MA, Belyakov A V. Wollastonite raw materials and their applications (a review). Glass and Ceramics. 1995;52: 237–40.

2. Wang H, Chen J, Yang W, Feng S, Ma H, Jia G, et al. Effects of Al_2O_3 addition on the sintering behavior and microwave dielectric properties of $CaSiO_3$ ceramics. J Eur Ceram Soc. 2012;32(3):541–5.

3. Nour WMN, Mostafa AA, Ibrahim DM. Recycled wastes as precursor for synthesizing wollastonite. Ceram Int. 2008;34(1):101–5.

4. Liu X, Ding C. Characterization of plasma sprayed wollastonite powder and coatings. Surf Coatings Technol. 2002;153(2–3):173–7.

5. Kotsis I, Balogh A. Synthesis of wollastonite. Ceram Int. 1989;15(2):79–85.

6. Magallanes-Perdomo M, De Aza AH, Mateus AY, Teixeira S, Monteiro FJ, De Aza S, et al. In vitro study of the proliferation and growth of human bone marrow cells on apatite-wollastonite-2M glass ceramics. Acta Biomater. 2010;6(6):2254–63.

7. Tamimi F, Kumarasami B, Doillon C, Gbureck U, Nihouannen D Le, Cabarcos EL, et al. Brushite-collagen composites for bone regeneration. Acta Biomater. 2008;4(5):1315–21.

8. Zhang NL, Molenda JA, Fournelle JH, Murphy WL, Sahai N. Effects of pseudowollastonite (CaSiO3) bioceramic on in vitro activity of human mesenchymal stem cells. Biomaterials. 2010;31(30):7653–65.

9. Lin K, Zhai W, Ni S, Chang J, Zeng Y, Qian W. Study of the mechanical property and in vitro biocompatibility of $CaSiO_3$ ceramics. Ceram Int. 2005;31(2):323–6.

10. Risbud M, Saheb DN, Jog J, Bhonde R. Preparation, characterization and in vitro biocompatibility evaluation of poly(butylene terephthalate)/wollastonite composites. Biomaterials. 2001;22(12):1591–7.

11. Gandolfi MG, Shah SN, Feng R, Prati C, Akintoye SO. Biomimetic calcium-silicate cements support differentiation of human orofacial mesenchymal stem cells. J Endod. 2011;37(8):1102–8.

12. Azeena S, Subhapradha N, Selvamurugan N, Narayan S, Srinivasan N, Murugesan R, et al. Antibacterial activity of agricultural waste derived wollastonite doped with copper for bone tissue engineering. Mater Sci Eng C. 2017;71:1156–65.

13. Gao C, Peng S, Feng P, Shuai C. Bone biomaterials and interactions with stem cells. Bone Research. 2017;5;17059.

14. Gao C, Feng P, Peng S, Shuai C. Carbon nanotube, graphene and boron nitride

nanotube reinforced bioactive ceramics for bone repair. Acta Biomaterialia. 2017;61:1-20.

15. Cannillo V, Colmenares-Angulo J, Lusvarghi L, Pierli F, Sampath S. In vitro characterisation of plasma-sprayed apatite/wollastonite glass-ceramic biocoatings on titanium alloys. J Eur Ceram Soc. 2009;29(9):1665-77.

16. Vakalova T V., Pogrebenkov VM, Karionova NP. Solid-phase synthesis of wollastonite in natural and technogenic siliceous stock mixtures with varying levels of calcium carbonate component. Ceram Int. 2016;42(15):16453–62.

17. Gal'perina MK, Lykhina NS. Study of optimum conditions of synthesizing wollastonite. Glas Ceram. 1976;33(3):172–5.

18. Gallini S, Jurado JRR, Colomer MTT. Synthesis and characterization of monazite-type Sr:LaPO prepared through coprecipitation. J Eur Ceram Soc. 2005;25(12):2003–7.

19. Wang H, Zhang Q, Yang H, Sun H. Synthesis and microwave dielectric properties of CaSiO3 nanopowder by the sol-gel process. Ceram Int. 2008;34(6):1405–8.

20. Chen C-C, Ho C-C, Lin S-Y, Ding S-J. Green synthesis of calcium silicate bioceramic powders. Ceram Int. 2015;41(4):5445–53.

21. Vichaphund S, Kitiwan M, Atong D, Thavorniti P. Microwave synthesis of wollastonite powder from eggshells. J Eur Ceram Soc. 2011;31(14):2435–40.

22. Huang XH, Chang J. Synthesis of nanocrystalline wollastonite powders by citrate-nitrate gel combustion method. Mater Chem Phys. 2009;115(1):1–4.

23. Faure J, Drevet R, Lemelle A, Ben Jaber N, Tara A, El Btaouri H, et al. A new sol-gel synthesis of 45S5 bioactive glass using an organic acid as catalyst. Mater Sci Eng C. 2015;47:407–12.

24. Arcos D, Vallet-Regí M. Sol-gel silica-based biomaterials and bone tissue regeneration. Acta Biomaterialia. 2010;6:2874–88.

25. Hench LL. Sol-gel materials for bioceramic applications. Curr Opin Solid State Mater Sci. 1997;2(5):604–10.

26. Chen Q-Z, Li Y, Jin L-Y, Quinn JMW, Komesaroff PA. A new sol–gel process for producing Na_2O-containing bioactive glass ceramics. Acta Biomater. 2010;6(10):4143–53.

27. Abu R, Yahya R, Neon S. Production of High Purity Amorphous Silica from Rice Husk. Procedia Chem. 2016;19:189–95.

28. Ismail H, Shamsudin R, Abdul Hamid MA. Effect of autoclaving and sintering on the formation of β-wollastonite. Mater Sci Eng C. 2016;58:1077–81.

29. Mohammadi M, Alizadeh P, Atlasbaf Z. Effect of frit size on sintering, crystallization and electrical properties of wollastonite glass-ceramics. J Non Cryst Solids. 2011;357(1):150–6.

30. Klimesch DS, Ray A. The use of DTA/TGA to study the effects of ground quartz with different surface areas in autoclaved cement : Quartz pastes. Part 1: A method for evaluating DTA/TGA results. Thermochim Acta. 1996;289(1):41–54.

31 Meiszterics A, Rosta L, Peterlik H, Rohonczy J, Kubuki S, Henits P, et al. Structural characterization of gel-derived calcium silicate systems. J Phys Chem A. 2010;114(38):10403–11.

32. Li HC, Wang DG, Chen CZ, Weng F, Shi H. Influence of different amount of Na_2O additive on the structure, mechanical properties and degradability of bioactive wollastonite. Ceram Int. 2016;42(1):1439–45.

33. Swann GEA, Patwardhan S V. Application of Fourier Transform Infrared Spectroscopy (FTIR) for assessing biogenic silica sample purity in geochemical analyses and palaeoenvironmental research. Clim Past. 2011;7(1):65–74.

34. Sainz MA, Pena P, Serena S, Caballero A. Influence of design on bioactivity of novel $CaSiO_3$-$CaMg(SiO_3)_2$ bioceramics: In vitro simulated body fluid test and thermodynamic simulation. Acta Biomater. 2010;6(7):2797–807.

35. Samudrala R, Reddy GVN, Manavathi B, Azeem PA. Synthesis, characterization and cytocompatibility of ZrO_2 doped borosilicate bioglasses. J Non Cryst Solids. 2016;447:150–5.

36. Long LH, Chen LD, Bai SQ, Chang J, Lin KL. Preparation of dense β-$CaSiO_3$ ceramic with high mechanical strength and HAp formation ability in simulated body fluid. J Eur Ceram Soc. 2006;26(9):1701–6.

34. Ni S, Chang J. In vitro degradation, bioactivity, and cytocompatibility of calcium silicate, dimagnesium silicate, and tricalcium phosphate bioceramics. J Biomater Appl. 2009; 24(4):139-58.

35. Meiszterics A, Rosta L, Peterlik H, Rohonczy J, Kubuki S, Henits P, et al. Structural characterization of gel-derived calcium silicate systems. J Phys Chem A. 2010;114(38):10403–11.

36. Li HC, Wang DG, Chen CZ, Weng F, Shi H. Influence of different amount of Na_2O additive on the structure, mechanical properties and degradability of bioactive wollastonite. Ceram Int. 2016;42(1):1439–45.

37. Naghizadeh F, Abdul Kadir MR, Doostmohammadi A, Roozbahani F, Iqbal N, Taheri MM, et al. Rice husk derived bioactive glass-ceramic as a functional bioceramic: Synthesis, characterization and biological testing. J Non Cryst Solids. 2015;427:54–61.

38. Samudrala R, Abdul Azeem P, Penugurti V, Manavathi B. In vitro evaluation of niobia added soda lime borosilicate bioactive glasses. J Alloys Compd. 2018;764:1072-78.

39. Lin K, Zhai D, Zhang N, Kawazoe N, Chen G, Chang J. Fabrication and characterization of bioactive calcium silicate microspheres for drug delivery. Ceram Int. 2014;40(2):3287–93.

40. Samudrala R, Abdul Azeem P, Penugurti V, Manavathi B. Cytocompatibility studies of titania-doped calcium borosilicate bioactive glasses in-vitro. Mater Sci Eng C. 2017;77:772–9.

41. Aguiar H, Serra J, González P, León B. Structural study of sol-gel silicate glasses by IR and Raman spectroscopies. J Non Cryst Solids. 2009;355(8):475–80.

42. El-Rashidy AA, Waly G, Gad A, Hashem AA, Balasubramanian P, Kaya S, et al. Preparation and in vitro characterization of silver-doped bioactive glass nanoparticles fabricated using a sol-gel process and modified Stöber method. Journal of Non-Crystalline Solids. 2017; 483:26-36.

43. Liu X, Ding C, Chu PK. Mechanism of apatite formation on wollastonite coatings in simulated body fluids. Biomaterials. 2004;25(10):1755–61.

44. Magallanes-Perdomo M, Luklinska ZB, De Aza AH, Carrodeguas RG, De Aza S, Pena P. Bone-like forming ability of apatite-wollastonite glass ceramic. J Eur Ceram Soc. 2011;31(9):1549–61.

45. Hoppe A, Güldal NS, Boccaccini AR. A review of the biological response to ionic dissolution products from bioactive glasses and glass-ceramics. Biomaterials. 2011;32: 2757–74.

46. Li HC, Wang DG, Chen CZ. Effect of sodium oxide and magnesia on structure, in vitro bioactivity and degradability of wollastonite. Mater Lett. 2014;135:237–40.

47. Ni S, Chang J. In vitro degradation, bioactivity, and cytocompatibility of calcium silicate, dimagnesium silicate, and tricalcium phosphate bioceramics. J Biomater Appl. 2009; 24(2):139-158.

48. Sinkó K, Meiszterics A, Rosta L. Comparative study of calcium silicate bulk systems produced by different methods. In: Progress in Colloid and Polymer Science. 2008;135:130-138.

49. Li HC, Wang DG, Hu JH, Chen CZ. Effect of various additives on microstructure, mechanical properties, and in vitro bioactivity of sodium oxide-calcium oxide-silica-phosphorus pentoxide glass-ceramics. J Colloid Interface Sci. 2013; 405:296-304.

50. Meiszterics A, Sinkó K. Sol-gel derived calcium silicate ceramics. Colloids Surfaces A Physicochem Eng Asp. 2008;319(1–3):143–8.

51. Zhang F, Chang J, Lu J, Lin K, Ning C. Bioinspired structure of bioceramics for bone regeneration in load-bearing sites. Acta Biomater. 2007; 3(6):896-904.

52. Jin Z, Wu R, Shen J, Yang X, Shen M, Xu W, et al. Nonstoichiometric wollastonite bioceramic scaffolds with core-shell pore struts and adjustable mechanical and biodegradable properties. J Mech Behav Biomed Mater. 2018; 88:140-149.

53. Lin K, Chang J, Zeng Y, Qian W. Preparation of macroporous calcium silicate ceramics. Mater Lett. 2004; 58(15):2109-2113.

Chapter 4

A comparative study on *in vitro* behaviour of bio-waste derived wollastonite with chemically derived wollastonite

This chapter compared the in vitro bioactivity, change in pH of SBF solution, degradation rate, antibacterial activity and cell proliferation ability of wollastonite (β-$CaSiO_3$) ceramics synthesized by present sol-gel method using bio-waste resources such as rice husk ash (RHA) and eggshells with β-$CaSiO_3$ prepared using tetraethylorthosilicate (TEOS) and calcium nitrate tetra hydrate ($Ca(NO_3)_2.4H_2O$) by conventional sol-gel method.

4.1 Introduction

Calcium silicate ceramics have been identified as bioactive and prospective candidates for bone tissue engineering applications [1–3]. Researchers have reported that bone tissue can be produced on calcium silicate ceramics with hydroxyl carbonated apatite layer deposition [4, 5]. Moreover, these ceramics can support the attachment of human bone derived cells (HBDC), their proliferation and differentiation [6–8]. The conventional starting materials used to synthesize calcium silicates are calcium oxide (CaO) and silica (SiO_2). Commercial calcium oxide and calcium nitrate tetra hydrate ($Ca(NO_3)_2.4H_2O$) are the normal sources of calcium oxide. The sources of silica are commercial silica, tetraethylorthosilicate (TEOS) and sodium silicate (Na_2SiO_3). However, some of these materials are expensive.

Researchers have made several efforts to recycle natural waste as an alternative source to reduce causing damage to the ground and environmental pollution. Many studies have been performed to produce calcium silicates from waste as resources in different synthesis procedures and these calcium silicates exhibit a range of properties. S. Vichaphund et al. [9] synthesized wollastonite ($CaSiO_3$) powder by microwave assisted solid-state reaction using eggshells as a calcium oxide source and silica. R. Abd Rashid et al. [10] prepared wollastonite from Malaysian limestone and silica sand via solid-state route, which exhibited quantitatively good bioactivity charactereristics. H. Ismail et al. [11] produced wollastonite using rice husk as a source of silica and commersial calcium oxide by autoclaving and sintering method. S. Azeena et al. [12] reported a synthesis of wollastonite from rice straw ash as silica source and calcium nitrate by sol-gel method. Y. Wang et al. [13] produced wollastonite by silicon slag from zirconium oxychloride production industries with the addition of certain amount of calcium oxide. S.S. Hossain et al. [14] fabricated wollastonite using eggshells and rice husk ash by solid-state reaction.

In spite of various methods that have been reported for preparation of calcium silicate ceramics, sol-gel synthesized calcium silicates have proven to be potential candidates for its biomedical application due to their enhanced chemical homogeneity and higher bioactivity [15, 16]. The traditional powder manufacture technology using melt-quenching method or solid-state sintering for the fabrication of calcium silicate ceramics requires more than 1200 °C temperature; in contrast, the sol-gel technique requires reasonably low temperature of 800 °C [17]. A typical sol-gel method for synthesis of calcium silicate requires gelation of TEOS and ($Ca(NO_3)_2.4H_2O$) via acid or base hydrolysis of TEOS [18, 19]. TEOS hydrolysis is extremely slow in neutral medium and this method requires the addition of acid or base catalyst during gelation. Without any catalyst, the presence of water alone leads to elastic homogenious gel formation, which requires long drying time [19]. In the current study, we report a new approach for the synthesis of calcium silicate using silica and calcium oxide obtained from rice husk and eggshells, respectively, by sol-gel method. The method provides evidence for cost-effective synthesis, environmentally beneficial and effective utilization of bio-waste for the fabrication of sustainable calcium silicate ceramics.

The objective of this work was to compare the systematic and detailed investigations of sol-gel synthesized wollastonite using rice husk ash and eggshells as starting materials (denoted as NCS) with TEOS and $Ca(NO_3)_2.4H_2O$ as starting materials (denoted as CCS) in terms of bioactivity, degradation rate, antibacterial activity, cytocompatibility and cell proliferation.

4.2 Results and discussion

4.2.1 Thermal analysis

Fig. 4.1 displays thermogravimetric analysis (TGA) and differential thermal analysis (DTA) of samples after drying them at 120 °C. From the TGA curves of both the samples, it

is confirmed that all residuals can be eliminated before 700 °C. Therefore, 700 °C temperature was chosen for the stabilisation of two samples. The exothermic peak on DTA curves for samples NCS (Fig. 4.1(a)) and CCS (Fig. 4.1(b)) at 772 °C and 870 °C respectively indicate the crystallisation temperature (T_C) for ceramics. Therefore, samples NCS and CCS were sintered for 2 hours at 802 °C and 900 °C (~ T_C + 30 °C) respectively for optimum crystal growth.

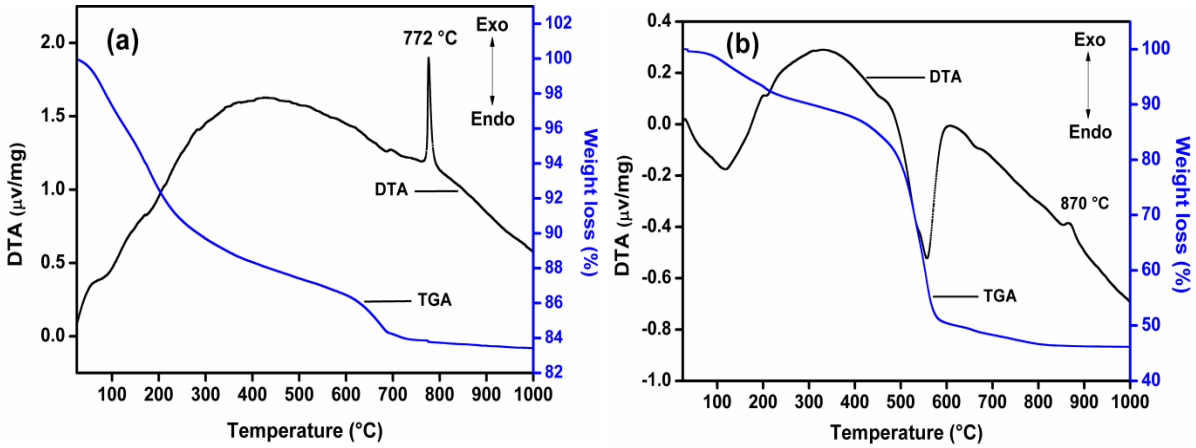

Fig. 4.1 TG-DTA curves of (a) NCS and (b) CCS samples after dried at 120 °C

4.2.2 Structural characterization

The phase formation of the samples NCS and CCS which were sintered at 802 °C and 900 °C respectively were examined by XRD. The XRD peak patterns (Fig. 4.2) of both the samples showed very similar trend and well matched with JCPDS file no: 84-0655 of β-wollastonite phase [20]. It is also noticed that the peak intensities of NCS powder were slightly higher than that of CCS; this observation indicates that the calcium silicate synthesized from RHA and eggshell has good crystallization. The average crystallite size was calculated as ~ 48.3 nm for NCS and ~ 62.8 nm for CCS using Debye Scherrer's equation. Fig. 4.3 shows the particle size distribution by dynamic light scattering obtained from HORIBA-SZ-100 particle size analyzer [21]. The average particle size of NCS ceramics was

obtained as ~ 42.4 nm and for CCS ceramics ~ 55.4 nm. These results are in close agreement with the crystallite size obtained from the XRD patterns.

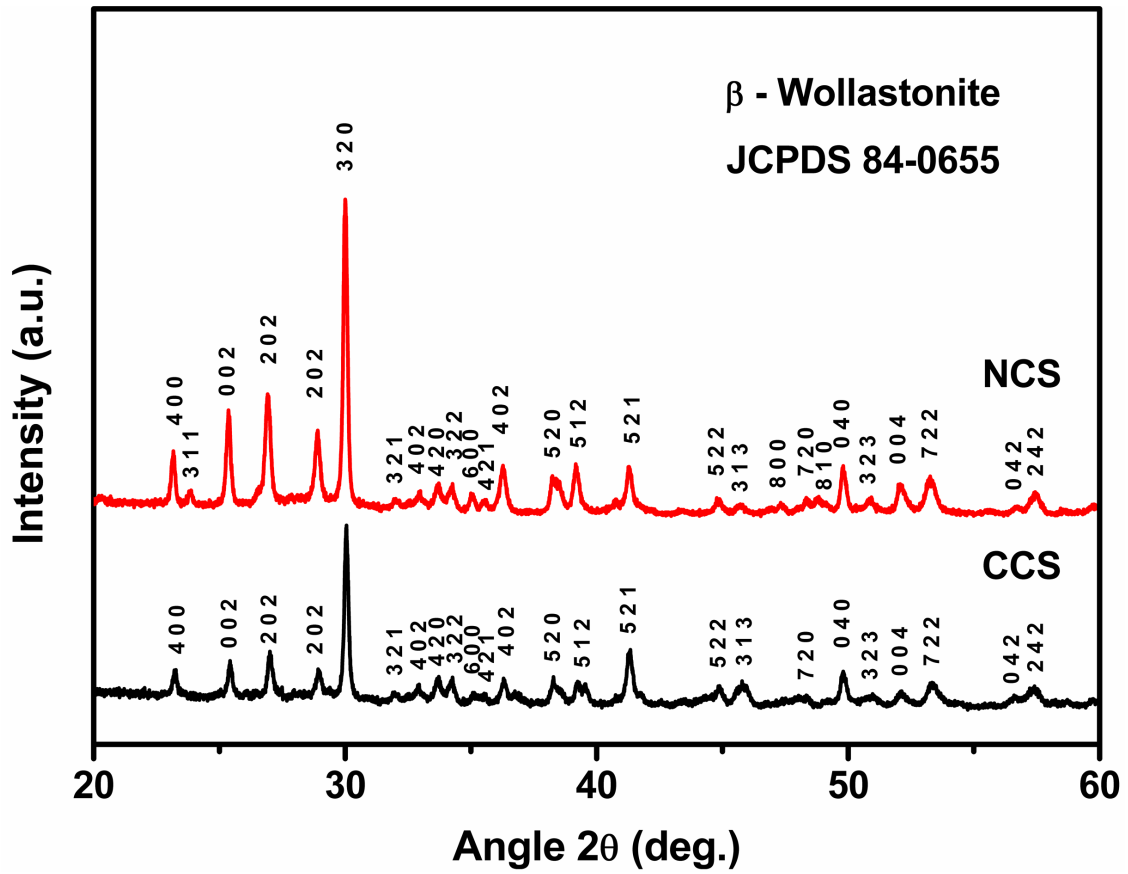

Fig. 4.2 XRD patterns of NCS and CCS ceramics after sintering

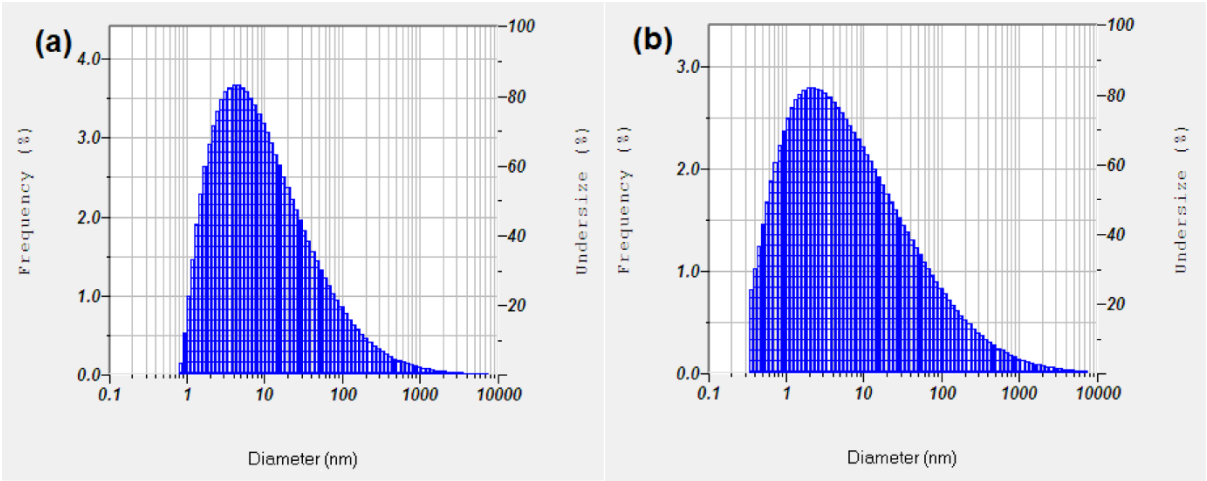

Fig. 4.3 Particle size distribution of (a) NCS and (b) CCS ceramics

The surface morphology was studied using scanning electron microscopy (SEM) while energy dispersive spectroscopy (EDS) was used to find the elements presented in the ceramic materials. Fig. 4.4 shows SEM-EDS results of NCS and CCS samples. SEM micrographs of NCS sample showed porous surface, rough and irregular surface morphology. On the other hand, a smooth surface with a small number of holes was observed on CCS sample. The EDS spectra predictably reveal the presence of Ca, Si and O in both samples. No additional impure elements were identified.

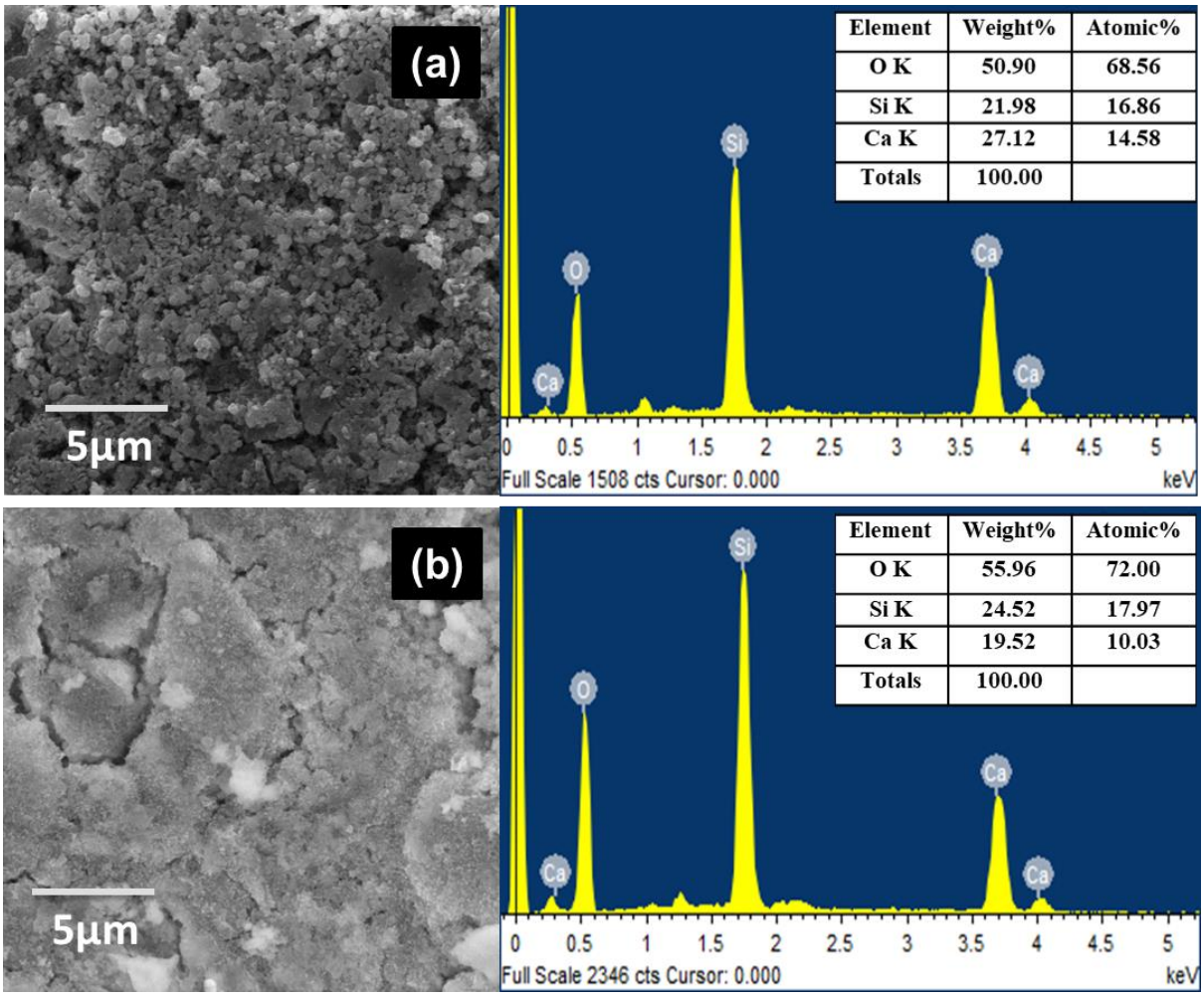

Fig. 4.4 Morphologies and elemental spectra of sintered (a) NCS and (b) CCS ceramics

Fourier transform infrared spectroscopy was performed on sintered ceramic powders and the transmittance spectra are presented in Fig. 4.5. The IR spectra peaks at ~ 450, ~ 520

and ~ 566 cm^{-1} were attributed to bending or rocking motion in Si-O-Si bonds [22, 23]. The peaks observed at ~ 642, ~ 684 and ~ 725 cm^{-1} were characteristic of Si-O-Si symmetric stretching vibration [22–24] whereas the band observed at 1022 - 1076 cm^{-1} could be ascribed to Si-O-Si asymmetric stretching vibration. The band at 902 - 943 cm^{-1} was associated with non-bridging bond of Si-O-NBO [25]. Moreover, the presence of peaks at ~ 1635 cm^{-1} and ~ 3435 cm^{-1} were attributed to the existence of adsorbed moisture [26, 27] and the presence of carbonate band at 1418-1477 cm^{-1} may be due to the ambient carbon dioxide employed during sintering process [10]. The intensity of FTIR bands strongly depends on the degree of crystallinity and their exact position on type of crystalline phase. In the present study the peak positions of NCS and CCS ceramics were precisely coincides with each other and were coincides with characteristic of infrared bands associated with β phase of wollastonite [28] but slight intensity variations in peaks were observed. The low frequency absorption band (450 cm^{-1}) is stronger in NCS than in CCS ceramic which indicated better crystallinity of NCS sample and the results are in agreement with XRD results. In the region of frequencies of symmetric stretching vibration of bridge bonds Si-O-Si in tetrahedra [SiO_4], one high intense band at ~ 725 cm^{-1} is observed in CCS than in NCS to indicate the high symmetry of complex anions [29–31].

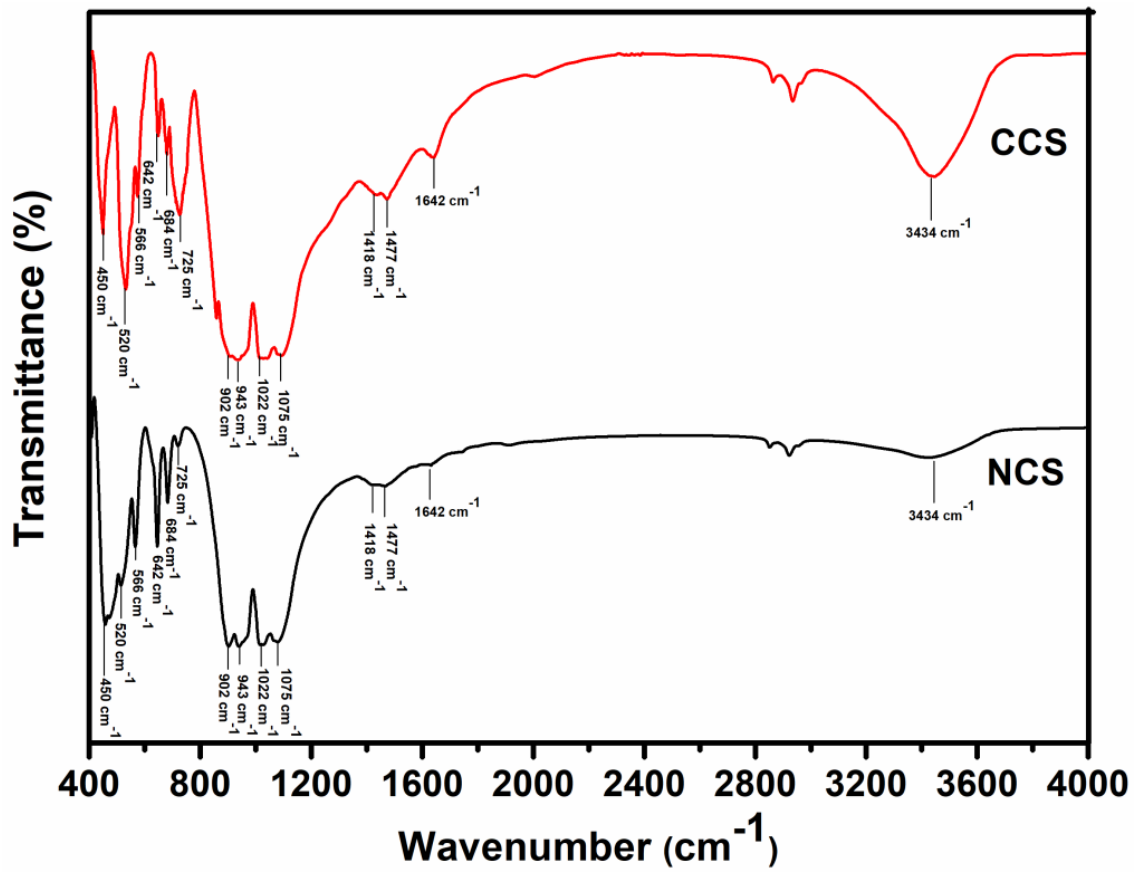

Fig. 4.5 FTIR spectra of NCS and CCS ceramic samples after sintering

4.2.3 In vitro bioactivity

Fig. 4.6 shows X-ray diffraction patterns of the ceramics after immersion in SBF solution for 3, 7 and 14 days. From the XRD results (002), (211), (222), (213), (004) and (313) reflections were observed that were in agreement with the hydroxyapatite (Ca_{10} $(PO_4)_6$ $(OH)_2$) phase (JCPDS no: 09-0432), and increasing amount of hydroxyapatite phase were detected with increase in soaking time. After 14 days of soaking, the diffraction intensity of matrix wollastonite phase almost completely disappeared and was substituted with hydroxyapatite as the major phase for NCS samples, whereas traces of wollastonite phase were still noticed for CCS samples. These results revealed that calcium silicate ceramic prepared from RHA and eggshell shows better growth rate of hydroxyapatite on its surface, which could be due to its surface microstructure. The kinetics of the hydroxyapatite

nucleation depends on surface factors of the compounds such as surface chemistry and microstructure. Nano crystalline porous and irregular surface morphology provides maximum number of nucleation sites for hydroxyapatite deposition because of high surface energy of grain boundaries [32, 33].

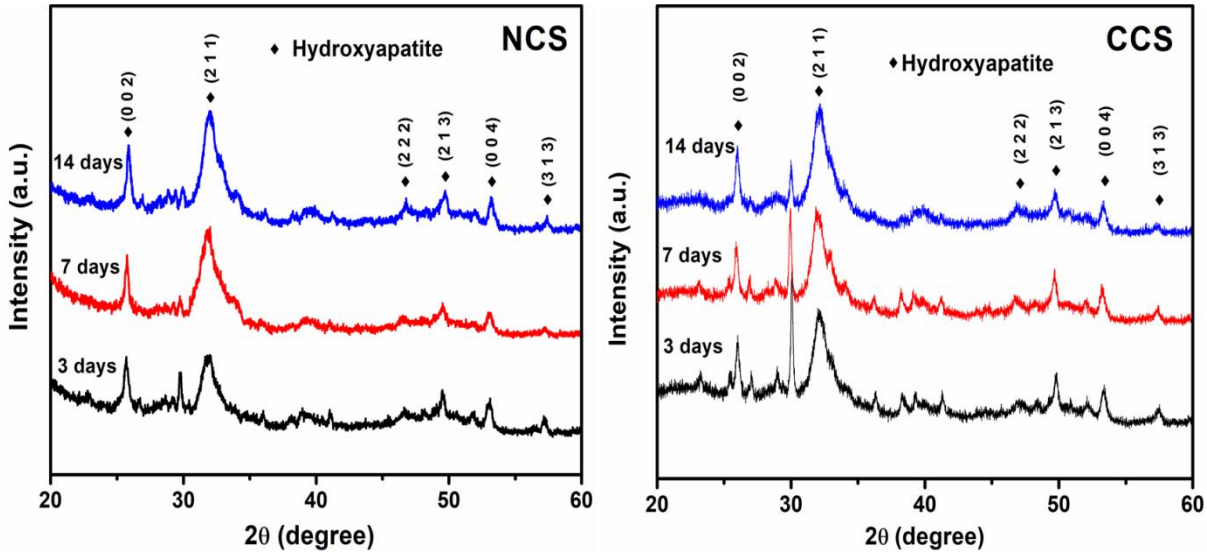

Fig. 4.6 XRD patterns of the NCS and CCS ceramics after immersion in SBF solution for 3, 7, 14 days

Fig. 4.7 and 4.8 displays the surface micrographs and EDS spectra of SBF immersed NCS and CCS ceramics surface, respectively. The surface micrographs showed more obvious evidence for new precipitated hydroxyapatite phase by the presence of white colour spherical shaped particles with agglomeration on the sample surface. However, it can be clearly seen that the development of apatite phase on NCS ceramics surface was higher with more compactness than that on CCS ceramics, which illustrates high biological activity of NCS ceramics. EDS analysis results showed that the newly precipitated phase after soaking in SBF solution contains mainly Ca, P and O. However, Si was still present in the sediments on CCS samples after 14 days of incubation. The NCS sample after incubation in SBF solution for 14 days generated a Ca:P of 1.94 whereas for CCS sample it was about 1.91. The obtained

atomic ratio of Ca:P after 14 days of soaking showed the formation of carbonated hydroxyapatite (CHA) on the surface of the ceramics [34].

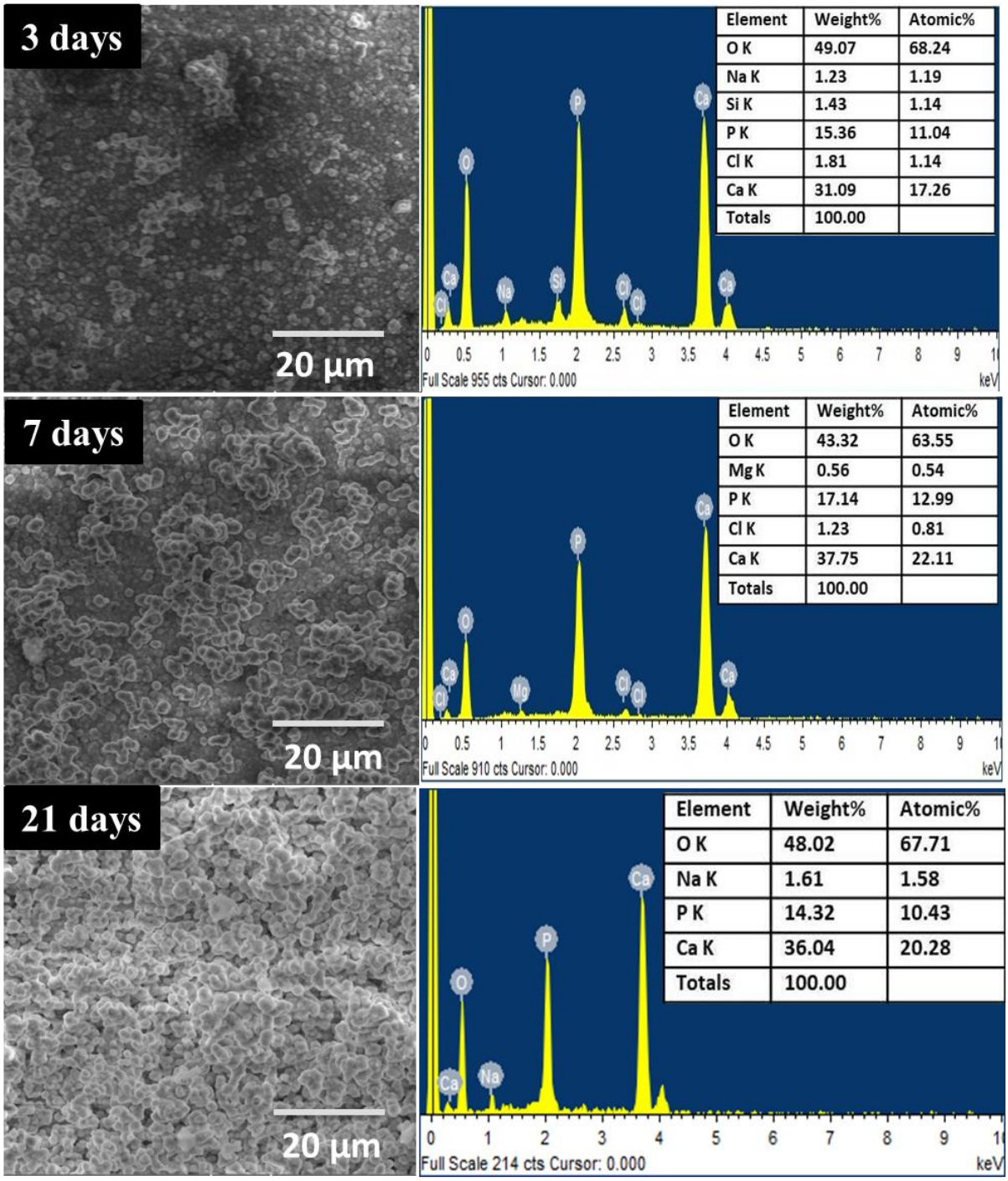

Fig. 4.7 SEM - EDS of NCS after soaking in SBF solution for 3, 7, 14 days

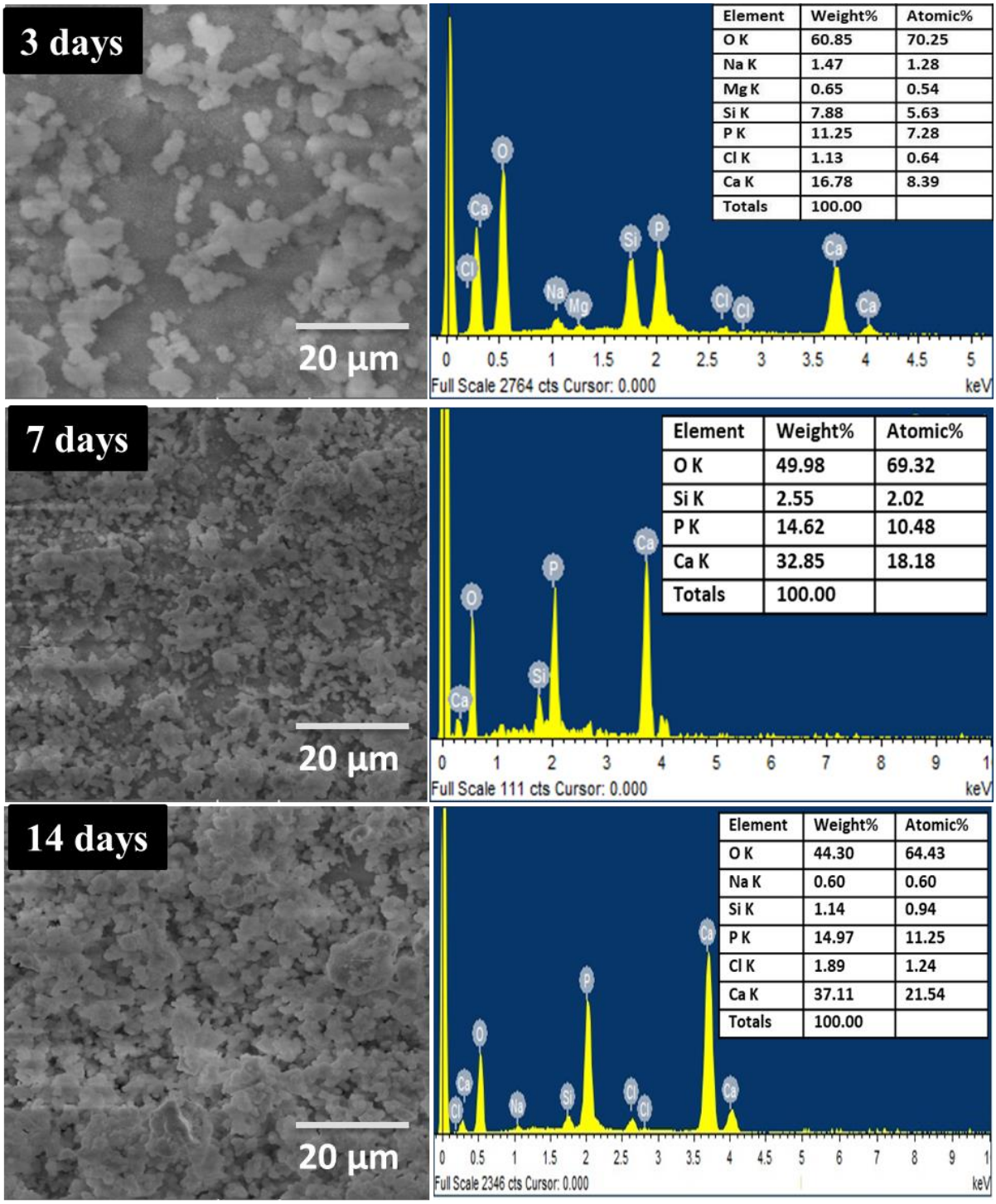

Fig. 4.8 SEM - EDS of CCS after soaking in SBF solution for 3, 7, 14 days

FTIR spectra (Fig. 4.9) showed the characteristic peaks after biomimetic process in SBF solution, the peaks resulting from the original phase of the ceramics got weaker and some new peaks appeared at ~ 563, ~ 800 and ~ 960 cm^{-1} related to Si-OH [35, 36]. This was

the result of network dissolution by the action of H^+ or H_3O^+ ions from the solution on Si-O-Si bonds, which formed silanol [Si (OH) $_4$] groups. On prolonged soaking period, calcium ions first got attached to silanol groups leading to the crystallization of hydroxyapatite. The appearance of a peak at ~ 601 cm^{-1} along with ~ 1033 cm^{-1} and ~ 1093 cm^{-1} indicates the characteristics of crystalline hydroxyapatite [25, 37]. Moreover it can be seen that the peaks in NCS ceramics became stronger than in CCS ceramics. The small shoulder at ~ 874 cm^{-1} along with band at 1418-1487 cm^{-1} corresponding to the C-O stretching of the carbonate group (CO_3^{2-}) was also observed, which revealed the growth of carbonated hydroxyapatite (CHA) on the samples [38].

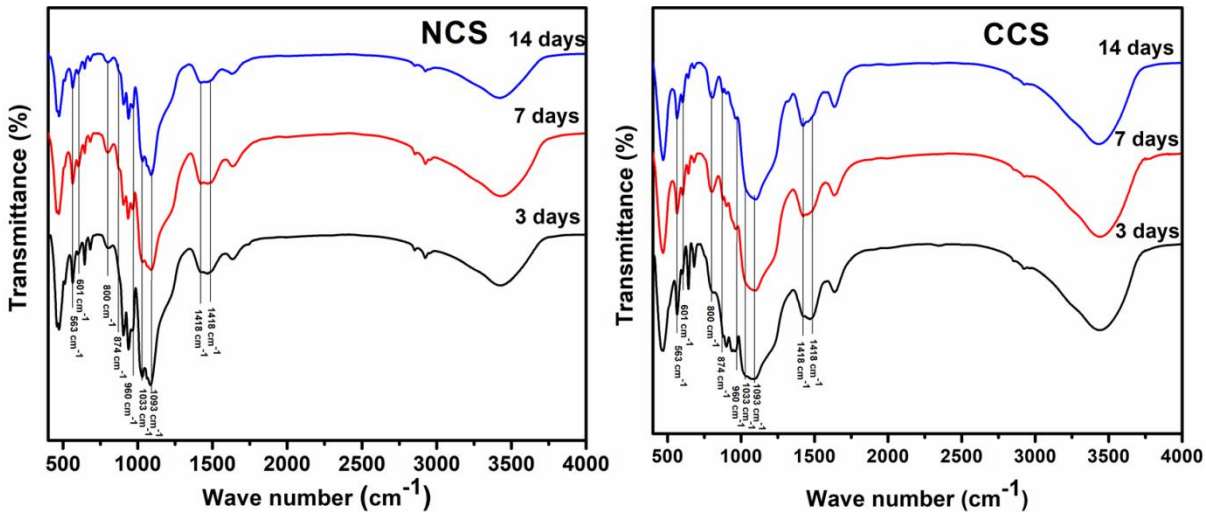

Fig. 4.9 FTIR spectra of NCS and CCS ceramics after immersion in SBF solution for 3, 7, 14 days

4.2.4 Change in pH of SBF solution

Fig. 4.10 illustrates the variation in pH level of SBF solution for the duration of immersion from day 1 to 14 days. The controlled pH level of SBF solution prior to soaking is 7.4. The pH level of the solution increased rapidly during initial immersion period (up to 5 days) for both the ceramics in accordance with previous reports [39]. After 5 days, the increase in pH level of the solution becomes relatively slow. After day 12, the increase in pH

level was maximum for CCS (from 7.4 to 8.03±0.015), whereas this increase was minimum for NCS (from 7.4 to 7.7±0.014). These results demonstrate that the pH values found for NCS samples were lower than for CCS samples which may be assumed because of slow degradation rate of NCS as compared to CCS ceramics. The release of Ca^{2+} ions is accountable for increase in pH value as the ions are replaced with H^+ or H_3O^+ ions in solution due to which concentration of OH^- ions increases. The increase in pH value become slower with prolonged time because of the solution becomes supersaturated and ion exchange reaction ultimately ceases [4, 40].

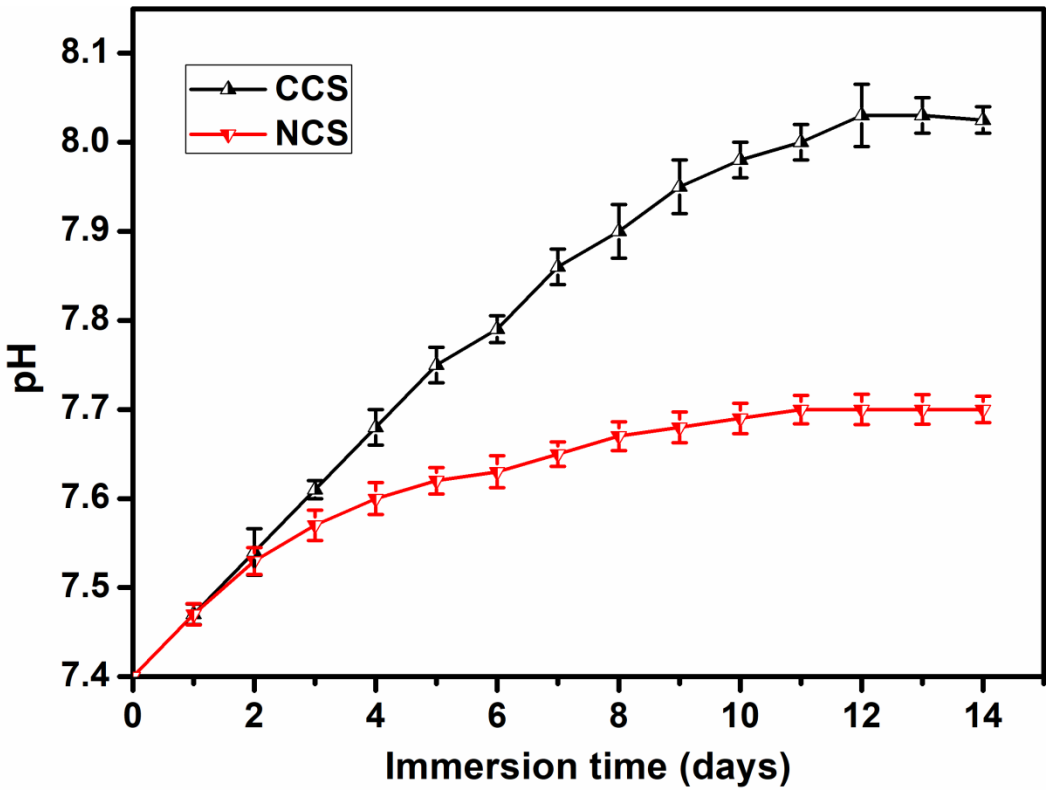

Fig. 4.10 Variation in pH of SBF solution for NCS and CCS ceramics with immersion time

4.2.5 Degradation

The degradation rate (weight loss %) of NCS and CCS ceramics was carried out in Tris-HCl solution for a time period from 1 to 21 days and the results are presented in Fig. 4.11. It was evident the degradation rate increased almost linearly on immersion time for both

the samples. A significant difference in rate of degradation was observed in ceramics. After one day, the degradation rate of NCS ceramics reached ~ 2.5% while for CCS ceramics it was ~ 4.25% and after 21 days, the degradation rate of NCS ceramics reached ~ 21.5% while for CCS ceramics it was ~ 42.7%. Degradability is one of the important features that the bioactive material must fulfil [41]. The rate of degradation is closely related to the bioactivity of the material. Network connectivity and microstructure are the main factors that affect the degradability and hence bioactivity. A very high rate of degradation produces high concentration of ions, which is responsible for higher pH change in surrounding environment. Cellular proliferation is not possible to stimulate if low ionic concentrations resulted from very slow dissolution rates [42]. The current study revealed that the prepared NCS ceramics presented considerable degradation rate in Tris-HCl solution and its degradation rate was lower than CCS ceramics over the whole immersion period, suggesting its use as a potential material in biomedical applications.

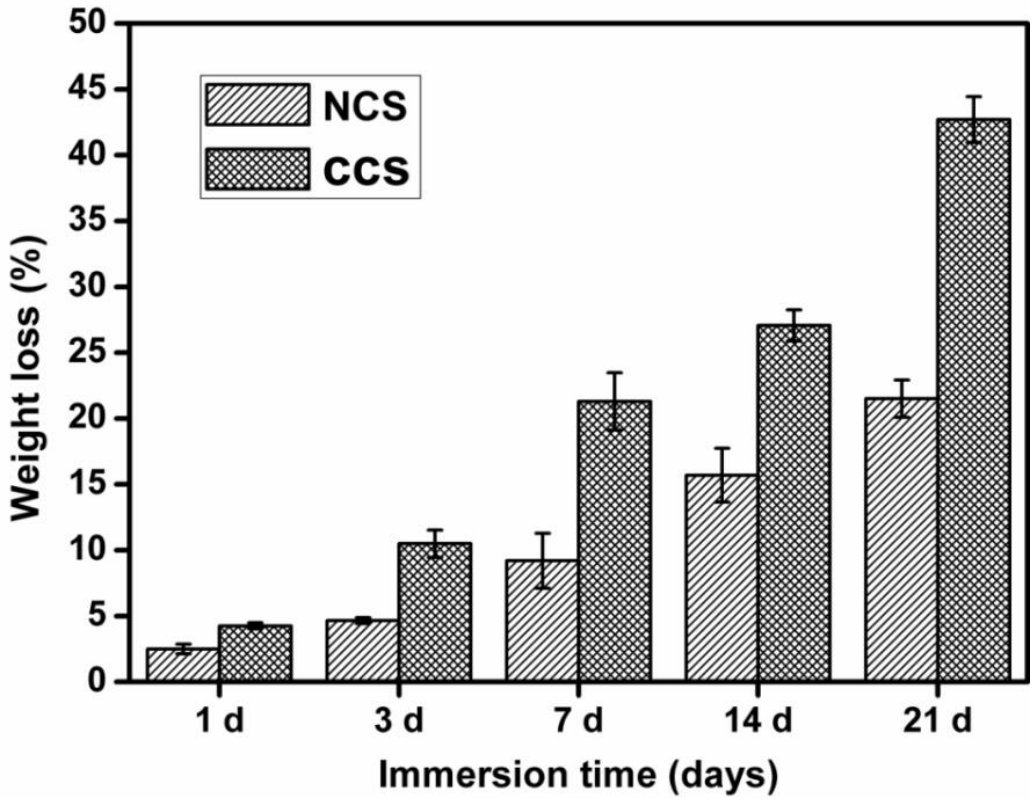

Fig. 4.11 Weight loss of NCS and CCS as a function of immersion time in Tris-HCl

4.2.6 Cytocompatibility

Cytocompatibility was investigated using MTT assay of MG-63 cells cultured with ceramic samples at various concentration (1000 µg/mL to 50 µg/mL). MTT assay is based on the cell metabolic ability in converting MTT to formazan crystals with live cells, where these crystals give out a coloured product when dissolved in acidified isopropanol, measured as optical density (OD) values. The optical density values give an indicator for the respective number of viable cells. The results of cell cytocompatibility study are profiled in Fig. 4.12(a). As can be observed from the results, there is no significant difference in the cell viability of MG-63 cells after treating with different dosage (1000 µg/mL to 50 µg/mL) of NCS and CCS ceramics compared to controlled cell viability. Moreover, cell viability is unaffected by ceramic particles. As per the International Organization for Standardization (ISO) 10993 – 5: 2009, biological evaluation of medical devices - part 5: tests for *in vitro* cytotoxicity – if the relative cell viability for the highest concentration of the sample is greater than 70 % of the control group, then the material shall be considered non-cytotoxic [43]. In the present study, the cell viability in NCS ceramics was greater than 85 % even at higher concentration (1000 µg/mL). Therefore the cytocompatible nature of NCS ceramics is amply confirmed along with CCS ceramics.

The cytocompatibility test results showed the non-toxic nature of NCS and CCS ceramic particles when treated with MG-63 cells for 24 h at various concentrations (1000 µg/mL to 50 µg/mL). However, the MTT assay was also used to evaluate the effect of the ceramic particles on cell proliferation. MG-63 cells were treated with conditioned medium obtained from incubation of 200 µg/mL ceramic particles in DMEM containing 10% FBS. Cell viability plots of the control group and after being treated with NCS and CCS ceramic particles were obtained on 1, 3, 5 and 7 days (Fig. 4.12 (b)). The results showed NCS

ceramic particles had a positive role in simulating cell proliferation along with CCS ceramic particle. Significant increase in cell viability in NCS ceramic samples was observed compared with control group at 1, 3, 5 and 7 days of incubation time. It is speculated that the biological response of the cells depends on the release of Ca^{2+} ion concentration resulted from dissolution of compounds. For example, a Ca^{2+} ion concentration of 2-6 mM favored cell survival and proliferation, whereas slightly higher concentration of 6-10 mM favored differentiation and matrix mineralization and the concentration beyond 10 mM provide to be detrimental to cells [42, 44].

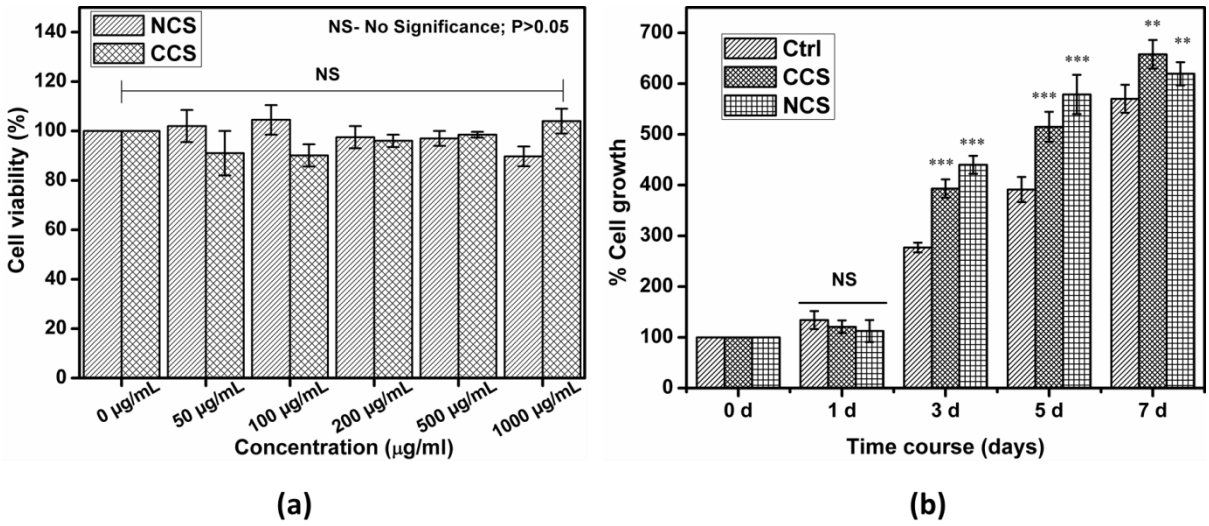

Fig. 4.12 Cell viability (a) and proliferation (b) of NCS and CCS ceramics with MG-63 cells using MTT assay ***P<0.001, ** P<0.01, *P<0.05 was used as significant

4.2.7 Antimicrobial activity

The antimicrobial activity of NCS and CCS ceramics was determined against *E.coli* and *S.aureus* bacteria by means of disc diffusion technique in discs of 10 mm diameter. Antibacterial activity was assessed by determining the diameter of inhibition zone against bacteria after 24 hours of incubation. Surprisingly an excellent inhibition zone was observed for NCS ceramics on two different bacteria (Fig.4.13). The inhibition zone was measured as 16.5 mm for *E. coli* and 15 mm for *S. aureus*, which can be seen in Fig. 4.13(b) by the

creation of grey colour bacterial inhibition region. This is actually an important result that proves the antibacterial activity of NCS ceramics. From the results it is also observed that *E.coli* showed higher pathogenic inhibition than *S.aureus*. This is because of a much thicker peptidoglycan layer for the distinctive *S. aureus* [45]. However, no inhibition zones appeared on CCS ceramics which shows that there was no bactericidal activity of CCS ceramics. Therefore, it was presumed that calcium silicate ceramic, which was synthesised using calcined eggshells powder as well as RHA as source materials, inhibited bacterial growth around the sample. The antimicrobial activity of NCS ceramics could be due to calcinated eggshells. It is reported that calcium oxide produced in eggshell that is calcined at a temperature of about 900 °C can impart antimicrobial activity to the composition [46–48]. Bacterial adhesion to the implant material is the main cause of implantation infections that lead to the failure of implanted material. Several studies have been reported on ion based modification by doping the antibacterial agent (Ag, Cu and Zn) for improving antimicrobial activity of calcium silicate ceramics. This ion based modification may also affect structural integrity and toxicity levels. However, the present prepared calcium silicate using calcined eggshells showed potential action on microbial growth inhibition without doping by any antibacterial agent. Thus the prepared NCS ceramics could be a potential candidate for biomedical applications.

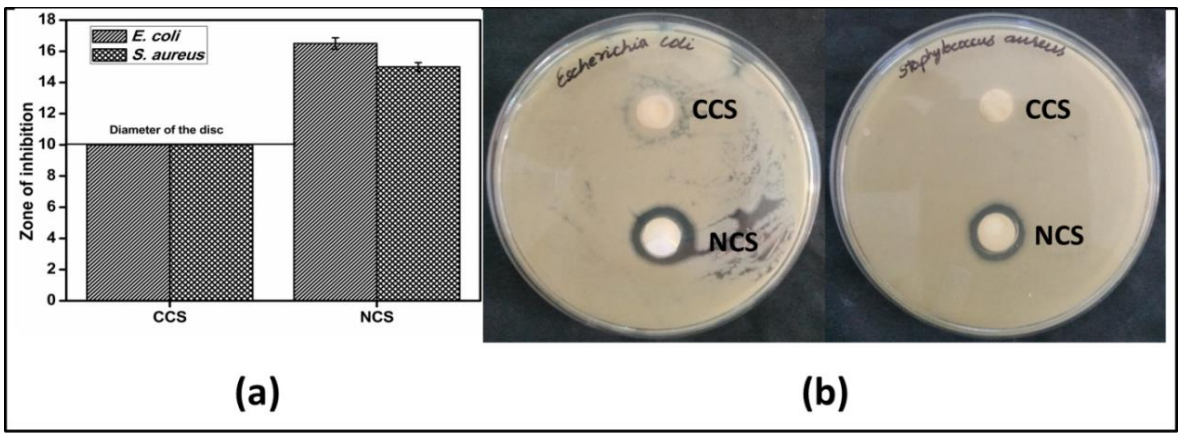

Fig. 4.13 Zone of inhibition results for NCS and CCS on *E.coli* and *S.aureus* after 24 h

4.3 Conclusion

This study compared the *in vitro* bioactivity, degradation rate, antibacterial activity, cytocompatibility and cell proliferation of wollastonite (β-$CaSiO_3$) ceramics synthesized by sol-gel method using bio-waste resources such as rice husk ash (RHA) and eggshells with β-$CaSiO_3$ prepared using tetraethylorthosilicate (TEOS) and calcium nitrate tetra hydrate (($Ca(NO_3)_2.4H_2O$). *In vitro* bioactivity results clearly showed that apatite crystals were close-packed and fine, and the growth rate was faster on NCS ceramics than on CCS ceramics. Degradation results demonstrated that NCS has slow dissolution rate than CCS ceramics. The most noticeable antimicrobial study demonstrated that NCS samples exhibit significant antimicrobial activity against *E. coli* and *S. aureus.* Cell culture study revealed that NCS ceramic particle were found to be biocompatible and demonstrate cell proliferative ability. Therefore, the results of the present study provide new insights into the development of calcium and silica-based materials from bio-waste and further enhance the significant benefits of calcium silicate in the biomedical field.

4.4 References

1. Lin K, Zhai W, Ni S, Chang J, Zeng Y, Qian W. Study of the mechanical property and in vitro biocompatibility of $CaSiO_3$ ceramics. Ceram Int. 2005;31(2):323-6.

2. Liu X, Morra M, Carpi A, Li B. Bioactive calcium silicate ceramics and coatings. Biomedicine and Pharmacotherapy. 2008;62(8):526-9.

3. De Aza PN, Luklinska ZB, Anseau MR, Hector M, Guitián F, De Aza S. Reactivity of a wollastonite-tricalcium phosphate Bioeutectic(®) ceramic in human parotid saliva. Biomaterials. 2000; 21(17):1735-41.

4. Liu X, Ding C, Chu PK. Mechanism of apatite formation on wollastonite coatings in simulated body fluids. Biomaterials. 2004;25(10):1755–61.

5. Ismail H, Shamsudin R, Abdul Hamid MA, Rozidawati A. Mechanism of Apatite Formation on β-wollastonite Sample Surface Synthesized from Rice Husk Ash. Sains Malaysiana. 2016; 45(12):1779-85.

6. Ni S, Chang J, Chou L, Zhai W. Comparison of osteoblast-like cell responses to calcium silicate and tricalcium phosphate creamics in vitro. J Biomed Mater Res - Part B Appl Biomater. 2007; 80(1):174-83.

7. Wang C, Lin K, Chang J, Sun J. Osteogenesis and angiogenesis induced by porous β-CaSiO3/PDLGA composite scaffold via activation of AMPK/ERK1/2 and PI3K/Akt pathways. Biomaterials. 2013; 34(1):64-77.

8. Xu S, Lin K, Wang Z, Chang J, Wang L, Lu J, et al. Reconstruction of calvarial defect of rabbits using porous calcium silicate bioactive ceramics. Biomaterials. 2008;29(17):2588–96.

9. Vichaphund S, Kitiwan M, Atong D, Thavorniti P. Microwave synthesis of wollastonite powder from eggshells. J Eur Ceram Soc. 2011;31(14):2435–40.

10. Abd Rashid R, Shamsudin R, Abdul Hamid MA, Jalar A. In-vitro bioactivity of wollastonite materials derived from limestone and silica sand. Ceram Int. 2014; 40(5):6847-53.

11. Ismail H, Shamsudin R, Abdul Hamid MA. Effect of autoclaving and sintering on the formation of β-wollastonite. Mater Sci Eng C. 2016;58:1077–81.

12. Azeena S, Subhapradha N, Selvamurugan N, Narayan S, Srinivasan N, Murugesan R, et al. Antibacterial activity of agricultural waste derived wollastonite doped with copper for bone tissue engineering. Mater Sci Eng C. 2017;71:1156–65.

13. Wang Y, Song J, Guo Q, Xi X, Hou G, Wei G, et al. The environmental sustainability of synthetic wollastonite using waste from zirconium oxychloride production. J Clean Prod. 2016; 172:2576-84.

14. Hossain SS, Roy PK. Study of physical and dielectric properties of bio-waste-derived synthetic wollastonite. J Asian Ceram Soc. 2018; 6(3):289-98.

15. Arcos D, Vallet-Regí M. Sol-gel silica-based biomaterials and bone tissue regeneration. Acta Biomaterialia. 2010;6:2874–88.

16. Faure J, Drevet R, Lemelle A, Ben Jaber N, Tara A, El Btaouri H, et al. A new sol-gel synthesis of 45S5 bioactive glass using an organic acid as catalyst. Mater Sci Eng C. 2015;47:407–12.

17. Hench LL, West JK. The Sol-Gel Process. Chem Rev. 1990;90(1):33–72.

18. Chrysafi R, Perraki T, Kakali G. Sol-gel preparation of $2CaO{\cdot}SiO_2$. J Eur Ceram Soc. 2007; 27(2-3):1707-10.

19. Meiszterics A, Sinkó K. Sol-gel derived calcium silicate ceramics. Colloids Surfaces A Physicochem Eng Asp. 2008;319(1–3):143–8.

20. Li HC, Wang DG, Chen CZ. Effect of zinc oxide and zirconia on structure, degradability and in vitro bioactivity of wollastonite. Ceram Int. 2015;41(8):10160–9.

21. Flower GL, Latha SV, Rao KV. Novel characterization of nanosilver fluid through ultrasonic studies supported by UV-Vis spectroscopy, DLS and TEM studies. J Mol Liq. 2016; 221:333-8.

22. Swann GEA, Patwardhan S V. Application of Fourier Transform Infrared Spectroscopy (FTIR) for assessing biogenic silica sample purity in geochemical analyses and palaeoenvironmental research. Clim Past. 2011;7(1):65–74.

23. El-Kady AM, Ali AF, Rizk RA, Ahmed MM. Synthesis, characterization and microbiological response of silver doped bioactive glass nanoparticles. Ceram Int. 2012;38(1):177–88.

24. Dong Z, Yang Q, Mei M, Liu L, Sun J, Zhao L, et al. Preparation and characterization of fluoride calcium silicate composites with multi-biofunction for clinical application in dentistry. Compos Part B Eng. 2018; 143:243-9.

25. Li HC, Wang DG, Chen CZ, Weng F, Shi H. Influence of different amount of Na_2O additive on the structure, mechanical properties and degradability of bioactive wollastonite. Ceram Int. 2016;42(1):1439–45.

26. Evangeline B, Azeem PA, Prasada Rao R, Swati G, Haranath D. Structural and luminescent features of cerium doped $CaZrO_3$blue nanophosphors. J Alloys Compd. 2017; 705:618-23.

27. Lucacel Ciceo R, Trandafir DL, Radu T, Ponta O, Simon V. Synthesis, characterisation and in vitro evaluation of sol-gel derived SiO_2-P_2O_5-CaO-B_2O_3 bioactive system. Ceram Int. 2014; 40(7)9517-24.

28. Vakalova T V., Karionova NP, Pogrebenkov VM, Vereshchagin VI, Gorbatenko V V. Features of solid phase synthesis of wollastonite from natural and technogenic raw material. Refract Ind Ceram. 2010; 51(4):295-01.

29. Tuzhovska ZS, Dutova KP, Bobkova NM, Tuzhovka V V. Study of the structure and the crystallization process of calcium metasilicate glass by ir spectroscopy. J Appl Spectrosc. 1974; 20(6):772-4.

30. Handke M, Sitarz M, Rokita M, Galuskin E. Vibrational spectra of phosphate-silicate biomaterials. In: Journal of Molecular Structure. 2003. 651:39-54.

31. Sitarz M, Handke M, Mozgawa W. FTIR studies of the cyclosilicate-like structures. In: Journal of Molecular Structure. 2001. 596(1-3):185-9.

32. Surmenev RA, Surmeneva MA, Ivanova AA. Significance of calcium phosphate coatings for the enhancement of new bone osteogenesis - A review. Acta Biomaterialia. 2014. 10(2):557-79.

33. Ergun C, Evis Z, Webster TJ, Sahin FC. Synthesis and microstructural characterization of nano-size calcium phosphates with different stoichiometry. Ceram Int. 2011; 37(3):971-7

34. Sainz MA, Pena P, Serena S, Caballero A. Influence of design on bioactivity of novel $CaSiO_3$-$CaMg(SiO_3)_2$ bioceramics: In vitro simulated body fluid test and thermodynamic simulation. Acta Biomater. 2010; 6(7):2797-807.

35. Catauro M, Bollino F, Renella RA, Papale F. Sol-gel synthesis of SiO2-CaO-P2O5 glasses: Influence of the heat treatment on their bioactivity and biocompatibility. Ceram Int. 2015; 41(10):12578-88.

36. Innocenzi P. Infrared spectroscopy of sol-gel derived silica-based films: A spectra-microstructure overview. J Non Cryst Solids. 2003; 316:(2-3):309-19.

37. Li P, Ohtsuki C, Kokubo T, Nakanishi K, Soga N, Nakamura T, et al. Process of formation of bone-like apatite layer on silica gel. J Mater Sci Mater Med. 1993; 4(2):127-31.

38. Barralet J, Best S, Bonfield W. Carbonate substitution in precipitated hydroxyapatite: An investigation into the effects of reaction temperature and bicarbonate ion concentration. J Biomed Mater Res. 1998; 41:79-86.

39. Wang K, Leng Y, Lu X, Ren F, Geb X, Ding Y. Theoretical analysis of calcium phosphate precipitation in simulated body fluid. Biomaterials. 2005; 26(10):1097-108.

40. Zia R, Riaz M, Maqsood S, Anjum S, Kayani Z, Hussain T. Titania doped bioactive ceramics prepared by solid state sintering method. Ceram Int. 2015; 41(7):8964-72.

41. Hench LL, Polak JM. Third-generation biomedical materials. Science. 2002;

295(5557):1014-7.

42. Hench LL. The story of Bioglass®. In: Journal of Materials Science: Materials in Medicine. 2006;17(11):967–78.

43. International Organization for Standardization. Biological evaluation of medical devices - Part 5: Tests for in vitro cytotoxicity. Iso 10993–5. 2009. p. 10993-5.

44. Maeno S, Niki Y, Matsumoto H, Morioka H, Yatabe T, Funayama A, et al. The effect of calcium ion concentration on osteoblast viability, proliferation and differentiation in monolayer and 3D culture. Biomaterials. 2005; 26(23):4847-55.

45. Ou SF, Chung RJ, Lin LH, Chiang YC, Huang CF, Ou KL. A mechanistic study on the antibacterial behavior of silver doped bioceramic. J Alloys Compd. 2015; 629:362-7.

46. Ohshima Y, Takada D, Namai S, Sawai J, Kikuchi M, Hotta M. Antimicrobial Characteristics of Heated Eggshell Powder. Biocontrol Sci. 2015; 20(4):239-46.

47. Wellman-Labadie O, Picman J, Hincke MT. Antimicrobial activity of cuticle and outer eggshell protein extracts from three species of domestic birds. Br Poult Sci. 2008; 49(2):133-43.

48. Wellman-Labadie O, Lakshminarayanan R, Hincke MT. Antimicrobial properties of avian eggshell-specific C-type lectin-like proteins. FEBS Lett. 2008; 582(5):699-704.

Chapter 5

In vitro evaluation of silver doped wollastonite synthesized from bio-waste

Present chapter throws light on the dopant effect on structural and biological properties of wollastonite ceramics. The orthopedic implants bring with it the risk of adherence and colonization of bacteria on the implant surface, which causes the failure of implant and bacterial infections. As silver (Ag) is an antibacterial agent that shows strong biocidal effect against 12 species of bacteria including Staphylococcus aureus (S. aureus) and Escherichia coli (E. coli), Ag was doped into wollastonite with the objective of improving antibacterial activity, where Ag doping concentration varied from 2 mol.% to 6 mol.% and its effect on in vitro bioactivity, degradation rate, change in pH of SBF solution and antimicrobial activity of wollastonite was studied.

5.1 Introduction

The necessity of implantation for damaged or diseased parts of the body is not only for mechanical support but also to restore their physiological functions. This indubitably has been the motivating factor for research into the developing of new materials in biomedical applications. Bioactive materials are a class of biomaterials, having two primary important properties of biocompatibility and bioactivity [1]. The first property deals with the acceptance of material with surrounding tissues by not being toxic, injurious and not causing immunological rejection while the latter has the ability to form a bond with living tissues under physiological conditions. The bioactive materials, comprising of bioactive glasses and ceramics explored for biomedical applications are mainly of three types calcium silicate, borate and phosphate based materials [2, 3]. Materials based on calcium silicate received warm response as bioactive materials, and they have found applications in repairing hard tissue texture and for regeneration as well as for ossicular prostheses and alveolar ridge resorption [4, 5].

Wollastonite ($CaSiO_3$) is the most common calcium silicate ceramic; it has proven to be a potential candidate for scaffolds for bone tissue engineering (BTE) as it shows excellent bioactivity and biocompatibility [2, 6–8]. *In vitro* and *in vivo* studies results revealed that it has the ability to form bond with soft tissues, hard tissues and form carbonated hydroxyapatite (CHA) layer on its surface. This layer has similar chemical and crystallographic construction as bone mineral phase and exhibits osteoconductive properties for bone growth [9, 10]. The addition of small amount of transition metal ions (Ti, Zr, Cu, Zn, Mg, Ag) in calcium silicate ceramics enhances their osteogenic properties, thereby promoting the attachment, proliferation and differentiation of human mesenchyme stem cells and osteoblast cells [11, 12]. Titanium (Ti) and zirconia (Zr) have been traditionally used as

implantable materials in orthopedic applications as they have shown excellent biocompatibility with the host tissue [13]. Thus the incorporation of these ions into calcium silicate ceramics improves chemical stability and supports the proliferation of human bone derived cells (HBDC) [14–16]. The addition of copper (Cu) ions contributes to antibacterial properties and enhances the mechanical strength as Cu ions have hypoxia-mimicking ability; they potentiate endogenous cell growth or signals for bone growth [17–19]. On the other hand, it has been demonstrated that magnesium (Mg) ions plays significant role in bone remodeling and skeletal growth. Mg substituted calcium silicate ceramics have poor degradation rate [20, 21]. All the above mentioned elements are important trace elements for a living human body, and these are considered important for preserving human activities.

The orthopedic implant brings with it the risk of adherence and colonization of bacteria on the implant surface, which causes the failure of implant and bacterial infections [22]. It has been reported in several instances that silver (Ag) is an antibacterial agent that shows strong biocidal effect against 12 species of bacteria including *Staphylococcus aureus* (*S. aureus*) and *Escherichia coli* (*E. coli*). Thus Ag doped bioactive materials have received significant attention in the modern time period [22–24].

Therefore, the objective of the present study is to test the bioactivity, degradation rate and antibacterial activity of silver incorporated wollastonite synthesized using rice husk ash (RHA) and eggshell by sol-gel technique.

5.2 Results and discussion

5.2.1 Thermal analysis

TGA and DTA curves of the samples W, 2AgW, 4AgW and 6AgW (pure wollastonite, 2 mol.% Ag, 4 mol.% Ag and 6 mol.% Ag doped wollastonite ceramics are

denoted as W, 2AgW, 4AgW and 6AgW, respectively) are shown in Fig. 5.1. From TGA curves, it is observed that the thermal decomposition takes place in different steps. The weight loss below ~150 °C was ascribed to the elimination of physically adsorbed humidity water from the pores of the gel, which is reflected in DTA curves as a small endothermic peak around 90 °C [25]. While, the next step of weight loss which involved from ~220 to ~600 °C was reflected in the exothermic hump in the DTA curves of all the four samples and centered at ~415, ~382, ~370 and ~340 °C for samples W, 2AgW, 4AgW and 6AgW, respectively, which was attributed to the low temperature decarbonation [26]. The final weight loss which involved from ~600 to ~750 °C was attributed to the high temperature decarbonation [26, 27]. On the other hand, from the TGA curves for the silver doped samples (2AgW, 4AgW and 6AgW), it is observed that the total weight loss of the samples increased with increase in silver percentage [28]. In the DTA curve of pure sample, the exothermic peak at 778 °C indicated the crystallization temperature for wollastonite and it was observed that the substitution of Ag at the expense of Ca caused a shift of crystalline temperature to lower value (situated on DTA curves of the samples 2AgW, 4AgW and 6AgW at 725 °C, 700 °C and 705 °C respectively). It is also observed that the peak height and sharpness of these exothermic peaks were decreased for 2AgW, 4AgW and 6AgW samples; it shows that the amount of wollastonite crystalline phase decreased with increase in Ag content [29, 30], which further supported XRD results.

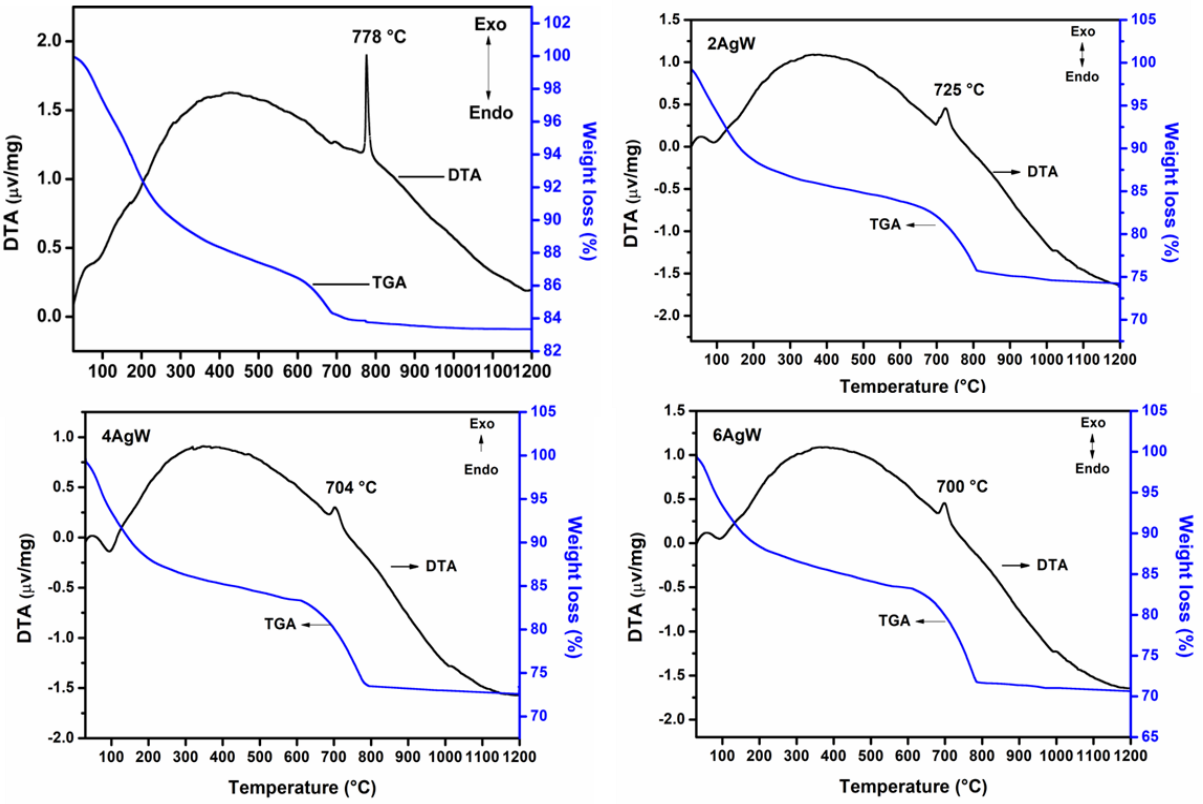

Fig. 5.1 TG-DTA curves of samples (a) W, (b) 2AgW, (c) 4AgW and (d) 6AgW

5.2.2 Structural characterization

The XRD patterns of W, 2AgW 4AgW and 6AgW powder samples sintered at 800 °C are shown in Fig. 5.2. All the diffraction peaks of sample W were indexed to β-wollastonite (JCPDS file no: 75-1396) [31, 32] and no other peaks were observed. The XRD patterns of 2AgW, 4AgW and 6AgW typically resembled the pure wollastonite phase and though no significant changes were observed, the maximum intensity peak at 29.96° decreased gradually, which indicated that there was a decrease in crystallinity with the increase in silver concentration from 2 to 6 mol.%. It was also found that the diffraction peak at 31.27° corresponded to AgO (JCPDS file No. 75-0969) [33] and the intensity of AgO peak increased with increase in silver concentration. The average crystallite size was estimated by Scherrer's formula ($D = K\lambda/\beta\cos\theta$) using full width half maxima (FWHM), which shows that the crystallite size slightly reduced from W to 6AgW as shown in Table 5.1.

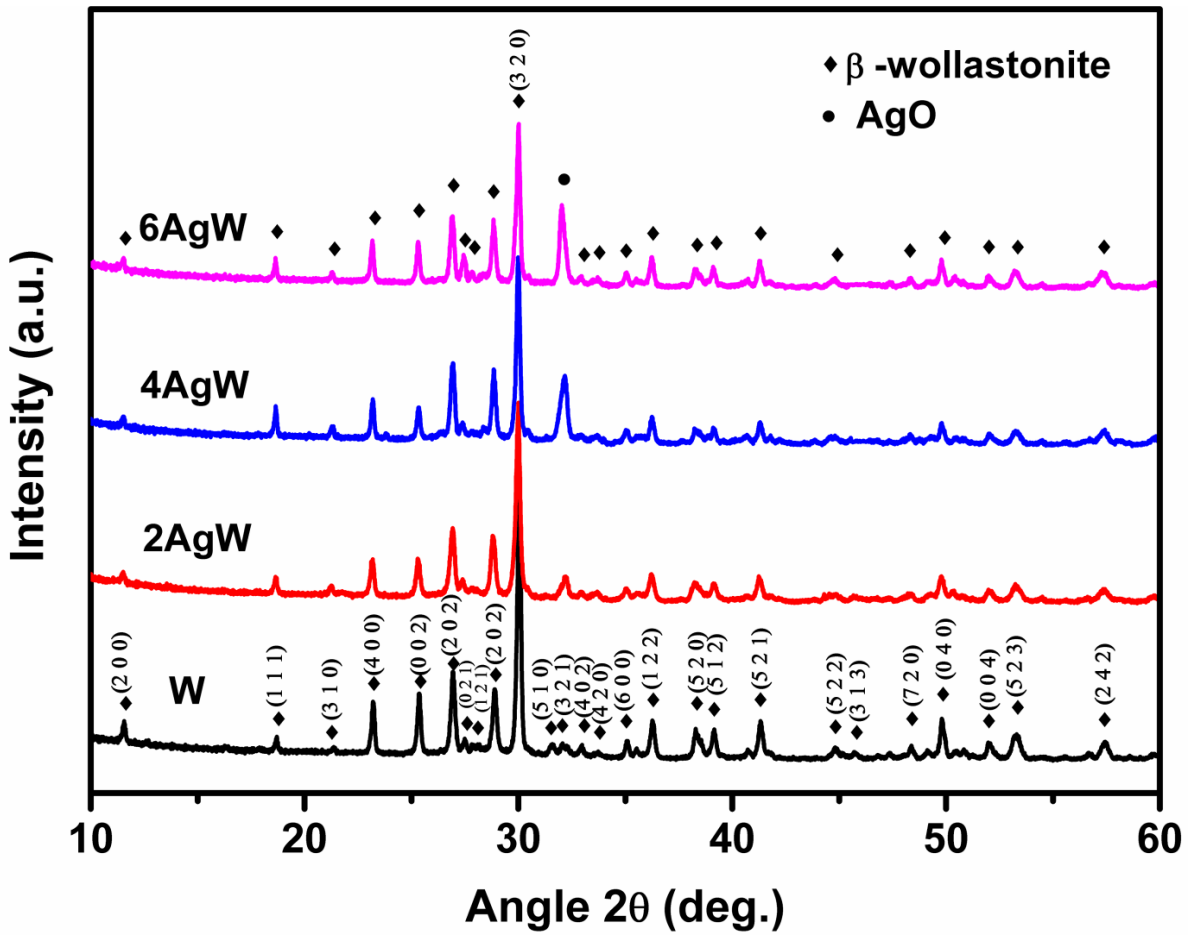

Fig. 5.2 XRD patterns of samples W, 2AGW, 4AgW and 6AgW

Table 5.1 Calculation of crystallite size for pure and silver doped wollastonite

Sr. no.	Samples	Average crystallite size (D) nm
01	W	76 ± 2.8
02	2AgW	56 ± 2.0
03	4AgW	39 ± 3.1
04	6AgW	35 ± 1.6

The surface morphology along with elemental spectra obtained from SEM- EDS analysis for pure and silver doped wollastonite ceramic pellets after sintering at 800 °C is presented in Fig. 5.3. SEM images of pure and silver doped wollastonite show porous surface, rough and irregular surface morphology. With increase of silver concentration in the wollastonite phase, larger porous structure appeared [34, 35]. However, the quantitative analysis of pure and silver doped wollastonite was analyzed by EDS spectra. The chemical

composition of pure wollastonite was confirmed by the presence of elements such as Ca, Si and O, whereas EDS spectra of silver doped wollastonite confirmed the existence of Ca, Si, O and Ag.

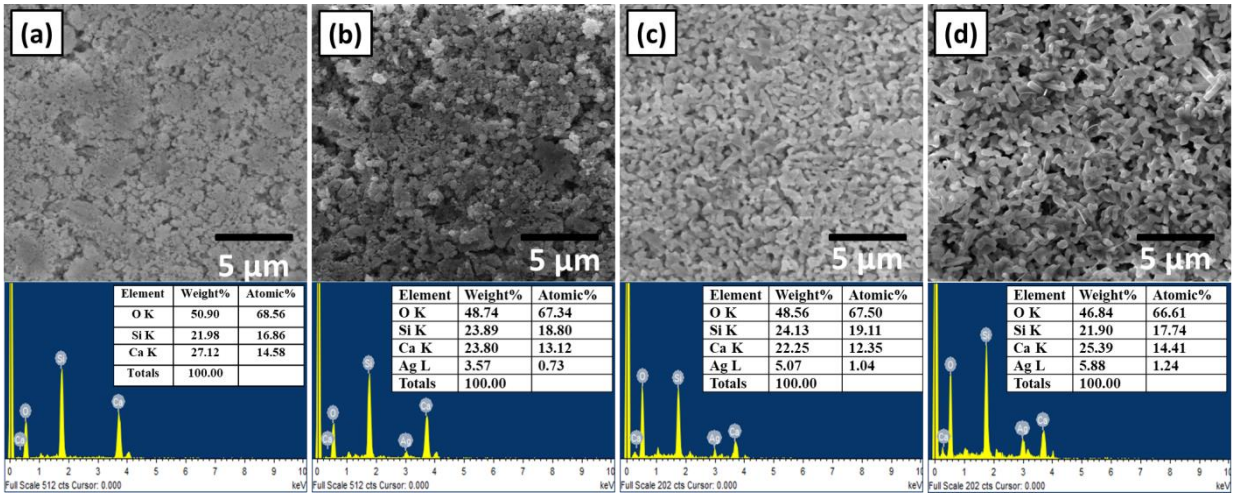

Fig. 5.3 SEM micrographs and corresponding EDS spectra ceramic pellets (a) W, (b) 2AgW, (c) 4AW and (d) 6AWA

Fig. 5.4 denotes the FTIR spectra of pure and silver doped wollastonite samples. For all samples, the characteristic bands corresponding to Si-O-Si asymmetric stretching mode was observed at 1021–1088 cm^{-1} and Si-O-Si symmetric stretching mode was identified at 646-684 and 800 cm^{-1} [36]. In addition, the IR absorption band located at 474-568 cm^{-1} was assigned to bending mode of Si-O-Si and the band situated at 903-943 cm^{-1} was attributed to non-bridging oxygen bonds (NBO) of Si-O-NBO [37]. On the other hand, the absorption peaks at 1635 cm^{-1} and 3437 cm^{-1} belonged to the O-H stretching vibrations [16]. In the FTIR spectra of 2AgW, 4AgW and 6AgW samples, no other significant difference was observed in the IR absorption bands with respect to pure wollastonite. However, it can be seen that the intensity of the silicate absorption bands decreased with increase in silver concentration. It was also found that a slight shift in wavenumber from 474 cm^{-1} to 456 cm^{-1} occurred, from

pure to silver doped wollastonite, which confirms the formation of silver incorporated wollastonite ceramics.

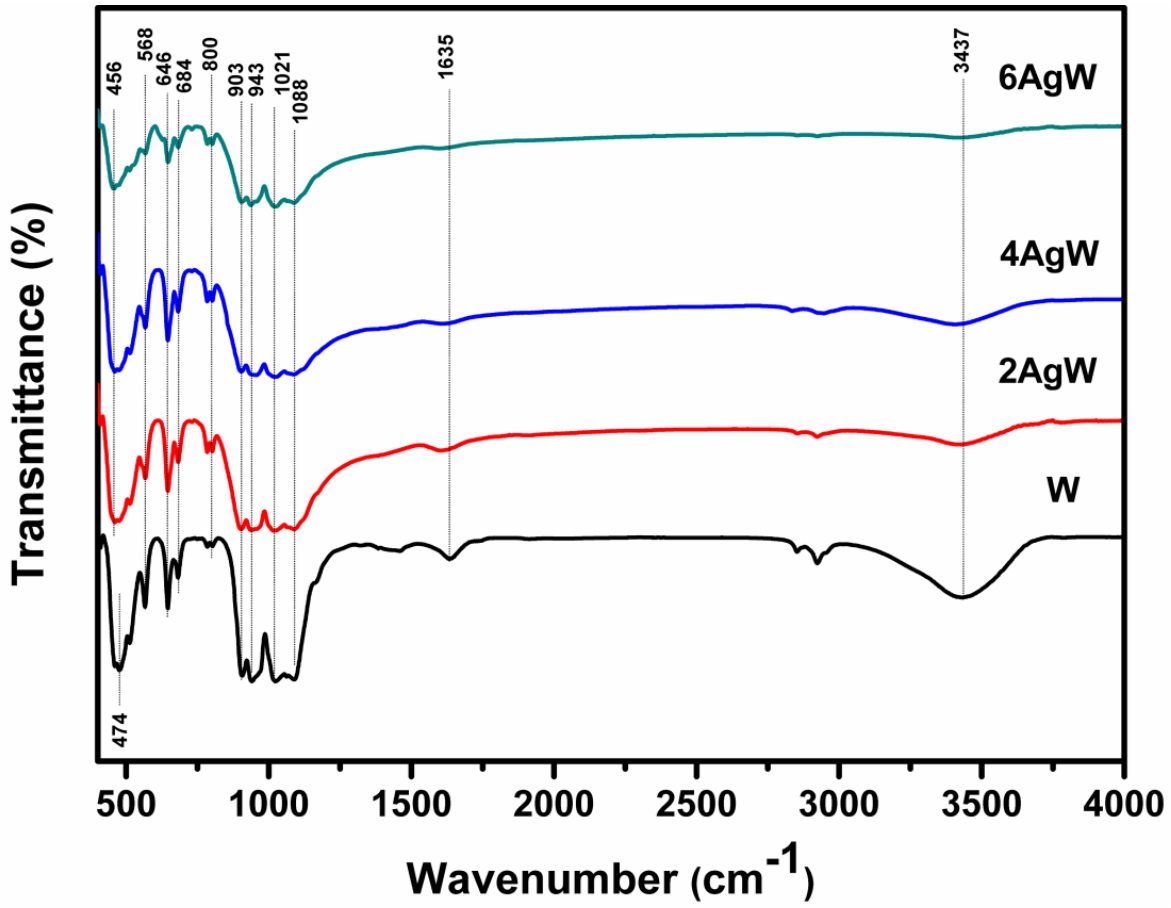

Fig. 5.4 FTIR Spectra of pure and silver doped wollastonite

5.2.3 In vitro bioactivity

In vitro bioactivity was examined by means of hydroxyapatite layer formation ability on the surface of the samples in SBF solution. Fig. 5.5 illustrates the XRD pattern of pure and silver doped wollastonite after being soaked for 7 days (Fig 5.5(a)) and 21 days (Fig. 5.5(b)) in SBF solution. The XRD pattern clearly shows the representative diffraction peaks of hydroxyapatite in all the samples in accordance with JCPDS No. 09-0432 [38, 39]. The diffraction intensity of original wollastonite phase reduced significantly and was replaced with hydroxyapatite. Further, the peak intensities of hydroxyapatite increase with increasing

exposure time in SBF solution from 7 days to 21 days. It can also be observed that the intensity of these diffraction peaks increased from W to 6AgW, demonstrating silver doped wollastonite exhibit higher hydroxyapatite mineralization on their surface compared to pure wollastonite, which further supported SEM-EDS and FTIR analysis.

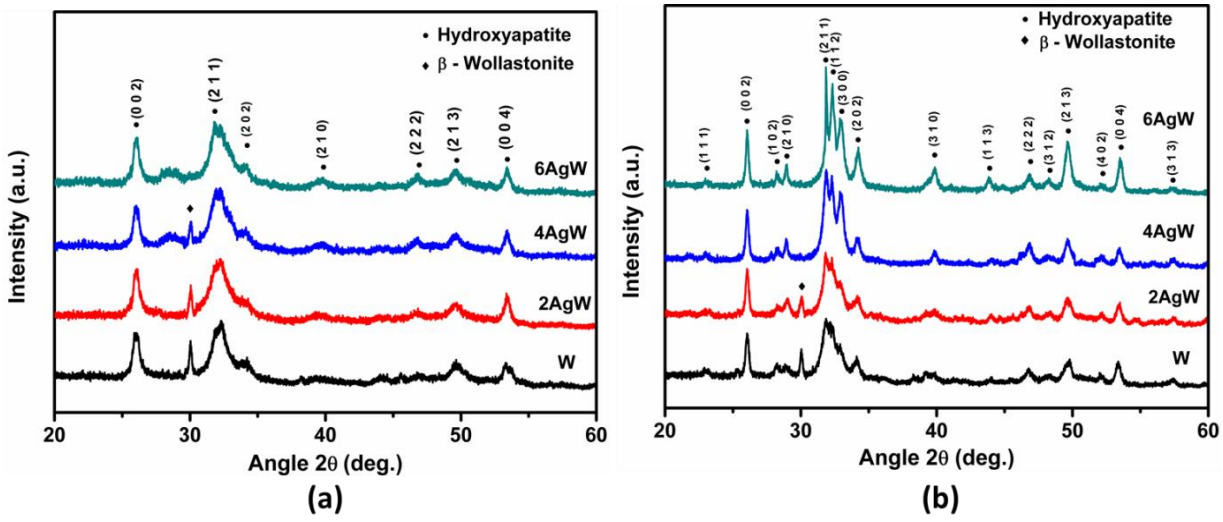

Fig. 5.5 XRD patterns of undoped and silver doped wollastonite after (a) 7 days and (b) 21 days of soaking in SBF solution

Fig. 5.6 displays the surface morphologies and corresponding elemental spectra obtained from SEM-EDS analysis for the pellets of W, 2AgW, 4AgW and 6AgW after immersion in SBF solution for 14 days. The formation of apatite layer on the surface of the samples ensures the formation of spherical shaped grains with agglomeration at lower magnification (Fig. 5.6(a_1, b_1, $c_1$and d_1)). Higher magnification SEM images (Fig. 5.6(a_2, b_2, c_2 and d_2)) demonstrated that each of these calcium phosphate spheres like grains consists of a large number of tiny flake-like crystals of calcium phosphate in good agreement with previous reports [40, 41]. The micrographs of silver doped wollastonite revealed that higher apatite nucleation on their surface than pure wollastonite and confirmed the addition of silver facilitates apatite nucleation in as prepared wollastonite [35, 42, 43]. The EDS spectra confirmed the chemical composition of hydroxyapatite by the presence of elements such as P,

Ca and O (Fig. 5.6(a_3, b_3, c_3 and d_3)).

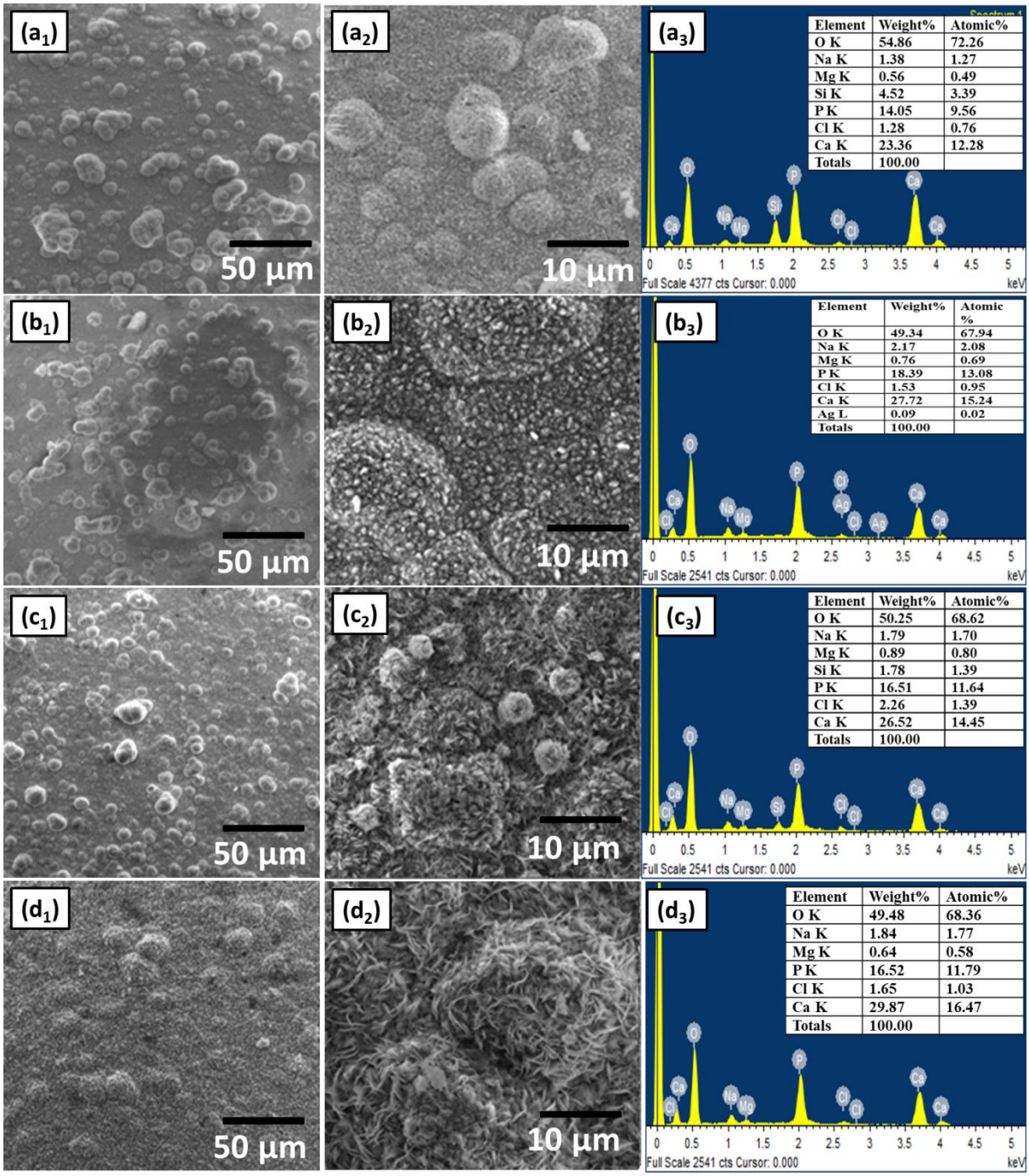

Fig. 5.6 SEM micrographs and EDS spectra of ceramics (a) W, (b) 2AgW, (c) 4AgW and (d) 6AgW after immersion in SBF solution for 14 days

Fig. 5.7 shows FTIR spectra of W, 2AgW, 4AgW and 6AgW samples after immersion in SBF solution. It is found that the silicate absorption bands corresponding to the

wollastonite phase decreased in intensity and the FTIR spectra showed new peaks positioned at 563, 607, 875, 1033, 1093, 1418 and 1468 cm^{-1} after 7 days (Fig. 5.7(a)) of incubation in SBF solution. The absorption bands at 563, 607, 1033 and 1093 cm^{-1} assigned to the phosphate (PO_4^{3-}) group, in which the band at 563-607 cm^{-1} is the characteristic feature of crystalline phosphate in hydroxyapatite [44]. In addition, the absorption bands corresponding to the carbonate group (CO_3^{2-}) were observed at 1418, 1468 and 875 cm^{-1} [16], after being soaked in SBF solution. The outcomes suggested that the formation of hydroxyapatite is in the form of hydroxyl carbonate apatite (HCA) [32, 45]. Furthermore, silicate absorption bands were almost completely disappeared and phosphate absorption peaks appeared as major peaks after 21 days (Fig. 5.7(b)) of soaking in SBF solution.

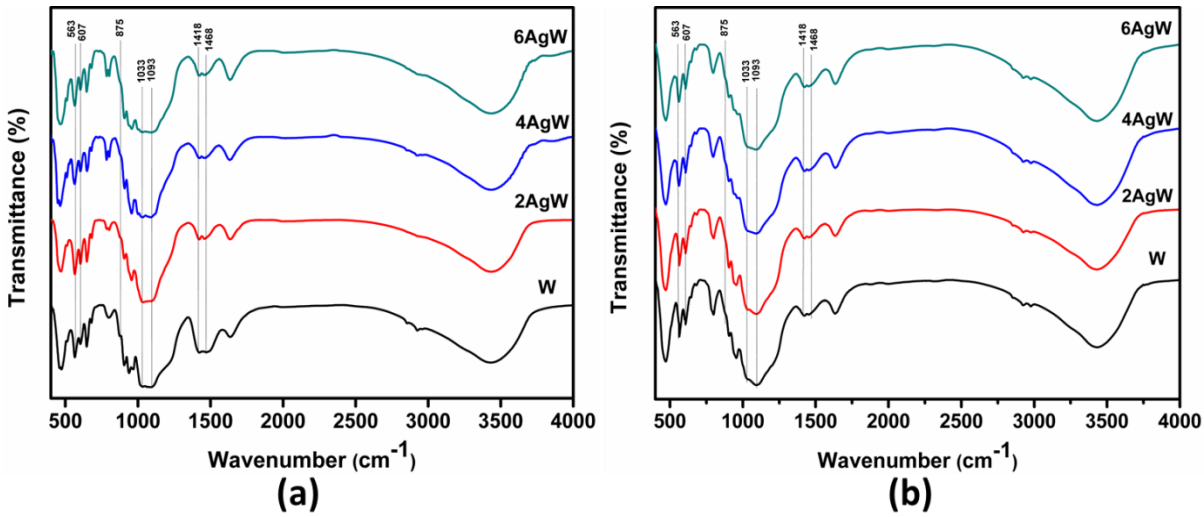

Fig. 5.7 FTIR spectra pure and silver doped wollastonite after (a) 7 days (b) 21 days of soaking in SBF solution

5.2.4 Change in pH of SBF solution

The variation in pH value of SBF solution during the first 14 days of immersion of W, 2AgW, 4AgW and 6AgW pellets was shown in Fig. 5.8. The variation in pH value of SBF is associated with the mechanism of nucleation and the development of hydroxyapatite layer on

the surface of bioactive specimens [46]. It is proposed that, when the bioactive specimen is immersed in SBF solution the cationic ions (Ca^{+2}) on surface of specimen are exchanged with H^+ and H_3O^+ ions from the solution resulting in the rapid increase of pH value of the solution at early immersion period [37, 47]. This ion leaching leads to silanol formation at higher pH level and then absorption of phosphate and calcium ions from SBF solution, as result growth of hydroxyapatite layer on the surface of specimen [48]. In the present study, a slight decrease in pH value of the solution was observed at very initial stage of immersion for silver incorporated wollastonite samples; this decrease is predicted by the initial rapid release of silver ions into the SBF solution [43]. After that considerable rise in pH value of the solution was observed. This could be due to the dissolution of Ca^{+2} ions into the solution [35, 43]. The pH values of SBF solution in W, 2AgW, 4AgW and 6AgW samples after 14 days of immersion were 7.68, 7.65, 7.63 and 7.60 respectively. It is seen that the increase in concentration of Ag in wollastonite phase reduces the pH value of SBF solution [49].

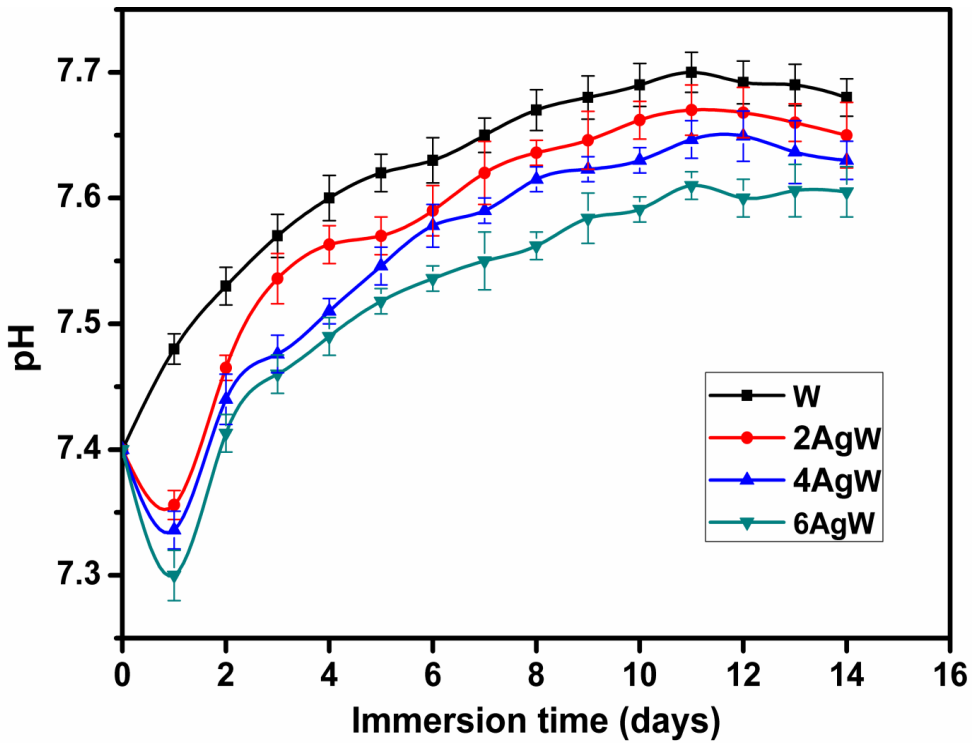

Fig. 5.8 Variations of pH value of SBF solution for pure and silver doped wollastonite with immersion time

5.2.5 Degradation

Wollastonite is a promising candidate for hard tissue regeneration because of its excellent bioactivity and osteogenic properties. However, the high dissolution rate of wollastonite, which is accountable for higher pH level in surrounding environment [37, 50], has a limit on its clinical applications. Fig. 5.9 shows the average weight loss of triplicate ceramic blocks with standard deviation as a function of immersion time in Tris-HCl solution. The weight loss was increased with increase in immersion time. After 21 days of immersion, the weight loss of the samples W, 2AgW, 4AgW and 6AgW is 24.39±1.23%, 22.89±0.24%, 21.16±0.38% and 18.86±0.55% respectively. It shows that the incorporation of Ag into wollastonite phase reduces the dissolution rate of wollastonite. Wollastonite structure contains SiO_4 tetrahedral network and Ca^{+2} ions form the link between two SiO_4 tetrahedral with non-bridging oxygen groups. These non-bridging oxygen groups are crucial in the exchange of Ca^{+2} ions with H^+ or H_3O^+ from the surrounding solution leading to higher dissolution rate of wollastonite and consequently increase in pH value of the solution. In the current study, the incorporation of silver into wollastonite at the expense of calcium would decrease the number of non-bridging oxygen groups [51] and reduce the dissolution rate of ceramic, signifying a potential preferable material for biomedical applications.

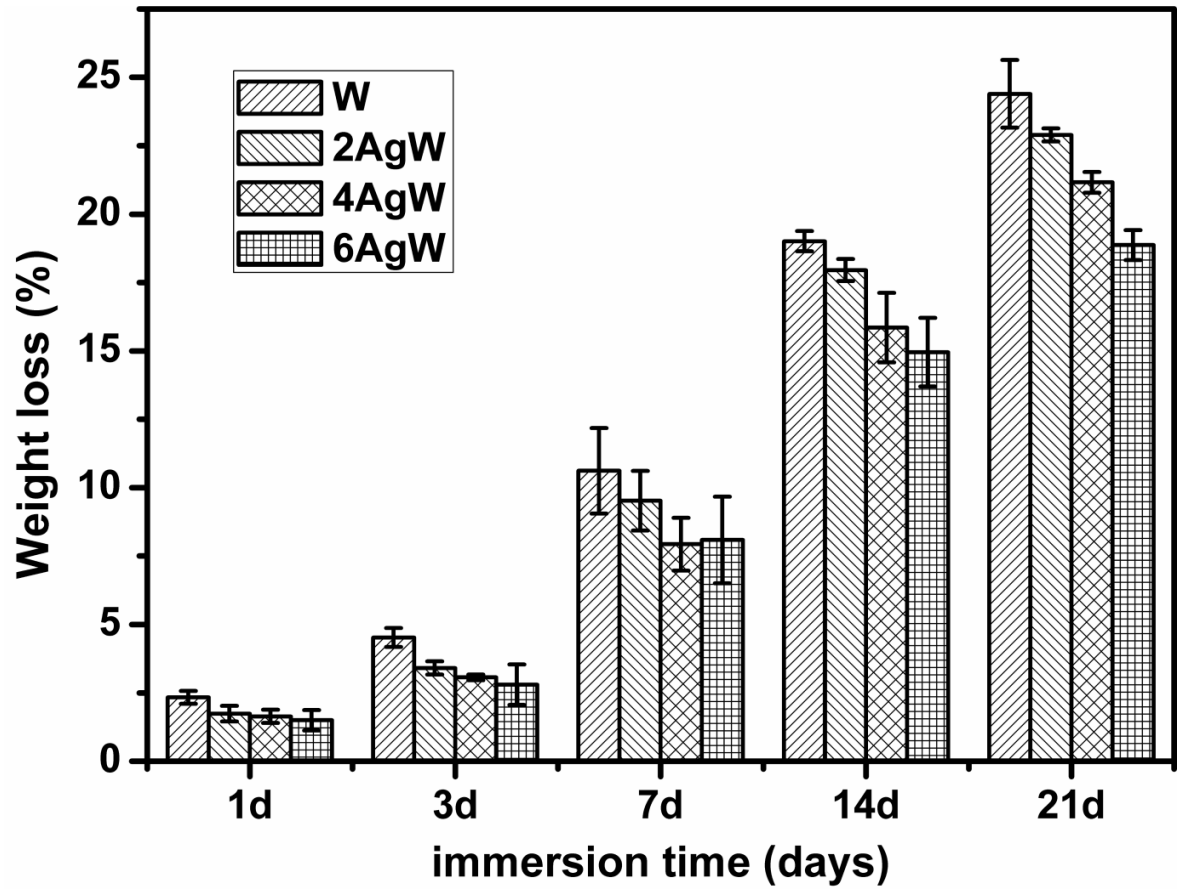

Fig. 5.9 Weight loss% for pure and silver doped wollastonite with immersion time in Tris-HCl solution

5.2.6 Antimicrobial activity

Antimicrobial assay revealed that W, 2AgW, 4AgW and 6AgW samples showed antibacterial effect against two possible sources of infection in wound curing, such as *E. coli* and *S. aureus* as shown in Fig. 5.10. Fig. 5.10 (a) and (b) demonstrate the zone of inhibition around the disc in agar plate, after 24 hours and 48 hours of incubation time, respectively. After 24 hours, the zone of inhibition by W was found to be 13 ± 0.3 mm and 12 ± 0.23 mm against *E. coli* and *S. aureus*, respectively. Therefore, W showed bactericidal activity. This is due to the bactericidal activity of CaO, which was obtained from eggshell and used in synthesis of wollastonite [52]. However, the zone of inhibition against *E. coli* was found to increase from 13 ± 0.3 mm (W) to 17.5 ± 0.24 mm (6AgW). Similarly the zone of inhibition against *S. aureus* increased from 12 ± 0.23 mm (W) to 16.5 ± 0.29 mm (6AgW). From the

results, it is very much clear that silver doped wollastonite showed elevated levels of microbial inhibition zone than pure wollastonite (Fig. 5.11a) resulting in enhanced antimicrobial activity of wollastonite [29, 53]. The samples were kept in incubator for another 24 hours to precisely observe the effect of silver. At this point, significant inhibition zone was found around silver doped wollastonite against both the pathogens, and the diameter of inhibition region was found to increase with increase in silver doping level (Fig. 5.11b). However, pure wollastonite no longer shows antibacterial activity due to the loss of CaO bactericidal ability. Hence, silver doped wollastonite effectively inhibits bacteria. On the other hand, the region of inhibition against *E. coli* was found to be larger than the region of inhibition against *S. aureus* because of the low thickness of cell wall [54].

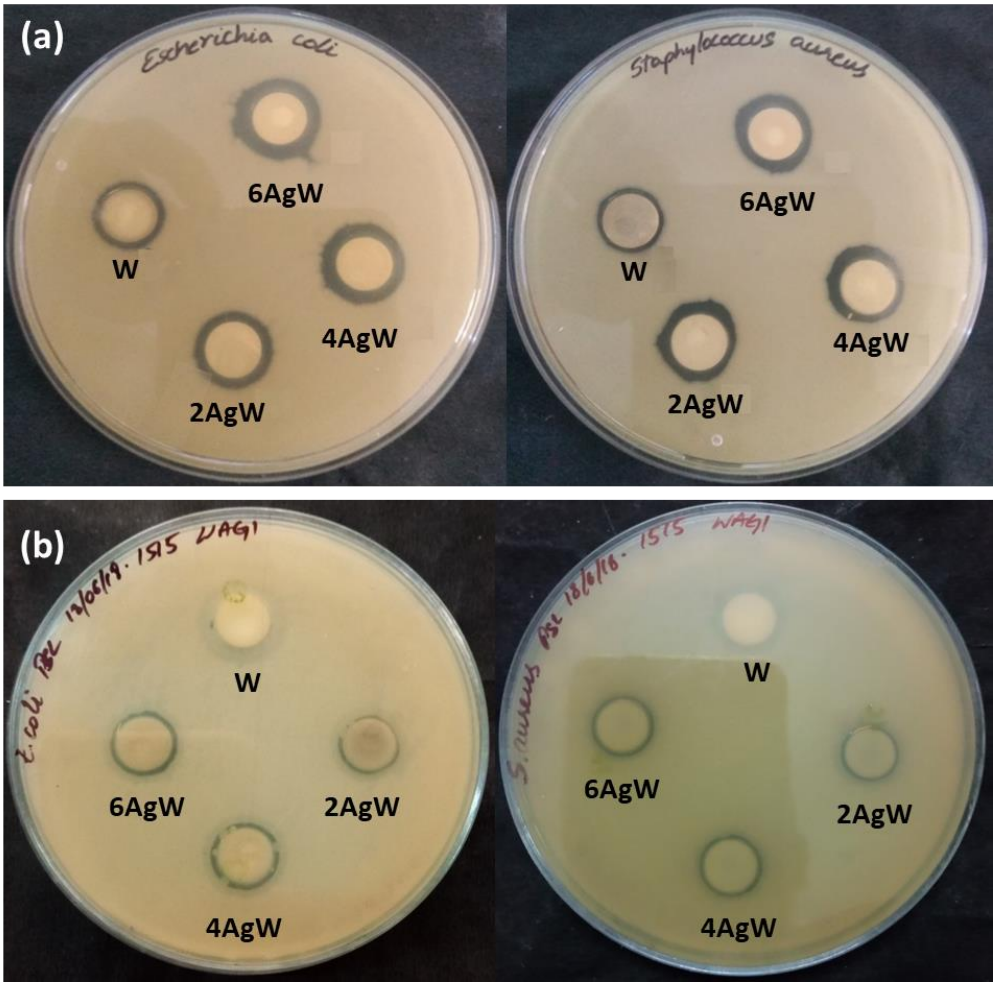

Fig. 5.10 Antimicrobial activity of pure and silver doped wollastonite after (a) 24 hours and (b) 48 hours against *E. coli* and *S. aureus*

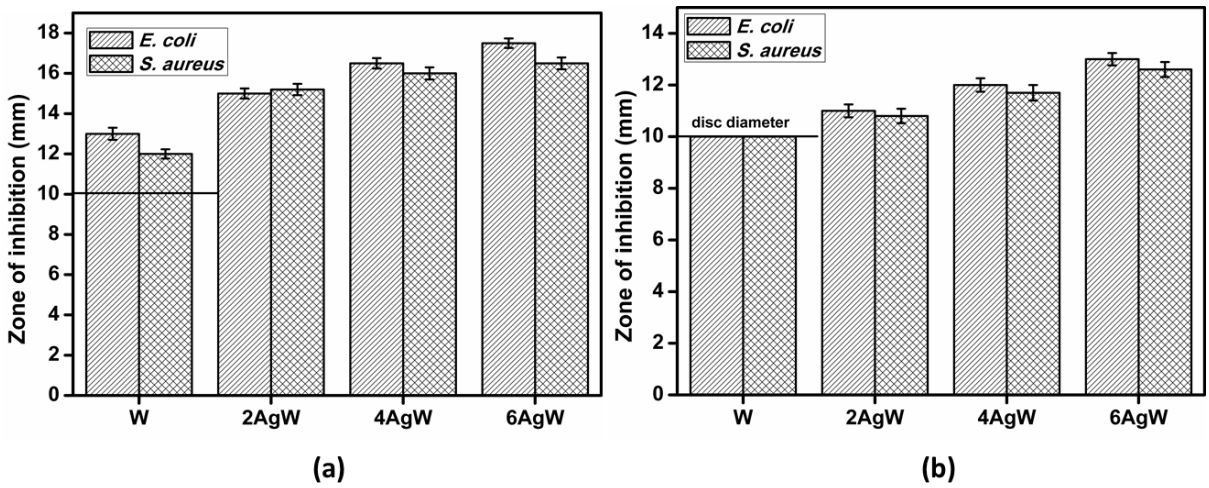

Fig. 5.11 Zone of inhibition graph for all silver doped samples against E. coli and S. aureus after (a) 24 hours and (b) 48 hours

5.3 Conclusion

In the present study, wollastonite and silver doped wollastonite with various concentrations (2, 4 and 6 mol.%) of silver were successfully prepared by sol-gel method using bio-waste such as rice husk ash (RHA) and eggshells. Powder X-ray Diffractometer (XRD) analysis proved the crystallization of pure phase β-wollastonite and silver doped wollastonite after suitable heat treatment (800 °C for 2 hours) according to the thermogravimetric and differential thermal analysis (TG/DTA) results. *In vitro* bioactivity study shows the promising apatite layer formation on the surface of pure and Ag doped wollastonite ceramic pellets and the addition of Ag result in the enhancement of apatite layer development on the surface of the samples. Degradation study revealed that the addition of silver decreases the degradation rate wollastonite. The antimicrobial activity test demonstrates that Ag doped wollastonite exhibits excellent inhibition zone of pathogens such as *E. coli* and *S. aureus* than pure form of wollastonite. Therefore, these biological studies evidently shown that developed Ag doped wollastonite is cost effective and environmentally beneficial. Besides, it is a potential biomaterial that may find applications in bone tissue engineering.

5.4 References

1. Hench LL. Bioceramics: From Concept to Clinic. J Am Ceram Soc. 1991;74(7):1487–510.

2. Gao C, Peng S, Feng P, Shuai C. Bone biomaterials and interactions with stem cells. Bone Research. 2017; 5:17059.

3. Hench LL., Wilson J. An Introduction to Bioceramics. World Sci. 1993;41–75.

4. Best SM, Porter AE, Thian ES, Huang J. Bioceramics: Past, present and for the future. J Eur Ceram Soc. 2008;28(7):1319–27.

5. Hench LL. The story of Bioglass®. In: Journal of Materials Science: Materials in Medicine. 2006; 17(11):967–78.

6. Lin K, Zhai W, Ni S, Chang J, Zeng Y, Qian W. Study of the mechanical property and in vitro biocompatibility of $CaSiO_3$ ceramics. Ceram Int. 2005;31(2):323–6.

7. Zhang NL, Molenda JA, Fournelle JH, Murphy WL, Sahai N. Effects of pseudowollastonite ($CaSiO_3$) bioceramic on in vitro activity of human mesenchymal stem cells. Biomaterials. 2010;31(30):7653–65.

8. Magallanes-Perdomo M, De Aza AH, Mateus AY, Teixeira S, Monteiro FJ, De Aza S, et al. In vitro study of the proliferation and growth of human bone marrow cells on apatite-wollastonite-2M glass ceramics. Acta Biomater. 2010;6(6):2254–63.

9. Magallanes-Perdomo M, Luklinska ZB, De Aza AH, Carrodeguas RG, De Aza S, Pena P. Bone-like forming ability of apatite-wollastonite glass ceramic. J Eur Ceram Soc. 2011;31(9):1549–61.

10. Xu S, Lin K, Wang Z, Chang J, Wang L, Lu J, et al. Reconstruction of calvarial defect of rabbits using porous calcium silicate bioactive ceramics. Biomaterials. 2008;29(17):2588–96.

11. No YJ, Li JJ, Zreiqat H. Doped calcium silicate ceramics: A new class of candidates for synthetic bone substitutes. Materials. 2017; 10(2):153.

12. Hoppe A, Güldal NS, Boccaccini AR. A review of the biological response to ionic dissolution products from bioactive glasses and glass-ceramics. Biomaterials. 2011; 32.2757–74.

13. Geetha M, Singh AK, Asokamani R, Gogia AK. Ti based biomaterials, the ultimate choice for orthopaedic implants - A review. Progress in Materials Science. 2009; 54:397–425.

14. Wu C, Ramaswamy Y, Soeparto A, Zreiqat H. Incorporation of titanium into calcium silicate improved their chemical stability and biological properties. J Biomed Mater Res - Part A. 2008;86(2):402–10.

15. Ramaswamy Y, Wu C, Van Hummel A, Combes V, Grau G, Zreiqat H. The responses of osteoblasts, osteoclasts and endothelial cells to zirconium modified calcium-silicate-based ceramic. Biomaterials. 2008;29(33):4392–402.

16. Samudrala R, Abdul Azeem P, Penugurti V, Manavathi B. Cytocompatibility studies of titania-doped calcium borosilicate bioactive glasses in-vitro. Mater Sci Eng C. 2017;77:772–9.

17. Popescu RA, Magyari K, Vulpoi A, Trandafir DL, Licarete E, Todea M, et al. Bioactive and biocompatible copper containing glass-ceramics with remarkable antibacterial properties and high cell viability designed for future in vivo trials. Biomater Sci. 2016;4(8):1252–65.

18. Azeena S, Subhapradha N, Selvamurugan N, Narayan S, Srinivasan N, Murugesan R, et al. Antibacterial activity of agricultural waste derived wollastonite doped with copper for bone tissue engineering. Mater Sci Eng C. 2017;71:1156–65.

19. Li J, Zhai D, Lv F, Yu Q, Ma H, Yin J, et al. Preparation of copper-containing bioactive glass/eggshell membrane nanocomposites for improving angiogenesis, antibacterial activity and wound healing. Acta Biomater. 2016; 36:254-66.

20. Diba M, Goudouri OM, Tapia F, Boccaccini AR. Magnesium-containing bioactive polycrystalline silicate-based ceramics and glass-ceramics for biomedical applications. Curr Opin Solid State Mater Sci. 2014;18(3):147–67.

21. Diba M, Tapia F, Boccaccini AR, Strobel LA. Magnesium-Containing Bioactive Glasses for Biomedical Applications. Int J Appl Glas Sci. 2012; 36:254-66.

22. Balamurugan A, Balossier G, Laurent-Maquin D, Pina S, Rebelo AHS, Faure J, et al. An in vitro biological and anti-bacterial study on a sol-gel derived silver-incorporated bioglass system. Dent Mater. 2008;24(10):1343–51.

23. Kawashita M, Tsuneyama S, Miyaji F, Kokubo T, Kozuka H, Yamamoto K. Antibacterial silver-containing silica glass prepared by sol-gel method. Biomaterials. 2000;21(4):393–8.

24. Zhao G, Stevens SE. Multiple parameters for the comprehensive evaluation of the susceptibility of Escherichia coli to the silver ion. BioMetals. 1998;11(1):27–32.

25. Izquierdo-Barba I, Salinas AJ, Vallet-Regí M. In vitro calcium phosphate layer formation on sol-gel glasses of the CaO-SiO_2 system. J Biomed Mater Res. 1999;47(2):243–50.

26. Klimesch DS, Ray A. The use of DTA/TGA to study the effects of ground quartz with different surface areas in autoclaved cement : Quartz pastes. Use of the semi-isothermal thermogravimetric technique. Thermochim Acta. 1997; 306(1-2):159-165.

27. Wilburn F. Handbook of Thermal Analysis of Construction Materials. Thermochim

Acta. 2003.

28. Mariappan CR, Ranga N. Influence of silver on the structure, dielectric and antibacterial effect of silver doped bioglass-ceramic nanoparticles. Ceram Int. 2017;43(2):2196–201.

29. Reddy MV, Pathak M. Sol-gel combustion synthesis of Ag doped CaSiO3: in vitro bioactivity, antibacterial activity and cytocompatibility studies for biomedical applications. Mater Technol. 2018; 33(1):33-47.

30. Hu AM, Li M, Dali DLM, Liang KM. Crystallization and properties of a spodumene-willemite glass ceramic. Thermochim Acta. 2005; 437(1-2):110-113.

31. Palakurthy S, K. VGR, Samudrala RK, P. AA. In vitro bioactivity and degradation behaviour of β-wollastonite derived from natural waste. Mater Sci Eng C. 2019;98:109-117.

32. Li HC, Wang DG, Chen CZ, Weng F, Shi H. Influence of different amount of Na_2O additive on the structure, mechanical properties and degradability of bioactive wollastonite. Ceram Int. 2016;42(1):1439–45.

33. Shen W, Li P, Feng H, Ge Y, Liu Z, Feng L. The bactericidal mechanism of action against Staphylococcus aureus for AgO nanoparticles. Mater Sci Eng C. 2017;75:610–9.

34. Yazdimamaghani M, Vashaee D, Assefa S, Walker KJ, Madihally S V., Köhler GA, et al. Hybrid macroporous gelatin/bioactive-glass/nanosilver scaffolds with controlled degradation behavior and antimicrobial activity for bone tissue engineering. J Biomed Nanotechnol. 2014; 10(6):911-31.

35. El-Rashidy AA, Waly G, Gad A, Hashem AA, Balasubramanian P, Kaya S, et al. Preparation and in vitro characterization of silver-doped bioactive glass nanoparticles fabricated using a sol-gel process and modified Stöber method. Journal of Non-Crystalline Solids. 2017; 483:26-36.

36. Nakamoto K. Infrared and Raman Spectra of Inorganic and Coordination Compounds. Applied Organometallic Chemistry. 1997;13: 408 p.

37. Li HC, Wang DG, Chen CZ. Effect of zinc oxide and zirconia on structure, degradability and in vitro bioactivity of wollastonite. Ceram Int. 2015;41(8):10160–9.

38. Ji L, Wang W, Jin D, Zhou S, Song X. In vitro bioactivity and mechanical properties of bioactive glass nanoparticles/polycaprolactone composites. Mater Sci Eng C. 2015;46:1–9.

39. Vadera N, Ashokan A, Gowd GS, Sajesh KM, Chauhan RP, Jayakumar R, et al. Manganese doped nano-bioactive glass for magnetic resonance imaging. Mater Lett. 2015;160:335–8.

40. Zhang Y, Mizuno M, Yanagisawa M, Takadama H. Bioactive behaviors of porous apatite- and wollastonite-containing glass-ceramic in two kinds of simulated body fluid. J Mater Res. 2003;18(2):433–41.

41. Balamurugan A, Balossier G, Kannan S, Michel J, Rebelo AHS, Ferreira JMF. Development and in vitro characterization of sol-gel derived $CaO-P_2O_5-SiO_2$-ZnO bioglass. Acta Biomater. 2007;3(2):255–62.

42. Ciraldo FE, Liverani L, Gritsch L, Goldmann WH, Boccaccini AR. Synthesis and characterization of silver-doped mesoporous bioactive glass and its applications in conjunction with electrospinning. Materials (Basel). 2018; 11(5):692.

43. Goh YF, Alshemary AZ, Akram M, Abdul Kadir MR, Hussain R. Bioactive Glass: An In-Vitro Comparative Study of Doping with Nanoscale Copper and Silver Particles. J Appl Glas Sci. 2014; 5(3):255-266.

44. Ohtsuki C, Kokubo T, Takatsuka K, Yamamuro T. Compositional dependence of bioactivity of glasses in the system $CaO-SiO_2-P_2O_5$. Its in vitro evaluation. J Ceram Soc Japan Int ed. 1991;99(1):2–7.

45. Izquierdo-Barba I, Salinas AJ, Vallet-Regí M. Effect of the continuous solution exchange on the in vitro reactivity of a $CaO-SiO_2$ sol-gel glass. J Biomed Mater Res. 2000; 51(2):191-9.

46. Dobrádi A, Enisz-Bódogh M, Kovács K, Korim T. Bio-degradation of bioactive glass ceramics containing natural calcium phosphates. Ceram Int. 2016;42(2):3706–14.

47. Bohner M, Lemaitre J. Can bioactivity be tested in vitro with SBF solution? Biomaterials. 2009; 30(12):2175-9.

48. Liu X, Ding C, Chu PK. Mechanism of apatite formation on wollastonite coatings in simulated body fluids. Biomaterials. 2004;25(10):1755–61.

49. Seyed Shirazi SF, Gharehkhani S, Cornelis Metselaar HS, Nasiri-Tabrizi B, Yarmand H, Ahmadi M, et al. Ion size, loading, and charge determine the mechanical properties, surface apatite, and cell growth of silver and tantalum doped calcium silicate. RSC Adv. 2015;6(1):190–200.

50. Liu Z, Chan KC, Liu L, Guo SF. Bioactive calcium titanate coatings on a Zr-based bulk metallic glass by laser cladding. Mater Lett. 2012; 82:67-70.

51. El-Kady AM, Ali AF, Rizk RA, Ahmed MM. Synthesis, characterization and microbiological response of silver doped bioactive glass nanoparticles. Ceram Int. 2012;38(1):177–88.

52. Ohshima Y, Takada D, Namai S, Sawai J, Kikuchi M, Hotta M. Antimicrobial Characteristics of Heated Eggshell Powder. Biocontrol Sci. 2015; 20(4):239-46.

53. Ni S, Li X, Yang P, Ni S, Hong F, Webster TJ. Enhanced apatite-forming ability and antibacterial activity of porous anodic alumina embedded with CaO-SiO_2-Ag_2O bioactive materials. Mater Sci Eng C. 2016; 58:700-8

54. Ou SF, Chung RJ, Lin LH, Chiang YC, Huang CF, Ou KL. A mechanistic study on the antibacterial behavior of silver doped bioceramic. J Alloys Compd. 2015; 629:362-367.

Chapter 6

Effect of zirconia on structural, mechanical and biological properties of bio-waste derived wollastonite ceramics

In this chapter, the effect of partial substitution of zirconia (ZrO_2) on structural, biological and mechanical properties of wollastonite were described. As Zr shows superior biocompatibility, osseointegration and good mechanical strength, it is speculated that the incorporation of zirconia into wollastonite will significantly improve their mechanical and biological properties. Zr was doped into wollastonite with the objective of improving mechanical properties and degradability, where Zr doping concentration varied from 1 to 5 mol.% and its effect on in vitro bioactivity, degradation, mechanical properties and cytocompatibility of wollastonite were studied.

6.1 Introduction

Calcium silicate-based ceramics mainly include wollastonite, akermanite, diopside, merwinite and bredigite ceramics have been focused in recent years because they support the attachment, proliferation and differentiation of osteoblasts like cells such as human mesenchymal stem cells [1–3]. Ca and Si are two ions that are dissolute from these ceramics. Ca ion plays an important role in cell reaction in bioceramics including cell proliferation and differentiation into osteoblast [4]. Si is one of the most significant trace elements in the human body, which acts as a key controller of bone calcification and helps to improve bone density and prevent osteoporosis, specifically at the early stage of bone formation [5, 6]. It has also been reported that the dissolution products from calcium silicates enhance the effect of insulin-like growth factor on cell proliferation [7]. Moreover, calcium silicate ceramics show better mechanical properties compared to other calcium phosphate ceramics [8, 9].

Wollastonite ($CaSiO_3$) with a monoclinic crystal structure belongs to the group of calcium silicate ceramics. It exists in two forms: low temperature form β – wollastonite (β – $CaSiO_3$) and high temperature form α – wollastonite (α – $CaSiO_3$) [10–12]. It has received attention for its ability to contribute to hard tissue regeneration due to its progressive bio-functionalities [13, 14]. Siriphannon et al. [15] showed that apatite growth rate on wollastonite was faster than on A-W glass ceramics and other bioactive glass ceramics. *In vitro* cell culture assessments demonstrated that wollastonite ceramics can support the attachment of osteoblast-like cells and bone marrow mesenchymal stem cell, their proliferation and differentiation [16–18]. However, the degradation rate of wollastonite ceramics is relatively high, leading to abrupt change in pH value of local environment by dissolution ions which may negatively affect surrounding cells [19]. Additionally, the high soluble rate is likely reason for failure of scaffold construction before the creation of appropriate extracellular matrix (ECM) and new bone. Therefore the dissolution rate of

wollastonite should be monitored for better clinical applications. Furthermore, wollastonite ceramics were mechanically not strong enough as bone substitutes for load-bearing sites. The problem can be resolved by emerging multiphase bioceramics with improved mechanical properties and less soluble phases [20, 21].

Zirconium (Zr) has been a traditionally used material to prepare prosthetic devices as it shows superior biocompatibility and good mechanical properties [22]. Literature reports indicated that the Zr ions exhibit excellent osseointegration [23]. The incorporation of zirconia has been reported to increase mechanical properties and reduce the dissolution rate of materials [24–27]. Therefore, it is speculated that the incorporation of zirconia into wollastonite will significantly improve their mechanical and biological properties. The β-wollastonite produced via sol-gel process, utilizing eggshells and rice husk ash (RHA) as sources of calcium oxide and silica showed excellent *in vitro* bioactivity and cytocompatibility but mechanically not strong and showed a slightly higher dissolution rate. Therefore, in the current study, zirconium oxynitrate hydrate ($Zr(NO_3)_2$. x H_2O) as zirconia precursor was used to produce zirconia-containing wollastonite with the objective of achieving improved dissolution rate, biological properties, and mechanical properties that are as close as possible with those of the human bone.

6.2 Results and discussion

6.2.1 Thermal analysis

TG and DTA measurement results of W, 1ZrW, 3ZrW and 5ZrW (pure wollastonite, 1mol.% ZrO_2, 3 mol.% ZrO_2 and 5 mol.% ZrO_2 doped wollastonite ceramics denoted as W, 1ZrW, 3ZrW and 5ZrW, respectively) dried gels are shown in Fig. 6.1. These gel samples were undergoing three distinct stages of mass loss. The first stage of mass loss at 30 - 220 °C is large mass loss related to the release of residual water [28]. The second stage of mass loss

occurred at 220 - 500 °C, due to low temperature decarbonation and the third stage of mass loss occurred at 500 - 750 °C due to high temperature decarbonation [29]. The weight loss was found to be constant in all samples after 800 °C. Furthermore, the total weight loss increased with increase in zirconia content, which could be related to additional nitrate decomposition in 1ZrW, 3ZrW and 5ZrW samples [26]. From the DTA curves of the samples, a significant exothermic peak related to the beginning of crystallization was observed at 778 °C for W, 794 °C for 1ZrW, 802 °C for 3ZrW and 816 °C for 5ZrW, respectively. These results showed that the addition of zirconia in wollastonite phase increased its crystallization temperature [30]. Therefore, according to TG-DTA results, 850 °C was chosen as sintering temperature.

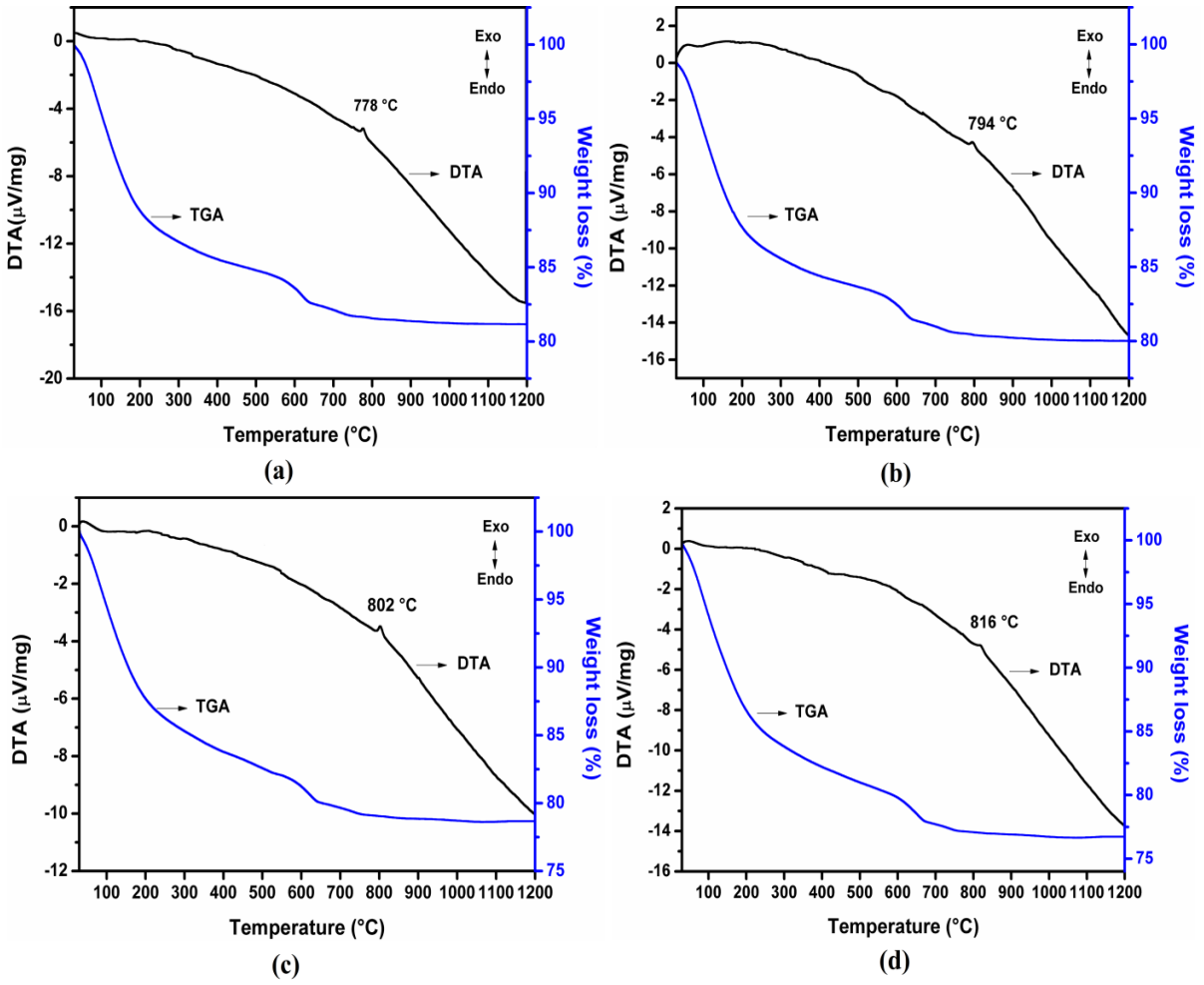

Fig. 6.1 TG-DTA curves of dried gels for (a) W, (b) 1ZrW, (c) 3ZrW and (d) 5ZrW

6.2.2 Structural Characterization

XRD patterns of sintered Zr-W ceramic powders are illustrated in Fig. 6.2. The observed diffraction peaks for undoped sample were completely identical to standard β-wollastonite pattern (JCPDS file no: 84-0655). XRD patterns of 1ZrW, 3ZrW and 5ZrW showed no phase change, and diffraction peaks of β- wollastonite and ZrO_2 (JCPDS file no: 70-7359) were detected. Though the main peaks of ZrO_2 (2θ = 29.95, 34.96 and 49.73°) are very close to β-$CaSiO_3$ (2θ = 29.97, 35.03 and 49.75°), it is difficult to distinguish them [31]. However, the maximum intensity peak at 2θ = 29.97° was decreased gradually in 1, 3 and 5 mol% zirconia added wollastonite, indicating that there was a decrease in crystallinity of wollastonite with the incorporation of zirconia [26, 31, 32]. The average crystalline size were calculated as ~ 50.8 nm for pure wollastonite, ~ 61.23 nm for 1ZrW, ~ 86.1 nm for 3ZrW and ~ 104.6 nm for 5ZrW using Debye Scherrer's equation.

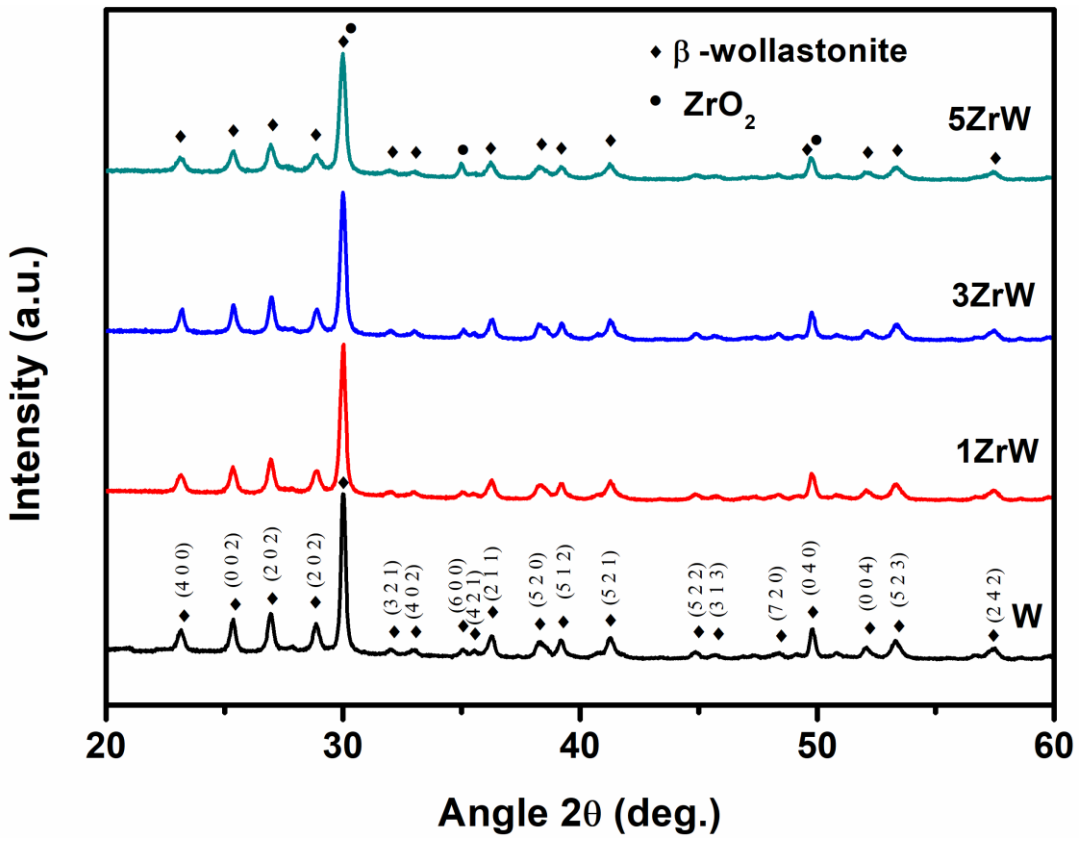

Fig. 6.2 XRD patterns of pure and zirconia added wollastonite

The surface morphologies and their respective quantitative elemental analysis of sintered Zr-W ceramics are shown in Fig. 6.3. The surface of pure wollastonite showed coarse and irregular morphology. When zirconia is incorporated, the surface became smooth and appeared dense [31]. The elemental composition of the synthesized pure and zirconia incorporated wollastonite was analysed by EDS spectra. EDS spectra confirmed elemental composition of pure wollastonite with the existence Ca, Si and O whereas EDS spectra of 1ZrW, 3ZrW and 5ZrW ceramics revealed the presence of Zr along with Ca, Si and O elements. Moreover, the atomic percentage of Zr was found to increase from 1ZrW to 5ZrW.

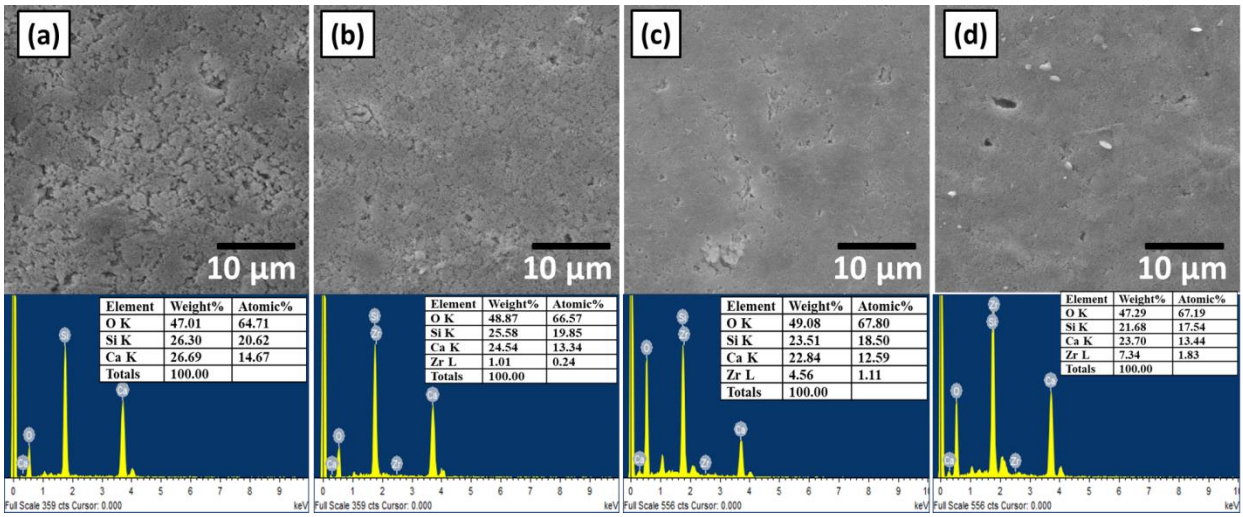

Fig. 6.3 SEM micrographs and EDS spectra of ceramics (a) W, (b) 1ZrW, (c) 3ZrW and (d) 5ZrW

The FTIR spectra from pure and zirconia added wollastonite ceramics are presented in Fig. 6.4. From FTIR spectra, the peaks at ~ 641 and ~ 684 cm^{-1} correspond to the symmetric stretching vibration Si-O-Si and the band at 1021-1076 cm^{-1} corresponds to asymmetric stretching vibration Si-O-Si were identified [33]. Moreover, the IR spectra peaks at ~ 462, ~ 514 and ~ 566 cm^{-1} allocated to the bending vibration in Si-O-Si bonds were identified. Two non-bridging oxygen (NBO) bonds of Si-O-NBO were found at ~ 904 and ~ 946 cm^{-1} [34, 35]. In addition, the occurrence of peaks at ~ 1635 and ~ 3432 cm^{-1} were ascribed to adsorbed moisture [36]. On the addition of zirconia into wollastonite phase, the peak at ~ 462 cm^{-1}

which corresponds to the bending vibration in Si-O-Si bonds slightly shifted to the lower wavenumber part. Moreover, another asymmetric stretching vibration Si-O-Si at ~ 725 cm^{-1} was identified and the intensity of this peak increased with increase in zirconia content.

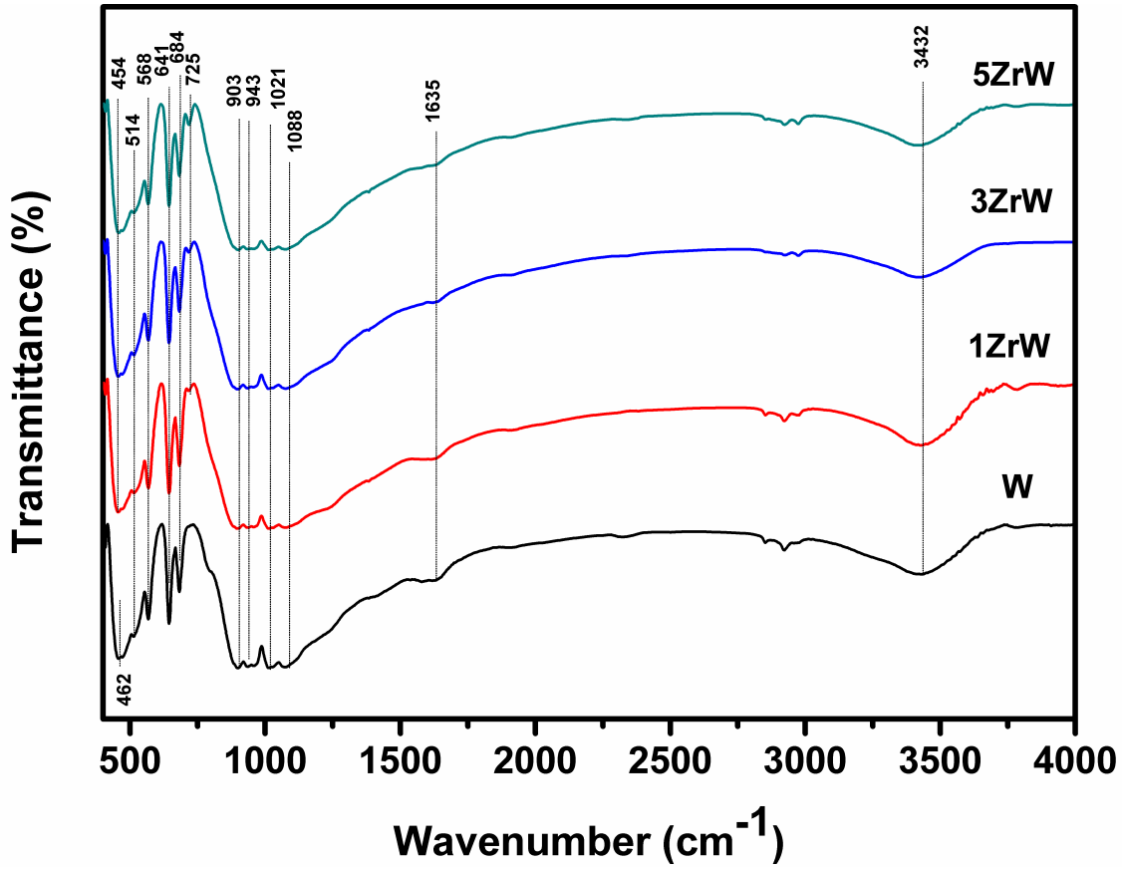

Fig. 6.4 FTIR spectra pure and zirconia incorporated wollastonite

6.2.3 In vitro bioactivity

The prerequisite for an implant to bond to living bone is the growth of hydroxyapatite on its surface. Therefore, the hydroxyapatite forming ability of prepared Zr-W ceramics on the surface was assessed using *in vitro* test in SBF. XRD analysis was carried out to characterize the precipitated agglomerates. Fig. 6.5 illustrates XRD patterns of Zr-W ceramics after 21 days of soaking in SBF. XRD peaks matched well with standard peaks at 2θ = 25.87, 31.78, 49.46 and 53.14 and were assigned to (0 0 2), (2 1 1), (2 1 3) and (0 0 4) crystalline planes of hydroxyapatite in accordance with standard JCPDS file no: 09-0432 [37,

38]. Additionally, the peak intensities of hydroxyapatite for 1ZrW, 3ZrW and 5ZrW ceramics were found to decrease on increasing zirconia content.

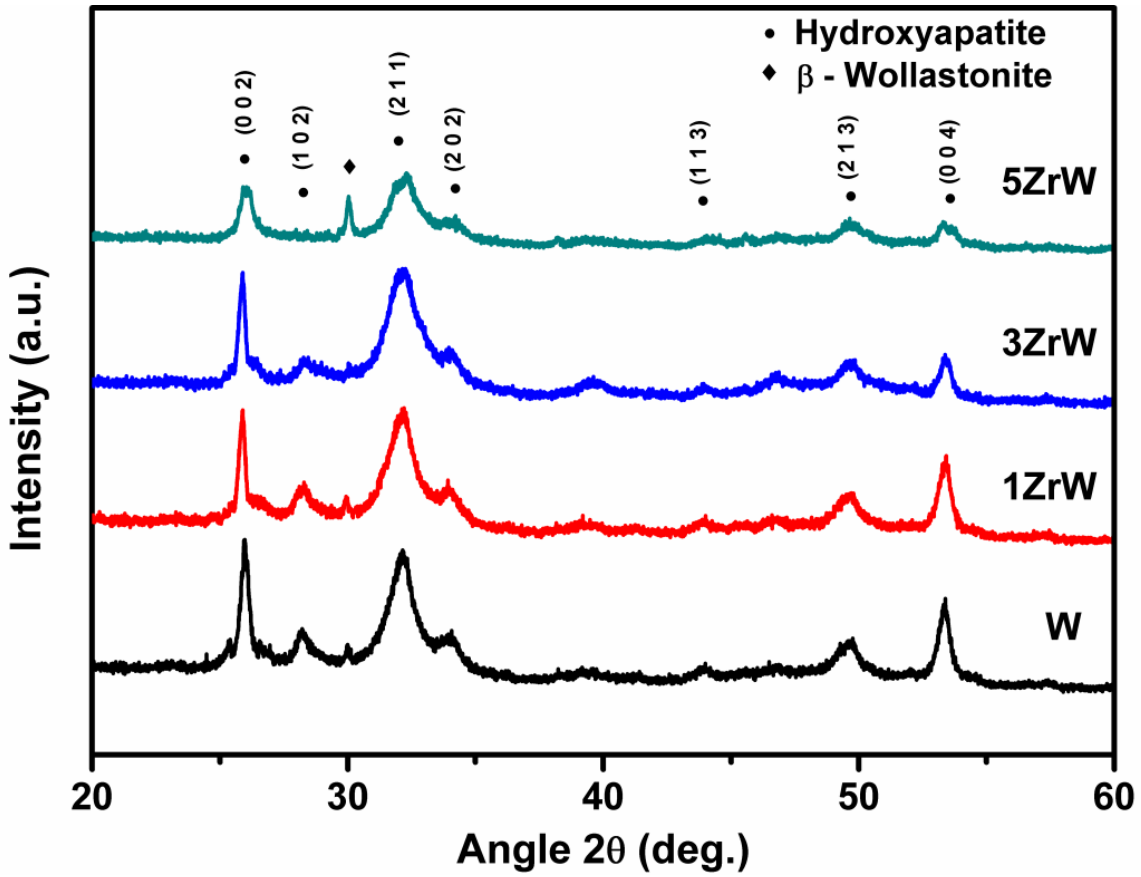

Fig. 6.5 XRD patterns of Zr-W ceramics after immersion in SBF for 21 days

The surface micrographs and equivalent EDS spectra of Zr-W ceramic specimens after immersion in SBF solution for 14 days are shown in Fig. 6.6. The surface of the specimens containing 0 mol.% of zirconia was completely precipitated by spherical like agglomerated hydroxyapatite crystals [39, 40]. While the quantity of spherical shaped agglomerated crystals decreased with increase in zirconia concentration. This could be due to the bioinert nature of zirconia. However, a trivial quantity of apatite crystals can be seen on the surface of ceramics containing 5 mol.% of zirconia. In addition, EDS analysis indicates that the spherical agglomerated crystals were composed of mainly Ca and P ions.

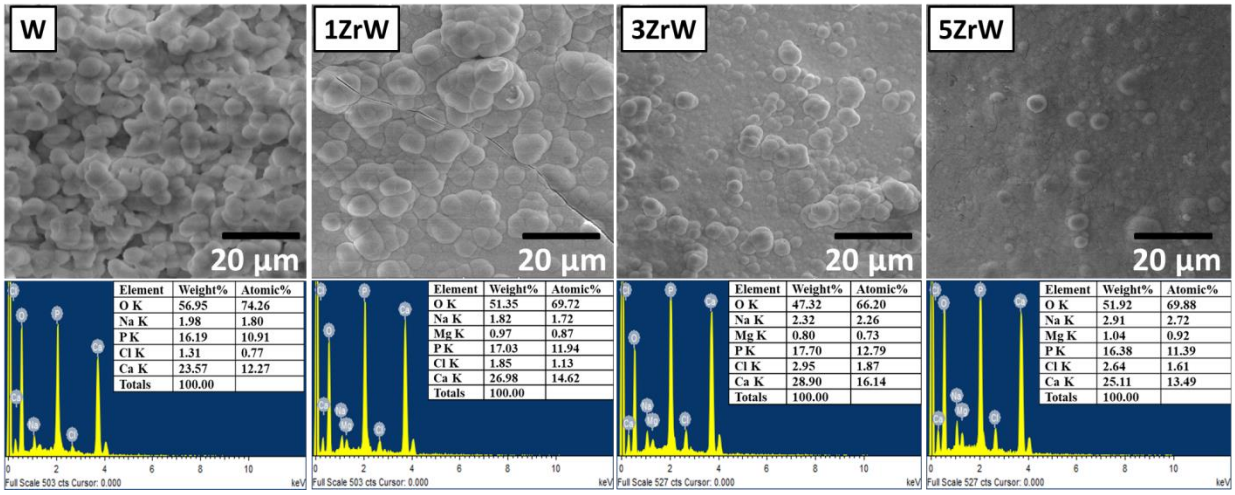

Fig. 6.6 Surface micrographs and EDS spectra of Zr-W ceramics after immersion in SBF for 14 days

FTIR spectroscopy was also studied after immersion in SBF to monitor the apatite growth rate of zirconia incorporated wollastonite ceramics. The infrared spectra of W, 1ZrW, 3ZrW and 5ZrW after soaking in SBF for 21 days are described in Fig. 6.7. After immersion in SBF for 21 days, well-resolved infrared bands at ~ 1418, ~ 1487 and ~ 875 cm^{-1} were assigned to C-O vibrations of carbonate group (CO_3^{2-}) [41, 42], while the infrared bands at ~ 563, ~ 603, ~ 1093 and ~ 1033 cm^{-1} were assigned to phosphate group (PO_4^{3-}); in particular, the double peaks at ~ 563 and ~ 603 cm^{-1} were characteristic of crystalline P-O bonds in hydroxyapatite as can be clearly observed for pure wollastonite [43, 44]. The infrared absorption peaks at ~ 563 and ~ 603 cm^{-1} could also be observed on FTIR spectrum of 1ZrW, 3ZrW and 5ZrW ceramics, but the intensities decreased with increase in zirconia content in the ceramics. These results combined with SEM-EDS and XRD analysis show evidence of *in vitro* bioactivity of the prepared Zr-W ceramics with the formation of apatite while the growth rate decreased with increase of zirconia content in the wollastonite phase, indicating that excessive zirconia incorporation inhibits apatite forming ability of wollastonite.

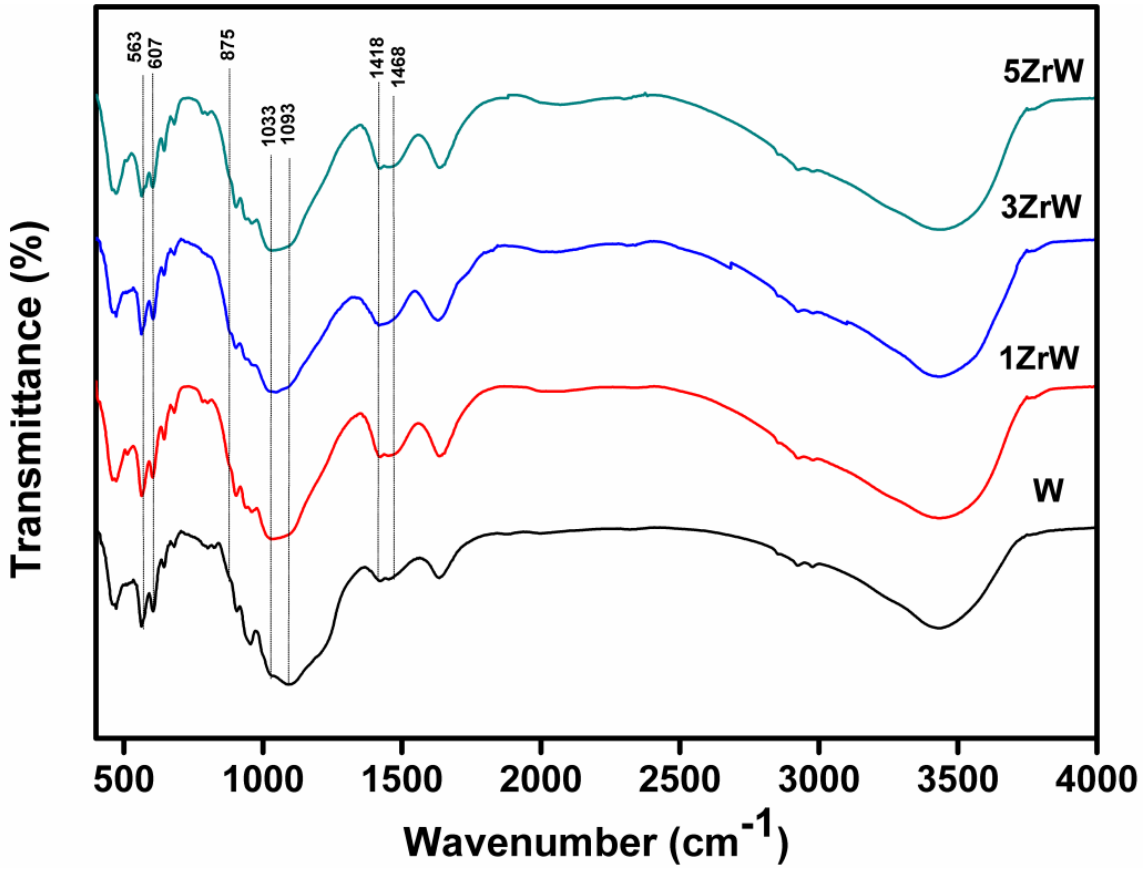

Fig. 6.7 FTIR patterns of Zr-W ceramics after immersion in SBF for 21 days

6.2.4 Change in pH of SBF solution

Fig. 6.8 illustrates the plots of pH variation of SBF versus immersion time for W, 1ZrW, 3ZrW and 5ZrW specimens. As can be observed from Fig. 6.8, all ceramics showed similar tendency in pH change during immersion time; That is, there is rapid increase in pH during initial soaking hours for up to 4 days, and beyond this, pH increases slowly until 11 days of soaking, and then pH value remains constant till the final testing time of 14 days. The change in pH value of SBF basically followed the same trend as for bioactive material, which is directly related to release of ions due to the dissolution of material in the media [25, 40, 45]. In the present study, zirconia added wollastonite ceramics showed lower pH change compared to pure wollastonite. Therefore, the incorporation of zirconia for CaO made the degradation rate of wollastonite slower, which is further confirmed from degradation studies.

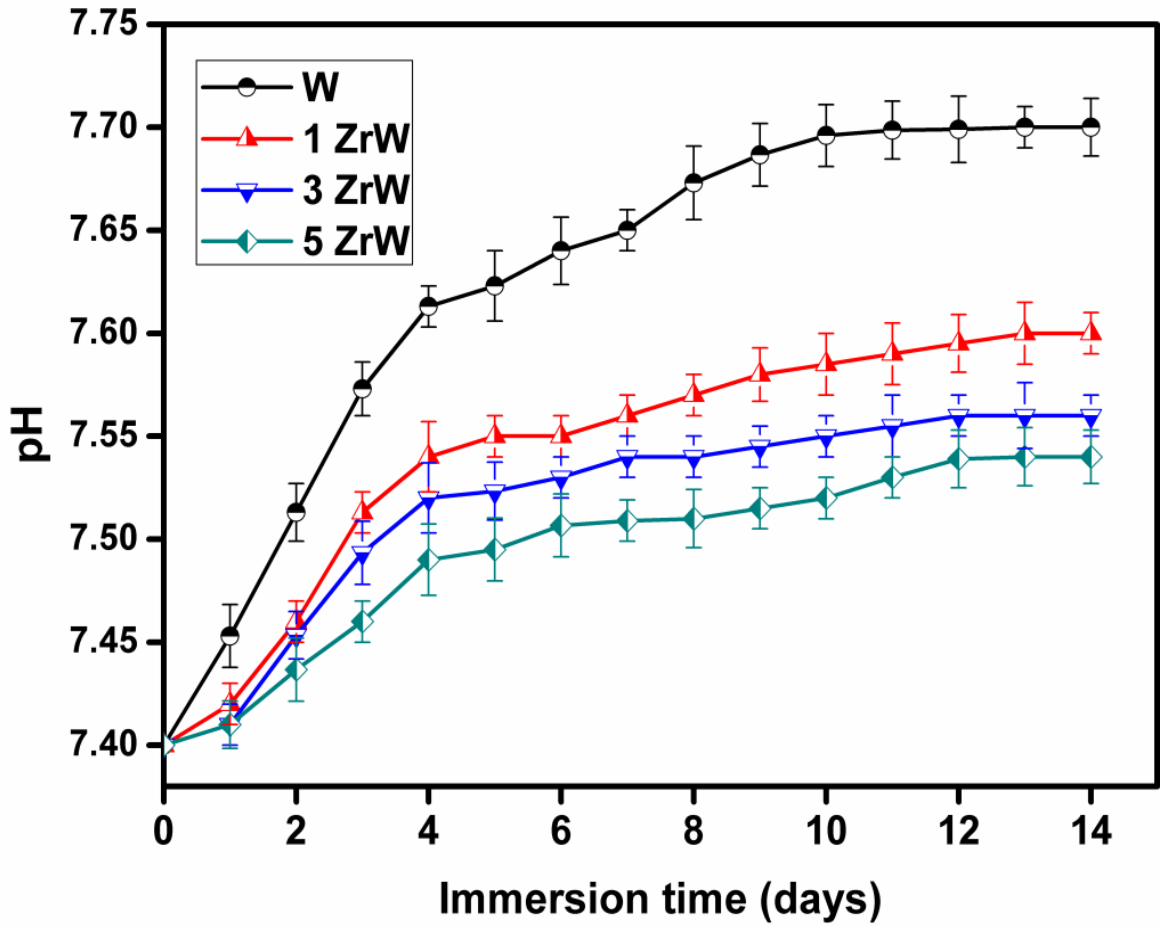

Fig. 6.8 Change in pH value of SBF for W, 1ZrW, 3ZrW and 5ZrW specimens with immersion time

6.2.5 Degradation

The effect of incorporation of zirconia on degradability of wollastonite was studied by immersing it in Tris-HCl buffer solution. Fig. 6.9 displays the percentage of weight loss of Zr-W ceramics verses immersion period in Tris-HCl buffer solution. It can be understood that the weight loss of all specimens increased with immersion time. After 21 days of immersion, the weight loss of specimens W, 1ZrW, 3ZrW and 5ZrW was 17.16%, 14.54%, 13.61% and 11.33% respectively. Pure wollastonite specimens showed higher weight loss compared to zirconia added wollastonite, which indicates that incorporation of zirconia resulted in decrease of degradation rate significantly ($P<0.05$). Wollastonite ceramics have been reported to be high degradable materials, and that degradability is regulated by crystallinity, grain size,

microstructure, surface area, etc. [21, 46, 47]. In the present work, incorporation of zirconia into wollastonite phase made the microstructure compact and dense, as can be seen from SEM images in Fig. 6.3. Therefore, the specimens incorporated with zirconia were not easily attacked by Tris-HCl buffer solution, resulting in lower degradation rate.

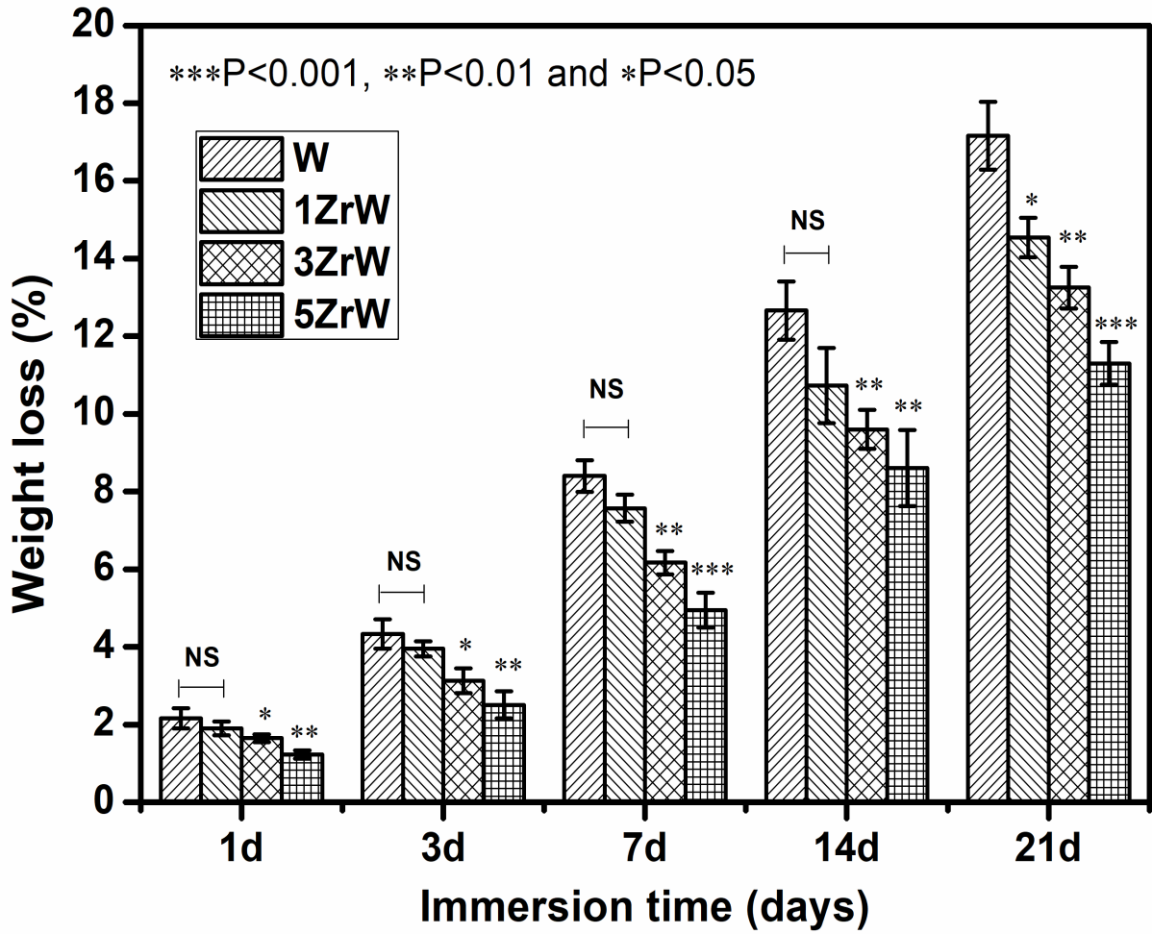

Fig. 6.9 Weight loss% of W, 1ZrW, 3ZrW and 5ZrW ceramics in Tris-HCl buffer solution, ***P<0.001, **P<0.01 and *P<0.05 was used as significant

6.2.6 Cytocompatibility

The quantitative assessment of cytotoxicity test is expressed by calculating relative cell viability. Fig. 6.10 shows the percentage of cell viability of MG-63 cells cultured with various concentrations (50µg/mL - 1000 µg/mL) of W, 1ZrW, 3ZrW and 5ZrW samples extracts for 48 hours. As can be seen from Fig. 6.10, different concentrations of W, 1ZrW,

3ZrW and 5ZrW samples extracts do not show significant change (P>0.05) in the viability of relative cells compared to controlled cell viability. Moreover, cell viability is not affected by the sample extracts even at higher concentration (1000 µg/mL), indicating that pure and zirconia doped wollastonite ceramics have no toxic influence on MG-63 cells. Biological evaluation of medical devices - part 5: tests for *in vitro* cytotoxicity (ISO 10993 – 5: 2009) stated that if the relative cell viability is greater than 70 % of the control group for the maximum concentration of the sample extract, then the material shall be considered non-cytotoxic [48].

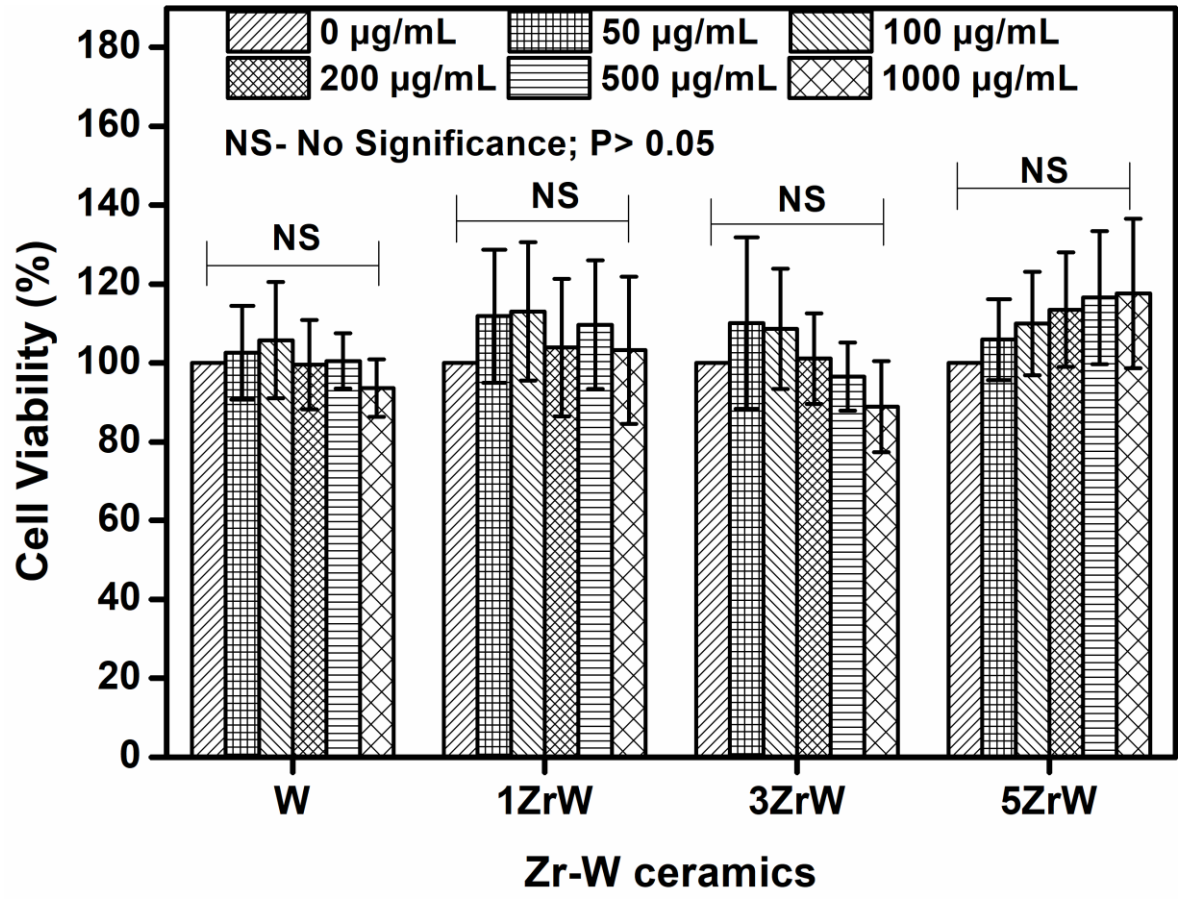

Fig. 6.10 Cell viability of Zr-W ceramics with MG-63 cell using MTT assay

6.2.7 Mechanical properties

Microhardness and compressive strength of Zr-W ceramics with varying zirconia content was presented in Fig. 6.11 (a & b). It is vibrant to see that the addition of zirconia in

wollastonite phase significantly enhanced ($P<0.05$) its microhardness and compressive strength. Microhardness value increased from 19.3 ± 1.3 HV with 0 mol% zirconia to 45.1 ± 2.8 HV with 5 mol% zirconia. While the compressive strength ranges from 40 ± 2.4 MPa for 0 mol% zirconia to 86 ± 2.1 MPa for 5 mol% zirconia. Effect of incorporation of zirconia on the bending strength and modulus of elasticity of wollastonite is demonstrated in Fig. 6.12. It can be observed that the bending strength and elasticity modulus improved significantly ($P<0.05$) with increase of zirconia content. The bending strength and elasticity modulus of pure wollastonite were estimated to be 10.2 ± 0.7 MPa and 1.44 ± 0.1 GPa, respectively. After incorporation with zirconia, the bending strength and elasticity modulus of 5ZrW ceramics increased to 23.6 ± 1.2 MPa and 5.8 ± 0.2 GPa. The addition of zirconia greatly improves mechanical properties due to its exceptional reinforcing capability. Many aspects such as crystallinity, amount of crystalline phases present, crystalline size, surface morphology and porosity distribution have an influence on mechanical properties [49, 50]. Moreover, existence of more than one crystalline phase in ceramics can also result in complex mechanical behaviour [51, 52]. For bone defect applications, synthetic bone implant materials must have mechanical properties that match the natural bone. These values must at least be in the range of cancellous bone [53]. The compressive strength of human vertebral bone (load bearing site) is in the range of 24 - 43 MPa, and while femoral cancellous bone (load bearing site) is in the range of 48 – 80 MPa [47, 54]. Consequently, the compressive strength of prepared Zr-W ceramics which is in the range of 40 ± 2.4 – 86 ± 2.1 MPa may be appropriate for load bearing applications.

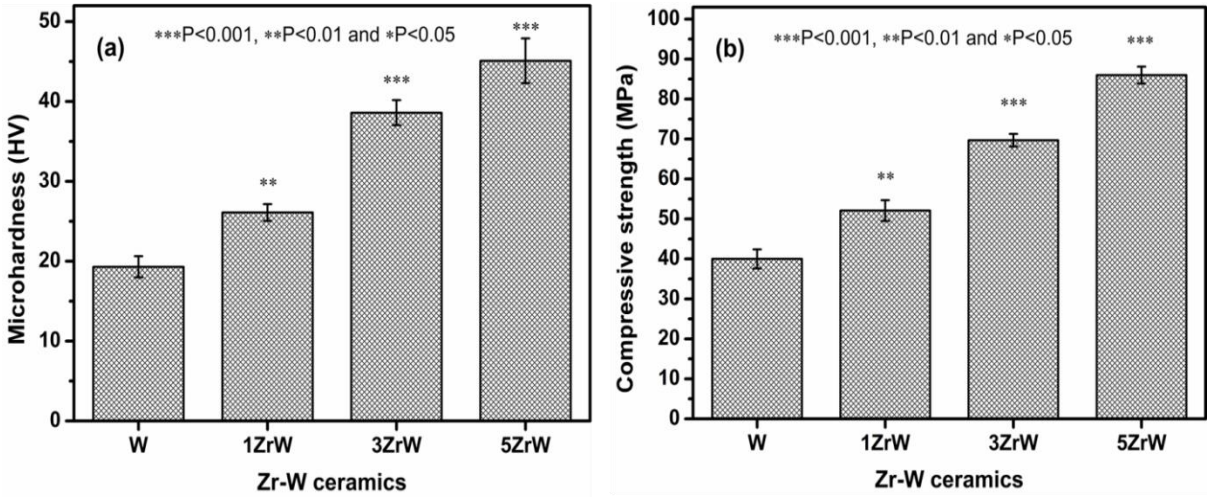

Fig. 6.11 Results of (a) micro hardness and (b) compressive strength of Zr-W ceramics, ***P<0.001, **P<0.01 and *P<0.05 was used as significant

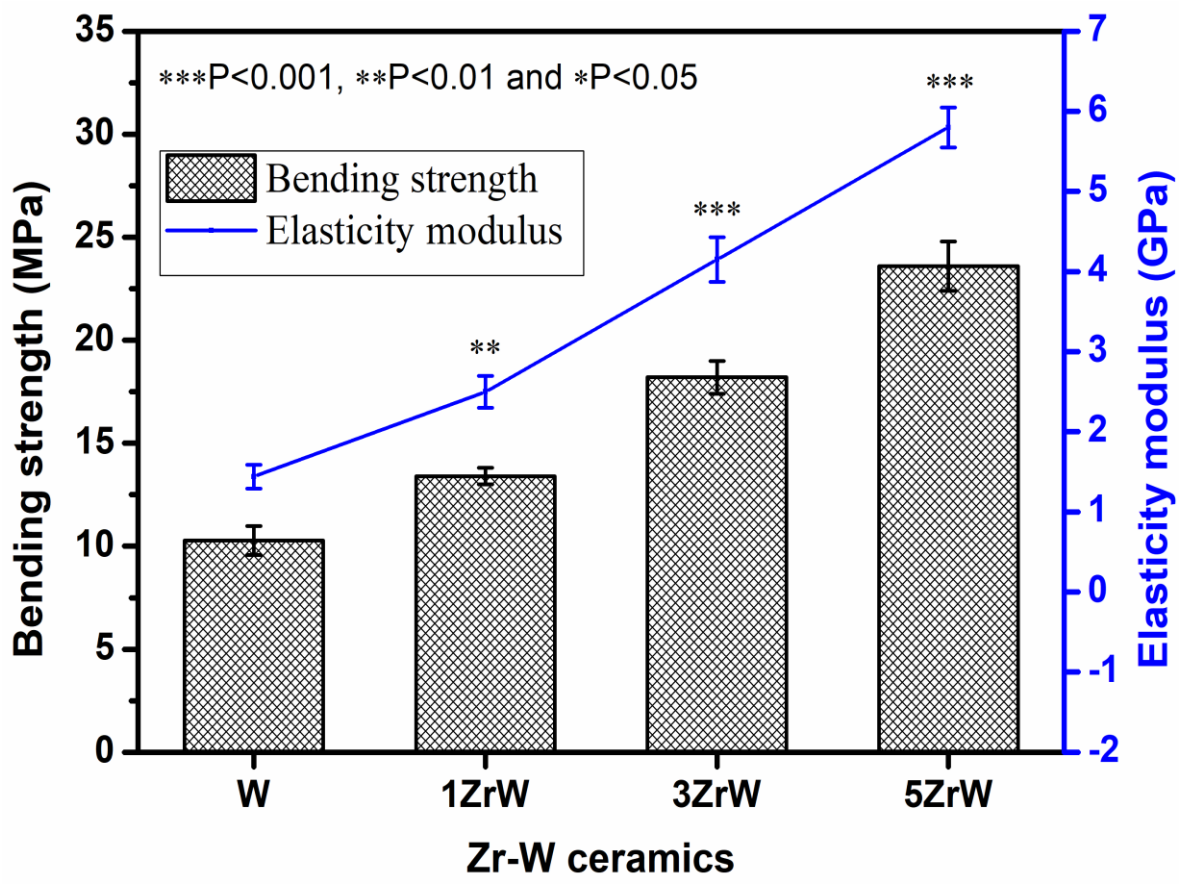

Fig. 6.12 Results of bending strength and elasticity modulus of Zr-W ceramics, ***P<0.001, **P<0.01 and *P<0.05 was used as significant

6.3 Conclusion

Bioactive ceramics of zirconia-containing wollastonite were fabricated via sol-gel technique, utilising bio-waste such as eggshells as calcium oxide source and rice husk ash (RHA) as silica source. The incorporation of zirconia into wollastonite phase could increase mechanical properties. The microhardness and compressive strength increased from 19.3 ± 1.3 to 45.1 ± 2.8 HV and 40 ± 2.4 to 86 ± 2.1 MPa, respectively, with increase in zirconia content from 0 to 5 mol%. The bending strength and elasticity modulus increased from 10.2 ± 0.7 to 23.6 ± 1.2 MPa and 1.44 ± 0.1 to 5.8 ± 0.2 GPa, respectively. *In vitro* studies results revealed that the prepared Zr-W ceramics show good bioactivity with the formation of hydroxyapatite while apatite forming rate slightly decreased with increase in zirconia content. Degradation test result showed that the addition of zirconia decreased the degradation rate of wollastonite. Cytocompatibility test demonstrated Zr-W ceramics have no toxic effect on MG-63 cells. Therefore, this study suggests that Zr-W ceramics could be promising cost effective biomaterials that may be recommended for bone tissue engineering.

6.4 References

1. Elsayed H, Romero AR, Molino G, Brovarone CV, Bernardo E. Bioactive glass-ceramic foam scaffolds from "inorganic gel casting" and sinter-crystallization. Materials (Basel). 2018; 11(3):349.
2. Gandolfi MG, Shah SN, Feng R, Prati C, Akintoye SO. Biomimetic calcium-silicate cements support differentiation of human orofacial mesenchymal stem cells. J Endod. 2011;37(8):1102–8.
3. Ding SJ, Shie MY, Wang CY. Novel fast-setting calcium silicate bone cements with high bioactivity and enhanced osteogenesis in vitro. J Mater Chem. 2009; 19(8):1183-1190.
4. Sun J, Wei L, Liu X, Li J, Li B, Wang G, et al. Influences of ionic dissolution products of dicalcium silicate coating on osteoblastic proliferation, differentiation and gene expression. Acta Biomater. 2009; 5(4):1284-93.
5. Carlisle EM. Silicon: A possible factor in bone calcification. Science (80-). 1970; 167(3916):279-80.
6. Zhou X, Zhang N, Mankoci S, Sahai N. Silicates in orthopedics and bone tissue engineering materials. Journal of Biomedical Materials Research - Part A. 2017: 105(7):2090-2102.
7. Midha S, van den Bergh W, Kim TB, Lee PD, Jones JR, Mitchell CA. Bioactive Glass Foam Scaffolds are Remodelled by Osteoclasts and Support the Formation of Mineralized Matrix and Vascular Networks In Vitro. Adv Healthc Mater. 2013; 2(3):490-9.
8. Su CC, Kao CT, Hung CJ, Chen YJ, Huang TH, Shie MY. Regulation of physicochemical properties, osteogenesis activity, and fibroblast growth factor-2 release ability of β-tricalcium phosphate for bone cement by calcium silicate. Mater Sci Eng C. 2014; 37:156-63.
9. Kunjalukkal Padmanabhan S, Gervaso F, Carrozzo M, Scalera F, Sannino A, Licciulli A. Wollastonite/hydroxyapatite scaffolds with improved mechanical, bioactive and biodegradable properties for bone tissue engineering. Ceram Int. 2013; 39(1):619-627.
10. Zhang N, Molenda JA, Fournelle JH, Murphy WL, Sahai N. Effects of pseudowollastonite ($CaSiO_3$) bioceramic on in vitro activity of human mesenchymal stem cells. Biomaterials. 2010; 31(30):7653-7665.
11. Magallanes-Perdomo M, De Aza AH, Mateus AY, Teixeira S, Monteiro FJ, De Aza S, et al. In vitro study of the proliferation and growth of human bone marrow cells on apatite-wollastonite-2M glass ceramics. Acta Biomater. 2010;6(6):2254–63.
12. Palakurthy S, K. VGR, Samudrala RK, P. AA. In vitro bioactivity and degradation behaviour of β-wollastonite derived from natural waste. Mater Sci Eng C. 2019;98.109-117.

13. Zhang NL, Molenda JA, Fournelle JH, Murphy WL, Sahai N. Effects of pseudowollastonite ($CaSiO_3$) bioceramic on in vitro activity of human mesenchymal stem cells. Biomaterials. 2010;31(30):7653–65.

14. Lin K, Zhai W, Ni S, Chang J, Zeng Y, Qian W. Study of the mechanical property and in vitro biocompatibility of $CaSiO_3$ ceramics. Ceram Int. 2005; 31(2):323-326.

15. Siriphannon P, Kameshima Y, Yasumori A, Okada K, Hayashi S. Influence of preparation conditions on the microstructure and bioactivity of α-$CaSiO_3$ ceramics: Formation of hydroxyapatite in simulated body fluid. J Biomed Mater Res. 2000; 52(1):30-39.

16. Ni S, Chang J, Chou L. A novel bioactive porous $CaSiO_3$ scaffold for bone tissue engineering. J Biomed Mater Res - Part A. 2006; 76(1):196-205.

17. Ni S, Chang J, Chou L, Zhai W. Comparison of osteoblast-like cell responses to calcium silicate and tricalcium phosphate creamics in vitro. J Biomed Mater Res - Part B Appl Biomater. 2007; 80(1):174-83.

18. Wang C, Lin K, Chang J, Sun J. Osteogenesis and angiogenesis induced by porous β-$CaSiO_3$/PDLGA composite scaffold via activation of AMPK/ERK1/2 and PI3K/Akt pathways. Biomaterials. 2013; 34(1):64-77.

19. Kohn DH, Sarmadi M, Helman JI, Krebsbach PH. Effects of pH on human bone marrow stromal cells in vitro: Implications for tissue engineering of bone. J Biomed Mater Res. 2002; 60(2):292-9.

20. Luo T, Wu C, Zhang Y. The in vivo osteogenesis of Mg or Zr-modified silicate-based bioceramic spheres. J Biomed Mater Res - Part A. 2012; 100(9):2269-77.

21. Cannillo V, Colmenares-Angulo J, Lusvarghi L, Pierli F, Sampath S. In vitro characterisation of plasma-sprayed apatite/wollastonite glass-ceramic biocoatings on titanium alloys. J Eur Ceram Soc. 2009; 29(9):1665-1677.

22. Ramaswamy Y, Wu C, Van Hummel A, Combes V, Grau G, Zreiqat H. The responses of osteoblasts, osteoclasts and endothelial cells to zirconium modified calcium-silicate-based ceramic. Biomaterials. 2008;29(33):4392–402.

23. Piconi C, Maccauro G. Zirconia as a ceramic biomaterial. Biomaterials. 1999.

24. Li HC, Wang DG, Chen CZ. Effect of zinc oxide and zirconia on structure, degradability and in vitro bioactivity of wollastonite. Ceram Int. 2015;41(8):10160–9.

25. Zhu Y, Zhang Y, Wu C, Fang Y, Yang J, Wang S. The effect of zirconium incorporation on the physiochemical and biological properties of mesoporous bioactive glasses scaffolds. Microporous Mesoporous Mater. 2011; 143(2-3):311-319.

26. Montazerian M, Yekta BE, Marghussian VK, Bellani CF, Siqueira RL, Zanotto ED. Bioactivity and cell proliferation in radiopaque gel-derived CaO-P_2O_5-SiO_2-ZrO_2 glass and glass-ceramic powders. Mater Sci Eng C. 2015; 55:436-447.

27. Hong KJ, Kim JM, Kim HS. Microstructure and properties of CaO-ZrO_2-SiO_2 glass-

ceramics prepared by sintering. J Eur Ceram Soc. 2003; 23(13):2193-2202.

28. Ismail H, Shamsudin R, Abdul Hamid MA. Effect of autoclaving and sintering on the formation of β-wollastonite. Mater Sci Eng C. 2016;58:1077–81.

29. Klimesch DS, Ray A. The use of DTA/TGA to study the effects of ground quartz with different surface areas in autoclaved cement : Quartz pastes. Part 1: A method for evaluating DTA/TGA results. Thermochim Acta. 1996;289(1):41–54.

30. Yu B, Liang K, Gu S. Effect of ZrO_2 on crystallization of CaO-P_2O_5-SiO_2 glasses. Ceram Int. 2002; 28(6):695-698.

31. Shuai C, Feng P, Yang B, Cao Y, Min A, Peng S. Effect of nano-zirconia on the mechanical and biological properties of calcium silicate scaffolds. Int J Appl Ceram Technol. 2015; 12(6):1148-1156.

32. Yin P, Yuan JW, Liu LH, Xiao T, Lei T. Effect of ZrO_2 on the bioactivity properties of gel-derived CaO-P_2O_5-SiO_2-SrO glasses. Ceram Int. 2017; 43(13):9691-9698.

33. Paluszkiewicz C, Blazewicz M, Podporska J, Gumuła T. Nucleation of hydroxyapatite layer on wollastonite material surface: FTIR studies. Vib Spectrosc. 2008; 48(2):263-268.

34. Meiszterics A, Rosta L, Peterlik H, Rohonczy J, Kubuki S, Henits P, et al. Structural characterization of gel-derived calcium silicate systems. J Phys Chem A. 2010;114(38):10403–11.

35. Swann GEA, Patwardhan S V. Application of Fourier Transform Infrared Spectroscopy (FTIR) for assessing biogenic silica sample purity in geochemical analyses and palaeoenvironmental research. Clim Past. 2011;7(1):65–74.

36. Palakurthy S, P AA, K VR. In vitro evaluation of silver doped wollastonite synthesized from natural waste for biomedical applications. Ceram Int. 2019; 45(18):25044-25051.

37. Palakurthy S, Azeem PA, Venugopal Reddy K, Penugurti V, Manavathi B. A comparative study on in vitro behavior of calcium silicate ceramics synthesized from biowaste resources. J Am Ceram Soc. 2019; 103(2):933-943.

38. Kaur G, Pickrell G, Kimsawatde G, Homa D, Allbee HA, Sriranganathan N. Synthesis, cytotoxicity, and hydroxyapatite formation in 27-Tris-SBF for sol-gel based CaO-P_2O_5-SiO_2-B_2O_3-ZnO bioactive glasses. Sci Rep. 2014; 4:4392.

39. Shuai C, Gao C, Nie Y, Hu H, Zhou Y, Peng S. Structure and properties of nano-hydroxypatite scaffolds for bone tissue engineering with a selective laser sintering system. Nanotechnology. 2011; 22:285703.

40. Liu X, Ding C, Chu PK. Mechanism of apatite formation on wollastonite coatings in simulated body fluids. Biomaterials. 2004;25(10):1755–61.

41. Gozalian A, Behnamghader A, Daliri M, Moshkforoush A. Synthesis and thermal behavior of Mg-doped calcium phosphate nanopowders via the sol gel method. Sci Iran. 2011; 18(6):1614-1622.

42. Landi E, Tampieri A, Mattioli-Belmonte M, Celotti G, Sandri M, Gigante A, et al. Biomimetic Mg- and Mg,CO_3-substituted hydroxyapatites: synthesis characterization and in vitro behaviour. J Eur Ceram Soc. 2006; 26(13):2593-2601.

43. Ohtsuki C, Kokubo T, Yamamuro T. Mechanism of apatite formation on CaO-SiO_2-P_2O_5 glasses in a simulated body fluid. J Non Cryst Solids. 1992; 143:84-92.

44. Yang Z, Jiang Y, Yu LX, Wen B, Li F, Sun S, et al. Preparation and characterization of magnesium doped hydroxyapatitegelatin nanocomposite. J Mater Chem. 2005; 15(18):1807-1811.

45. Magallanes-Perdomo M, Luklinska ZB, De Aza AH, Carrodeguas RG, De Aza S, Pena P. Bone-like forming ability of apatite-wollastonite glass ceramic. J Eur Ceram Soc. 2011;31(9):1549–61.

46. Hoppe A, Güldal NS, Boccaccini AR. A review of the biological response to ionic dissolution products from bioactive glasses and glass-ceramics. Biomaterials. 2011;32:2757–74.

47. Zhang F, Chang J, Lu J, Lin K, Ning C. Bioinspired structure of bioceramics for bone regeneration in load-bearing sites. Acta Biomater. 2007; 3(6):896-904.

48. International Organization for Standardization. Biological evaluation of medical devices - Part 5: Tests for in vitro cytotoxicity. Iso 10993–5. 2009.

49. Wang H, Pallav P, Isgrò G, Feilzer AJ. Fracture toughness comparison of three test methods with four dental porcelains. Dent Mater. 2007; 23(7):905-10.

50. Li HC, Wang DG, Meng XG, Chen CZ. Effect of ZrO2 additions on the crystallization, mechanical and biological properties of MgO-CaO-SiO_2-P_2O_5-CaF_2 bioactive glass-ceramics. Colloids Surfaces B Biointerfaces. 2014; 118:226-233.

51. Gorman CM, Hill RG. Heat-pressed ionomer glass-ceramics. Part II. Mechanical property evaluation. Dent Mater. 2004; 20(3):252-261.

52. Stanton KT, O'Flynn KP, Kiernan S, Menuge J, Hill R. Spherulitic crystallization of apatite-mullite glass-ceramics: Mechanisms of formation and implications for fracture properties. J Non Cryst Solids. 2010; 356(35-36):1802-1813.

53. Ignatius AA, Wolf S, Augat P, Claes LE. Composites made of rapidly resorbable ceramics and poly(lactide) show adequate mechanical properties for use as bone substitute materials. J Biomed Mater Res. 2001; 57(1):126-31.

54. Hench LL. Bioceramics: From Concept to Clinic. J Am Ceram Soc. 1991;74(7):1487–510.

Chapter 7

Structural and biological properties of diopside ceramics ($CaMgSi_2O_6$) derived from bio-waste

This chapter throws light on the extension of method of preparation for calcium silicate-based bioceramics such as diopside ($CaMgSi_2O_6$), akermanite ($Ca_2MgSi_2O_7$), bredigite ($Ca_7Mg(SiO_4)_4$), merwinite ($Ca_3MgSi_2O_8$), monticellite ($CaMgSiO_4$), hardystonite ($Ca_2Zn(Si_2O_7)$ and baghdadite ($Ca_3ZrSi_2O_9$). Among various calcium silicates-based bioceramics, diopside with the crystal structure of monoclinic, has received much attention on account of its quite interesting properties in terms of good compressive strength, mechanical stability and bending strength, and controllable degradation rate. It shows good hydroxyapatite formation rate and has excellent in vivo osteoinduction. Therefore, we have synthesized diopside bioceramics from RHA and eggshell via sol-gel method, while also determining the degradation rate, apatite-forming ability, biocompatibility and mechanical properties for bone tissue reconstruction and repair.

7.1 Introduction

Calcium phosphates, calcium silicates and calcium sulphates are representative of commonly used bioactive materials [1, 2]. Tricalcium phosphate and hydroxyapatite are ceramics based on calcium phosphates, which have molecular composition equivalent to that of human bone [3], are potentially used in orthopedic applications for bone tissue repair and extensively studied to induce bone regeneration because of its exceptional adaptation under human body environment [4, 5]. However, low mechanical strength, fracture toughness and slow degradation rate of calcium phosphates have hindered its broader applications as orthopedic implants [6].

Calcium silicate – based biomaterials including bioglass, $CaSiO_3$ and Ca – Si – x (x = Zr, Ti, Zn, Mg, Sr) ceramics, are an emerging subject of research for bone tissue engineering [7–9]. Literature reports have shown that the release of Ca and Si ions at specific concentrations induces osteoblasts cells proliferation and differentiation being a significant feature of calcium silicate – based biomaterials [10]. Furthermore, the relatively widespread range of chemical compositions of calcium silicate – based bioceramics can greatly impact mechanical properties, making them capable of stress and load-bearing orthopedic applications [11].

Magnesium ions in mammalian bodies are the fourth most abundant cations and in combination with sodium and calcium ion channels, play a key role in mammalian cells, stabilizing DNA and stimulating cell growth and proliferation. The role of Mg^{2+} ions in adhesion and growth of osteoblastic cells to degraded magnesium compound has been clearly revealed in many *in vitro* examinations [12, 13]; thus magnesium is a very important component in bioceramics to enhance biological properties [14, 15]. Diopside ($CaMgSi_2O_6$), akermanite ($Ca_2MgSi_2O_7$), merwinite ($Ca_3MgSi_2O_8$), bredigite ($Ca_7MgSi_4O_{16}$) and

monticellite ($CaMgSiO_4$) are pure phase ceramics belonging to the magnesium containing calcium silicates group, which have been examined for their potential applications as bone substitutes. Among these, calcium magnesium silicates, diopside with the crystal structure of monoclinic, has received much attention on account of its quite interesting properties in terms of good compressive strength, mechanical stability and bending strength [16] and controllable degradation rate [17]. It shows good hydroxyapatite formation rate and has excellent *in vivo* osteoinduction [17, 18]. Diopside finds use in a wide variety of clinical applications such as bone and dental root implants [19], surgery hemostasis applications [20], drug delivery [21] and in *in vivo* imaging [22].

Different synthesis techniques have already been described for diopside ceramics such as solid state sintering [23], co-precipitation process [24], sol-gel technique [25] and hydrothermal methods [26]. Precursor materials used in these processes are commercial CaO or $Ca(NO_3)_2.4H_2O$ and commercial SiO_2 or tetraethyl orthosilicate (TEOS). However the raw materials are expensive and have limitations when used for bulk synthesis. Moreover, these methods require high temperature treatment. The objective of the current work is to report a cost effective synthesis of diopside using bio-waste such as rice husk as a source of silica and eggshells as a source of calcium oxide through sol-gel technique, while also determining the degradation rate, apatite-forming ability, biocompatibility and mechanical properties for bone tissue reconstruction and repair.

7.2 Results and discussion

7.2.1 Thermal analysis

The thermal stability and phase transformations of dried gel were studied using simultaneous TG-DTA investigation. Fig. 7.1 displays the TG-DTA plots of synthesized diopside gel after it was dried. The TGA curve exhibited mainly three distinct steps of weight

loss: the initial weight loss step was seemed at 30 – 150 °C with a comparable weight loss of ~13.8 % and it was observed in DTA curve as an endothermic hump at ~100 °C, ascribed to the removal of residual water [27]. The next step of weight loss which occurred between 150 – 450 °C showed a broad exothermic hump with a trivial weight loss of ~7.9, which was associated with the dehydration of chemically adsorbed water [27, 28]. The final step of weight loss was more prominent, which can be observed at 450 – 750 °C showed an endothermic peak around 530 °C, while the corresponding weight loss of ~12.6, ascribed to the elimination of by-products from incomplete condensation of the precursors, most likely decarbonation as well as the removal of nitrate ions from Mg $(NO_3)_2$. $6H_2O$ [29, 30]. It was observed that mass loss becomes constant after 750 °C. In the DTA curve, the exothermic peak observed at ~776 °C is presumed to be caused by the crystallization of dried gel powder into diopside. The exothermic crystallization peak value thus obtained was compared with the previously reported results of diopside produced using different starting materials and by various synthesis methods (Table 7.1). It is clearly indicated that the crystallization temperature is dependent of method of preparation and the starting materials. The crystallization temperature revealed that the diopside prepared from RHA and eggshells by the present sol-gel method crystallized at lower temperature when compared to previous investigations by other researchers, except that the dried diopside gel powder prepared by the sol–gel method using metal alkoxides and metal salts as starting materials.

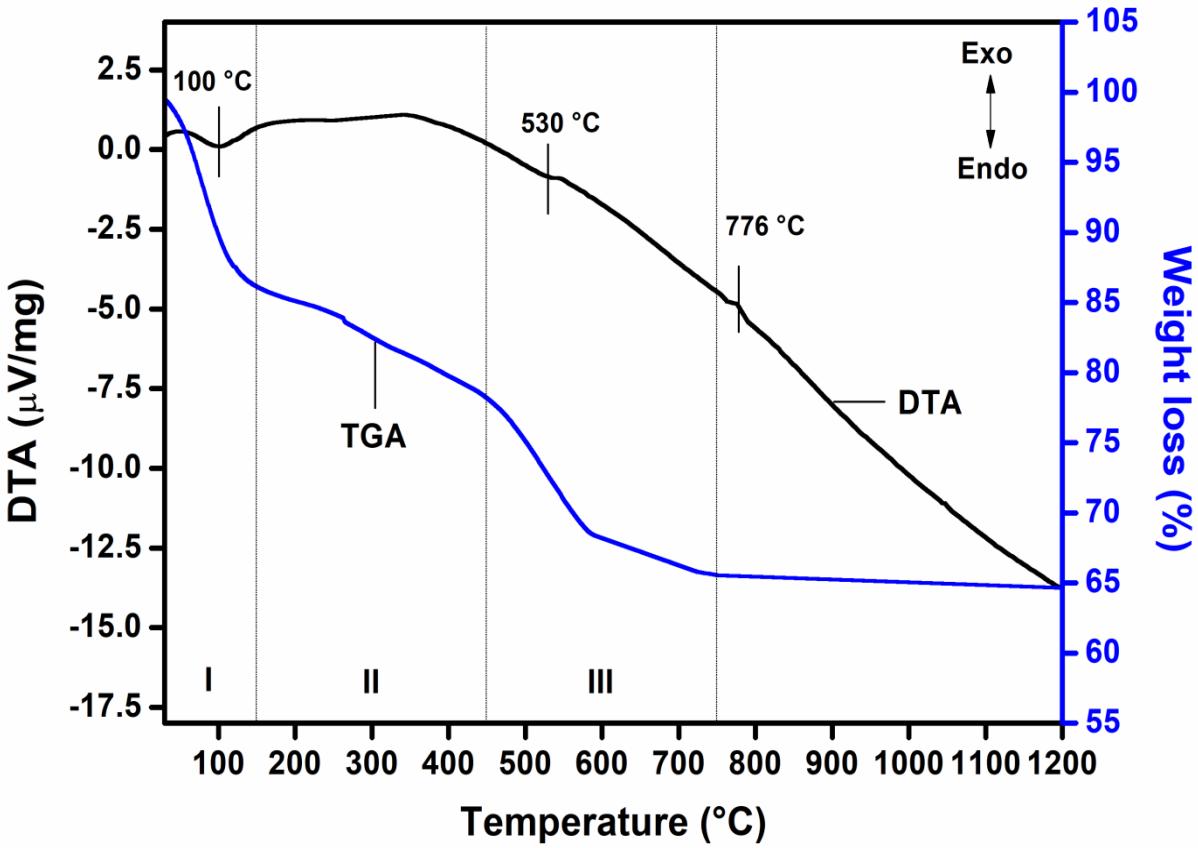

Fig. 7.1 TG-GTA curves of diopside samples

Table 7.1 Crystallization temperature of diopside synthesized using various starting materials and by different synthesis methods

Preparation method	Starting materials	Crystallization temperature (°C)	Ref.
Sol-gel	Rice husk ash, eggshells and $Mg(NO_3)_2 \cdot 6H_2O$	776	Present study
Solid-state reaction	SiO_2 , $CaCO_3$ and MgO	882	[31]
Coprecipitation	TEOS, $Ca(NO_3)_2 \cdot 4H_2O$ and $Mg(NO_3)_2 \cdot 6H_2O$	845	[24]
Sol-gel	TEOS, $Ca(OC_2H_5)_2$ and $Mg(OC_2H_4OC_2H_5)_2$	840	[32]
Sol-gel	TEOS, $Ca(NO_3)_2 \cdot 4H_2O$ and $MgCl_2 \cdot 6H_2O$	751	[33]
Ball milling assisted solid-state reaction	SiO_2, eggshell and MgO	880	[34]
Solid-state reaction	Rice husk ash, eggshell and MgO	870	[35]

7.2.2 Structural characterization

The quantitative Rietveld refinement analysis of XRD powder data was performed using generalised structure analysis system (GSAS) along with graphical user interface EXPGUI [36, 37]. Fig. 7.2 shows the Rietveld plot for the sintered sample at 800 °C. The results showed the presence of monoclinic diopside ($CaMgSi_2O_6$) phase. Further from the XRD pattern, the structural parameters of crystalline phase and refinement reliability factor were obtained using GSAS software and are given in Table 7.2. The value of pattern-dependent disagreement factor (R_{WP}) was obtained as 7.93% and no other possible impurity was observed. Thus the results showed that the prepared ceramics from eggshells and RHA by the present sol-gel technique possess sharp, intense and highly crystalline peaks which corresponded to pure diopside phase at low sintering temperature of 800 °C. The average crystalline size was calculated as ~34.93 nm on high intensity diffraction peaks by Scherrer's equation. Literature reports showed that pure phase of diopside was obtained in the temperature range of 1100 – 1300 °C. Moreover, akermanite and monticellite phases were the secondary phases which are generally observed during the preparation of diopside [17, 24, 33, 38]. The present results revealed that the pure phase of diopside was obtained at a temperature of 800 °C, which was significantly low compared to previous studies. The low sintering temperature could be due to the method that was adopted to use RHA and eggshell as alternative sources.

Table 7.2 Rietveld refinement quality parameters of prepared diopside sample

Parameter	Rietveld Result
Formula	$CaMgSi_2O_6$
Crystal system	Monoclinic
Space group	C 1 2/c 1
Unit cell parameters	a = 9.7415 (3), b = 8.9323 (3) and c= 5.2504 (1) $\alpha = \gamma = 90$ and $\beta = 106.233$
R_{WP} (%)	7.93
Chi squared χ^2	1.819
Volume ($Å^3$)	438.65 (3)

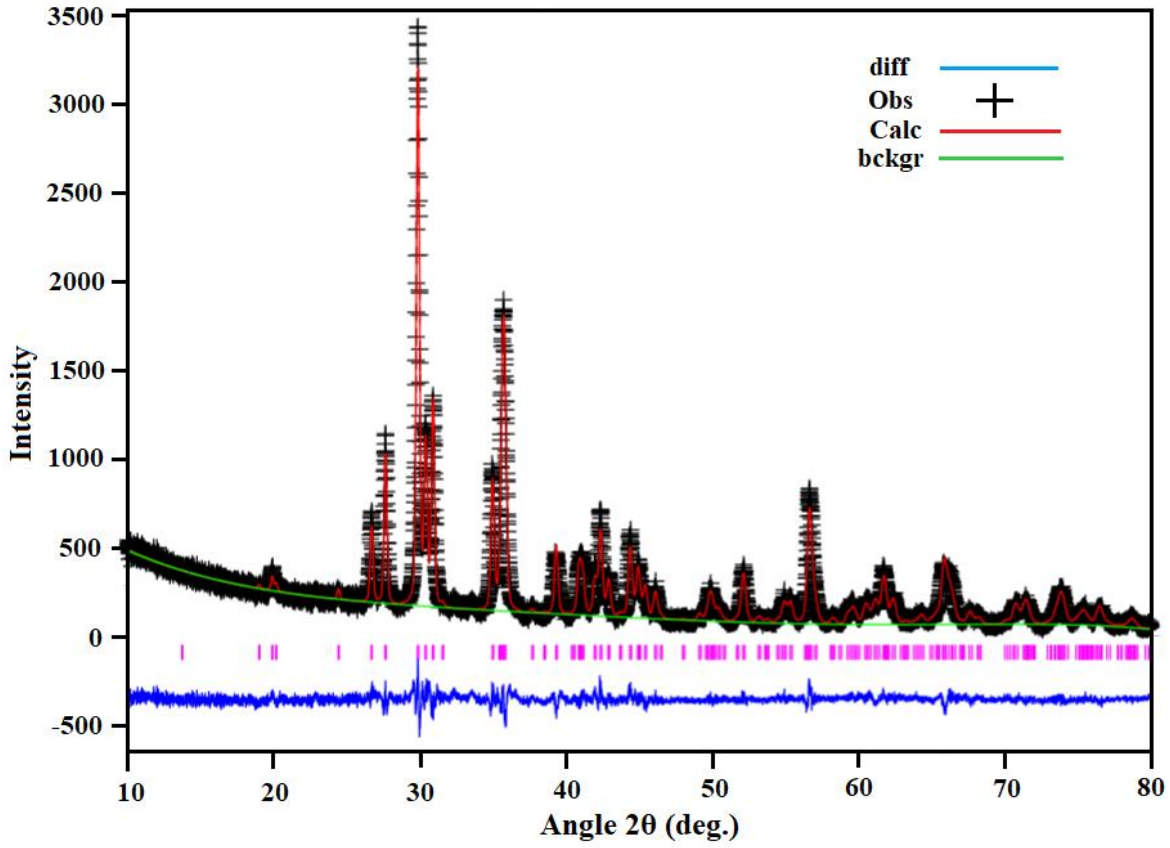

Fig. 7.2 GSAS Rietveld refinement plot for the prepared diopside ceramic

The morphological parameters of synthesized diopside ceramics were analyzed by SEM-EDS. Fig. 7.3 shows the surface micrographs and relative elemental spectra of diopside pellets sintered at 800 °C. SEM image of surface of diopside pellets shows porous surface with agglomerated spherical particles of about 0.3 µm – 0.44 µm in diameter. The appearance of pores on the surface of diopside pellets might be due to the release of volatile materials through calcination and sintering procedure. Porous and agglomerated surface shows significant role in the interaction of bioceramic implants in the surrounding tissues [39, 40]. The EDS spectra show the presence of all indispensable elements like Ca, Mg, Si and O. No extra impure elements were detected, which further supports the XRD data that pure diopside phase was achieved from eggshell and RHA at 800 °C.

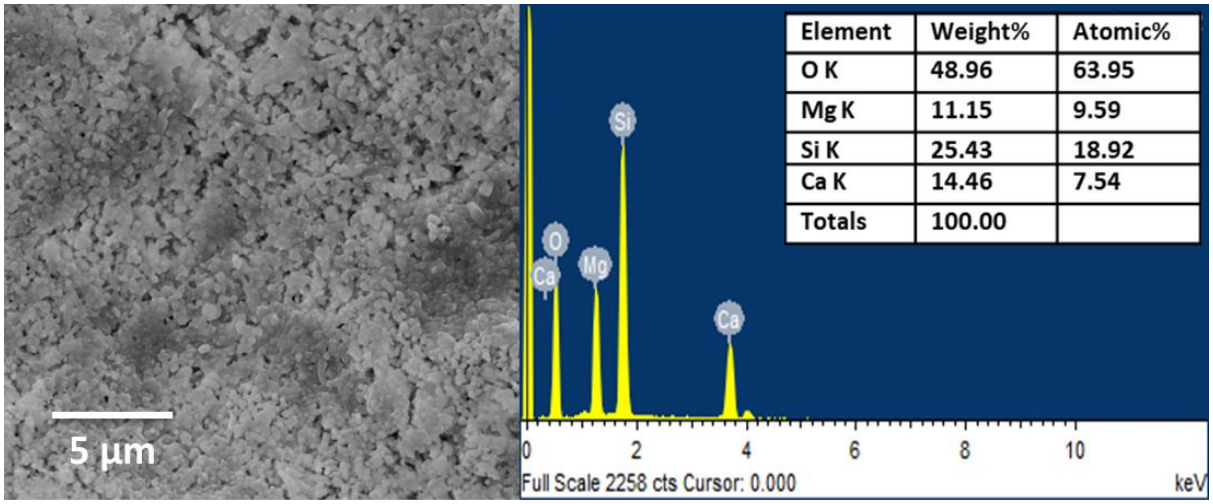

Fig. 7.3 SEM-EDS of sintered diopside sample

All characteristic functional groups related to diopside were detected in FTIR spectra (Fig. 7.4) of sintered specimens at 800 °C. Non-bridging bending vibration mode of (NBO) O – Ca – O (NBO) was observed at ~ 415 cm^{-1} and the bands at ~ 470 and ~ 510 cm^{-1} represent the non-bridging bending vibration mode of (NBO) O – Mg – O (NBO). The sharp peaks at ~ 630 and ~ 675 cm^{-1} showed bending mode of (NBO) Si – O – Si (NBO), while the band at ~ 865 cm^{-1} was attributed to stretching of Si – O (NBO) linkages. The IR spectra peaks observed at ~ 964 and ~ 1070 cm^{-1} were ascribed to stretching mode of Si – O (BO). Moreover, stretching vibration band at 3434 cm^{-1} was associated with moisture absorption. These observations were in agreement with previously described diopside functional groups [41–43].

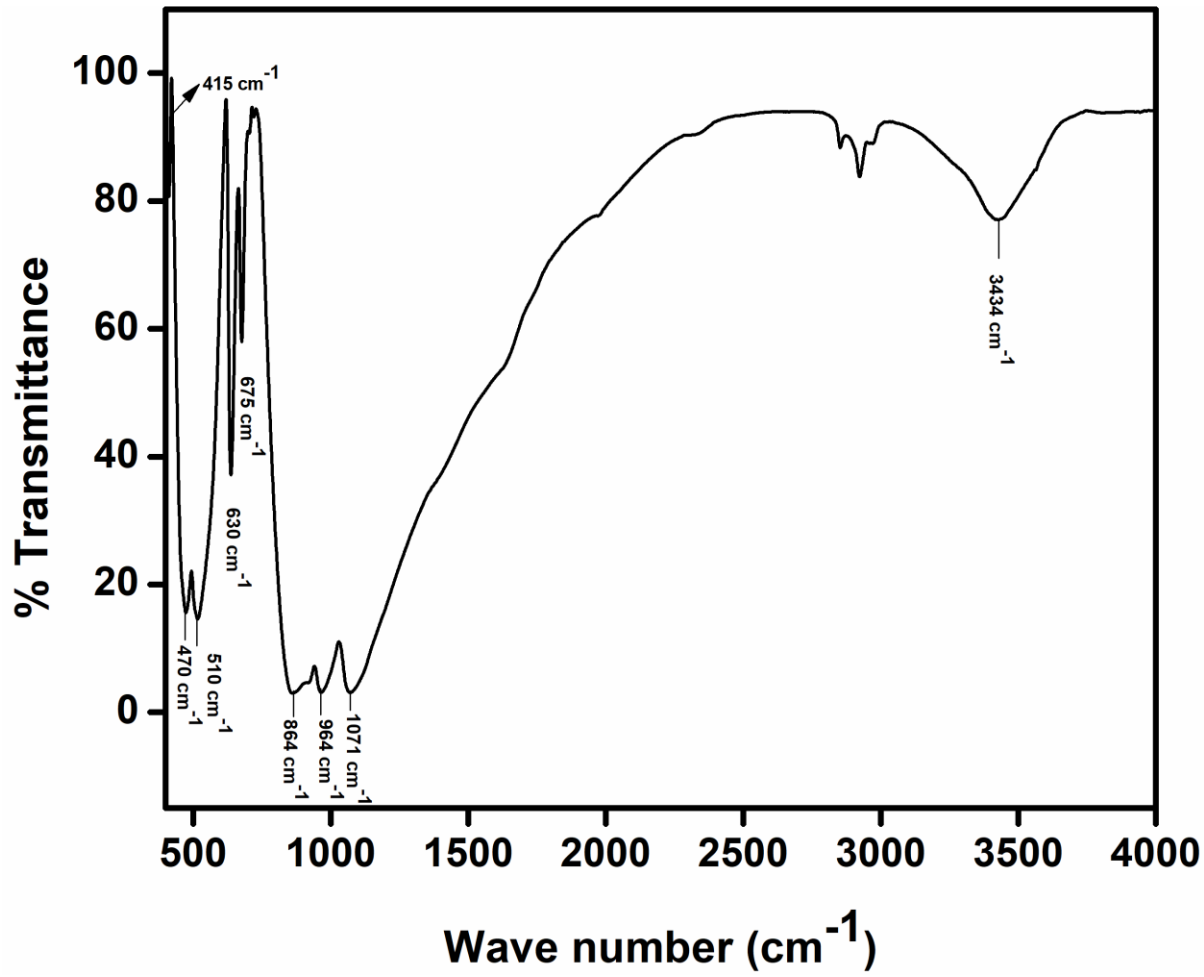

Fig. 7.4 FTIR spectra of diopside ceramics

7.2.3 In vitro bioactivity

Surface crystallinity of diopside ceramics immersed in SBF for 3, 7, 14 and 21 days was examined by XRD patterns (Fig. 7.5) to evaluate hydroxyapatite deposition. XRD record of diopside ceramics soaked in SBF for 3 days, which did not show a significant new crystallinity phase, while the crystalline peaks of diopside started becoming less intense with passage of immersion time which demonstrates that dissolution of diopside, happens first, enabling subsequently the precipitation of hydroxyapatite. The precipitation of small peaks at 2θ = 25.87 (0 0 2) and 31.78 (2 1 1) appeared to be the secondary phase after 7 days of immersion consistent with the reports in JCPDS file No. 09-0432 of hydroxyapatite. The intensity of XRD peaks related to hydroxyapatite marginally increased in samples that had

been immersed for 14 days, but the diopside phase was still dominant. When the surface was analyzed after 21 days of immersion, the hydroxyapatite peaks improved and a few more hydroxyapatite peaks (2θ = 34.04 (2 0 2), 46.71 (2 2 2) and 53.14 (0 0 4)) appeared as trivial phase. These results indicate that the diopside prepared from eggshell and RHA has the ability to form hydroxyapatite in early stages of soaking time in accordance with the literature reports [17, 25, 33].

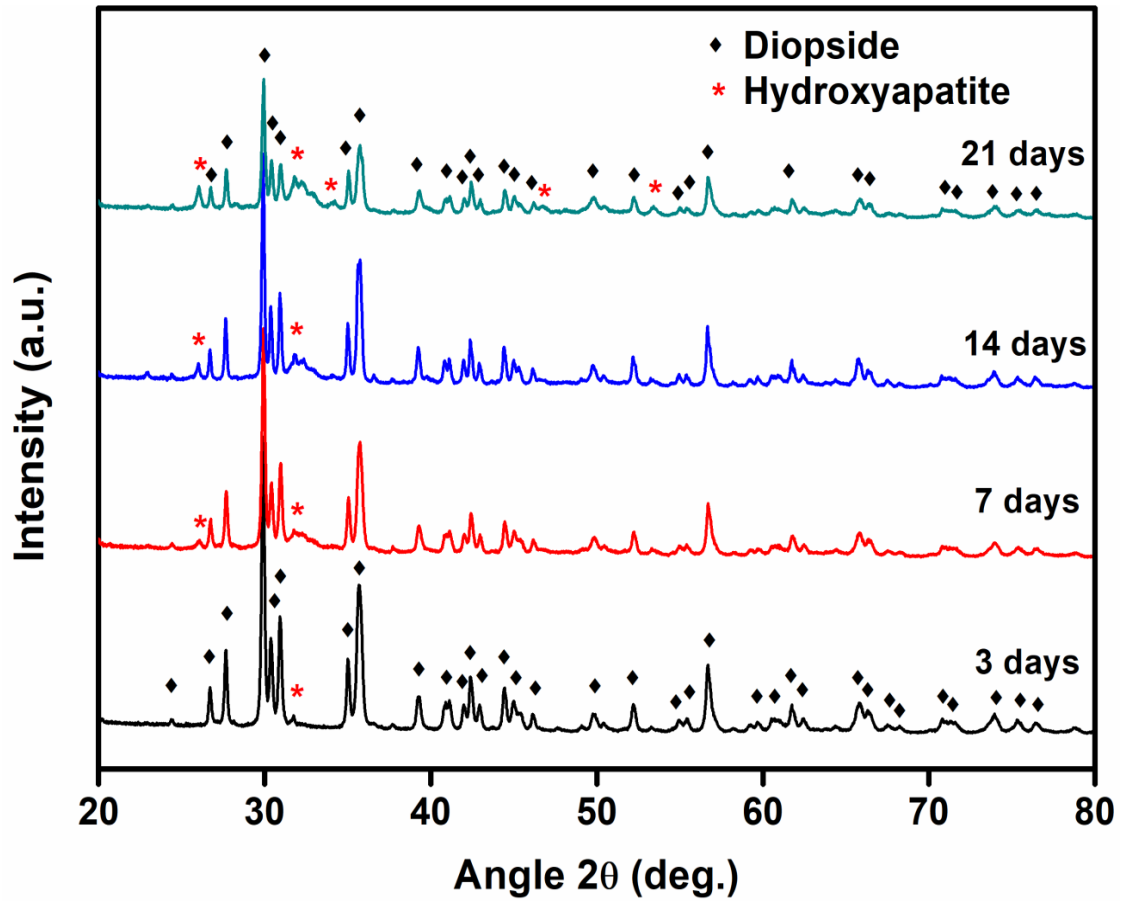

Fig. 7.5 XRD patterns of diopside ceramics after immersion in SBF for 3, 7, 14 and 21 days

SEM photographs of diopside pellets after being immersed for 14 days in SBF showed leaf-like particles formation on their surface (Fig. 7.6). These particles increased in number and were consistently distributed on the sample that had been immersed for 21 days (Fig. 7.6 (b)). The formation of leaf-like particles on diopside pellets was very similar to those of SEM micrographs of hydroxyapatite particle on the surface of bioactive ceramics in

previous reports [24]. Further, EDS spectra of formed leaf-like particles shows the existence of P along with Ca, Mg, Si, O and the P content increased as a result of increasing the time period of immersion from 14 to 21 days.

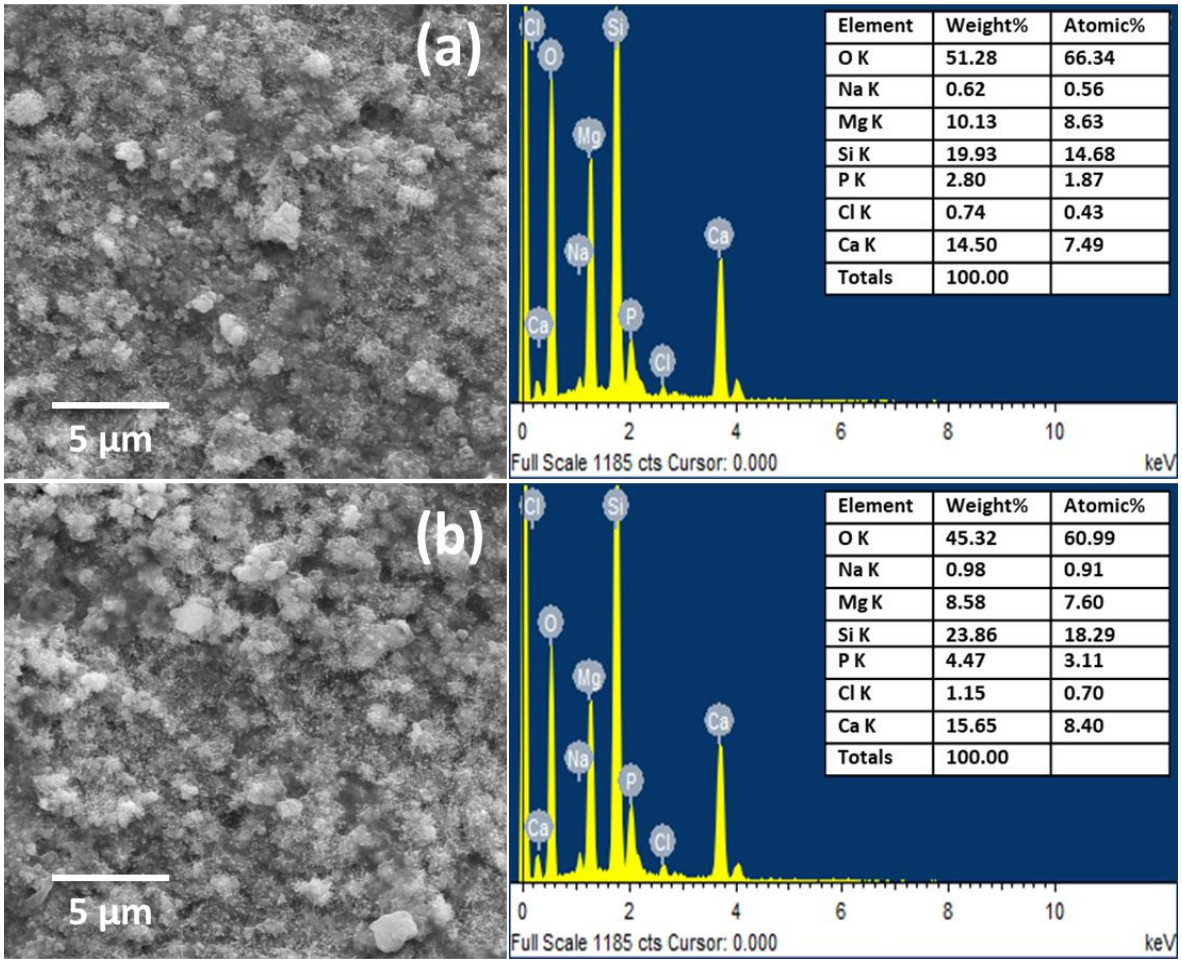

Fig. 7.6 SEM-EDS of diopside (a) after 14 days and (b) after 21 days of immersion in SBF

Fig. 7.7 illustrates the FTIR spectra of hydroxyapatite formation on diopside specimen surface 14 days after soaking in SBF. The FTIR analysis of diopside after immersion in SBF demonstrated that the peaks at ~ 630 and ~ 675 cm^{-1} related to bending mode of silicates become less intense. The peaks at ~ 470 and ~ 510 cm^{-1} corresponding to O – Mg – O were substituted with phosphate bending vibration modes at ~ 485 and 607 cm^{-1}, while the phosphate stretching bands were witnessed at ~ 964 and ~ 1082 cm^{-1}. The presence of phosphate peaks was evidence of the growth of hydroxyapatite on the surface of diopside

after soaking it in SBF. Moreover, the peak at ~ 1405 cm^{-1} was attributed to the carbonate functional group, indicating that carbonated hydroxyapatite (CHA) layer formed on the surface of the sample [44]. The band at ~ 1635 cm^{-1} was evidence of the bending vibrational mode of absorbed H_2O, while the stretching vibrational band at ~ 3434 cm^{-1} was related to moisture absorption [43, 45].

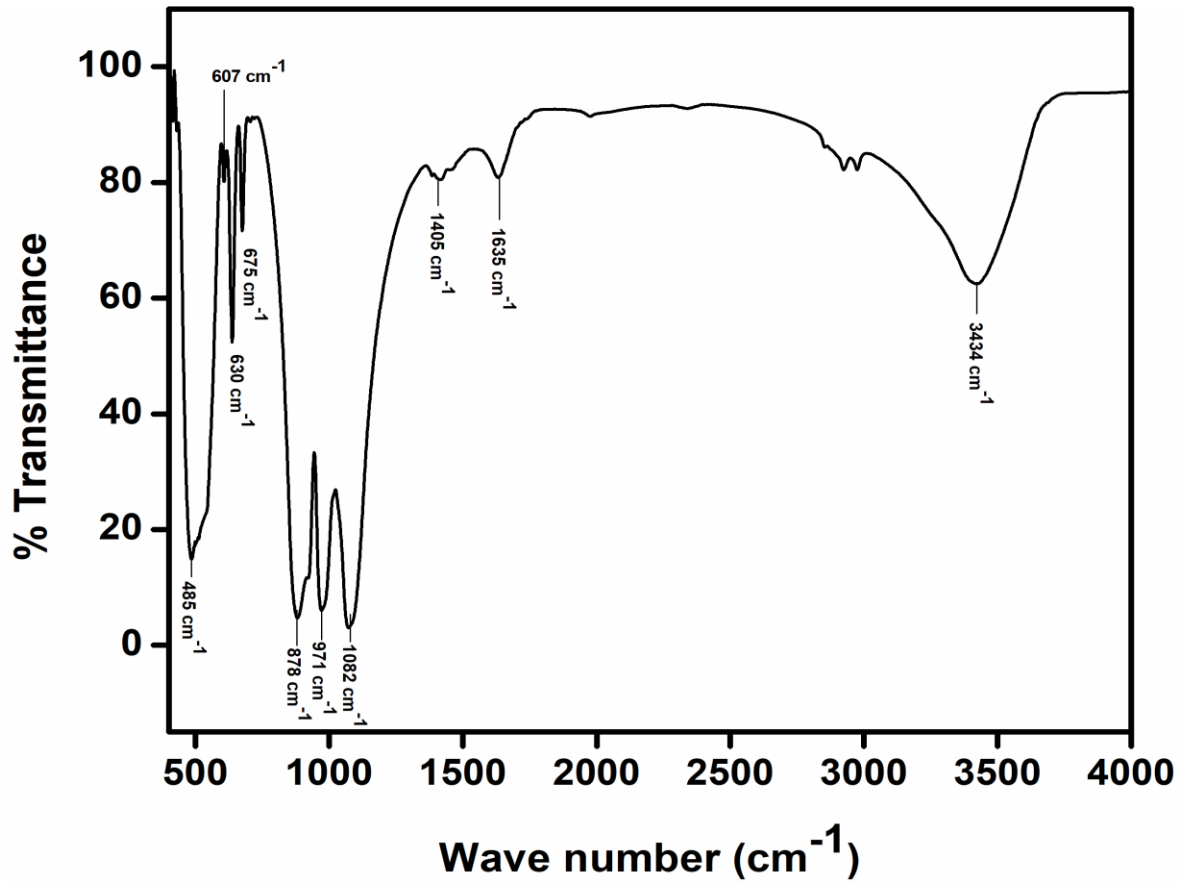

Fig. 7.7 FTIR spectra of diopside after immersion in SBF for 14 days

7.2.4 Change in pH of SBF solution

Variation in pH of SBF as an effect of soaking of diopside pellets is associated with apatite forming ability and degradability. Prior to soaking, fresh SBF had pH value of 7.4, though the pH level increased to a maximum value of ~7.56 after 9 days of immersion, and thereafter the pH value remained constant (Fig. 7.8). Two factors have been reported that lead the change in pH level of SBF; the first is the ion leaching from bioceramics to physiological

fluid i.e. diopside releases Ca^{2+} and Mg^{2+} ions from its surface into SBF, thereby leaving vacancies. These vacancies are filled with H^+ and H_3O^+ ions from SBF, leading to rise in pH level of SBF. The next is the saturation of SBF by means of acid silica [19, 41]. However, the present results showed a pH range of 7.4 – 7.56 when diopside specimens immersed in SBF were slightly lower compared to reports in the literature [16, 46], demonstrating a favourable environment for *in vivo* bone cell culture.

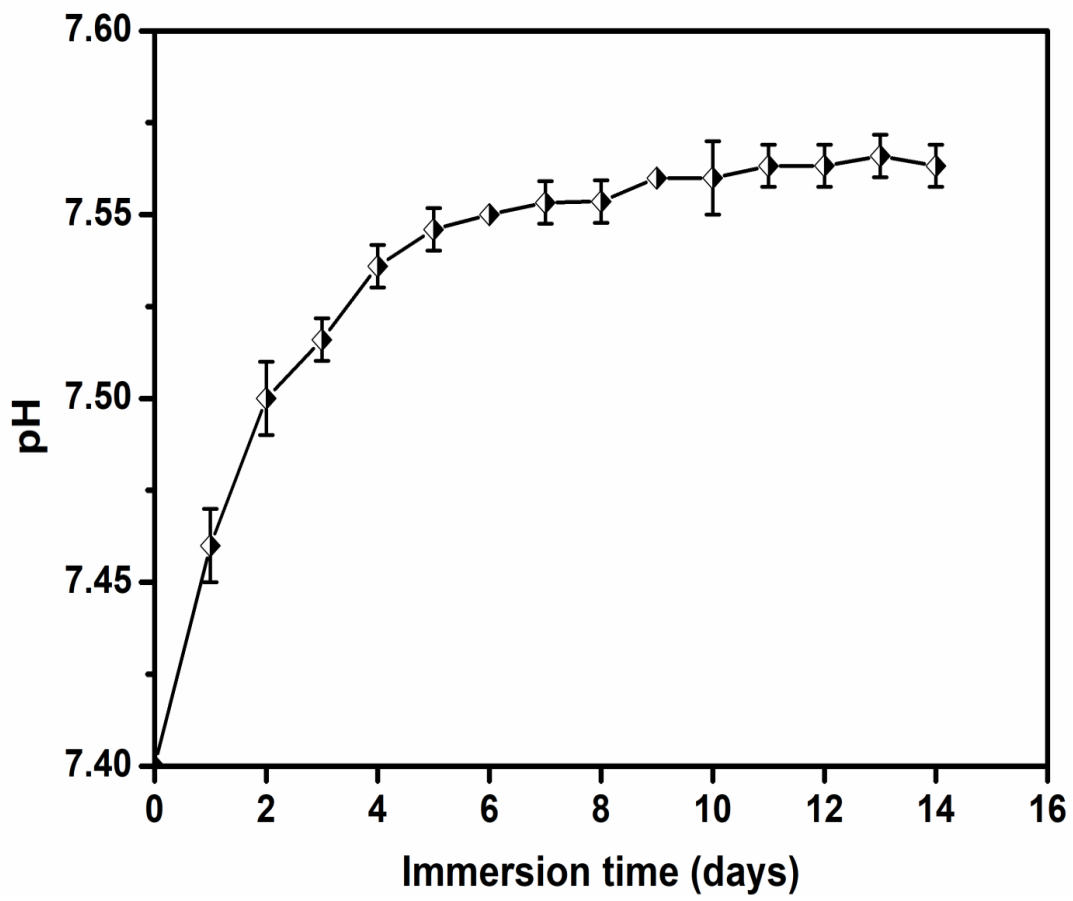

Fig. 7.8 The change of pH value in SBF solution with different immersion times for diopside

7.2.5 Degradation

Degradation of diopside ceramics in SBF is presented in Fig. 7.9. The prepared diopside samples showed a continuous degradation in SBF with increasing immersion period. The weight loss profile increased linearly with increasing immersion time; nevertheless the

overall weight loss was only 1.7% after 28 days of immersion. Previous studies reported that diopside has extremely low degradation rate in SBF owing to the existence of Mg in the crystal structure. The presence of higher bonding energy Mg – O bonds in diopside crystal system makes it more stable and inhibits ion release from the crystal lattice, resulting in a lower degradation rate [47]. The present study demonstrated that diopside ceramics prepared from eggshell and RHA were degradable in a physiological environment; nevertheless, the total weight loss was only 1.7% after soaking it in SBF for 28 days, which is in good agreement with reports available in the literature [16, 17]. Therefore, diopside ceramics with lower rates of dissolution compared to conventional bioceramics might be potential candidates for load-bearing orthopedic applications.

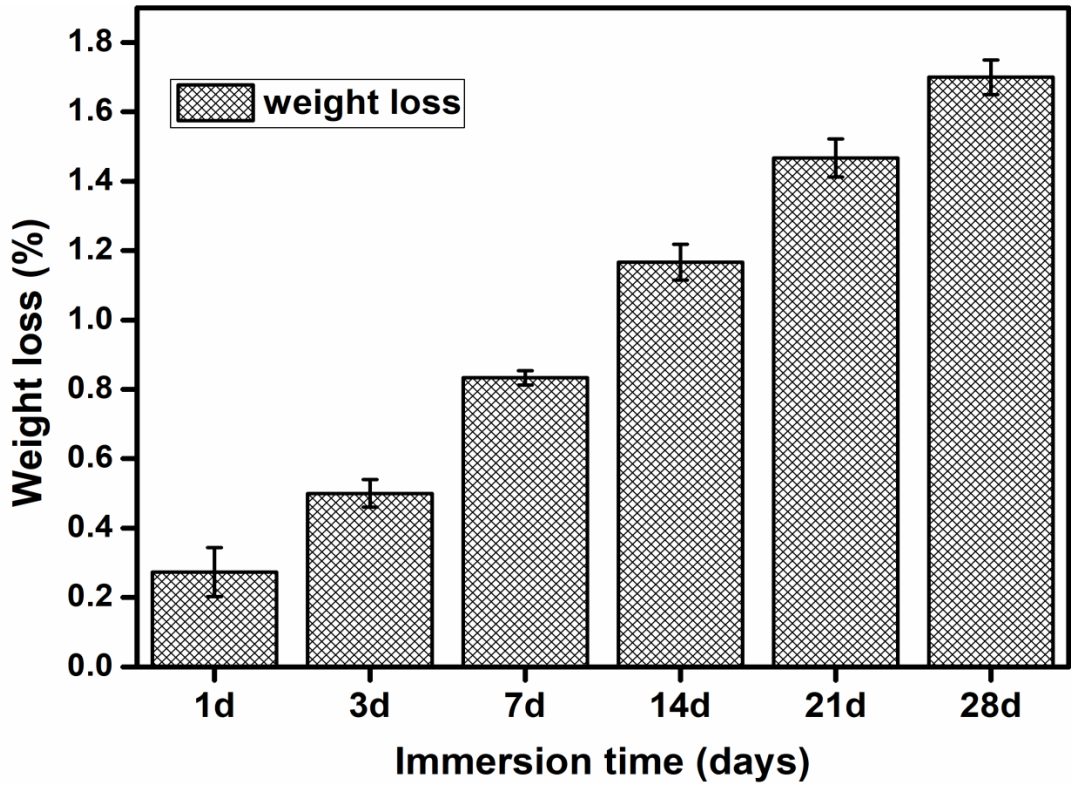

Fig. 7.9 Weight loss of diopside ceramics with different immersion times in SBF solution

7.2.6 Cytocompatibility

The quantitative evaluation of the *in vitro* cytocompatibility assessment is given by calculating the relative percentage of cell viability. Fig. 7.10 represents the relative cell

viability (in %) of osteoblast-like MG-63 cells treated with different dosages of sample dilutions. As can be seen from Fig. 7.10, there is no significant variation in MG-63 cell viability after 48 hours of culture with different dosages (1000μg/mL to 50μg/mL) of sample dilutions. According to biological evaluation of medical devices (Part 5: tests for *in vitro* cytocompatibility (ISO 10993 - 5: 2009)), if the relative cell viability is less than 70% after culture with material then the material has cytotoxic potential. In the present study, it was shown that cell viability is greater than 70% for diopside samples at different concentrations, which revealed the great cytocompatibility potential of prepared diopside ceramics. Furthermore, it has been observed from proliferation assay (Fig. 7.11) that ionic dissolution from diopside ceramics has a clear impact on osteoblasts like cell proliferation. A positive effect on stimulating cell proliferation was observed when the concentrations were between 1.25 and 12.5 mg/mL and after that the stimulatory effect decreased with increasing concentration. The dilution extracts even showed an inhibitory effect on cell proliferation when the concentration was increased to 100 mg/mL in agreement with the previous reports [48]. It has been reported that the proliferation response of the cells depends primarily on the concentration of Ca^{2+} and Mg^{2+} ions released by the ceramics dissolution. For example, Mg^{2+} concentrations of 5 – 10 mM induced proliferation rate of human bone marrow stromal cells, while higher concentrations of Mg^{2+}, that is concentration greater than 20 mM were found to be cytotoxic [12, 49]. Osteoblasts proliferation and differentiation induced by Ca^{2+} concentrations of 2 – 4 mM, and extracellular matrix mineralization were found for medium concentrations of 6 – 8 mM, while cytotoxicity was noticed for Ca^{2+} concentrations of larger than 10 mM [50]. In the present study, cytocompatibility and cell proliferation test results strongly indicate that the synthesized diopside has excellent biocompatibility.

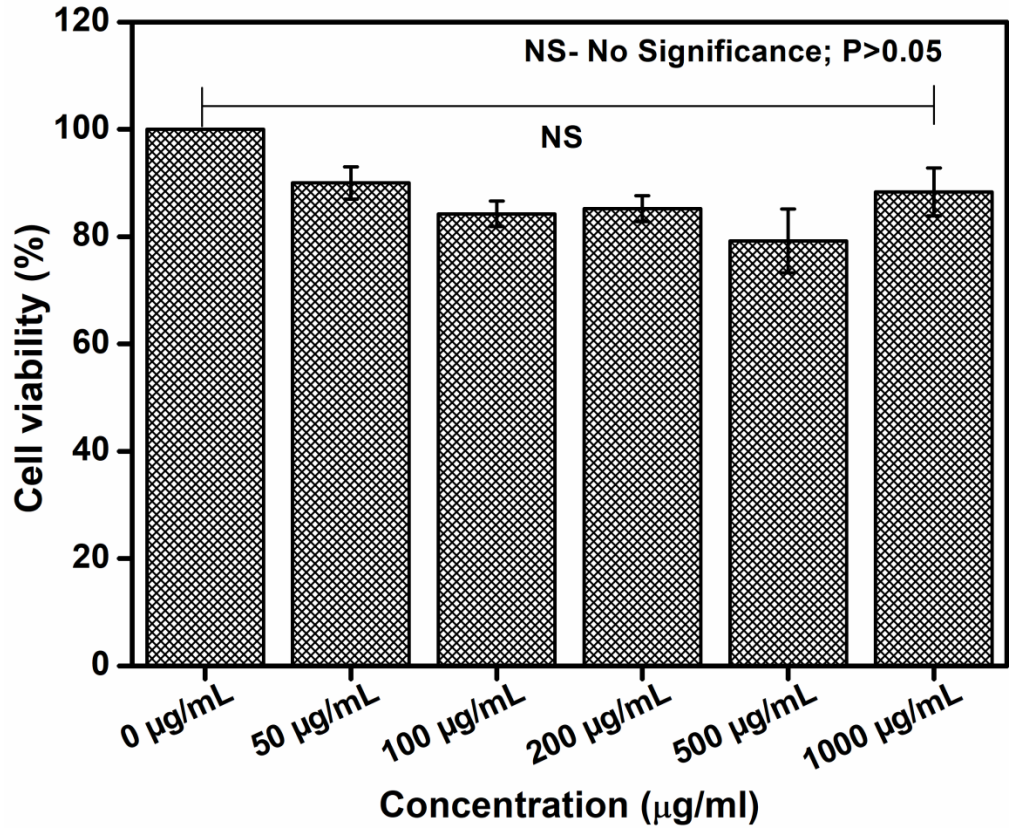

Fig. 7.10 Cell viability of diopside with osteoblast-like MG-63 cells using MTT assay

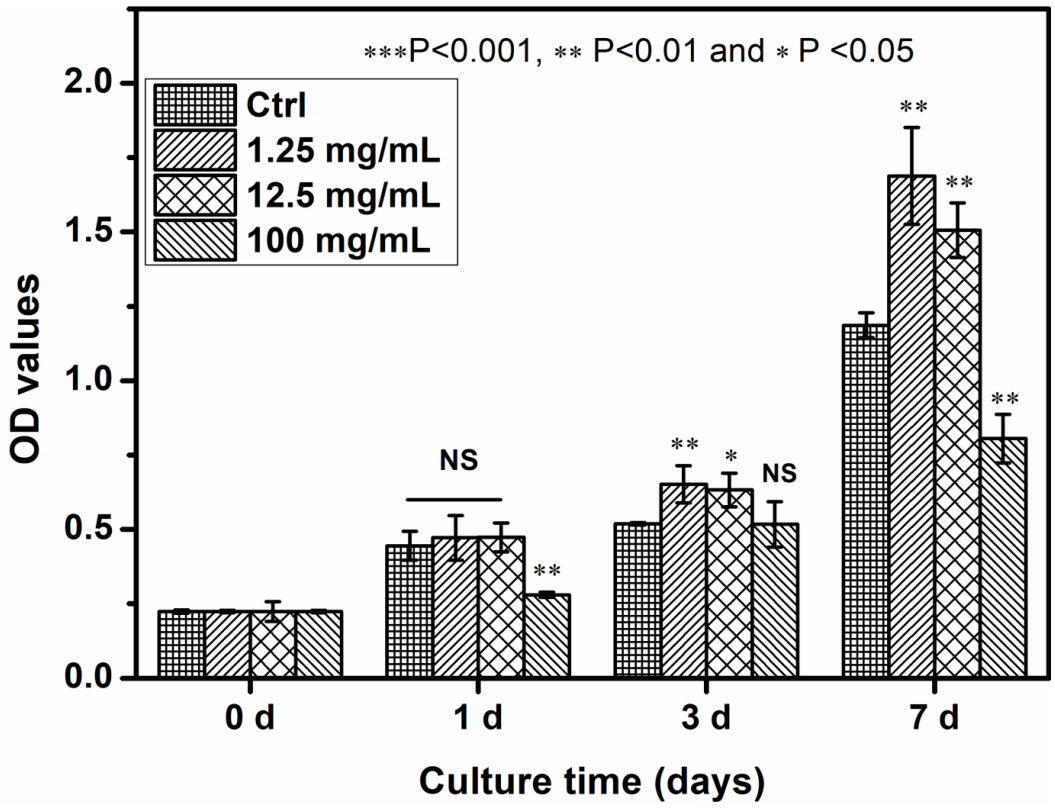

Fig. 7.11 Cell proliferation results of diopside ceramics with osteoblast-like MG-63 cells

7.2.7 Mechanical properties

Experimental determinations of some of the mechanical properties on prepared diopside ceramics in comparison with the previous reported results figure in Table 7.3. The fracture toughness and microhardness values were obtained at five different positions on specimen surface, given the mean value of fracture toughness is about 2.8±0.3 MPa $m^{1/2}$ and microhardness is about 7.31±0.1 GPa. The image of Vickers indentation on polished surface of diopside specimen at 4.9 N loads can be seen in Fig. 7.12. The compressive strength, elasticity modulus and bending strength of diopside were estimated to be 210 ± 12.5, 17.5 ± 2.3 GPa and 86.7 ± 7.3 MPa, respectively. The possible reason for the difference in the mechanical properties of diopside in Table 7.3 could be on account of particles size, pore size and pore distribution. Mechanical properties are highly dependent on particle size, pore size and pore distribution of a material during sintering process. The smaller the particles size, the smaller the pores between adjacent particles, resulting in better mechanical properties of the material [51, 52]. However, the diopside ceramics prepared in the present study possessed good mechanical properties, which are in the range for human cortical bone (Table 7.4), suggesting their potential in applications pertaining to repair of human bones.

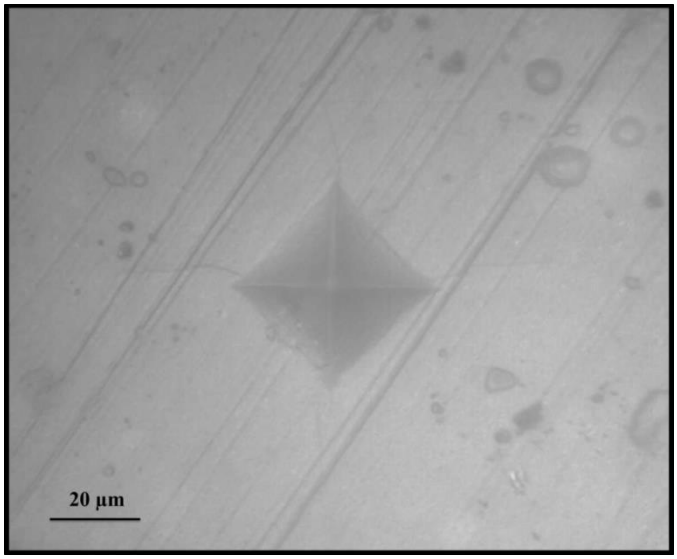

Fig. 7.12 Vickers indentation on diopside ceramics at 4.9 N loads

Table 7.3 Mechanical properties of diopside prepared by different raw materials and methods

Synthesis method	**Starting materials**	**Mechanical properties**					**Ref.**
		Hardness (GPa)	Compressive strength (MPa)	Fracture toughness (MPa $m^{1/2}$)	Bending strength (MPa)	Elasticity modulus (GPa)	
Sol-gel	RHA, eggshells and Mg $(NO_3)_2$ 6 H_2O	7.31 ± 0.1	210 ± 12.5	2.8 ± 0.3	86.7 ± 7.3	17.5 ± 2.3	Present study
Solid-state reaction	SiO_2, $CaCO_3$ and MgO	-	-	3.5	300	170	[38]
Ball milling assisted solid-state reaction	SiO_2, eggshell and MgO	11.5 ± 2.6	-	4 ± 0.3	350 ± 7	112 ± 17	[34]
Ball milling assisted sol-gel	TEOS, $Ca(NO_3)_2{\cdot}4H_2O$ and $Mg(NO_3)_2{\cdot}6H_2O$	-	210 ± 7	-	-	-	[42]
Sol-gel combustion method	TEOS, Eggshell and $Mg(NO_3)_2{\cdot}6H_2O$	-	78 ± 4.4	-	-	3.19 ± 0.4	[43]
Coprecipitation	TEOS, $Ca(NO_3)_2{\cdot}4H_2O$ and $Mg(NO_3)_2{\cdot}6H_2O$	-	1.36 ± 0.3	-	-	0.06 ± 0.02	[16]
Sol-gel	TEOS, $Ca(NO_3)_2{\cdot}4H_2O$ and $MgCl_2{\cdot}6H_2O$	-	8.17 ± 2.3	-	-	-	[53]

Table 7.4 Mechanical properties of diopside in comparison with human bone

Property	**Diopside ($CaMgSi_2O_6$)**	**Cortical bone**	**Cancellous bone**
Microhardness	7.31±0.1 GPa	-	-
Compressive strength	210 ± 12.5 MPa	100-230 MPa	2-12MPa
Fracture toughness	2.8 ± 0.3 MPa $m^{1/2}$	2-12 MPa $m^{1/2}$	-
Bending strength	86.7 ± 7.3 MPa	50-150 MPa	-
Elasticity modulus	17.5 ± 2.3 GPa	7-30 GPa	0.5-0.05 GPa

In vitro mechanical integrity of diopside ceramics was studied by evaluating the compressive strength after soaking it in SBF. Fig. 7.13 illustrates the stress-strain curves under compression (Fig. 7.13(a)) and a plot of compressive strength verses soaking time (Fig. 7.13(b)). As revealed in Fig 7.13, a decrease in compressive strength was obvious in SBF

immersed samples, where the compressive strength value for 28 day SBF immersed samples was reduced to 120 ± 9 MPa. The main reason behind the decrease in compressive strength is the dissolution of ions from a bioactive material resulting in degradation and loss in mechanical strength during soaking in SBF. Apatite formation at a later stage leads to enhancement in the mechanical properties [54]. In the present work, the prepared diopside ceramics showed excellent compressive strength which was nearly similar to the compressive strength of human cortical bone (100-230 MPa) even after 28 days immersion in SBF [55].

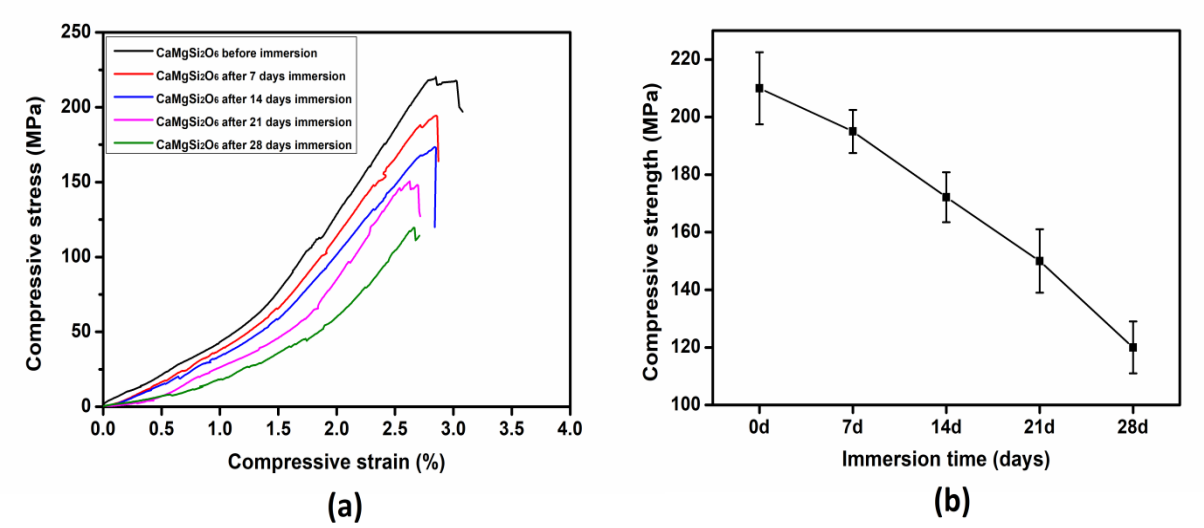

Fig. 7.13 Compressive stress-strain curves (a) and change of compressive strength (b) with different immersion times in SBF solution for diopside ceramic samples

Mechanical stability is a significant factor to prevent the collapse of scaffold structure before the formation of proper extracellular matrix (ECM) and new bone [56]. Literature reports have shown that the compressive strength of diopside scaffolds reduced to 30% for 14 days SBF immersed samples and this reduction for bioglass scaffolds was 54% and for wollastonite scaffolds it was 60% [16, 57]. The present study has shown that after 14 days of immersion in SBF, the compressive strength of prepared diopside ceramics decreased by about 18%. The data demonstrate that diopside ceramics prepared from RHA and eggshells not only have mechanical properties appropriate for human cortical bone, but also show

excellent *in vitro* mechanical stability. Moreover, these excellent mechanical properties and mechanical stability of diopside ceramics show them to be very reliable as strengthening materials to develop biocomposites.

7.3 Conclusion

Pure phase diopside was successfully prepared at significantly low temperature (800 °C) from rice husk ash (RHA) and eggshell using sol-gel method. The prepared diopside ceramics possessed good mechanical properties especially compressive strength (210 ± 12.5 MPa), fracture toughness (2.8 ± 0.3 MPa $m^{1/2}$), bending strength (86.7 ± 7.3 MPa) and elasticity modulus (17.5 ± 2.3 GPa) values in the range seen in human cortical bone, as well as improved mechanical stability and slow degradation rate. Biological studies results demonstrated that the synthesized diopside ceramics exhibited good apatite forming-ability, and cytocompatibility as well as stimulatory effect on osteoblasts like cell proliferation. Therefore, diopside ceramics prepared from RHA and eggshells might be potential low cost candidate for use as bioactive implant in bone tissue engineering as well as safe reinforcement material in the manufacture of biocomposites.

7.4 References

1. Miguez-Pacheco V, Hench LL, Boccaccini AR. Bioactive glasses beyond bone and teeth: Emerging applications in contact with soft tissues. Acta Biomaterialia. 2015; 13:1-15.
2. Gao C, Peng S, Feng P, Shuai C. Bone biomaterials and interactions with stem cells. Bone Research. 2017;5:1-33.
3. Eliaz N, Metoki N. Calcium phosphate bioceramics: A review of their history, structure, properties, coating technologies and biomedical applications. Materials (Basel). 2017; 10:1-104.
4. Ahn ES, Gleason NJ, Nakahira A, Ying JY. Nanostructure Processing of Hydroxyapatite-based Bioceramics. Nano Lett. 2001; 1:149-153.
5. Xin R, Leng Y, Chen J, Zhang Q. A comparative study of calcium phosphate formation on bioceramics in vitro and in vivo. Biomaterials. 2005; 26:6477-6486.
6. Miranda P, Pajares A, Saiz E, Tomsia AP, Guiberteau F. Mechanical properties of calcium phosphate scaffolds fabricated by robocasting. J Biomed Mater Res - Part A. 2008; 85A:218-227.
7. Hench LL. Biomaterials: A forecast for the future. In: Biomaterials. 1998; 19:1419-1423.
8. Wu C, Chang J, Wang J, Ni S, Zhai W. Preparation and characteristics of a calcium magnesium silicate (bredigite) bioactive ceramic. Biomaterials. 2005; 26:2925-2931.
9. Ramaswamy Y, Wu C, Van Hummel A, Combes V, Grau G, Zreiqat H. The responses of osteoblasts, osteoclasts and endothelial cells to zirconium modified calcium-silicate-based ceramic. Biomaterials. 2008; 29:4392-4402.
10. Valerio P, Pereira MM, Goes AM, Leite MF. The effect of ionic products from bioactive glass dissolution on osteoblast proliferation and collagen production. Biomaterials. 2004; 25:2941-2948.
11. Wu C, Chang J. A review of bioactive silicate ceramics. Biomedical Materials (Bristol). 2013; 8:1-12.
12. Yoshizawa S, Brown A, Barchowsky A, Sfeir C. Magnesium ion stimulation of bone marrow stromal cells enhances osteogenic activity, simulating the effect of magnesium alloy degradation. Acta Biomater. 2014; 10:2834-2842.
13. Wu L, Feyerabend F, Schilling AF, Willumeit-Römer R, Luthringer BJC. Effects of extracellular magnesium extract on the proliferation and differentiation of human osteoblasts and osteoclasts in coculture. Acta Biomater. 2015; 27:294-304.
14. He D, Zhuang C, Chen C, Xu S, Yang X, Yao C, et al. Rational Design and Fabrication of Porous Calcium-Magnesium Silicate Constructs That Enhance Angiogenesis and Improve Orbital Implantation. ACS Biomater Sci Eng. 2016; 2:1519-1527.

15. Diba M, Tapia F, Boccaccini AR, Strobel LA. Magnesium-Containing Bioactive Glasses for Biomedical Applications. Int J Appl Glas Sci. 2012; 3:221-253.

16. Wu C, Ramaswamy Y, Zreiqat H. Porous diopside (CaMgSi2O6) scaffold: A promising bioactive material for bone tissue engineering. Acta Biomater. 2010; 6:2237-2245.

17. Wu C, Chang J. Degradation, bioactivity, and cytocompatibility of diopside, akermanite, and bredigite ceramics. J Biomed Mater Res - Part B Appl Biomater. 2007; 83:153-160.

18. Nonami T. Developmental Study of Diopside for Use as Implant Material. MRS Proc. 1991; 252:87-92.

19. Jafari Baghjeghaz M, Salahinejad E. Enhanced sinterability and in vitro bioactivity of diopside through fluoride doping. Ceram Int. 2017; 43:4680-4686.

20. Wei J, Lu J, Yan Y, Li H, Ma J, Wu X, et al. Preparation and Characterization of Well Ordered Mesoporous Diopside Nanobiomaterial. J Nanosci Nanotechnol. 2012; 11:10746-10749.

21. Saravanan C, Sasikumar S. Bioactive Diopside (CaMgSi2O6) as a Drug Delivery Carrier – A Review. Curr Drug Deliv. 2012; 9:583-587.

22. Lecointre A, Bessière A, Priolkar KR, Gourier D, Wallez G, Viana B. Role of manganese in red long-lasting phosphorescence of manganese-doped diopside for in vivo imaging. Mater Res Bull. 2013; 48:1898-1905.

23. Yamamoto S, Nonami T, Hase H, Kawamura N. Fundamental study on apatite precipitate ability of CaO-MgO-SiO_2 compounders employed pseudo body solution of application for biomaterials. J Aust Ceram Soc. 2012; 48:180-184.

24. Iwata NY, Lee GH, Tokuoka Y, Kawashima N. Sintering behavior and apatite formation of diopside prepared by coprecipitation process. Colloids Surfaces B Biointerfaces. 2004; 34:239-245.

25. Choudhary R, Vecstaudza J, Krishnamurithy G, Raghavendran HRB, Murali MR, Kamarul T, et al. In-vitro bioactivity, biocompatibility and dissolution studies of diopside prepared from biowaste by using sol-gel combustion method. Mater Sci Eng C. 2016; 68:89-100.

26. Bozadjiev L, Doncheva L. METHODS FOR DIOPSIDE SYNTHESIS. J Univ Chem Technol Metall. 2006; 41:125-128.

27. Palakurthy S, P AA, K VR. In vitro evaluation of silver doped wollastonite synthesized from natural waste for biomedical applications. Ceram Int. 2019; 45:25044-25051.

28. Oki A, Parveen B, Hossain S, Adeniji S, Donahue H. Preparation and in vitro bioactivity of zinc containing sol-gel-derived bioglass materials. J Biomed Mater Res - Part A. 2004; 69:216-221.

29. Ismail H, Shamsudin R, Abdul Hamid MA. Effect of autoclaving and sintering on the

formation of β-wollastonite. Mater Sci Eng C. 2016;58:1077–81.

30. Montazerian M, Yekta BE, Marghussian VK, Bellani CF, Siqueira RL, Zanotto ED. Bioactivity and cell proliferation in radiopaque gel-derived CaO-P_2O_5-SiO_2-ZrO_2 glass and glass-ceramic powders. Mater Sci Eng C. 2015; 55:436-447.

31. Iwata N, Yokoyama M, Ishinabe A, Tsuchiya T, Tsunakawa S. Preparation and characterization of sodium and iron-containing diopside crystal by several methods from solution. Mater Res Soc Symp - Proc. 1999; 547:243-248.

32. Nonami T, Takahashi C, Yamazaki J. Synthesis of diopside by alkoxide method and coating on titanium. Nippon Seramikkusu Kyokai Gakujutsu Ronbunshi/Journal Ceram Soc Japan. 1995; 103:703-708.

33. Iwata NY, Lee GH, Tsunakawa S, Tokuoka Y, Kawashima N. Preparation of diopside with apatite-forming ability by sol-gel process using metal alkoxide and metal salts. Colloids Surfaces B Biointerfaces. 2004; 33:1-6.

34. Kazemi A, Abdellahi M, Khajeh-Sharafabadi A, Khandan A, Ozada N. Study of in vitro bioactivity and mechanical properties of diopside nano-bioceramic synthesized by a facile method using eggshell as raw material. Mater Sci Eng C. 2017; 71:604-610.

35. Choudhary R, Venkatraman SK, Bulygina I, Senatov F, Kaloshkin S, Anisimova N, et al. Biomineralization, dissolution and cellular studies of silicate bioceramics prepared from eggshell and rice husk. Mater Sci Eng C. 2021; 118:1-7.

36. Toby BH. EXPGUI , a graphical user interface for GSAS . J Appl Crystallogr. 2001; 34:210-213.

37. Evangeline B, Azeem PA, Prasada Rao R, Swati G, Haranath D. Structural and luminescent features of cerium doped $CaZrO_3$blue nanophosphors. J Alloys Compd. 2017; 710:618-623.

38. Nonami T, Tsutsumi S. Study of diopside ceramics for biomaterials. J Mater Sci Mater Med. 1999; 10:475-479.

39. Saiz E, Goldman M, Gomez-Vega JM, Tomsia AP, Marshall GW, Marshall SJ. In vitro behavior of silicate glass coatings on Ti6Al4V. Biomaterials. 2002; 23:3749-3756.

40. Lakshmi R, Velmurugan V, Sasikumar S. Preparation and Phase Evolution of Wollastonite by Sol-Gel Combustion Method Using Sucrose as the Fuel. Combust Sci Technol. 2013; 185:1777-1785.

41. Zouai S, Harabi A, Karboua N, Harabi E, Chehlatt S, Barama SE, et al. A new and economic approach to synthesize and fabricate bioactive diopside ceramics using a modified domestic microwave oven. Part 2: Effect of P_2O_5 additions on diopside bioactivity and mechanical properties. Mater Sci Eng C. 2016; 61:553-563.

42. Najafinezhad A, Abdellahi M, Ghayour H, Soheily A, Chami A, Khandan A. A comparative study on the synthesis mechanism, bioactivity and mechanical properties of three silicate bioceramics. Mater Sci Eng C. 2017; 72:259-267.

43. Choudhary R, Venkatraman SK, Chatterjee A, Vecstaudza J, Yáñez-Gascón MJ, Pérez-Sánchez H, et al. Biomineralization, antibacterial activity and mechanical properties of biowaste derived diopside nanopowders. Adv Powder Technol. 2019; 30:1950-1964.

44. Barralet J, Best S, Bonfield W. Carbonate substitution in precipitated hydroxyapatite: An investigation into the effects of reaction temperature and bicarbonate ion concentration. J Biomed Mater Res. 1998; 41:79-86.

45. Sasikumar S, Vijayaraghavan R. Synthesis and Characterization of Bioceramic Calcium Phosphates by Rapid Combustion Synthesis. J Mater Sci Technol. 2010; 26:1114-1118.

46. Shahrouzifar MR, Salahinejad E, Sharifi E. Co-incorporation of strontium and fluorine into diopside scaffolds: Bioactivity, biodegradation and cytocompatibility evaluations. Mater Sci Eng C. 2019;

47. Vallet-Regí M, Salinas AJ, Román J, Gil M. Effect of magnesium content on the in vitro bioactivity of CaO-MgO- SiO_2-P_2O_5 sol-gel glasses. J Mater Chem. 1999; 9:515-518.

48. Wu C, Chang J. Degradation, bioactivity, and cytocompatibility of diopside, akermanite, and bredigite ceramics. J Biomed Mater Res - Part B Appl Biomater. 2007; 83:153-160.

49. Nabiyouni M, Brückner T, Zhou H, Gbureck U, Bhaduri SB. Magnesium-based bioceramics in orthopedic applications. Acta Biomaterialia. 2018; 66:23-43.

50. Maeno S, Niki Y, Matsumoto H, Morioka H, Yatabe T, Funayama A, et al. The effect of calcium ion concentration on osteoblast viability, proliferation and differentiation in monolayer and 3D culture. Biomaterials. 2005; 26:4847-4855.

51. Lu J, Lu Z, Peng C, Li X, Jiang H. Influence of particle size on sinterability, crystallisation kinetics and flexural strength of wollastonite glass-ceramics from waste glass and fly ash. Mater Chem Phys. 2014; 148:449-456.

52. Narayan R. Biomedical materials. Biomedical Materials. 2009.

53. Ghomi H, Emadi R, Javanmard SH. Fabrication and characterization of nanostructure diopside scaffolds using the space holder method: Effect of different space holders and compaction pressures. Mater Des. 2016; 91:193-200.

54. He D, Zhuang C, Xu S, Ke X, Yang X, Zhang L, et al. 3D printing of Mg-substituted wollastonite reinforcing diopside porous bioceramics with enhanced mechanical and biological performances. Bioact Mater. 2016; 1:85-92.

55. Gerhardt LC, Boccaccini AR. Bioactive glass and glass-ceramic scaffolds for bone tissue engineering. Materials (Basel). 2010; 3:3867-3910.

56. Hutmacher DW. Scaffolds in tissue engineering bone and cartilage. Biomaterials. 2000; 21:2529-2543.

57. Wu C, Ramaswamy Y, Boughton P, Zreiqat H. Improvement of mechanical and biological properties of porous CaSiO3 scaffolds by poly(d,l-lactic acid) modification. Acta Biomater. 2008; 4:343-353.

Chapter 8

Summary and conclusions

In this chapter, brief summary and conclusions drawn from the investigations carried out on in vitro bioactivity, degradation rate, mechanical properties, cytocompatibility and cell proliferation ability of bio-waste derived wollastonite ($CaSiO_3$) ceramics substituted with trace metal oxide (Ag, Zr and Mg) are discussed along with future prospective of the research work.

8.1 Summary

The research work presented in this thesis has been focused mainly on two aspects:

1. Synthesis of β-wollastonite (β-$CaSiO_3$) though sol-gel method using natural resources such as rice husk as a source of silica and eggshells as a source of calcium oxide. Wollastonite is a promising bone implant material because of its advanced bio-functionalities, excellent bioactivity and biocompatibility.

2. Improving the structural, mechanical properties and dissolution behaviour of wollastonite with various trace metal oxide (Ag, Zr and Mg) additions.

Initially, β-wollastonite was prepared using bio-waste such as rice husk ash (RHA) as a source of silica and eggshells as a source of calcium oxide through sol-gel method. The optimum calcination and sintering temperatures required to obtain pure phase of β-wollastonite were achieved using thermal analysis. The *in vitro* apatite forming ability, degradation behaviour and mechanical properties of synthesized wollastonite were discussed. Later, β-wollastonite was also prepared using tetraethylorthosilicate (TEOS) and calcium nitrate tetrahydrate ($Ca(NO_3)_2.4H_2O$) by conversional sol-gel method. The results of *in vitro* bioactivity, degradation, antibacterial activity, and cell proliferation studies for β-wollastonite synthesized from natural resources and through chemical methods were compared by observing their performance under the same experimental conditions.

In order to enhance the structural properties, antibacterial activity and dissolution behaviour of wollastonite, silver (Ag) was chosen as a dopant element because (i) Ag is an antibacterial agent that shows strong biocidal effect against 12 species of bacteria, including Staphylococcus aureus (S. aureus) and Escherichia coli (E. coli) (ii) the incorporation of silver into wollastonite at the expense of calcium would decrease the number of non-bridging

oxygen groups and reduce the dissolution rate. Ag was doped into wollastonite, where Ag doping concentration varied from 2 to 6 mol.% and its effect on the properties of β-wollastonite was studied.

As Zr shows superior biocompatibility, osseointegration and good mechanical strength, it is speculated that the incorporation of zirconia into wollastonite will significantly improve the mechanical and biological properties. Zr was doped into wollastonite with the objective of improving mechanical properties and degradation rate, where Zr doping concentration varied from 1 to 5 mol.% and its effect on the bioactivity, degradation rate, cytocompatibility and mechanical properties of wollastonite was studied.

Further, the study focused on extension of method of preparation for calcium silicate-based bioceramics such as diopside ($CaMgSi_2O_6$), akermanite ($Ca_2MgSi_2O_7$), bredigite ($Ca_7Mg(SiO_4)_4$), merwinite ($Ca_3MgSi_2O_8$), monticellite ($CaMgSiO_4$), hardystonite ($Ca_2Zn(Si_2O_7$) and baghdadite ($Ca_3ZrSi_2O_9$). Among various calcium silicates-based bioceramics, diopside with the crystal structure of monoclinic, has received much attention on account of its quite interesting properties in terms of good compressive strength, superior mechanical stability and bending strength and controllable degradation rate. It shows good hydroxyapatite formation rate and has excellent *in vivo* osteoinduction. Therefore, diopside bioceramics were synthesized from natural resources such as rice husk as a source of silica and eggshells as a source of calcium oxide via sol-gel method; the degradation rate, apatite-forming ability, biocompatibility and mechanical properties for bone tissue reconstruction and repair were also assessed for diopside bioceramics.

X-ray fluorescence (XRF) spectrometer, Thermo gravimetric and differential thermal analyzer (TG-DTA), X-ray diffraction (XRD), Fourier transform infrared (FTIR) spectroscopy (FTIR), Scanning electron microscopy- Energy dispersive spectrometry (SEM-

EDS) and Particle analyzer were used to characterize the prepared samples. Bioactivity was studied based on the rate of hydroxyapatite formation using *in vitro* experiments in simulated body fluid (SBF). Weight loss studies were performed in Tris-HCl buffer solutions to know the degradation behaviour of the synthesized ceramics according to ISO 10993 "Biological evaluation of biomedical devices-Part 14: Identification and quantification of degradation products from ceramics. Cytocompatibility was estimated for osteoblast-like cells (MG – 63) using MTT assay. Mechanical properties such as microhardness and fracture toughness were tested using micro Vickers hardness tester, while compressive strength, bending strength and elasticity modules were tested using universal testing machine.

8.2 Conclusions

β-wollastonite was successfully achieved at relatively low temperature (850 °C) sintering from natural resources such as rice husk ash (RHA) as a source of silica and eggshells as a source of calcium oxide through sol-gel method. *In vitro* biological studies results revealed that the prepared wollastonite samples exhibited good bioactivity with faster growth rate of hydroxyapatite and no toxic effect on osteoblast-like MG-63 cells. The mechanical properties revealed good compressive strength (40.77 ± 2.46 MPa) and Micro-hardness (20.14 ± 1.85 HV) values. Furthermore, the apatite crystals were close-packed and fine, and the growth rate was faster on wollastonite that was prepared from natural resources (NCS) than on wollastonite prepared from chemicals (CCS). Degradation results demonstrated that NCS has lower dissolution rate than CCS ceramics. The most noticeable antimicrobial study demonstrated that NCS samples exhibit significant antimicrobial activity against *E. coli* and *S. aureus*. Cell culture study revealed that NCS ceramic particles were found to be cytocompatible and demonstrate cell proliferative ability along with CCS ceramic particles.

Silver (Ag) doped wollastonite ceramics showed the promising apatite layer formation on their surface and the addition of Ag result in the enhancement of apatite layer formation rate. Degradation study revealed that the addition of silver decreases the degradation rate of wollastonite. The antimicrobial activity test demonstrated that Ag doped wollastonite exhibits excellent inhibition zone of pathogens such as *E. coli* and *S. aureus* than pure form of wollastonite.

The incorporation of zirconia into wollastonite phase could increase mechanical properties. The microhardness and compressive strength increased from 19.3 ± 1.3 to 45.1 ± 2.8 HV and 40 ± 2.4 to 86 ± 2.1 MPa, respectively, with increase in zirconia content from 0 to 5 mol%. The bending strength and elasticity modulus increased from 10.2 ± 0.7 to 23.6 ± 1.2 MPa and 1.44 ± 0.1 to 5.8 ± 0.2 GPa, respectively. *In vitro* studies results revealed that the prepared Zr-W ceramics show good bioactivity with the formation of hydroxyapatite while apatite forming rate slightly decreased with increase in zirconia content. Degradation test result showed that the addition of zirconia decreased the degradation rate of wollastonite. Cytocompatibility test demonstrated Zr-W ceramics have no toxic effect on MG-63 cells.

Further, Pure phase diopside was successfully obtained at significantly low temperature (800 °C) from rice husk ash (RHA) and eggshell using sol-gel method. The prepared diopside ceramics possessed good mechanical properties especially compressive strength (210 ± 12.5 MPa), fracture toughness (2.8 ± 0.3 MPa $m^{1/2}$), bending strength (86.7 ± 7.3 MPa) and elasticity modulus (17.5 ± 2.3 GPa) values in the range seen in human cortical bone, as well as improved mechanical stability and slow degradation rate. Biological studies results demonstrated that the synthesized diopside ceramics exhibited good apatite forming-ability, and cytocompatibility as well as stimulatory effect on osteoblasts like cell proliferation.

Based on the above observations, it may be conclude that the calcium silicate-based bioceramics derived from natural resources showed good bioactivity, biodegradation, cytocompatibility and mechanical properties. Therefore, these calcium silicate-based ceramics prepared from rice husk ash and eggshells might be potential low cost candidate for use as bioactive implant in bone tissue engineering as well as safe reinforcement material in the manufacture of biocomposites scaffolds. The work also provides evidence that the method is effective for accelerating utilisation as well as recycling of waste volumes to generate bioceramics for synthetic bone substitutes.

8.3 Future

- In order to utilize the beneficial effects of ions released and to enhance the biological performance of prepared calcium silicate-based ceramics in the direction of specific host response, future developments may explicitly examine the kinetics of specific ion release.
- The prepared calcium silicate-based materials can be processed into porous ceramic scaffolds using scaffold fabrication techniques to avail oneself of the benefits of porous scaffolds like patient-derived cells seeding capacity and drug loading capacity into the scaffolds.
- Calcium silicate-based ceramics/polymer composite scaffolds can be obtained for specific bone grafts by monitoring their proportions.
- Detailed biocompatibility experiments can be done along with *in vivo* animal models.

List of publications

1. Srinath Palakurthy, Abdul azeem P, Venugopal reddy K, Samudrala Rajkumar. **In vitro bioactivity and degradation behaviour of β-wollastonite derived from natural waste**. Mater Sci Eng C. 2019;98:109-117. doi:10.1016/j.msec.2018.12.101.

2. Srinath Palakurthy, Abdul azeem P, Venugopal reddy K. **In vitro evaluation of silver doped wollastonite synthesized from natural waste for biomedical applications**. Ceram Int. 2019; 45(18):25044-25051. doi:10.1016/j.ceramint.2019.03.169.

3. Srinath Palakurthy, Abdul azeem P, Venugopal reddy K, Vasudevarao Penugurti, Bramanandam Manavathi. **A comparative study on in vitro behavior of calcium silicate ceramics synthesized from biowaste resources**. J Am Ceram Soc. 2019; 103(2):933-943. doi:10.1111/jace.16745.

4. Srinath Palakurthy, Abdul azeem P, Venugopal reddy K, Vasudevarao Penugurti, Bramanandam Manavathi. **Zirconia-containing wollastonite ceramics derived from bio waste resources for bone tissue engineering**. Biomed. Mater. 2020; 15(5): 055025. doi:10.1088/1748-605x/ab975d.

5. Srinath Palakurthy, Abdul azeem P, Venugopal reddy K. **Review on calcium silicate-based bioceramics in bone tissue engineering**. Int J Appl Ceram Technol. 2020; 17(5):2450-2464. https://doi.org/10.1111/ijac.13577

6. Srinath Palakurthy, Venugopal reddy K, Sushil Patel, Abdul azeem P. **A cost effective SiO_2–CaO– Na_2O bio-glass derived from bio-waste resources for biomedical applications**. Prog. Biomater. 2020;9:239-248. doi:10.1007/s40204-020-00145-0.

7. Srinath Palakurthy, Abdul Azeem P, Venugopal Reddy K, Chiranjeevi Padala, Bramanandam Manavathi, Prasada Rao R. **A novel cost-effective approach to fabricate diopside bioceramics: a promising ceramics for orthopedic applications**. Advanced Powder Technology, 2021; 32(3):875-884. https://doi.org/10.1016/j.apt.2021.01.038

AIP Proceedings

1. Srinath Palakurthy, Abdul azeem P., Venugopal reddy K., Rajkumar Samudrala, Synthesis and in vitro bioactivity of SiO_2-CaO-Na_2O glass using bio-waste resources, AIP Conference Proceedings 2115, 030233 (2019); https://doi.org/10.1063/1.5113072

2. Srinath Palakurthy, Abdul azeem P, Venugopal reddy K, Sol-gel synthesis of SiO_2-CaO-Na_2O bio-ceramics using bio-waste, in: AIP Conf. Proc., 2020. doi:10.1063/5.0017238.

List of papers presented in National/International Conferences

1. Presented a paper entitled "***In vitro* bioactivity of wollastonite derived from natural waste for biomedical applications**" in the International Conference "Recent Trends in Materials Science and Technology 2018 (ICMST 2018)" organized by Indian Institute of Space Science and Technology (IIST) jointly with Materials Research Society of India (MRSI), held during October 10^{th}-13^{th}, 2018, at VSSC, Thiruvananthapuram.

2. Presented a paper entitled "***In vitro* Evaluation of Silver Doped Wollastonite Synthesized from Natural Waste**" in the International Conference "Advanced ceramics and Nano materials for Sustainable Developments (ACeND - 2018)" organized by Indian Ceramic Society Karnataka chapter held during September 9^{th}-21^{th}, 2018, at Christ deemed to university, Bengaluru, India.

3. Presented a paper entitled "**Synthesis of cost effective SiO_2-CaO-Na_2O bio-glass using Bio waste resources**" in the International Conference "63^{rd} DAE Solid State Physics Symposium (DAE-SSPS 2018)" organized by Bhabha Atomic Research Centre, Mumbai, India held during December 18^{th}-22^{th}, 2018, at Guru Jambheshwar University of Science and Technology, Hisar, Haryana

4. Presented a paper entitled "***In vitro* bioactivity of zirconia-containing wollastonite synthesized from natural resources**" in the International Conference "Advanced functional materials and devices" held during February 26^{th}-28^{th}, 2019, at National Institute of Technology, Warangal.

5. Presented a paper entitled "**Sol-gel Synthesis of SiO_2-CaO-Na_2O Bio-Ceramics using Bio-Waste**" in the International Conference "64^{rd} DAE Solid State Physics Symposium (DAE-SSPS 2019)" organized by Bhabha Atomic Research Centre, Mumbai, India, held during December 18^{th}-22^{th}, 2019, at Indian Institute of Technology, Jodhpur, Rajasthan.

Received: 12 May 2020 | Revised: 12 May 2020 | Accepted: 9 June 2020

DOI: 10.1111/ijac.13577

ORIGINAL ARTICLE

International Journal of Applied Ceramic Technology

Review on calcium silicate-based bioceramics in bone tissue engineering

Palakurthy Srinath | P. Abdul Azeem | K. Venugopal Reddy

Department of Physics, National Institute of Technology Warangal, Warangal, India

Correspondence
P. Abdul Azeem, Department of Physics, National Institute of Technology Warangal, Warangal 506004, India.
Email: drazeem2002@yahoo.com

Abstract

Calcium (Ca) and silica (Si) ions have attracted intense interest in biomedical applications. The two ions are directly involved in many biological processes; for instance, Ca plays a key role in regulating cellular responses to bioceramics, promoting cell growth, and differentiation into osteoblasts. Si plays a significant role in bone calcification and is helpful for bone density improvement and inhibiting osteoporosis. Calcium silicate ceramics including a large group of trace metal containing calcium silicate-based compounds are involved in biomedical applications such as repairing hard tissue texture, bone scaffolds, bone cements, or implant coatings. The aim of the study is to provide a comprehensive overview of developments in research on calcium silicate-based ceramics, such as wollastonite ($CaSiO_3$), diopside ($CaMgSi_2O_6$), akermanite ($Ca_2MgSi_2O_7$), bredigite ($Ca_7Mg(SiO_4)_4$), merwinite ($Ca_3MgSi_2O_8$), monticellite ($CaMgSiO_4$), hardystonite ($Ca_2Zn(Si_2O_7)$, and baghdadite ($Ca_3ZrSi_2O_9$), including degradation, apatite mineralization, and mechanical properties. Finally, the biological in vitro and in vivo presentation for bone tissue repair are summarized, which show promise with regard to application of calcium silicate-based ceramics as bone repair and replacement materials.

KEYWORDS

bioactivity, bioceramics, bone, calcium silicate

1 | INTRODUCTION

Bone has high regeneration potential, and can repair itself when the wound is smaller than the "critical size defect" while the newly formed bone is indistinguishable from healthy ones. The nonregenerative threshold of bone fracture is called critical sized defect (CSD).[1,2] In such cases, extensive studies have been reported for bone repair, including autografts and allografts using autologous and allogeneic transplantations. Autografts are the gold standard for bone repair in which cancellous iliac bone is taken from the same patient and used as a graft. Autografts have indispensable components needed to achieve osteoconduction, osteogenesis, and osteoinduction without the risk of an immunogenic response because they are perfectly histocompatible.[3] However, autograft transplants are very expensive techniques, and they are associated with substantial donor site injury, illness, disability, scarring, and the risks of surgery: bleeding, inflammation, infection, and chronic pain. Autologous transplantations may be a null treatment option in cases where the defect site needs larger bones than is possible or obtainable.[4] Allogeneic transplantation is the process of bone grafting in which bone is taken from a living human donor, or from a cadaver (freeze-dried bone), or from xenografts (animal origin). Allografts are associated with low revascularization and integration compared to autografts. Moreover, they demonstrate different kinetics of remodeling, risks of immunogenic response, and the transmission of viral pathologies.[5]

The prerequisites for establishment of bone replacements and the limitations mentioned have been detailed above and,

Materials Science & Engineering C 98 (2019) 109–117

Contents lists available at ScienceDirect

Materials Science & Engineering C

journal homepage: www.elsevier.com/locate/msec

In vitro bioactivity and degradation behaviour of β-wollastonite derived from natural waste

Srinath Palakurthy, Venu Gopal Reddy K., Raj Kumar Samudrala, Abdul Azeem P.*

Department of Physics, National Institute of Technology Warangal, Warangal 506004, India

ARTICLE INFO

Keywords:
Sol-gel method
Hydroxyapatite
Biomedical applications
Wollastonite

ABSTRACT

Calcium silicate ceramics, in particular wollastonite ($CaSiO_3$), is the most commonly used bioactive material for bone regeneration and repairing applications. The present study aims to synthesize cost effective wollastonite using natural waste materials such as rice husk ash (RHA) and eggshells, sources of silica and calcium oxide respectively. Wollastonite was prepared by sol-gel method and based on thermogravimetric and differential thermal analysis (TG/DTA) results the samples were sintered at 850 °C. X-ray diffractometer (XRD) revealed that the sintered samples possess single phasic β-wollastonite. The assessment of bioactivity was examined using *in vitro* studies by immersing the pellets in simulated body fluid (SBF) for different time periods (3, 7, 14, 21 days). The growth of hydroxyapatite layer on the surface of the sample was analysed using XRD, Fourier transform infrared (FTIR) spectroscopy and Scanning electron microscopy-energy dispersive spectrometer (SEM-EDS). The significant change in pH of the SBF solution was observed during the first 11 days of immersion, after which the pH was saturated. Biodegradation test was performed in SBF and Tris buffer solutions according to ISO 10993-14 standard, and the test revealed that the ceramic pellets showed lower degradation rates with slow dissolution of ionic species. MTT assay demonstrated that the prepared wollastonite exhibits cytocompatibility with MG-63 cells at different dosage (1000–50 μg/mL) for 48 h. The results suggested that β-wollastonite can be a low cost bioactive material, which can be useful in biomedical applications.

1. Introduction

Wollastonite is the most extensively studied calcium silicate ceramic. It has a wide combination of properties such as thermal stability, low thermal conductivity, corrosion resistance, chemical inertness and low dielectric constant [1,2]. Wollastonite is used in ceramics to reduce the baking temperature and duration, as filling agent in rubber, paper and plastic, as milking agent in paint, bonding agents for abrasives, and metallurgical applications [3,4]. Wollastonite is a polymeric substance existing in two mineral forms: low temperature form; where β-wollastonite crystallizes in a chain silicate and high temperature form; where α-wollastonite crystallizes in a triclinic lattice [5].

Wollastonite has also been studied for being a promising bone implantable material because of its advanced bio-functionalities, excellent bioactivity and biocompatibility [6–10] The presence of Ca and Si ions in wollastonite shows its important role in the formation of hydroxyapatite layer, affects mineralization process and plays a role in bone bonding mechanism [11,12]. The ion products released from calcium silicate ceramics could promote gene expression and improve the efficiency of insulin-like growth factor (IGF), which is especially related to cell proliferation. Wollastonite ceramic shows better performance in terms of mechanical properties such as higher bending strength and fracture toughness when compared with calcium phosphate and Hydroxyapatite (HA) [13,14]. However, the relatively high dissolution rate of wollastonite, which accounts for higher pH level in the surrounding environment, has a limit on its clinical applications. The problem can be solved by emerging multiphase materials comprising highly dissolvable phases [15].

Different methods went into the preparation of wollastonite: solid phase reaction [16,17], co-precipitation [18], sol-gel method [19], hydrothermal method [20], microwave synthesis [21] and solution combusting method [22]. Synthesis technique plays an important role in biomedical application of wollastonite. Sol-gel derived wollastonite exhibit unique surface chemistry and higher bioactivity [23–26]. In sol-gel process, metal alkoxides like tetraethylorthosilicate (TEOS) and tetramethylorthosilicate (TMOS) were used as silica precursor and calcium nitrate tetra hydrate ($Ca(NO_3)_2{\cdot}4H_2O$) was used as calcium oxide precursor. However, these precursors are expensive. The present work provides an environmentally beneficial and cost-free production of wollastonite by using Rice husk ash (RHA) and eggshells which form

* Corresponding author.
E-mail address: drazeem2002@nitw.ac.in (A.A. P.).

https://doi.org/10.1016/j.msec.2018.12.101
Received 7 May 2018; Received in revised form 11 December 2018; Accepted 25 December 2018
Available online 29 December 2018

Received: 29 May 2019 | Revised: 25 July 2019 | Accepted: 8 August 2019

DOI: 10.1111/jace.16745

ORIGINAL ARTICLE

Journal of the American Ceramic Society

A comparative study on in vitro behavior of calcium silicate ceramics synthesized from biowaste resources

Srinath Palakurthy[1] | **P. Abdul Azeem**[1] | **K. Venugopal Reddy**[1] | **Vasudevarao Penugurti**[2] | **Bramanandam Manavathi**[2]

[1]Department of Physics, National Institute of Technology Warangal, Warangal, India

[2]Department of Biochemistry, School of Life Science, University of Hyderabad, Hyderabad, India

Correspondence
P. Abdul Azeem, Department of Physics, National Institute of Technology Warangal, Warangal 506004, India.
Email: drazeem2002@yahoo.com

Funding information
Science and Engineering Research Board; MHRD, Government of India

Abstract

Calcium silicate ceramics have received significant attention for biomedical applications for their excellent bioactivity and osteoconduction properties. Sol-gel process is extensively used for the fabrication of calcium silicates. In sol-gel process, calcium nitrate tetra hydrate ($Ca(NO_3)_2{\cdot}4H_2O$) and tetraethylorthosilicate (TEOS) are used as precursors. However, these precursors are expensive. The objective of this work was to compare in vitro behavior of calcium silicate ($CaSiO_3$) produced using biowaste such as rice husk ash (RHA) and eggshells (coded; NCS) with $CaSiO_3$ prepared using TEOS and $Ca(NO_3)_2{\cdot}4H_2O$ (coded; CCS). Thermal investigation results revealed that the crystallization temperature for NCS is relatively lower (772°C) than for CCS (870°C). Bioactivity was studied in vitro using simulated body fluid (SBF) with respect to mineralization rate of hydroxyapatite. Mineralization of a greater hydroxyapatite was observed on NCS ceramics than CCS ceramics after incubation for 3, 7, 14 days in SBF solution, which was confirmed using X-ray diffractometer, Fourier transform infrared spectroscopy, scanning electron microscopy-energy dispersive spectroscopy. Degradation studies were conducted in Tris-HCl solution and the test results revealed that NCS ceramics has lower dissolution rate than CCS ceramics. The antimicrobial assay has shown that NCS samples exhibit significant zone of inhibition against *Escherichia coli* and *Staphylococcus aureus* which confirmed that the $CaSiO_3$ prepared from RHA and eggshell can prevent bacteria from adhering to the surface. In addition cell culture studies revealed that NCS ceramics possess good cytocompatibility with MG-63 cells and significantly promoted cell proliferation.

KEYWORDS

bioactivity, calcium silicate, hydroxyapatite, sol-gel

1 | INTRODUCTION

Calcium silicate ceramics have been identified as bioactive and prospective candidates for bone tissue engineering applications.[1–3] Researchers have reported that bone tissue can be produced on calcium silicate ceramics with hydroxyl carbonated apatite layer deposition.[4,5] Moreover, these ceramics can support the attachment of human bone-derived cells, their proliferation and differentiation.[6–8] The conventional starting materials used to synthesize calcium silicates are calcium oxide (CaO) and silica (SiO_2). Commercial calcium oxide and calcium nitrate tetra hydrate ($Ca(NO_3)_2{\cdot}4H_2O$) are

Ceramics International 45 (2019) 25044–25051

Contents lists available at ScienceDirect

Ceramics International

journal homepage: www.elsevier.com/locate/ceramint

In vitro evaluation of silver doped wollastonite synthesized from natural waste for biomedical applications

Srinath Palakurthy, Abdul Azeem P*, Venugopal Reddy K

Department of Physics, National Institute of Technology Warangal, Warangal, 506004, India

ARTICLE INFO

Keywords:
Sol-gel method
Bioactivity
Antibacterial activity
Wollastonite
Rice husk ash (RHA) and eggshells

ABSTRACT

The present study deals with a detailed investigation of bioactivity, degradation and antibacterial activity of silver doped wollastonite ($CaSiO_3$) synthesized using natural waste. Natural waste such as rice husk ash (RHA) and eggshells have been used as precursors for extracting silica (SiO_2) and calcium oxide (CaO) respectively. Silver oxide (AgO) (0, 2, 4 and 6 mol%) doped wollastonite at the expense of CaO were synthesized through sol-gel process, and were characterised with thermogravimetric and differential thermal analysis (TG/DTA), X-ray diffractometer (XRD), Fourier transform infrared (FTIR) spectroscopy and Scanning electron microscopy-energy dispersive spectrometer (SEM-EDS). Thermal analysis revealed that the crystallization temperature of all samples was below 800 °C, and so all samples were sintered at this temperature. The bioactivity was explored *in vitro*, employing simulated body fluid (SBF) and the hydroxyapatite phase formation was confirmed by XRD. FTIR spectra showed the presence of characteristic functional groups, while, surface morphology was observed using SEM images, revealing the spherical shape of hydroxyapatite. The chemical constituents of apatite were confirmed by EDS spectra. The degradation study results have shown that degradation rate of silver doped wollastonite decreased with increase in silver content. Antibacterial activity was tested using disk diffusion method against different bacteria. Silver doped wollastonite showed good antibacterial activity and enhanced bioactivity.

1. Introduction

The necessity of implantation for damaged or diseased parts of the body is not only for mechanical support but also to restore their physiological functions. This indubitably has been the motivating factor for research into the developing of new materials in biomedical applications. Bioactive materials are a class of biomaterials, having two primary important properties of biocompatibility and bioactivity [1]. The first property deals with the acceptance of material with surrounding tissues by not being toxic, injurious and not causing immunological rejection while the latter has the ability to form a bond with living tissues under physiological conditions. The bioactive materials, comprising of bioactive glasses and ceramics explored for biomedical applications are mainly of three types calcium silicate, borate and phosphate based materials [2,3]. Materials based on calcium silicate received warm response as bioactive materials, and they have found applications in repairing hard tissue texture and for regeneration as well as for ossicular prostheses and alveolar ridge resorption [4,5].

Wollastonite ($CaSiO_3$) is the most common calcium silicate ceramic; it has proven to be a potential candidate for scaffolds for bone tissue engineering (BTE) as it shows excellent bioactivity and biocompatibility [2,6–8]. *In vitro* and *in vivo* studies results revealed that it has the ability to form bond with soft tissues, hard tissues and have carbonated hydroxyapatite (CHA) layer on its surface. This layer has similar chemical and crystallographic construction as bone mineral phase and exhibits osteo conductive properties for bone growth [9,10]. The addition of small amount of transition metal ions (Ti, Zr, Cu, Zn, Mg, Ag) in calcium silicate ceramics enhances their osteogenic properties, thereby promoting the attachment, proliferation and differentiation of human mesenchyme stem cells and osteoblast cells [11,12]. Titanium (Ti) and zirconia (Zr) have been traditionally used as implantable materials in orthopedic applications as they have shown excellent biocompatibility with the host tissue [13]. Thus the incorporation of these ions into calcium silicate ceramics improves chemical stability and supports the proliferation of human bone derived cells (HBDC) [14–16]. The addition of copper (Cu) ions contributes to antibacterial properties and enhances the mechanical strength as Cu ions have hypoxia-mimicking ability; they potentiate endogenous cell growth or signals for bone growth [17–19]. On the other hand, it has been demonstrated that magnesium (Mg) ions plays significant role in bone remodeling and

* Corresponding author.
E-mail address: drazeem2002@nitw.ac.in (A.A. P).

https://doi.org/10.1016/j.ceramint.2019.03.169
Received 14 November 2018; Received in revised form 21 February 2019; Accepted 21 March 2019
Available online 23 March 2019

IOP Publishing Biomed. Mater. 0 (2020) xxxxxx https://doi.org/10.1088/1748-605X/ab975d

Biomedical Materials

RECEIVED
19 April 2020

REVISED
21 May 2020

ACCEPTED FOR PUBLICATION
28 May 2020

PUBLISHED
xx xx xxxx

PAPER

Zirconia-containing wollastonite ceramics derived from biowaste resources for bone tissue engineering

Palakurthy Srinath[1], P Abdul Azeem[1], K Venugopal Reddy[1], Vasudevarao Penugurti[1] and Bramanandam Manavathi[2]

[1] Department of Physics, National Institute of Technology Warangal, Warangal 506004, India
[2] Department of Biochemistry, School of Life Science, University of Hyderabad, India

E-mail: drazeem2002@yahoo.com

Keywords: *in vitro* bioactivity, sol-gel method, wollastonite, mechanical properties

Abstract

Zirconia-containing wollastonite ($CaSiO_3$) ceramics with partial substitution of zirconia (1, 3 and 5 mol%) were prepared using eggshells and rice husk ash as source materials for calcium oxide and silica, respectively, through a sol–gel technique. The effect of incorporation of zirconia on *in vitro* bioactivity, mechanical properties, degradability and cytocompatibility of wollastonite was studied. Bioactivity was evaluated by *in vitro* assay using simulated body fluid while degradability was tested in Tris-HCl buffer solution for different time periods (1, 3, 7, 14 and 21 d) according to the ISO 10 993-14 standard. Human osteosarcoma (MG-63) cells were used to assess cytocompatibility with the MTT assay. X-ray diffractometry, Fourier transform infrared spectroscopy and scanning electron microscopy–energy dispersive spectroscopy were used to characterize the ceramics before and after *in vitro* studies. The results obtained showed that increasing the zirconia content in the wollastonite phase increases microhardness, compressive strength, bending strength and the elasticity modulus, while slightly decreasing the rate of formation of the hydroxyapatite layer. Moreover, the samples doped with zirconia had a lower degradation rate and it was noticed that cell viability is unaffected by the incorporation of zirconia.

1. Introduction

Calcium silicate-based ceramics, including wollastonite, akermanite, diopside, merwinite and bredigite, have been widely studied in recent years because they support the attachment, proliferation and differentiation of osteoblast-like cells such as human mesenchymal stem cells [1–3]. Ca and Si are two ions that dissolve from these ceramics. Ca ions play an important role in cell reactions in bioceramics including cell proliferation and differentiation into osteoblasts [4]. Si is one of the most significant trace elements in the human body, acting as a key controller of bone calcification and helping to improve bone density and prevent osteoporosis, specifically during the early stage of bone formation [5, 6]. It has also been reported that the dissolution products from calcium silicates enhance the effect of insulin-like growth factor on cell proliferation [7]. Moreover, calcium silicate ceramics show better mechanical properties than other calcium phosphate ceramics [8, 9].

Wollastonite ($CaSiO_3$), which has a monoclinic crystal structure, belongs to the group of calcium silicate ceramics. It exists in two forms: a low-temperature form called β-wollastonite (β-$CaSiO_3$) and a high-temperature form called α-wollastonite (α-$CaSiO_3$) [10–12]. It has received attention for its ability to contribute to hard tissue regeneration due to its progressive bio-functionalities [13, 14]. Siriphannon *et al* [15] showed that the apatite growth rate on wollastonite was faster than on A-W glass ceramics and other bioactive glass ceramics. *In vitro* cell culture assessments demonstrated that wollastonite ceramics can support the attachment of osteoblast-like cells and the proliferation and differentiation of bone marrow mesenchymal stem cells [16–18]. However, the degradation rate of wollastonite ceramics is relatively high, leading to abrupt changes in the pH value of the local environment by dissolution ions which may negatively affect surrounding cells [19]. Additionally, the high rate of solubility is a likely reason for failure of scaffold construc-

Contents lists available at ScienceDirect

Advanced Powder Technology

journal homepage: www.elsevier.com/locate/apt

Original Research Paper

A novel cost-effective approach to fabricate diopside bioceramics: A promising ceramics for orthopedic applications

Srinath Palakurthy [a], Abdul Azeem P. [a,*], Venugopal Reddy K. [a], Chiranjeevi Padala [b], Bramanandam Manavathi [b], Prasada Rao Rayavarapu [c]

[a] Department of Physics, National Institute of Technology Warangal, Warangal 506004, India
[b] Department of Biochemistry, School of Life Science, University of Hyderabad, India
[c] Centre for Materials for Electronics Technology, Panchawati, Pune, India

ARTICLE INFO

Article history:
Received 19 October 2020
Received in revised form 24 December 2020
Accepted 27 January 2021
Available online xxxx

Keywords:
Bioceramics
Bioactivity
Biocompatibility
Mechanical properties

ABSTRACT

The objective of the present study is to prepare low temperature diopside ($CaMgSi_2O_6$) ceramics from natural waste (Rice husk ash & eggshells) and study the physico-mechanical and *in vitro* biological properties. X-ray powder diffraction (XRD), thermogravimetric-differential thermal analysis (TG-DTA), scanning electron microscopy (SEM), Fourier transforms infrared (FTIR) and energy-dispersive spectrometry (EDS) were used to assess the crystalline phase, thermal behavior, microstructure, functional groups and composition, respectively. Degradation as well as mechanical stability was studied by testing the weight loss and compressive strength in dynamic mode of simulated body fluid (SBF) according to ISO 10993-14. The bioactivity of diopside samples was tested by means of ability and rate of apatite mineralization on the surface in static mode of SBF. Cytocompatibility by human osteoblast-like cells and their proliferation were studied using MTT assay. Results revealed that the pure phase of diopside was successfully attained at significantly low temperature (800 °C) with good mechanical properties, which were nearly similar to that of human cortical bone, and with enhanced mechanical stability. Diopside ceramics possessed apatite growth on its surface in SBF and exhibits excellent biocompatibility with MG-63 cells. These results suggested that prepared diopside can be a cost-effective bioceramics for potential orthopedic applications.

1. Introduction

Calcium phosphates, calcium silicates and calcium sulphates are representative of commonly used bioactive materials [1,2]. Tricalcium phosphate and hydroxyapatite are ceramics based on calcium phosphates, which have molecular composition equivalent to that of human bone [3], are potentially used in orthopedic applications for bone tissue repair and extensively studied to induce bone regeneration because of its exceptional adaptation under human body environment [4,5]. However, low mechanical strength, fracture toughness and slow degradation rate of calcium phosphates have hindered its broader applications as orthopedic implants [6].

Calcium silicate – based biomaterials including bioglass, $CaSiO_3$ and Ca – Si – x (x = Zr, Ti, Zn, Mg, Sr) ceramics, are an emerging subject of research for bone tissue engineering [7–9]. Literature reports have shown that the release of Ca and Si ions at specific concentrations induces osteoblasts cells proliferation and differentiation being a significant feature of calcium silicate – based biomaterials [10]. Furthermore, the relatively widespread range of chemical compositions of calcium silicate – based bioceramics can greatly impact mechanical properties, making them capable of stress and load-bearing orthopedic applications [11].

Magnesium ions in mammalian bodies are the fourth most abundant cations and in combination with sodium and calcium ion channels, play a key role in mammalian cells, stabilizing DNA and stimulating cell growth and proliferation. The role of Mg^{2+} ions in adhesion and growth of osteoblastic cells to degraded magnesium compound has been clearly revealed in many *in vitro* examinations [12,13]; thus magnesium is a very important component in bioceramics to enhance biological properties [14,15]. Diopside ($CaMgSi_2O_6$), akermanite ($Ca_2MgSi_2O_7$), merwinite ($Ca_3MgSi_2O_8$), bredigite ($Ca_7MgSi_4O_{16}$) and monticellite ($CaMgSiO_4$) are pure phase ceramics belonging to the magnesium containing calcium silicates group, which have been examined for their potential applications as bone substitutes. Among these, calcium

* Corresponding author.
E-mail address: drazeem2002@nitw.ac.in (P. Abdul Azeem).

https://doi.org/10.1016/j.apt.2021.01.038
0921-8831/

Please cite this article as: P. Srinath, P. Abdul Azeem, K. Venugopal Reddy et al., A novel cost-effective approach to fabricate diopside bioceramics: A promising ceramics for orthopedic applications, Advanced Powder Technology, https://doi.org/10.1016/j.apt.2021.01.038